Identification of novel cellular factors involved in HIV-1 latency

Vorgelegt beim Fachbereich Biologie der Technischen Universität Darmstadt

zur Erlangung des akademischen Grades

Doctor rerum naturalium

Dissertation von

Alexandra Borch

1. Referentin:	Prof. Dr. Beatrix Süß
2. Referent:	Prof. Dr. Alexander Löwer
3. Referent:	Prof. Dr. Klaus Cichutek

Darmstadt 2019

Die vorliegende Arbeit wurde unter der Leitung von Prof. Dr. Klaus Cichutek in der Arbeitsgruppe von Dr. Renate König „Host-Pathogen Interactions“ am Paul-Ehrlich-Institut in Langen angefertigt.

Die Betreuung seitens der Technischen Universität Darmstadt erfolgte durch Prof. Dr. Beatrix Süß vom Fachbereich Biologie.

Borch, Alexandra
Identification of novel cellular factors involved in HIV-1 latency
Beim Fachbereich Biologie, Technische Universität Darmstadt
Jahr der Veröffentlichung der Dissertation auf TUprints:2020
URN: urn:nbn:de:tuda-tuprints-112896
Datum der Einreichung: 02.10.2019
Datum der mündlichen Prüfung: 13.12.2019

Summary

Despite ongoing efforts, HIV-1 (the causative agent of AIDS) remains an unresolved health threat. Even though current therapy approaches efficiently block ongoing viral replication they cannot cure the infection due to the presence of a latent reservoir. It is of crucial importance to understand that this viral reservoir can fuel new rounds of viral replication and spread the infection. The viral reservoir is defined as cells (best-characterized are resting memory $CD4^+$ T cells) harboring a replication-competent provirus while not producing new progeny virus, a state that can be reversed. Strategies to eradicate the viral reservoir include the so-called 'shock and kill' approach, which is a two-step process, aiming in the first step to reactivate the latent reservoir, leading to the production of new viruses. In a second step, denoted as ‚kill', death of those virus-producing cells is induced by specific cells of the immune system. The identification of host factors involved in HIV-1 latency formation and maintenance is therefore a crucial step to support this and also other strategies.

This current study aimed at validating novel host factors involved in HIV-1 latency. For this, the results of a genome-wide siRNA screen performed in HEK293T cells infected with a single-cycle HIV-1 reporter virus expressing luciferase (HIVluc), served as starting point. This model elucidates potential host factors important for HIV-1 transcriptional processes and is per se not a model for HIV-1 latency, as luciferase is constantly expressed from the viral promoter. Nevertheless, we hypothesize that there is a certain overlap in host factors, which not only have an influence on HIV-1 transcription but also on latency formation/maintenance. This assumption was confirmed by publications on two host factors, namely BRD4 and CYLD, which were reported to be important for the maintenance of HIV-1 latency but were also identified in the primary screen to influence HIV-1 luciferase expression. Two differential approaches were followed to choose and validate initial screening hits: For the first approach, follow-up hits were chosen based on their capability to bind and/or modify chromatin. This selection criterion is based on the importance of the chromatin environment for the formation and maintenance of HIV-1 latency. In a first set of experiments, the initial screening setup was recapitulated for a selection of hits and TRRAP, an adaptor protein found in multiprotein chromatin complexes and involved in epigenetic regulation of transcription, was reconfirmed as hit. Further experiments aimed to identify a potential role of TRRAP in HIV-1 latency. For this, J-Lat cells, a Jurkat derived latency cell model, were depleted of TRRAP by shRNA or siRNA and stimulated with various latency reversing agents (LRAs) to test for an additive effect on latency. Despite intensive testing, a clear involvement of TRRAP on latency could not be definitely determined.

In the second approach, follow-up hits were chosen based on the availability of commercially available compounds, which target the respective primary hits. This approach is here referred to as druggability. Several compounds were chosen and tested for their potential action on latency reversal alone or in combination with LRAs. Auranofin was identified to enhance reversal of latency when applied in combination with all tested LRAs, i.e. TNFα, prostratin, SAHA or sodium butyrate in J-Lat cells and in combination with SAHA and sodium butyrate when tested in U1 cells. Following the identification of auranofin, compounds affecting the same proposed targets, i.e. PRDX5, and its upstream pathway member, i.e. TXNRD1, involved in the thioredoxin pathway, were tested. Whereas none of the additional compounds recapitulated the exact effect of auranofin, diminazene was identified to also have an effect on latency reversal, which was most effective when applied in combination with either TNFα or prostratin. This effect was much stronger than the one seen for auranofin, but was cell line specific as the effect was only seen in J-Lat but not in U1 cells. Verification of auranofin's (and diminazene's) proposed targets was tested by siRNA-mediated silencing, demonstrating a marginal increase in latency reversal, pointing towards the involvement of the associated system in latency reversal. Based on literature, auranofin targets the thioredoxin system involved in reactive oxygen species (ROS) detoxification and reduction of oxidized proteins. This process is crucial for the integrity of the cell. Diminazene, on the other hand, is likely to target the polyamine homeostasis, which participates in a plethora of processes and interactions. An imbalance in polyamines might also lead to a higher level of oxidized products, potentially linking it to the cellular redox state. Whether those pathways are interconnected needs to be determined in future studies. Nevertheless, both the redox system and the polyamine homeostasis are of crucial importance for the cell with a wide range of possible consequences upon their perturbation, which are likely to affect the proviral state.

In summary, in an unbiased systems-level approach, we identified two compounds that mediate latency reversal in combination with other LRAs. We propose further investigation of the two systems targeted by those compounds, which have not been (extensively) studied for an involvement in HIV-1 latency as they could support the targeting of the latent reservoir.

Zusammenfassung

Trotz anhaltender Bemühungen bleibt HIV-1 (der Erreger von AIDS) eine ungelöste Gesundheitsbedrohung. Gegenwärtige Therapieansätze blockieren effizient den viralen Lebenszyklus, können die Infektion jedoch nicht heilen, aufgrund des Vorhandenseins eines latenten Reservoirs. Es ist von entscheidender Bedeutung zu verstehen, daß das latente Reservoir neue Runden viraler Replikation initiieren und damit die Infektion weiter verbreiten kann. Das latente Reservoir ist definiert als Zellen (am besten charakterisiert sind ruhende $CD4^+$ T-Gedächtniszellen), die replikationskompetentes Provirus in ihrem Genom beherbergen können, ohne aktiv neue Viren zu produzieren, wobei dieser Zustand umkehrbar ist. Zu den Strategien der Reservoir Beseitigung gehört unter anderem der sogenannte "shock and kill" Ansatz, bei dem es sich um einen zweistufigen Prozess handelt, der im ersten Schritt darauf abzielt, das latente Reservoir zu reaktivieren und neue Viren zu produzieren. In einem zweiten Schritt, der als "kill" bezeichnet wird, wird der Tod dieser virusproduzierenden Zellen durch bestimmte Zellen des Immunsystems induziert. Die Identifikation von Wirtsfaktoren, die an der Etablierung und Aufrechterhaltung von HIV-1-Latenz beteiligt sind, ist daher ein entscheidender Schritt für diesen Therapieansatz (und andere).

Diese Studie hatte zum Ziel, Wirtsfaktoren zu validieren, die an HIV-1-Latenz beteiligt sind. Als Ausgangspunkt dienten hierzu die Ergebnisse eines genomweiten siRNA-Screenings in HEK293T-Zellen, die infiziert waren mit einem HIV-1 Reportervirus das Luciferase exprimiert. Dieses Modell deckt Wirtsfaktoren auf, die potenziell an HIV-1 Transkription und Translation beteiligt sind, und ist an sich kein HIV-1 Latenzmodel, da Luciferase ständig vom viralen Promotor exprimiert wird. Dennoch gehen wir davon aus, dass es eine Überlappung von Wirtsfaktoren gibt, die nicht nur eine Rolle bei der HIV-1 Transkription spielen, sondern auch an der HIV-1 Latenz Etablierung/Beibehaltung. Diese Annahme wurde durch Veröffentlichungen von zwei Wirtsfaktoren bestätigt, nämlich BRD4 und CYLD, die Einfluss auf HIV-1-Latenz nehmen und ebenfalls im primären Screening identifiziert wurden. Für die Auswahl und Validierung primärer Screening-Treffer wurden zwei unterschiedliche Ansätze verfolgt: Für den ersten Ansatz wurden Folgetreffer auf der Grundlage ihrer Fähigkeit, Chromatin zu binden und/oder zu modifizieren, ausgewählt. Dieses Auswahlkriterium basiert auf der Bedeutung der Chromatinumgebung für die Bildung und Aufrechterhaltung der HIV-1 Latenz. In einer ersten Reihe von Experimenten wurde das primäre Screening-Experiment rekapituliert und TRRAP, ein Adaptorprotein, das in Multiprotein Chromatinkomplexen vorkommt und an der epigenetischen Transkriptionsregulation beteiligt ist, wurde erneut als

Treffer bestätigt. Weitere Experimente zielten darauf ab, eine mögliche Rolle von TRRAP in der HIV-1-Latenz zu identifizieren. Dafür wurden J-Lat Zellen verwendet, ein von Jurkat-Zellen abstammendes Latenzmodel, die durch shRNA oder siRNA TRRAP depletiert wurden, gefolgt von Stimulierung mit verschiedenen latenzumkehrenden Wirkstoffen (LRAs), um einen additiven Effekt auf die Latenz zu testen. Trotz intensiver Tests konnte keine eindeutige Beteiligung von TRRAP an HIV-1-Latenz beobachtet werden.

Im zweiten Ansatz wurden Folgetreffer ausgewählt, die durch kommerziell erhältliche chemische Substanzen, inhibiert werden können. Dieser Ansatz wird hier als „Druggability“ bezeichnet. Mehrere Substanzen wurden ausgewählt und auf ihren möglichen Einfluß auf die Latenz allein oder in Kombination mit LRAs getestet. Es wurde festgestellt, dass Auranofin die Umkehrung der Latenz erhöht, wenn es in Kombination mit allen getesteten LRAs, sprich TNFα, Prostratin, SAHA oder Natriumbutyrat, in J-Lat Zellen und in Kombination mit SAHA und Natriumbutyrat in U1 Zellen angewandt wird. Nach der Identifizierung von Auranofin wurden Substanzen, welche dieselben Wirtsfaktoren ansteuern, d.h. PRDX5 und sein übergeordneter Partner TXNRD1, die am Thioredoxin System beteiligt sind, getestet. Hierbei wurde keine Substanz gefunden, die den Effekt von Auranofin identisch rekapitulierte, aber Diminazen wurde identifiziert, die Latenz zu beeinflussen. Am wirksamsten war die Anwendung von Diminazen in Kombination mit TNFα oder Prostratin, der erzielte Effekt war wesentlich höher als der von Auranofin erzielte Effekt, war allerdings Zelllinien spezifisch, da dieser nur in J-Lat aber nicht in U1 Zellen gefunden wurde. Die Bestätigung des vermeintlichen Targets von Auranofin (und Diminazen) durch siRNA-Versuche zeigte einen kleinen Effekt und unterstützt die Vermutung, dass das assoziierte System wirklich das Ziel der Substanz(en) ist. Basierend auf Literaturangaben, beeinflußt Auranofin das Thiol-redoxin Sytem, welches an der Reduktion von reaktive Sauerstoffspezien und oxidierte Proteine beteiligt ist. Die Funktionalität dieses Prozesses ist von entscheidender Wichtigkeit für die Zelle. Diminazen, auf der anderen Seite, beeinträchtigt wohl das Polyamin Gleichgewicht, welches an einer Fülle von Prozessen und Interaktionen beteiligt ist. Ein Ungleichgewicht in der Polyamin Homöostase könnte den zellulären Redox Status beeinflussen. Dies könnte auf eine Verbindung zwischen den beiden Systemen hindeuten. Ob diese Systeme allerdings wirklich miteinander verbunden sind oder nicht, muß experimentell bestätigt werden. Nichtdestotrotz, sind beide Systeme von hoher Bedeutung für die Zelle mit weitreichenden Konsequenzen und somit ist auch ein potentieller Einfluss auf den Status des Provirus wahrscheinlich.

Zusammenfassend läßt sich sagen, daß wir in einem unvoreingenommenen System-basierenden Ansatz zwei Substanzen identifiziert haben, die eine Umkehrung der Latenz in Kombination mit anderen LRAs vermitteln. Wir schlagen vor, beide Systeme, die

Targets von diesen Substanzen sind, genauer zu untersuchen, da dies bis dato noch nicht (intensiv) getestet wurde hinsichtlich eines Einflusses auf HIV-1 Latenz. Das Targeting dieser Systeme könnte helfen das latente Reservoir angreifbar zu machen.

Table of contents

1 Introduction

1.1 HIV - the virus and its life cycle

The human immunodeficiency virus (HIV) is the causative agent of the acquired immunodeficiency syndrome (AIDS) (Weiss, 1993). Since the beginning of the current epidemic in mid- to late 1970s (Greene, 2007), HIV/AIDS caused more than 35 million of deaths. By the end of 2017, over 36.9 million people were infected with HIV (http://aidsinfo.unaids.org/). And despite ongoing efforts in preventing disease transmission, allowing access to medication, financing education and research, HIV still remains one of the major public health issues today.

HIV originated from at least two independent zoonotic transmissions of the simian immunodeficiency virus (SIV) from chimpanzee (SIV_{cpz}) and has diversified into several subtypes and clades (Gao et al., 1999). The HIV-1 M (major) group is the cause of the ongoing epidemic. The other type, HIV-2, has occurred via cross species transmission from SIV infected sooty mangabey monkeys (SIV_{smm}) (Sharp and Hahn, 2011). HIV-2 is geographically confined to western Africa, is less virulent and shows a lower level of transmission upon exposure when compared to HIV-1 (Berry et al., 2002; Popper et al., 2000). HIV-2 will be not further considered in this scientific work.

HIV is member of the *Retroviridae* family and belongs to the genus *Lentivirus*. It is assigned to group VI of the Baltimore classification possessing two copies of a positive-sense single-stranded RNA genome, which replicates via a DNA intermediate. The virus encodes for nine genes: three structural genes *gag* (group specific antigen), *pol* (polymerase, encoding the reverse transcriptase and integrase) and *env* (envelope glycoprotein), two regulatory genes *tat* and *rev*, and four accessory genes *nef*, *vif*, *vpr*, and *vpu* (and *vpx* in case of HIV-2) (Vogt, 1997). A graphical scheme of the viral genome organization is shown in **Figure 1A**.

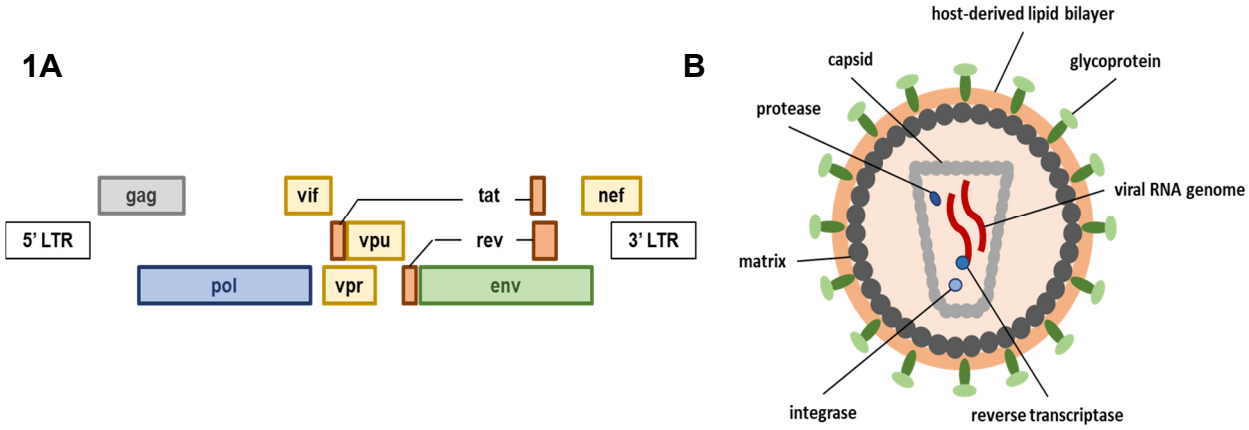

Figure 1: Genomic organization and virus composition of HIV-1. A) Organization of HIV-1 coding regions. **B)** Simplified presentation of HIV-1 particle. env= envelope, gag= group specific antigen, LTR= long terminal repeat, nef= negative regulatory factor, pol= polymerase, tat= transactivator of transcription, vif= viral infectivity factor, vpu= viral protein u, vpr= viral protein r. Adapted from Saliou et al., 2009.

The viral RNA genome is associated with viral proteins and enclosed by a conical shaped capsid made from p24, i.e. product of multiple cleaved Gag protein. A scheme of an HIV-1 virus is shown in **Figure 1B**. The capsid is further surrounded by matrix proteins and enveloped with cell derived lipid bilayer spiked with Env glycoprotein complexes, which mediate the first step in the viral life cycle, i.e. binding. A simplified graphical presentation of the life cycle is shown in **Figure 2**. Binding of the Env derived glycoprotein complex to its target receptor cluster of differentiation 4 (CD4), followed by co-receptor binding to either CC chemokine receptor 5 (CCR5) or CXC chemokine type 4 (CXCR4) (Wilen et al., 2012) leads to a conformational change in the glycoprotein and initiates fusion with the target cell membrane and release of the viral capsid into the cytoplasm. The viral RNA genome is reverse transcribed by the viral reverse transcriptase into double-stranded DNA (Hu and Hughes, 2012), transferred to the nucleus and integrated by the viral integrase into the host genome (Craigie and Bushman, 2012). The integrated virus is termed provirus. Upon integration, HIV-1 exploits the host transcription machinery. The preinitiation complex consisting of nuclear factor kappa-light-chain-enhancer of activated B cells (NFκB), nuclear factor of activated T cells (NFAT), and specificity protein (Sp1) facilitates RNA polymerase II binding to the viral promoter, i.e. 5' LTR, leading to low levels of viral transcripts (Roebuck and Saifuddin, 1999). Those transcripts are enough to form the trans-activator of transcription (Tat). Tat greatly enhances viral transcription and viral full-length mRNA production by binding to the trans-activating response element (TAR), an RNA stem-loop structure, following the recruitment of the positive transcriptional elongation factor (P-TEFb) consisting of cyclin dependent kinase 9 (CDK9) and

cyclin T1 (Nilson and Price, 2011). The viral mRNAs are exported into the cytoplasm, translation leads to viral protein formation, following assembly of immature virions including the packaging of the viral RNA genome and finally release via budding and maturation by viral protease.

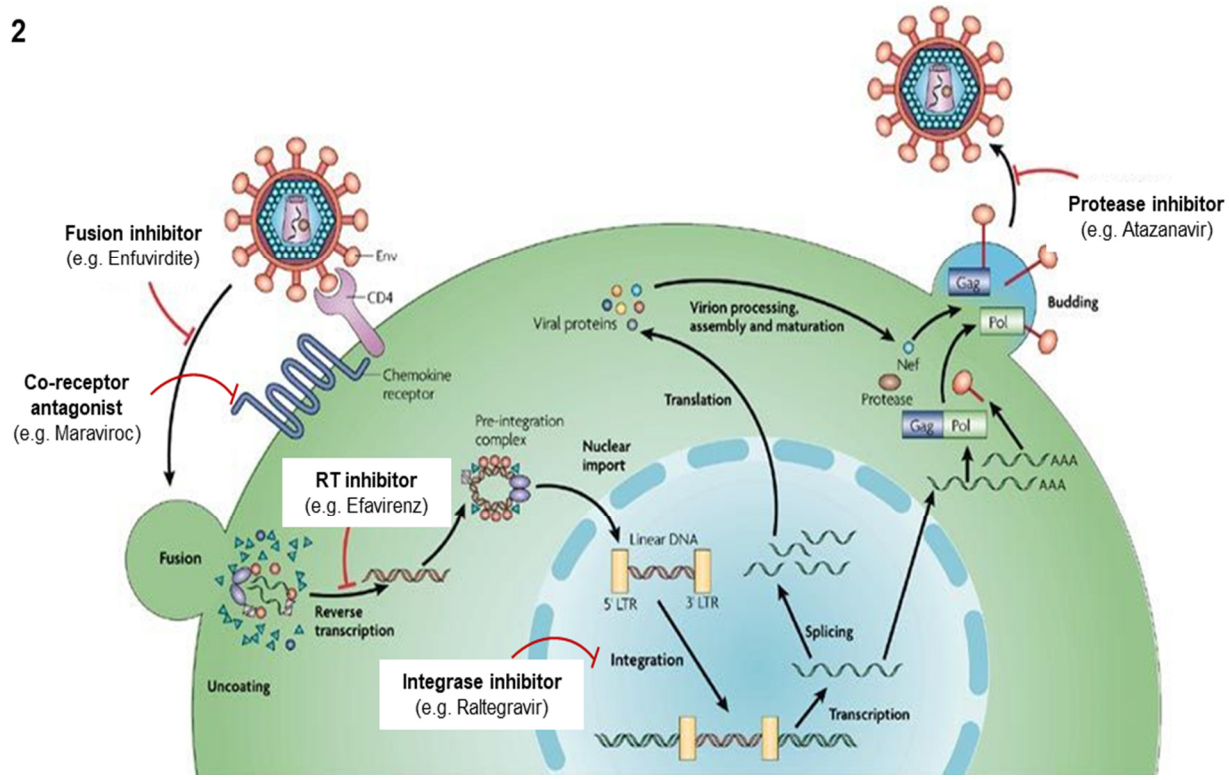

Figure 2: Simplified overview of the HIV-1 viral life cycle. The life cycle of HIV-1 follows defined steps, starting with attachment to the target cell, followed by entry, reverse transcription and integration into the host genome, synthesis of de novo viral proteins and assembly of those into new viral particles and their release. Possibilities to block the viral life cycle are indicated by red blocking lines RT= reverse transciptase. Adapted from Han et al., 2007.

1.2 HIV-1 disease progression and therapy

An untreated HIV-1 infection will progress towards AIDS development within three stages over the course of years and disease progression can be correlated to the viral load and to the counts of HIV-1 target cells, i.e. $CD4^+$ T lymphocyte counts (see **Figure 3**). The first stage, the acute infection phase, develops with flu-like symptoms within the first two to four weeks upon infection. During this time, the virus highly replicates and disseminates throughout the body, and $CD4^+$ T lymphocyte counts decrease drastically. This picture partially reverses, the viral load drops and $CD4^+$ T cell counts slightly recover (Perelson et al., 1997). This marks the beginning of the second phase. The second phase also known as the chronic phase, or asymptomatic phase, can last on average eight years and infected individuals do not show disease symptoms even though the viral load is slowly increasing while $CD4^+$ T cells counts are slowly decreasing. The transition into the final phase, the symptomatic phase, is marked by the onset of diverse physical symptoms. The constant depletion of $CD4^+$ T cells finally leads to an impaired immune system and opportunistic infections emerge. An untreated infected person will die due to the absence of an intact immune system (RKI-Ratgeber - HIV-Infektion/AIDS).

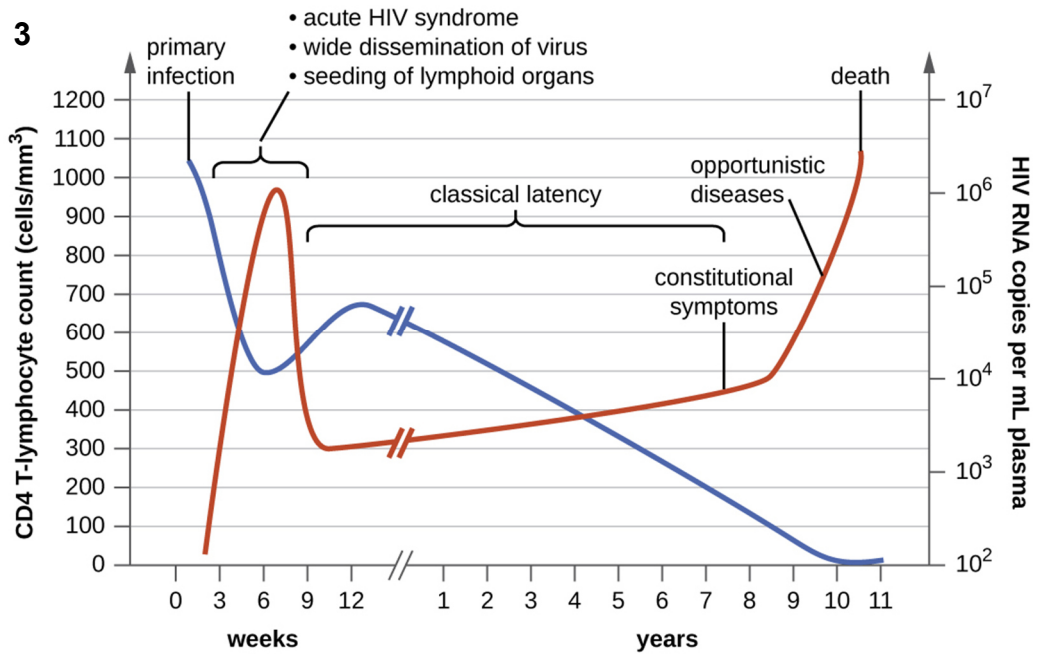

Figure 3: Overview of HIV-1 disease progression. Disease progression is measured by $CD4^+$ T cells counts in blue (left y-axis) and by viral load in red (right y-axis) in dependency of time (Pantaleo et al., 1993).

The first HIV-1 treatment was introduced as monotherapy in the late 1980s using azidothymidine (AZT) to block the reverse transcription step (Mitsuya et al., 1985), which is an essential step in the viral life cycle, but viral resistances quickly developed (Richman, 1990). Since the introduction of the highly active antiretroviral therapy (HAART, also known as the combined antiretroviral therapy (cART)) in 1995, disease progression towards AIDS can be halted (Egger et al., 1997; Palella et al., 1998; Perelson et al., 1997). Current recommendations for initial HAART regimens suggest a combination of three drugs, to effectively block the viral life cycle at various steps and to avoid the occurrence of viral resistances ("WHO | Updated recommendations on first-line and second-line antiretroviral regimens and post-exposure prophylaxis and recommendations on early infant diagnosis of HIV," 2019). HAART adherence will lead to a decline in the viral load below the detection limit of clinical assays and in line with this the likelihood of HIV-1 transmission is drastically reduced (Baeten and Overbaugh, 2003). Further, the life expectancy of an HIV-1 infected person who adheres to therapy is comparable to the life expectancy of an HIV-1 negative person (Wandeler et al., 2016). Despite the treatment advances, HAART is not a cure as it only suppresses ongoing HIV-1 infection. Therefore, adherence to therapy is a prerequisite to keep the viral loads below detection limit, which comes at the price of a daily and lifelong medication intake, to potential toxicities due to the long-term intake and at high expenses. While interruption of HAART will lead to viral rebound, occurrence of viral escape mutants and disease progression (Davey et al., 1999; Wang et al., 2011). This phenomenon of HIV persistence can be explained by the presence of a latent reservoir, i.e. cells harboring an intact provirus without producing viral products. Latently infected cells are not recognized by the immune system due to the absence of viral products and persist within the body for decades (Margolis, 2010). But latency is a reversible process and previously latent cells can be induced to produce and release progeny viruses to fuel new rounds of infection and spread of infection and reseeding of the viral reservoir. Therefore, current HIV research efforts are focusing on the comprehensive understanding of the latent reservoir. It is important to stress that a cure from HIV-1 infection will be only achieved if this reservoir is targeted.

In summary, the crux with HIV-1 infection is that it forms a latent reservoir, a tiny fraction of infected cells, which do not produce new viruses. But they can give rise to new progeny viruses, if latency is reversed and this in turn will start over the infection process. In the following sections the current understanding of latency establishment and reservoir formation are compiled, followed by the different current curing strategies.

1.3 Latency establishment - molecular mechanisms

Successful full-length viral transcription is needed as initial step towards the production of progeny virus and viral spread. Reversely, impairment of viral transcription will support the formation of latency, which can be evoked by several mechanisms and orchestrated from several levels. Up to now, several host factors have been identified to directly or indirectly affect latency formation. The different levels, which can independently but also jointly contribute to latency formation and maintenance, are highlighted below. Nevertheless, it is important to keep in mind, that true latent cells are very rare.

1.3.1 From the viral side - the presence of Tat

From the viral side, the absence of sufficient levels of Tat can be regarded as driver of latency. It was experimentally shown that Tat expression in trans inhibits latency formation (Pearson et al., 2008). Tat is a master regulator of HIV-1 transcription, which exploits the host machinery to efficiently increase viral transcription, if Tat levels exceed its threshold (Das et al., 2011).

1.3.2 Presence of transcription factors

From the cellular side, the absence of key transcription factors as e.g. NFκB p65/p50 heterodimers or NFAT impair initiation of transcription (Kinoshita et al., 1997; Nabel and Baltimore, 1987; Selliah et al., 2006; Yang et al., 1999). Those immediate acting transcription factors are usually kept in their inactive form or are sequestered but can be induced by external stimuli as e.g. by cytokines, growth factors, stress to viral and bacterial infections, without the need to be synthesized (Hiscott et al., 2001). Those transcription factors play a pivotal role in many cellular processes as cell differentiation, proliferation, immune responses and apoptosis. Due to this they are tightly regulated and constant activation of those has been linked to cancer development.

NFκB is kept in the cytoplasm by its interaction with IκB. Upon activation of diverse signaling pathways, IκB is phosphorylated by IκB kinase (IKK) complex, freeing NFκB complex which

translocate into the nucleus and initiates transcription of target genes including the provirus (Thompson et al., 1995). Cylindromatosis (CYLD) is a deubiquitinase, which targets IκB, which in turn prevents phosphorylation of IκB by IKK and therefore inhibits NFκB translocation (Mathis et al., 2015; Sun, 2010). Knockdown of CYLD has been shown to support reversal of latency (Manganaro et al., 2014). CYLD has been identified as hit in the initial screening and will be used as positive control.

1.3.3 Overcoming stalled RNA polymerase

Beyond the need of those positive acting transcription factors as NFκB, also RNA polymerase II (RNA Pol II) proximal-promoter pausing needs to be overcome to allow full-length production of pre-mRNA (Core and Lis, 2008; Zhou et al., 2012). Pausing of RNA Pol II shortly after initiation is an essential step in regulating gene expression. The P-TEFb complex is a key player in releasing this block. P-TEFb modifies the DRB sensitivity factor (DSIF) (Bourgeois et al., 2002), which leads to the displacement of the negative elongation factors (NELF) (Pagano et al., 2014; Wenzel et al., 2008) and stalled RNA pol II is released. Also, HIV-1 Tat is dependent on P-TEFb for full-length proviral mRNA procession. Since P-TEFb is of crucial importance for successful transcription by RNA Pol II, it is not surprising that it is tightly regulated on various levels.

Interestingly, P-TEFb is often found in association with bromodomain-containing protein 4 (BRD4), which supports the recruitment of P-TEFb to genes and their successful transcription (Jang et al., 2005). The bromodomain of BRD4 is an acetyllysine-binding motive and been found to bind acetylated histones (Dey et al., 2003). In the case of HIV-1 transcription, Tat relies and binds P-TEFb complex to achieve full-length viral mRNA procession and is in direct competition with BRD4, as they share the same P-TEFb binding site (Bisgrove et al., 2007). Knockdown of BRD4 or its inhibition by JQ1 has been found to support reactivation of latent HIV (Bisgrove et al., 2007; Li et al., 2013). Also, BRD4 has been identified as hit in the initial screening and will be used as positive control.

1.3.4 Modulation of chromatin

Changes in the chromatin i.e. epigenetic changes evoke another level of latency regulation and can support latency formation and maintenance. The DNA is spooled around nucleosomes, which form the basic building unit of chromatin and consist of DNA wrapped around a histone octamer, composed of each two proteins of H2A, H2B, H3 and H4 (Alberts et al., 2002; Luger et al., 1997). Histones are subjected to a variety of reversible modifications as methylation, acetylation, and phosphorylation among others (Luger and Richmond, 1998). The formation of densely packed chromatin, i.e. the formation of heterochromatin, can render whole regions transcriptionally silent, which can also affect the provirus. Even though it has been shown that HIV-1 preferentially integrates into intragenic regions of actively transcribed genes (Han et al., 2004; Lewinski et al., 2005). Nevertheless, the viral promoter has been found to be associated with two nucleosomes, i.e. Nuc-0 and Nuc-1 (Verdin et al., 1993), which is independent of its integration site. Nuc-1 is being situated around the proviral transcription start site and might impose a block to transcription. Those blocks can be derived from deacetylation of histone tails by a family of enzymes called histone deacetylases (HDACs), which leads to removal of acetyl groups from histone tails and with that to a spatial inaccessibility of transcription factors to the (viral) promoter (Yoshida et al., 2017). The action of HDACs can be reversed by histone acetyltransferase or by compound inhibition of HDACs. Also, histone methylation by histone methyltransferases (HMTs) as for example SUV39H1 (du Chéné et al., 2007), G9a (Imai et al., 2010) or EZH2 (Zhang et al., 2015) has been described to evoke a silencing effect by di- or tri-methylation of lysine residues on histones. Further, EZH2 is also being a partner in forming a repressive complex, which serves as binding platform for other chromatin remodelers and supporting by this heterochromatin formation (Friedman et al., 2011). The modification of histones is a reversible process and can be achieved e.g. by external stimuli which act for example by releasing NFκB heterodimer into the nucleus, which will in turn recruit co-activator complexes with histone acetyltransferase activity, leading to a remodeling of histones e.g. the proviral associated Nuc-1 and accessible DNA (Gerritsen et al., 1997; Perkins et al., 1997; Sheppard et al., 1999).

Further, direct DNA methylation, i.e. the formation of CpG islands, at the transcription start site has been shown to repress viral gene transcription (Blazkova et al., 2009, 2012; Palacios et al., 2012). It shall be noted, that gene transcription is a complex process, which includes the recruitment of many different factors, which in turn either directly or indirectly bind DNA or histones and consequently allow gene transcription. This process is tightly regulated on many different levels.

1.3.5 Proviral integration site and orientation

Another latency driving point is the integration site selection. HIV-1 predominately integrates into intronic regions of actively transcribed genes (Han et al., 2004; Schröder et al., 2002) with a preference for the open chromatin found in the outer shell of the nucleus, i.e. close to the nuclear membrane, and in close connection to nuclear pores (Marini et al., 2015). This is supported by findings showing that the components of the nuclear pore complex influence HIV-1 infection (König et al., 2008). In addition, also the viral integrase influences the choice of integration site, which needs to occur fast due to its short half-life (Manganaro et al., 2010). Further, also the orientation of provirus in relation to the host gene can influence latency establishment, as this may give rise to transcriptional interference. Known processes involve promoter occlusion and collision, which can give rise to read-through products or the absence of products (Greger et al., 1998; Han et al., 2008).

1.3.6 Post-transcriptional regulation

In addition, post-transcriptional regulation may also impact latency formation and maintenance, for example by retention of HIV-1 mRNA within the nucleus, or by regulation via host derived microRNAs (Huang et al., 2007; Van Lint et al., 2013) which can negatively impact on the newly formed viral mRNA or indirectly by affecting mRNAs levels of host factors needed (Ahluwalia et al., 2008).

1.4 HIV-1 target cells and reservoir formation

The target cells of HIV express CD4 as well as one of the chemokine co-receptors, i.e. CCR5 or CXCR4. Those surface receptors are found on $CD4^+$ T cells as well as on monocytes/ macrophages and on other cell types, whereas $CD4^+$ T cells are the major target of HIV-1.

$CD4^+$ T cells form a major part of the adaptive immunity orchestrating a panel of immune responses by e.g. supporting B cells in producing antibodies, activating macrophages, recruiting neutrophils and other immune cells through direct cell interaction or by the release of specific chemokines and cytokines (Zhu and Paul, 2008). They are originating in the bone marrow; transit to the thymus and further to the secondary lymphoid organs. Those cells are termed naïve $CD4^+$ T cells since they have not encountered their specific antigen. Upon exposure to their specific antigen via professional antigen presenting cells (APCs), they become activated and turn into $CD4^+$ T effector cells, which rapidly proliferate and activate other cells of the immune system in order to clear the body from the encountered antigen (Germain, 2002). The mounted immune response is stopped once the antigen is cleared and effector cells undergo apoptosis, while only a few will transition to become memory T cells. Those cells form a big part of the immunological memory and scan the environment for a reencounter with its specific antigen, being now able to mount an immune response faster and more efficient than upon its initial encounter (MacLeod et al., 2010). Since there are a broad range of $CD4^+$ T effector cells, it is not surprising that there is also a heterogeneous population of $CD4^+$ T memory cells, as e.g. T_{CM} (central memory), T_{TM} (transitional memory) and T_{EM} (effector memory) among others (Sallusto et al., 2004). T cell differentiation and memory formation is only incompletely understood but interaction with other cells, antigen exposure time and cytokine environment play a critical function. The differentiation of subtypes was initially based on their cell surface receptor expression, but differentiation based on their effector T cell origin or their tissue migration pattern might help to better classify and to sophistically distinguish the different $CD4^+$ memory T cells (Mahnke et al., 2013). Nevertheless, the shared feature of all memory T cells is their capability to persist in the body for years either by homeostatic proliferation or by low-level antigen-driven proliferation (Chomont et al., 2009). Those cells show lower levels of metabolism and RNA synthesis and are as well decreased in size when compared to effector $CD4^+$ T cells.

The $CD4^+$ T memory cells are the main and best-characterized reservoir for latent HIV-1 infection, which is experimentally supported as progeny virus can be recovered from those cells after stimulation (Chun et al., 1997; Finzi et al., 1997; Wong et al., 1997). This reservoir

is seeded early during infection. Thus, early administration of HAART leads to a reduced and genetically less divergent reservoir but does not inhibit reservoir formation (Chun et al., 1998; Eriksson et al., 2013; Strain et al., 2005).

Whether HIV-1 infects memory $CD4^+$ T cells directly or infects effector $CD4^+$ T cells which transition into memory $CD4^+$ T cells is a matter of ongoing debate. It is generally accepted that effector $CD4^+$ T cells are easily infected by HIV-1, which leads to a productive infection causing the formation and release of new infectious progeny viruses. When those cells become infected, most of them die within a short time due to the viral cytopathic effect or by cytotoxic T lymphocytes (CTL) induced cell death (Wei et al., 1995). The establishment of a latent infection in these cells might strictly depend on the right timing, i.e. the virus needs to infect the effector T cell at a moment when reverse transcription and integration can still happen while the cell is undergoing transition to become a memory T cell, a process which also involves chromatin rearrangement and differential gene expression, which also affects the provirus (Pace et al., 2011). One the other hand, *ex vivo* infection of primary $CD4^+$ memory T cells has been experimentally shown. Even though this process is less efficient, as memory $CD4^+$ T cells possess e.g. lower levels of CCR5 on their cell surface (Pierson et al., 2000) as well as lower dNTP levels (Baldauf et al., 2012; Goldstone et al., 2011) which negatively affects cell entry and reverse transcription. In any case, it shall be noted that latency formation is a rare process and one in one million memory T cells will carry a provirus that can be reactivated (Eriksson et al., 2013). The absence of viral products in latently infected cells renders those cells invisible to the immune system and so far, also no surrogate marker has been identified to allow direct targeting of infected cells. (Of note, CD32a, a member of the Fcγ receptor family, has been proposed as latency marker (Descours et al., 2017) while it could not been reproduced by others (Abdel-Mohsen et al., 2018; Badia et al., 2018)). On the other hand, activation of memory $CD4^+$ T cells, by its cognate antigen, will likely induce proviral transcription.

Of note, most studies on the latent reservoir have been carried out using $CD4^+$ memory T cells isolated from patient blood, as it easy to sample. But it might not capture the complete picture as not all memory cells are circulating as seen for tissue resident memory $CD4^+$ T cells (Wu et al., 2018). Further, HIV-1 positive cells can also be recovered from the lymph nodes, the gut-associated lymphoid tissues and from the central nervous system. Here, a potential influence of the prevalent microenvironment in those tissues cannot be excluded.

In addition, the participation of other cells in supporting viral dissemination as e.g. proposed for dendritic cells, and serving as potential reservoir, as e.g. proposed for macrophages and microglial cells is not fully elucidated but might put an additional level of complexity on understanding HIV-1 persistence.

1.5 Curing HIV-1 - what approaches are considered?

Finding a cure to HIV infection is the holy grail of ongoing research efforts and will only be achieved upon targeting of the latent reservoir. One differentiates between a sterilizing cure and a functional cure. In terms of sterilizing cure, no replication-competent proviruses will be found in a patient, the virus is eradicated from the patient (Xu et al., 2017). This type of cure will be difficult to achieve and even more difficult to prove due to limitations in e.g. the current HIV detection systems. A functional cure will be more likely achieved and can be described as remission, i.e. replication competent proviruses are present in the host, but no viral load can be detected, while HAART is not applied. Current curing efforts can be categorized in mainly four differential approaches (albeit more strategies will likely arise), as are stem cell transplants, genome editing, immune modulation and 'shock and kill', even though the categorization is not clearly defined and different strategies show overlap, share techniques or targets. In the following the main approaches are shortly summarized, but for this scientific work only the 'shock and kill' approach is of importance.

1.5.1 Stem cell transplant

The first person to be considered cured from HIV-1 was Timothy Brown, the so-called Berlin patient, and the achieved cure can be considered a sterilizing one. He received a stem cell transplant after chemotherapy failed to stop his leukemia. The transplant he received was from a donor carrying a homozygous Δ32 mutation in the CCR5 gene, which rendered the newly produced immune cells resistant to HIV-1 infection (Allers et al., 2011; Henrich et al., 2014; Hütter et al., 2009). The same approach was undertaken for the so-called London patient and the Dusseldorf patient, who are now considered patient two and three to be cured (Gupta et al., 2019). Of note, a similar approach has been undertaken for the so-called Boston patients, but resulted in viral rebound after prolonged remission, as the stem cell donors were not carrying the mutation in the CCR5 gene (Henrich et al., 2014). This highlights the importance for CCR5Δ32 mutation in order to block viral entry. Further, while those examples show that an HIV cure is feasible, it needs to be kept in mind that a stem cell therapy approach is dangerous, costly and not broadly practicable as the frequency of an human leukocyte antigen (HLA) matching and homozygous CCR5Δ32 donors is low. Besides this, not every HIV-1 positive patient will develop leukemia, which would justify such drastic and risky treatment.

1.5.2 Genome editing

Another approach investigated, comprises genome editing. Several targets are investigated and recent advances such as usage of CRISPR/Cas technology renders this approach feasible, as it allows the modification of the genome at a defined site. As examples, the knockdown of the CCR5 gene as well as double knockdown of both, CCR5 and CXCR4 genes, are investigated. If the vast majority of target cells were edited, then the cell entry of HIV would be impaired, and no new round of infection could be initiated (Tebas et al., 2014). It is also considered to use hematopoietic stem cells to introduce receptor knockouts; in this case the knockout would be transferred to daughter cells. Another investigated target is the virus itself. Targeting the incoming virus or the provirus by CRISPR/Cas could remove the virus from the host (Panfil et al., 2018). But also, this target is hard to reach, as reservoir cells may stay out of reach for sampling and due to the lack of a marker for latently infected cells, all HIV target cells would need to be edited. This highlights again the need for the identification of a specific latency marker, which would be a milestone in HIV latency research and would tremendously speed up the process of achieving a cure via genome editing (or other strategies). Nevertheless, up to now this technique is not fully developed to allow for highest efficiency by minimal off-target rate.

1.5.3 Immune modulation

Immune modulation aims to sustainably support/prime the immune system in fighting HIV better and more efficient. Examples include the modification of natural killer cells and $CD8^+$ T cells by expressing artificial T-cell receptors (TCR) or chimeric antigen receptors (CAR), which specifically bind to HIV, to enhance recognition and killing of infected cells (Liu et al., 2015). Also, the application of selected broadly neutralizing antibodies against HIV is in development (Kuhlmann et al., 2018; Sok and Burton, 2018). Those antibodies are found in around a quarter of infected individuals and possess the ability to neutralize the virus. The identification of broadly neutralizing will also support therapeutic vaccination research. Major drawback of this strategy is founded in the high mutation rate of the virus. It will be therefore likely that escape viruses will occur, and new rounds of infection can be initiated.

1.5.4 Shock and kill

This strategy comprises two critical steps. During the first step, denoted as ‘shock’, the latent reservoir is purged, i.e. proviral transcription is forced (Archin et al., 2014). Resulting viral products will render reactivated cells visible to the immune system. In the next step, denoted ‘kill’, the immune system will clear those cells. New rounds of viral infection can be inhibited by the administration of HAART. If all replication competent proviruses are purged, followed by subsequent killing, a cure is feasible. This is up to now the most researched category, focusing on the identification of latency reversing agents (LRA) by screening them for their action in different latency cell models. Due to the availability of e.g. compound or host-factor RNA interference (RNAi) libraries and the implementation of high throughput screens, the elucidation of novel LRA candidates is facilitated and accelerated. Several LRAs have been extensively studied as well as tested *in vivo*, but so far none of the tested LRAs could decrease the latent reservoir size nor increase remission time, if HAART was suspended (Lee et al., 2017; Rasmussen and Søgaard, 2018). The discovery of new LRAs (or host factors to be targeted) or the combination of two or more LRAs with distinct mechanistic actions presents a tool to reactivate the complete reservoir. Of note, there is accumulating evidence that the immune mediated killing of reactivated cells might be inefficient (Jones et al., 2014; Shan et al., 2012), this hurdle could be overcome by engineering the immune system (by strategies as immune modulation or others).

LRAs comprise a large set of compounds, with distinct mechanistically actions. Further, they can be categorized in either T cell activating or non-activating compounds (Spivak and Planelles, 2018). It was found that T cell activation would also induce proviral transcription, but also leads to cytokine production and unspecific T cell proliferation (Clutton et al., 2016), which would negatively affect the size of the latent reservoir. An overall immune activation by administration of antiCD3 antibodies and IL-2β *in vivo* was tested, which led to toxic effects in individuals (Kulkosky et al., 2002; Prins et al., 1999). Due to this, an overall activation is generally avoided but some level of T cell activation might be still needed for efficient proviral transcription.

In the following, examples of T cell activating and non-activating LRAs, which were used in this scientific work, will be listed including their proposed mechanisms of action.

1.5.4.1 T cell activating LRAs

One example for a T cell activating LRA is prostratin, which is a non-tumor-promoting phorbol ester naturally occurring in some plants (Gustafson et al., 1992; Zayed et al., 1977). Prostratin evokes its action by mimicking diacylglycerol, which binds to protein kinase C (PKC) family members, i.e. acting as a PKC agonist. This family comprises a large set of threonine/serine kinases (McKernan et al., 2012). Binding of PKC initiates downstream activation of NFκB (Jiang and Dandekar, 2015). NFκB proteins are dimeric transcription factors, which regulate the expression of genes involved in a broad range of biological functions as e.g. innate and adaptive immunity, inflammation and stress response. In the classical NFκB pathway, NFκB proteins are kept inactive by IκB proteins, sequestered in the cytoplasm. The phosphorylation of IκB by PKC, leads subsequently to its proteasomal degradation, released NFκB dimers (p65/p50) translocate to the nucleus and initiate transcription of target genes including the provirus. Constituent NFκB activation has been linked to cancer development (Rayet and Gélinas, 1999).

Another example of a T cell activating LRA is tumor necrosis factor alpha (TNFα). TNFα is an inflammatory cytokine, which regulates a wide range of biological processes. It is mainly produced by monocytes/ macrophages but also by other cells. TNFα evokes its action via TNF receptor engagement, which induces downstream signaling including NFκB activation via IκB phosphorylation (Sedger and McDermott, 2014).

1.5.4.2 Non-activating LRAs

As mentioned, there are also LRAs evoking their effect different from NFκB activation and therefore without overall cell activation. One intensely researched area is the inhibition of histone deacetylases (HDACs). HDACs comprise a group of enzymes, which can be divided in four classes (i.e. class I, II, III, and IV). HDACs catalyze the removal of acetyl groups from histones and other proteins. Acetylation and deacetylation are one mean of epigenetic control of gene expression. Blocking those enzymes by HDAC inhibitors (HDACi), leads to hyperacetylation of histones and to an ‘open’ chromatin conformation, rendering DNA accessible to transcription factors (Dokmanovic et al., 2007). Suberanilohydroxamic acid (SAHA; also known as vorinostat) is one prominent member of HDACi, as it blocks HDAC classes I, II, and IV (Xu et al., 2007) and is tested as an anti-cancer agent (Marks, 2007). Further, also sodium butyrate is an example of an HDACi acting on class I enzymes (Shirakawa et al., 2013). Sodium butyrate is a fatty acid derivative that can be found in some foods and is produced by bacteria from digestion of fibers in the large intestine (Li et al., 2012).

Another non-activating LRA is the recently identified JQ1. This compound inhibits bromodomain containing proteins, as e.g. bromodomain-containing protein 4 (BRD4). The inhibition of BRD4 leads to release of P-TEFb. Freed P-TEFb is hijacked by Tat and leads to increased proviral transcription. JQ1 has been shown to reverse latency when used in combination with e.g. prostratin in latency cell models (Li et al., 2013; Zhu et al., 2012).

1.6 How to measure the latent reservoir

In order to evaluate the effectiveness of curing strategies, the size of the latent reservoir and changes within need to be exactly determined. Up until now, the quantitative viral outgrowth assay (qVOA) is used as the gold standard to determine the size of the latent reservoir (Finzi et al., 1997, 1999). For this, resting $CD4^+$ T cells are isolated from HAART-treated HIV-1 positive donor blood, plated in a limiting dilution series and are fully activated by phytohaemagglutinin (PHA) and co-cultured with allogenic $CD8^+$ depleted peripheral blood mononuclear cells (PBMCs) from an HIV-1 negative donor. Reactivation of the latent reservoir followed by release of progeny virus and infection of bystander cells allows the amplification of virus and with this signal intensity. The detection is performed on culture supernatant by using standard p24 ELISA and the frequency of latently infected cells is calculated as infectious units per million cells (IUPM) (Norton et al., 2017). The advantage of this method is that it detects newly produced virus derived from reactivated reservoir cells, but it is time consuming, laborious and large quantities of cells (HIV-1 positive and allogenic PBMCs) are needed. Therefore, modifications have been implied to enhance the sensitivity and reproducibility of read-out and/or reducing the assay time by using e.g. HIV-1 permissive cell lines instead of allogenic PBMCs, ultra-sensitive p24 ELISA, or qPCR for viral RNA detection in the supernatant. Despite technical advances, it has been shown that not all replication-competent proviruses are reactivated upon stimulation and that multiple stimulations might be needed (Ho et al., 2013). Therefore, the qVOA is likely to underestimate the size of the latent reservoir.

PCR-based approaches can also be used to determine the size of the latent reservoir. One prominent example is the Alu-PCR performed on genomic DNA (derived from HIV-1 positive PBMCs or $CD4^+$ T cells). This approach uses primers which bind within a conserved region of the HIV-1 genome e.g. *gag* gene and within Alu elements of the host genome. Resulting fragments will be of varying size, depending on the distance of the provirus to the Alu element. A second (nested) PCR will be performed on top to amplify a fragment from the HIV-1 LTR. A standard containing a mix of cells with different HIV-1 integration sites is taken along to allow the calculation of the reservoir size. There are also other PCR-based approaches described, which e.g. directly amplify a fragment from the HIV-1 provirus with primers binding in highly conserved regions as e.g. LTR and *gag* gene, circumventing the need for a second PCR (Malnati et al., 2008). The general advantage of PCR-based approaches is that those are much faster in comparison to cell-culture based approaches (Henrich et al., 2017). The major drawback of PCR approaches is, however, that they cannot discriminate between replication-competent and replication-incompetent proviruses. The proportion of defective proviruses is

believed to be as high as 90% (Bruner et al., 2016). Due to this the reservoir is easily overestimated, and also a reduction in reservoir size will be not easily discriminated. Of note, there is a recent report on an advanced droplet digital PCR approach which allows the discrimination of intact and defective proviruses and their precise quantification (Bruner et al., 2019). The general implementation of this technique would allow to determine the reservoir size and to monitor it over time but requires designated equipment.

Besides measuring the reservoir size, there are also various possibilities to measure reactivation of latent provirus. Measuring of e.g. multiple spliced transcripts, full-length viral mRNA, presence of Tat protein or other viral products as an indication for reactivation, but results need to be carefully evaluated as not all measured products might lead to the production of infectious progeny virus.

1.7 Latency cell models

There have been many different latency models established, which aid to gain a more comprehensive understanding in latency formation and maintenance as well as to facilitate the discovery of host factors and/or compounds which can influence latency. Those latency models can be divided in cell line derived models, primary cell models and *in vivo* models. In the following the different models will be shortly summarized, with emphasis on cell line latency models utilized in this work.

1.7.1 Cell line derived latency models

Cell line derived latency models are easily cultivated, multiplied to high numbers and are not limited in their life span. Those cells are produced by transducing cell lines of interest with a commonly used HIV-1 laboratory strain, i.e. viruses that are well characterized and can be replication competent and may carry an additional reporter gene to allow facilitated detection. Those cell line derived latency models are a useful tool for a first-round evaluation of host targets or compounds for their potential effect to induce viral transcription.

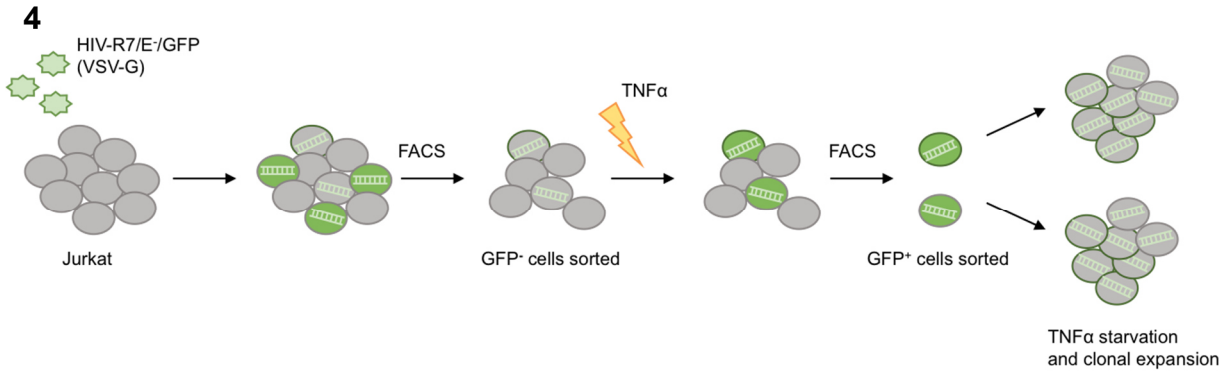

Figure 4: Graphical presentation of J-Lat cell production. Jurkat cells were infected with an HIV-1 derived reporter virus (*env* deleted by frameshift mutation, *nef* replaced by *gfp*, VSV-G pseudotyped). Four days post infection cells were sorted for GFP negative cells. Those cells were stimulated with TNFα for 24h, followed by sorting of GFP positive cells and single cell expansion. Resulting cells are different J-Lat clones, which do not show GFP expression on their own but upon stimulation. Scheme according to description by Jordan, Bisgrove, & Verdin, 2003.

The so-called J-Lat cells were derived from the parental Jurkat cells. The Jurkat cell line was established from peripheral blood from a male patient with acute T cell leukemia (Weiss et al., 1984). For the generation of J-Lat cells, the parental cells were transduced with an HIV-1 Δ*env* Δ*nef* GFP-reporter construct. GFP negative cells were sorted followed by activation with TNFα and sorted for GFP positive cells. Single cells were expanded and GFP expression faded without stimulation. Several clones exist, which vary in their degree to respond to different stimuli, as measured by GFP induction as a mean of proviral activation (Jordan et al., 2003). A graphical overview on J-Lat cell production is shown in **Figure 4**.

Another latency cell model tested are U1 cells, derived from the promonocytic U937 cell line. U1 cells were one of the first latency cell models established (Folks et al., 1987). This model possesses two copies of HIV-1 provirus, produces very low levels of viral mRNA under normal culture conditions and possesses mutations for the *tat* gene in both integrates (Emiliani et al., 1998). Proviral transcription can be efficiently induced by several LRAs, whereas latency is likely maintained by the mutated form of Tat (Perkins et al., 2008).

1.7.2 Primary latency models

There are several primary latency cell systems available, which are superior over cell lines for the common concerns and regarding the diversity of integration sites in comparison to clonally expanded latency cell lines. Primary latency cell models employ $CD4^+$ T cells (either with naïve or memory phenotype) isolated from uninfected PBMCs. Naïve $CD4^+$ T cells are activated, followed by infection with a modified or wild type HIV-1 strain, and allowed to return to a resting state. In order to promote the survival of transduced $CD4^+$ T cells the cultivation with feeder cells (Sahu et al., 2006), as well as the transduction with anti-apoptotic genes (Yang et al., 2009) has been proposed. Other models directly infect resting $CD4^+$ T cells and boost the number of infected cell by e.g. spin occulation (Swiggard et al., 2005) or the transduction with host factor antagonists' known to pose a block to the viral life cycle (Coiras et al., 2016). Even though primary derived latency models might recapitulate the HIV-1 reservoir found *in vivo* more closely, they are labor extensive, tedious and hardly result in enough latently infected cells to allow broad range screening of LRAs. In addition, also primary latency models of non-$CD4^+$ T cell origin exist. An overview of the different primary models is summarized by Bonczkowski et al., 2016.

1.7.3 *In vivo* latency models

In vivo models, as non-human primate (NHP) models or mouse models replenished with a human immune system, have been developed. The advantage of *in vivo* models is that they allow studying of a whole organisms and/or organs and with that the influence of different cell types and the microenvironment on pathogenesis, latency formation and reversal (Estes et al., 2018). Disadvantages of non-human primate models include the usage of SIV for infection, and most SIV strains are resistant to non-nucleoside reverse transcriptase inhibitors and further possess the accessory protein Vpx, which supports infection of e.g. resting cells and macrophages (Evans and Silvestri, 2013). For humanized mouse models it needs to be considered that engraftment and colonization of human cells takes long and that the size of the model limits the number of cells, which can be subsequently tested (Brooks et al., 2003; Policicchio et al., 2016).

1.8 High throughput screenings - a method to identify host factors involved in latency

The elucidation of novel host factors involved in latency can be challenging, but is indispensable for developing strategies, for instance, to reduce and/or to eradicate HIV reservoirs in patients. The implementation of high throughput screening (HTS) methods can propel the identification of novel factors. HTS are also commonly used in other research areas, for instance to identify novel cancer therapeutics. Prerequisite for performing an HTS are dedicated laboratory equipment like pipetting robotics. The experiment itself is run in an automated fashion with a throughput of thousands and more test substances, as e.g. compounds or biologicals, and therefore referred to as high throughput (Inglese and Auld, 2008). At first, the experimental question, which is supposed to be answered, needs to be formulated. The choice of an adequate test system, e.g. the cell line, needs to be carefully chosen. This is followed by the choice of the library, e.g. compound or RNAi (RNA interference) library. Those libraries are commercially available, and effort is put in the verification of target specificity. This is especially of importance for an RNAi approach, in which host factors are targeted by shRNA or siRNA, generating a stable or transient knockdown on mRNA level. RNAi technologies are known for their potential off-target effects, which need to be considered when interpreting the results (Campeau and Gobeil, 2011). Further, also the implementation of suitable controls is of crucial importance, as those will allow the assessment of the assay performance and data reliability. The assay is typically run in 96, 384 or higher well plate formats with an appropriate plate design to avoid systematic errors e.g. including the same controls for each plate but at varying position. The read-out is usually conducted with automated microscopes or plate readers measuring luciferase, or changes in absorbance, among others. In a last step, the generated raw data need to be analyzed with a suitable test to identify primary hits. Special attention needs to be given to the included negative controls, as they will determine the background signal, which is optimally not subject to high variation. High variation in background noise could easily mask real hits. The statistical test chosen for data analysis is dependent on the experimental design and Z-score or signal-to-noise/background have been proposed to discriminate hits (Caraus et al., 2015). Identified primary hits need to be further validated for example by (partial) repetition of the HTS, by a different approach or by a different test substance, e.g. shRNA instead of siRNA.

In summary, HTS are a powerful tool, which allow the identification of cellular factors, including also unexpected ones, in a rapid fashion. The conduction of an HTS needs special equipment and trained staff. The usage of proper controls, repeated measurements and an appropriate

statistical test for data evaluation can increase the robustness of an HTS. The identified primary hits need to be further validated either by repetition or by a different approach. This scientific work uses the results of a genome-wide siRNA screen (screening approach detailed in section 3.1, identified primary hits **Table S1**, Appendix) for the validation of host factors involved in HIV-1 latency.

1.9 Aim

The present study aims at the identification of host factors or compounds, which can support the reactivation of silent provirus as a first step in the 'shock and kill' approach. Starting point for this work are the primary hits derived from a genome-wide siRNA screen for host factors affecting transcription and (supposedly latency) of HIV-1 in HEK293T cells (detailed in **Figure 5**, primary hits identified **Table S1**, Appendix). Around 700 potential primary hits were identified, and some of those selected for follow-up experiments and validation. Two differential approaches will be pursued: I) identification of primary hits involved in chromatin binding/modification and testing whether these hits influence latency reversal alone or in combination with other known LRAs (TNFα, prostratin, SAHA, sodium butyrate) and II) identification of compounds that target primary hits (here referred to as druggability) and either reverse latency on their own or in combination with other known LRAs. As initial test systems HIV-1-infected HEK293T, J-Lat clones and U1 cell models are used to test for a potential effect upon host factor silencing or compound application. In a final setting, primary cells from HIV-1 positive patients on long-term HAART are tested for the reversal of latency upon compound application.

2 Materials and Methods

2.1 Materials

2.1.1 Plasmids, siRNAs, Oligonucleotides

2.1.1.1 Plasmids

Plasmids	Supplier	Reference
GIPZ CYLD shRNA_684	kind gift of L.Mangaro	RHS4430-200203337
GIPZ CYLD shRNA_685	kind gift of L.Mangaro	RHS4430-200306163
GIPZ CYLD shRNA_686	kind gift of L.Mangaro	RHS4430-200173983
GIPZ CYLD shRNA_687	kind gift of L.Mangaro	RHS4430-200303048
GIPZ CYLD shRNA_688	kind gift of L.Mangaro	RMM4431-200333126
GIPZ CYLD shRNA_689	kind gift of L.Mangaro	RHS4430-200206310
GIPZ non-silencing control	kind gift of K.Olivieri	RHS4346
pMD2.G (envelope expressing plasmid)	Addgene	#12259
psPAX2 (lentiviral packaging plasmid)	Addgene	#12260
TRIPZ BRD4 shRNA_004	kind gift of K.Olivieri	RHS4696-201896257
TRIPZ BRD4 shRNA_484	kind gift of K.Olivieri	RHS4696-201905323
TRIPZ BRD4 shRNA_487	kind gift of K.Olivieri	RHS4696-201906445
TRIPZ empty vector control	Dharmacon, Inc., Lafayette, US	RHS4750
TRIPZ TRRAP shRNA_538	Dharmacon, Inc., Lafayette, US	RHS4696-200704208
TRIPZ TRRAP shRNA_540	Dharmacon, Inc., Lafayette, US	RHS4696-200706835
TRIPZ TRRAP shRNA_543	Dharmacon, Inc., Lafayette, US	RHS4696-200700889
TRIPZ TRRAP shRNA_718	Dharmacon, Inc., Lafayette, US	RHS4696-200761563
TRIPZ TRRAP shRNA_720	Dharmacon, Inc., Lafayette, US	RHS4696-200766616
TRIPZ TRRAP shRNA_721	Dharmacon, Inc., Lafayette, US	RHS4696-200759422

2.1.1.2 Oligonucleotides

Oligonucleotide	Sequence (5' -> 3')	Application
ASXL3 fw	TTGCTCCCAGAAGTGGATAG	RT-qPCR
ASXL3 rev	CGTTGTTTGGTCCAGTAGTG	RT-qPCR
BRD4 fw	CTCAGAGTGGTGCTCAAGAC	RT-qPCR
BRD4 rev	AAGCGCTTCTTTATTGTTCC	RT-qPCR
CBX6 fw	AGGGAGCGTGAGCTGTATGG	RT-qPCR
CBX6 rev	GCTTCACCTTGCGGTTGATG	RT-qPCR
CCR5 fw	ATGATTCCTGGGAGAGACGC	qPCR
CCR5 probe	VIC-AACACAGCCACCACCCAAGTGATCA	qPCR
CCR5 rev	AGCCAGGACGGTCACCTT	qPCR

Oligonucleotide	Sequence (5' -> 3')	Application
CXXC1 fw	CAACGAGGGTGACAGTGATG	RT-qPCR
CXXC1 rev	CATTGCGCTCCTGCTCAAAC	RT-qPCR
CYLD fw	GAGAGTGTGACGCAGGAAAG	RT-qPCR
CYLD rev	GTGGTGAAGAACGGTCAAAG	RT-qPCR
GAG fw	GACGCTCTCGCACCCATCTC	RT-qPCR
GAG rev	CTGAAGCGCGCACGGCAA	RT-qPCR
GFP fw	CCACAACGTCTATATCATGGC	RT-qPCR
GFP rev	GATGTTGTGGCGGATCTTGA	RT-qPCR
HIV-1 M group fw	TACTGACGCTCTCGCACC	qPCR
HIV-1 M group probe	FAM-CTCTCTCCTTCTAGCCTC	qPCR
HIV-1 M group rev	TCTCGACGCAGGACTCG	qCR
KAT6B fw	AACGCGCTGTGAATAATGGG	RT-qPCR
KAT6B rev	TACAGGCACTGCATGTCTTG	RT-qPCR
MSH6 fw	ACCAAGAAGGGCTGTAAACG	RT-qPCR
MSH6 rev	ACAGAATTACTGGGCGACAC	RT-qPCR
P1 fw	GCGCTCTAGACGTATTACCGCCATGC	PCR
P2 rev	CTCCTTGATCAGCTCGCTCATGGTGGCAGATCCTCTAGTAGAG	PCR
P3 fw	GCAAACTGGGGCACAGATAATGTACAAGTAGCGGCCGC	PCR
P4 rev	GCGCCTCGAGCCTTCTGTTGGGTTAAC	PCR
P5 fw	CTCTACTAGAGGATCTGCCACCATGGCGAGCTGATCAAGGAG	PCR
P6 rev	GCGGCCGCTACTTGTACATTATCTGTGCCCCAGTTTGC	PCR
P7 seq	CGGCCGCATTAGTCTTCCAATTG	sequencing
PRDX5 fw	GGGAATCGACGTCTCAAGAG	RT-qPCR
PRDX5 rev	GGAGGGGTGGAGGAAGTAAT	RT-qPCR
RPL13A fw	CCTGGAGGAGAAGAGGAAAGAGA	RT-qPCR
RPL13A rev	TTGAGGACCTCTGTGTATTTGTCAA	RT-qPCR
RPS11 fw	GCCGAGACTATCTGCACTAC	RT-qPCR
RPS11 rev	ATGTCCAGCCTCAGAACTTC	RT-qPCR
SETD3 fw	CTGCGCTAGGGGAAGC	RT-qPCR
SETD3 rev	TCACTGGTCAGGTTCAAGAT	RT-qPCR
SMYD2 fw	AGCAAGGATTCTGGCCAAAC	RT-qPCR
SMYD2 rev	TCCTCTCCCGGCTTGATTTC	RT-qPCR
TRRAP fw	AGGAGCGACGGAAACGAAA	RT-qPCR
TRRAP rev	CCTCAAACTGACAGAATGGAGACA	RT-qPCR
TXNRD1 fw	GTTGGAGCATCCTATGTCGC	RT-qPCR
TXNRD1 rev	ATGCCATGTTCTTCCATGTGT	RT-qPCR
TXNRD2 fw	TCCACCCTAGGTCTGAAGG	RT-qPCR
TXNRD2 rev	ACCACCAGGAGATCATAGTC	RT-qPCR
USP22 fw	GCGAGGGCAACGTGGTAAAC	RT-qPCR
USP22 rev	TGCTGGAGGCCATGAAAGGG	RT-qPCR

All oligonucleotides were purchased from Eurofins MWG Operon, Ebersberg, Germany. fw= forward, seq= sequencing, rev=reverse

2.1.1.3 siRNAs

Oligonucleotide	Sequence	Supplier	Reference
all star	proprietary	Qiagen, Hilden, Germany	SI03650318
ASXL3 #1	UCAGAAGGCUCUAGAAAUA	Dharmacon, Inc., Lafayette, US	D-023422-01
ASXL3 #2	CCAAUUAGCUGCUCAGAAA	Dharmacon, Inc., Lafayette, US	D-023422-02
ASXL3 #3	GGACACAGCCAGCCAUUUA	Dharmacon, Inc., Lafayette, US	D-023422-03
ASXL3 #4	AAACUGAACAUGCCAACUA	Dharmacon, Inc., Lafayette, US	D-023422-04
CBX6 #1	GAAAGGGACGCAUCGAGUA	Dharmacon, Inc., Lafayette, US	D-009555-01
CBX6 #2	ACACAGAUCCGCCACAUGA	Dharmacon, Inc., Lafayette, US	D-009555-02
CBX6 #3	GGCCGAAUCCAUCAUCAAA	Dharmacon, Inc., Lafayette, US	D-009555-03
CBX6 #4	GAUGUGCAUUUCUCUGUCA	Dharmacon, Inc., Lafayette, US	D-009555-04
CXXC1 #1	ACACAGACCUGCAGAUCUU	Dharmacon, Inc., Lafayette, US	D-008545-01
CXXC1 #2	GGAAAUGGAACGCCGAUUC	Dharmacon, Inc., Lafayette, US	D-008545-02
CXXC1 #3	CAGCCCAGCUCCAAGUAUU	Dharmacon, Inc., Lafayette, US	D-008545-03
CXXC1 #4	CCAACAAGAUCCGGCAGAA	Dharmacon, Inc., Lafayette, US	D-008545-04
Hs_CYLD #2	AAGGGTAGAACCTTTGCTAAA	Qiagen, Hilden, Germany	SI00110082
Hs_CYLD #3	AAAGAACGATGTAGAATATTA	Qiagen, Hilden, Germany	SI00110089
Hs_CYLD #4	AAGGTTCATCCAGTCATAATA	Qiagen, Hilden, Germany	SI00110096
Hs_CYLD #5	CACCAAGATGCCCAATACCAA	Qiagen, Hilden, Germany	SI03059649
Hs_PRDX5 #1	CAGCCAGGAGGCGGAGTGGAA	Qiagen, Hilden, Germany	SI00096971
Hs_PRDX5 #2	CACCTGCAGCCTGGCACCCAA	Qiagen, Hilden, Germany	SI02638888
Hs_PRDX5 #5	TGGGAAGGAGACAGACTTATT	Qiagen, Hilden, Germany	SI03120712
Hs_PRDX5 #7	TGGGCCAGATTACTTCCTCCA	Qiagen, Hilden, Germany	SI05113248
Hs_TRRAP #1	CTGGCGCACATTATCGCCAAA	Qiagen, Hilden, Germany	SI00052591
Hs_TRRAP #3	CAGCACCTTTGTAACAAGTGTA	Qiagen, Hilden, Germany	SI00052598
Hs_TRRAP #3	AAGATTCGACAGCAAGTTAAA	Qiagen, Hilden, Germany	SI00052584
Hs_TRRAP #8	TTCCTGGTAGTTTGCGTGTAA	Qiagen, Hilden, Germany	SI05092605
Hs_TXNRD1 #1	CTGCAAGACTCTCGAAATTAT	Qiagen, Hilden, Germany	SI00050876
Hs_TXNRD1 #2	TGGCATCAAGTTTATAAGACA	Qiagen, Hilden, Germany	SI00050883
Hs_TXNRD1 #3	CCGACTCAGAGTAGTAGCTCA	Qiagen, Hilden, Germany	SI00050890
Hs_TXNRD1 #4	TGCCTGGCATTTGGTAGTATA	Qiagen, Hilden, Germany	SI00050897
Hs_TXNRD2 #1	ACGGTTTGCGGCGTTGCCAAA	Qiagen, Hilden, Germany	SI03090038
Hs_TXNRD2 #3	AACGCAGGCGAAGTTACTCAA	Qiagen, Hilden, Germany	SI03040527
Hs_TXNRD2 #5	ACCGTGGGTATCCATCCCACA	Qiagen, Hilden, Germany	SI00088494
Hs_TXNRD2 #6	CTCCGCGGCTTCGACCAGCAA	Qiagen, Hilden, Germany	SI00088480
KAT6B #1	GAACAUGGCUGCAUCAAAU	Dharmacon, Inc., Lafayette, US	D-019563-01
KAT6B #2	GCAGUUAACUAAUACACUU	Dharmacon, Inc., Lafayette, US	D-019563-02

Oligonucleotide	Sequence	Supplier	Reference
KAT6B #3	GAGGUGAAAUUAUAGACUU	Dharmacon, Inc., Lafayette, US	D-019563-03
KAT6B #4	GCAUAUUGGAAGAGCGUCA	Dharmacon, Inc., Lafayette, US	D-019563-17
Luciferase GL2	proprietary	Dharmacon, Inc., Lafayette, US	D-001100-01-20
Luciferase GL3	proprietary	Dharmacon, Inc., Lafayette, US	D-001400-01-20
MSH6 #1	GUAGAAAGAUGGCACAUAU	Dharmacon, Inc., Lafayette, US	D-019287-01
MSH6 #2	CGAAGUAGCCGCCAAAUAA	Dharmacon, Inc., Lafayette, US	D-019287-02
MSH6 #3	GAACAGAGCCUCCUGGAAU	Dharmacon, Inc., Lafayette, US	D-019287-03
MSH6 #4	GCUCUGAUGUGGAAUUUAA	Dharmacon, Inc., Lafayette, US	D-019287-04
negative con.	proprietary	Qiagen, Hilden, Germany	SI03650325
non-targeting #1	proprietary	Dharmacon, Inc., Lafayette, US	D-001210-01
non-targeting #3	proprietary	Dharmacon, Inc., Lafayette, US	D-001210-03
RPS27a	AAGCTGGAAGATGGACGTACT	Qiagen, Hilden, Germany	Custom siRNA
scramble 403	AAGGCCGTATCGTAATACTTC	Qiagen, Hilden, Germany	Custom siRNA
scramble 5701	AAGCCGCTTAGTAGTCTCGTA	Qiagen, Hilden, Germany	Custom siRNA
scramble 6105	AAGTAAGCTCGTGCGACGTAT	Qiagen, Hilden, Germany	Custom siRNA
scramble 984	AAGTAGCGAGTAATAGCCGCT	Qiagen, Hilden, Germany	Custom siRNA
scramble177	AAGGTAATTGCGCGTGCAACT	Qiagen, Hilden, Germany	Custom siRNA
scramble1777	AAGCGTTCGTCCTATGATCGA	Qiagen, Hilden, Germany	Custom siRNA
SETD3 #1	AAACACAGCUCGACAGUAC	Dharmacon, Inc., Lafayette, US	D-014808-01
SETD3 #2	GGUAAGAAGAGUCGAGUAA	Dharmacon, Inc., Lafayette, US	D-014808-02
SETD3 #3	CCAACAAACUACCCUUGAA	Dharmacon, Inc., Lafayette, US	D-014808-03
SETD3 #4	CCACACAAGCUAUACAUGA	Dharmacon, Inc., Lafayette, US	D-014808-04
SMYD2 #1	GCAAAGAUCAUCCAUAUAU	Dharmacon, Inc., Lafayette, US	D-020291-01
SMYD2 #2	GAAAUGACCGGUUAAGAGA	Dharmacon, Inc., Lafayette, US	D-020291-02
SMYD2 #3	GACAGUAACGUGUACAUGU	Dharmacon, Inc., Lafayette, US	D-020291-03
SMYD2 #4	GCACGCAACGUCAUUGAAG	Dharmacon, Inc., Lafayette, US	D-020291-04
TRRAP #1	GGACUUAACUGGAGAGGUU	Dharmacon, Inc., Lafayette, US	D-005394-01
TRRAP #2	GAAAGGAGCUUCUGAUUGC	Dharmacon, Inc., Lafayette, US	D-005394-02
TRRAP #3	CAAUGUAGCUCUGGAUAUA	Dharmacon, Inc., Lafayette, US	D-005394-03
TRRAP #4	CCUGGUAGUUUGCGUGUAA	Dharmacon, Inc., Lafayette, US	D-005394-19
USP22 #1	GGAGAAAGAUCACCUCGAA	Dharmacon, Inc., Lafayette, US	D-006072-01
USP22 #2	CAAAGCAGCUCACUAUGAA	Dharmacon, Inc., Lafayette, US	D-006072-02

Oligonucleotide	Sequence	Supplier	Reference
USP22 #3	GGAAGAUCACCACGUAUGU	Dharmacon, Inc., Lafayette, US	D-006072-04
USP22 #4	CCUUUAGUCUCAAGAGCGA	Dharmacon, Inc., Lafayette, US	D-006072-17

2.1.2 Antibodies

Antibody	Conju-gate	Species, Clonality	Appli-cation	Dilution	Supplier	Refer-ence
antiCD28	-	mouse, mc	cell activ.	2µg/ml	Miltenyi Biotec, Bergisch Gladbach, Germany	130-093-375
antiCD3	-	mouse, mc	cell activ.	2µg/ml	Miltenyi Biotec, Bergisch Gladbach, Germany	130-093-387
antiGAPDH	-	rabbit, mc	WB	1: 5,000	Cell Signaling Technology, Inc., Danvers, US	#2118
anti p24 (AG3.0)	-	mouse, mc	WB	1:500	kind gift from Dr. S. Norley	-
antiPRDX5	-	rabbit, pc	WB	1:1,000	Thermo Fisher Scientific Inc., Waltham, US	PA5-79864
antiTRRAP	-	rabbit, pc	WB	1:1,000	Cell Signaling Technology, Inc., Danvers, US	#3966
antiTubulin	-	mouse, mc	WB	1:3,000	Sigma Aldrich Corporation, St.Louis, US	T4026
antiTXNRD1	-	rabbit, mc	WB	1:1,000	Cell Signaling Technology, Inc., Danvers, US	#15140
antiTXNRD2	-	mouse, mc	WB	1:1,000	Cell Signaling Technology, Inc., Danvers, US	#12029
antiCD4	FITC	mouse, mc	FC	1:20	BioLegend®, San Diego, US	317407
antiCD25	PE	mouse, mc	cell iso., FC	1:11	Miltenyi Biotec, Bergisch Gladbach, Germany	130-091-024
antiCD69	PE	mouse, mc	cell iso., FC	1:11	Miltenyi Biotec, Bergisch Gladbach, Germany	130-092-160
antiHLA-DR	PE	mouse, mc	cell iso., FC	1:11	Miltenyi Biotec, Bergisch Gladbach, Germany	130-095-298
anti mouse IgG	HRP	goat, pc	WB	1:10,000	Cell Signaling Technology, Inc., Danvers, US	#7076
anti rabbit IgG	HRP	goat, pc	WB	1:10,000	Cell Signaling Technology, Inc., Danvers, US	#7074
anti rabbit IgG	HRP	goat, pc	ELISA	1:100,000	Jackson ImmunoResearch Ltd., Ely, UK	111-035-045

activ.= activation, ELISA= enzyme-linked immuno assay, FC= flow cytometry, FITC= fluorescein isothiocyanate, HRP= horseradish peroxidase, iso.= isolation, mc= monoclonal, pc= polyclonal, PE= phycoerythrin, WB= Western blot

2.1.3 Cell lines and bacterial strains

2.1.3.1 Cell lines

Cell line	Origin	Properties	RRID	Reference
HEK293T	human embryonic kidney	adherent cells	CVCL_0063	DuBridge et al., 1987
HEK293T/17	human embryonic kidney, clone 17	adherent cells	CVCL_1926	Pear, Nolan, Scott, & Baltimore, 1993
U1 HIV-1 infected U937 cell	human leukemic monocyte lymphoma	suspension cells, express show minimal constitutive expression of virus	CVCL_M769	Folks et al., 1987
J-Lat 8.4 HIV-1 (GFP^+, E^-) Jurkat cell	T acute lymphoblastic leukemia	suspension cells, upon stimulation express incomplete viral particles, possess *gfp* in place of *nef*	CVCL_8284	Jordan et al., 2003
J-Lat 6.3 HIV-1 (GFP^+, E^-) Jurkat cell	T acute lymphoblastic leukemia	suspension cells, upon stimulation express incomplete viral particles, possess *gfp* in place of *nef*	CVCL_8280	Jordan et al., 2003

2.1.3.2 Bacterial strains

Bacteria	Properties and genotype	Supplier
MAX Efficiency™ DH5α™ Competent Cells	F– Φ80lacZΔM15 Δ(lacZYA-argF) U169 recA1 endA1 hsdR17 (rk–, mk+) phoA supE44 λ– thi-1 gyrA96 relA1	Thermo Fisher Scientific Inc., Waltham, US
One Shot™ Stbl3™ Chemically Competent E. coli	F^- *mcr*B *mrrhsd*S20(r_B^-, m_B^-) *rec*A13 *sup*E44 *ara*-14 *gal*K2 *lac*Y1 *pro*A2 *rps*L20(Str^R) *xyl*-5 λ^- *leumtl*-1	Thermo Fisher Scientific Inc., Waltham, US

2.1.4 Compounds, solutions and general chemicals

2.1.4.1 Compounds

Compound	Stock solution	Solvent	Supplier	Catalogue number
4hydroxynonenal	80mM	C_2H_5OH	Santa Cruz Biotechnology, Inc., Dallas, US	sc-202019
Auranofin	20mM	DMSO	Tocris® a BioTechne® brand, Ltd., Minneapolis, US	4600
AZ505	5mM	DMSO	APExBIO, Houston, US	B1255
Benzoic Acid	500mM	C_2H_5OH	Sigma Aldrich Corporation, St.Louis, US	242381
Diminazene	0.5g/ml	H_2O	Sigma Aldrich Corporation, St.Louis, US	D7770
Docetaxel	10mM	DMSO	Sigma Aldrich Corporation, St.Louis, US	1885
Estramustine	250mM	DMSO	Santa Cruz Biotechnology, Inc., Dallas, US	sc-353281
Fotemustine	10mM	H_2O	Sigma Aldrich Corporation, St.Louis, US	F7307

Compound	Stock solution	Solvent	Supplier	Catalogue number
HOE140	750µM	H_2O	Tocris® a BioTechne® brand, Ltd., Minneapolis, US	3014
JQ1	20mM	DMSO	Sigma Aldrich Corporation, St.Louis, US	SML1524
Marimastat	50mM	DMSO	Sigma Aldrich Corporation, St.Louis, US	M2699
Mimosine	500mM	1M NH_4OH	Sigma Aldrich Corporation, St.Louis, US	M0253
Pazopanib	60mM	DMSO	Santa Cruz Biotechnology, Inc., Dallas, US	SC-396318
Prostratin	5mM	DMSO	Sigma Aldrich Corporation, St.Louis, US	P0077
SAHA	2.5mM	DMSO	Sigma Aldrich Corporation, St.Louis, US	SML0061
Sodium Butyrate	500mM	H_2O	Sigma Aldrich Corporation, St.Louis, US	B5887
Terameprocol	25mM	DMSO	Sigma Aldrich Corporation, St.Louis, US	T3455
TNFα	100µg/ml	H_2O	Miltenyi Biotec, Bergisch Gladbach, Germany	130-094-022
Vitamin B1	1M	H_2O	Santa Cruz Biotechnology, Inc., Dallas, US	SC-338735
Zonisamide solution	4.7mM	CH_3OH	Cerillant® by Sigma Aldrich Corporation, St.Louis, US	Z-005

2.1.4.2 Media, buffers and solutions

Media, Buffers & Solutions	Formulation
2% paraform-aldehyde (PFA)	20g Formaldehyde, add 1X PBS to 1L final volume, sterile filtrated, aliquoted and stored at -20°C
20X Tris-Acetate-EDTA (TAE) Buffer	800 mM Tris-HCl, 2.3% (v/v) acetic acid, 40mM EDTA, add H_2O to 1L final volume
Coomassie de-staining solution	40% (v/v) methanol, 7% (v/v) acetic acid, add H_2O to 1L final volume
Coomassie staining solution	0.5% (w/v) Coomassie® Brilliant Blue G-250, 40% (v/v) methanol, 7% (v/v) acetic acid, add H_2O to 1L final volume
MOPS buffer	50mM MOPS, 50 mM Tris, 0.1% (w/v) SDS, 1.025 mM EDTA Titriplex II
Phosphate-buffered saline (PBS) without $Ca^{2+}Mg^{2+}$	137mM NaCl, 2.7mM KCl, 1.47mM KH_2PO_4, 8.1mM Na_2HPO_4
RIPA complete lysis buffer	12.5ml Tris 1M pH 8 (25mM), 13.7ml NaCl 5 M (137mM), 5ml Glycerol (1% (v/v)), 0.5g SDS (0.1 % (w/v)), 2.5g Na-deoxycholate DOC (0.5% (w/v)), 5ml NP40 (1% (v/v)), 2ml EDTA 0.5M pH 8 (2mM) add H_2O to 500ml final volume
Tris-buffered saline with 1% (v/v) Tween 20 (TBS-T)	10mM Tris-HCl pH 8.0, 150mM NaCl, 0.05% (v/v) Tween-20, add H_2O to 1L final volume
Tris-EDTA (TE) buffer, pH 8.0	10mM Tris-HCl, 1mM EDTA Titriplex III

2.1.5 Equipment and Consumables

2.1.5.1 General laboratory equipment

General laboratory equipment	Supplier
Agarose gel electrophoresis apparatus	Mini-Sub Cell® GT System/ Sub-Cell® GT System, Bio-Rad Laboratories GmbH, Munich, Germany
Biological safety cabinet	HERAsafe, Thermo Fisher Scientific Inc., Waltham, US
	SterilGARD® III Advance, The Baker Company, Sanford, US
Blotting pads	Novex®, Life Technologies™, brand of Thermo Fisher Scientific Inc., Waltham, US
Centrifuges	Centrifuge 5810 R, Eppendorf AG, Hamburg, Germany
	Fresco 17 Microcentrifuge, Heraeus, Thermo Fisher Scientific Inc., Waltham, US
	Fresco 21 Microcentrifuge, Heraeus, Thermo Fisher Scientific Inc., Waltham, US
	Megafuge 40R, Heraeus, Thermo Fisher Scientific Inc., Waltham, US
	MiniSpin®, Eppendorf AG, Hamburg, Germany
	RC26 Plus, Sorvall, Thermo Fisher Scientific Inc., Waltham, US
CO_2 incubators	BBD 6220, Heraeus, Thermo Fisher Scientific Inc., Waltham, US
	HERAcell 240i, Thermo Fisher Scientific Inc., Waltham, US
Counting chamber	Neubauer-improved, Paul Marienfeld GmbH & Co. KG, Lauda-Königshofen, Germany
Gel blotting module	XCell II™ Blot Module, Novex®, Life Technologies™, brand of Thermo Fisher Scientific Inc., Waltham, US
Incubator shaker	Innova 4200/ 4230, New Brunswick Scientific, Eppendorf AG, Hamburg, Germany
Pipette (0.1-2.5µl, 0.5-10µL, 10-100µL, 50-200µL, 100-1000µL)	Eppendorf Reference®/ Eppendorf Research® plus, Eppendorf AG, Hamburg, Germany
Pipette filler	Pipetus®, Hirschmann Laborgeräte GmbH & Co. KG, Eberstadt, Germany
Platform shaker	Polymax 1040, Heidolph Instruments GmbH & Co. KG, Schwabach, Germany
Polyacrylamide gel electrophoresis Apparatus	XCell SureLock® Mini, Novex®, Thermo Fisher Scientific Inc., Waltham, US
Power supply	EV202, Consort bvba, Turnhout, Belgium
	PowerPac™ HC, Bio-Rad Laboratories, Inc., Hercules, US
Multichannel electronic pipettor (0.5-12.5 µL, 2-125 µL, 15-1250 µL)	Matrix Multichannel Electronic Pipettors, Thermo Fisher Scientific Inc., Waltham, US
Microscopes	Eclipse TS100, Nikon GmbH, Düsseldorf, Germany
	Leica DM IL, Leica Microsystems GmbH, Wetzlar, Germany
Scale	BP211D, Sartorius AG, Göttingen, Germany
Thermomixer	Eppendorf Thermomixer 5436, Eppendorf AG, Hamburg, Germany
UV/Vis spectrophotometer	GeneQuant pro, Amersham™, GE Healthcare GmbH, Solingen, Germany
Vortex mixer	Vortex-Genie 2, Scientific Industries, Inc., Bohemia, US

2.1.5.2 Consumables

General consumables	Source
Autoradiography film	Super RX, Fujifilm Europe GmbH, Düsseldorf, Germany
Cell culture flasks (25 cm^2, 75 cm^2, 175 cm^2)	CELLSTAR® Filter Cap Cell Culture Flasks, Greiner Bio-One GmbH, Frickenhausen, Germany
Cryogenic storage vials	Cryo.s™, Greiner Bio-One GmbH, Frickenhausen,Germany
Culture tube, with push cap	Sarstedt AG & Co., Nümbrecht, Germany
Cuvettes	Rotilabo®-disposable cuvettes, Carl Roth GmbH & Co. KG, Karlsruhe, Germany
Filter paper (Whatman paper)	GE Healthcare GmbH, Solingen, Germany
Filter unit (0.45µm)	Millex-HV Filter, Millipore, Merck KGaA, Darmstadt, Germany
Inoculating loops	L 200 - Ino-Loop™, Simport Scientific, Beloeil, Belgium
Microcentrifuge tubes (1 ml, 2 ml)	Sarstedt AG & Co., Nümbrecht, Germany
Microplate, transparent, 96 well, (F-bottom, U-bottom, V-bottom)	Greiner Bio-One GmbH, Frickenhausen,Germany
Microplate, white (96 well, 384 well)	Greiner Bio-One GmbH, Frickenhausen,Germany
Multidishes (6 well, 12 well, 24 well, 96 well)	Nunc Multidishes Nunclon™Δ, Nunc GmbH & Co. KG, Langenselbold, Germany
Pipette tips, with filter (10µl, 100µl, 300µl, 1000µl)	Biosphere® Pipette Tips, Sarstedt AG & Co., Nümbrecht, Germany
Pipette tips, with filter for multichannel electronic pipettors (12.5µl, 125µl, 1250µl)	Thermo Fisher Scientific Inc., Waltham, US
Pipettes, with filter (5ml, 10ml, 25ml)	Serological Pipettes, Greiner Bio-One GmbH, Frickenhausen, Germany
Pipettes, without filter	Aspirating Pipettes, Greiner Bio-One GmbH, Frickenhausen, Germany
Polypropylene tubes, conical (15ml, 50ml)	Greiner Bio-One GmbH, Frickenhausen, Germany

2.1.6 Databases

Database	Application	Source
DGIbd - Mining the Druggable Genome	Drug-Gene Interaction database	http://dgidb.genome.wustl.edu/ (Cotto et al., 2018)
DrugBank	Target/compound details	https://www.drugbank.ca/ (Law et al., 2014)
Genego	Target/compound details	proprietary
Primer-BLAST	Primer design	https://www.ncbi.nlm.nih.gov/tools/primer-blast/
PubMed	Information on host factors	https://www.ncbi.nlm.nih.gov/pubmed/
The Human Protein Atlas	Expression levels of host factors in different tissues	http://www.proteinatlas.org/ (Uhlén et al., 2015)
Therapeutic Target Database (TTD)	Target/compound details	http://bidd.nus.edu.sg/group/cjttd/ (Li et al., 2018)

2.1.7 Software

Software	Description	Supplier
FCS Express 4.0	FACS data processing	De Novo Software, Suite, US
Graph Pad Prism 7	Data processing	GraphPad Software, Inc.
Microsoft Office 2010	Basic writing and presentation programs	Microsoft Corporation, Washington, US
SDS v2.4	RT-qPCR data processing	Applied Biosystems, brand of Thermo Fisher Scientific Inc., Waltham, US
SnapGene Viewer 3.3.4	Cloning and plasmid organization system	GSL Biotech LLC, Chicago, US
Vector NTI Advance(R) 11.5.2	Cloning and plasmid organization system	Invitrogen, brand of Thermo Fisher Scientific Inc., Waltham, US

2.2 Methods

2.2.1 Molecular techniques

2.2.1.1 DNA amplification by PCR

For the generation of a new constant shRNA expressing backbone, PCR was used to specifically amplify fragments.

In short, primers were designed to allow amplification of the sequence of interest (*in silico* primer design with vector NTI software). A PCR master mix was set up (**Table 1**) and a PCR run under the indicated cycling conditions (**Table 2**) according to the KOD polymerase manual using TProfessional Thermocycler (Biometra GmbH, Göttingen, Germany). The annealing temperature of the primers was determined by vector NTI and is mentioned in the respective result paragraph. Successful amplification of PCR fragments was confirmed by fragment visualization after gel electrophoresis and by sequencing.

Table 1: Formulation of PCR mix for fragment amplification.

Component	Volume
KOD polymerase 2.5U/µl (Millipore, Merck KGaA, Darmstadt, Germany)	1.0µl
$MgSO_4$ (25mM)	3.0µl
dNTPs (2mM each)	5.0µl
template DNA (10ng)	Xµl
primer fw 10µM	1.5µl
primer rev 10µM	1.5µl
10X KOD buffer	5.0µl
add nuclease free H_2O to a final volume of	50.0µl

Table 2: Overview over PCR cycling conditions.

Step	Temperature	Time	
Polymerase activation	95°C	2min	
Denaturation	95°C	20s	repeat 30x
Annealing	variable	10s	
Extension	70°C	20s/kb	
Final extension	70°C	5min	
On hold	4°C	∞	

2.2.1.2 Restriction digestion of plasmids or PCR amplified fragments

Digestion of DNA sequences or plasmids with restriction enzymes produces blunt or unique sticky ends, which allows for exchange, deletion or insertion of fragments. Compatible ends can be ligated into a backbone, generating a modified plasmid. In general, a restriction digest was set up (**Table 3**) with two restriction enzymes in the correct buffer and incubated for 1h/1µg template at 37°C.

Purified PCR fragments for the generation of a new shRNA expressing backbone were restriction digested with XbaI and XhoI in diluted10X Buffer 4 (all New England Biolabs GmbH, Frankfurt am Main, Germany).

Cloning of shRNA sequences from the pGIPZ to the pTRIPZ backbone and further to the pRIPZ backbone was done by restriction digest of backbone and shRNA containing plasmid with the same restriction enzymes to produce compatible ends, which were joined by ligation. The moving of shRNA was done according to the manual using FastDigest MluI and FastDigest XhoI in diluted 10X Fast Digest Green buffer (all Thermo Fisher Scientific Inc., Waltham, US).

Table 3: Formulation of restriction digest.

Component	Volume
10X buffer	5µl
PCR fragment/DNA sample (≤ 5µg)	Xµl
Enzyme 1	1µl
Enzyme 2	1µl
add nuclease free H_2O up to a final volume of	50µl

2.2.1.3 Agarose gel electrophoresis

Gel electrophoresis was carried out in order to visualize and separate digested DNA fragments and PCR products.

For this, 0.4g – 0.75g LE agarose (Biozym Scientific GmbH, Hessisch Oldendorf, Germany) was weighed and mixed in 50ml 1X TAE buffer, yielding a 0.8% - 1.5% (w/v) agarose solution (lower agarose percentages for large fragments for restriction-digested backbones and higher agarose percentages for small fragments). The mixture was heated in a microwave oven until the agarose completely dissolved. 1:10,000 diluted Gel Red Nucleic Acid Stain (Biotium Inc., Fremont, US) was added, the gel was casted and allowed to solidify at room temperature. The gel electrophoresis chamber was assembled and filled with 1X TAE buffer. The sample was mixed with 1:6 diluted Gel Loading Dye (New England Biolabs GmbH, Frankfurt am Main,

Germany) and loaded on the gel along with 7µl of GeneRuler™ 1kb Plus DNA Ladder (Thermo Fisher Scientific Inc., Waltham, US). The applied voltage was 80V for preparative digestions, or 120V for analytical ones. The gel was visualized on a UV transilluminator (INTAS Science Imaging Instruments GmbH, Göttingen, Germany). For preparative digestions, samples were cut from the gel and used further.

2.2.1.4 Isolation of DNA fragments from agarose gel

After separation of DNA fragments by gel electrophoresis, the fragments were isolated from agarose. Using Nucleo® Gel and PCR Clean-up kit (Macherey-Nagel GmbH & Co. KG, Düren, Germany), the DNA fragment isolation was performed according to the manufacturer's protocol. The agarose piece was weighed, and 200µl NTI Binding Buffer per 100mg agarose was added. The mixture was heated to 50°C, incubated until agarose completely melted, loaded onto the provided column, and centrifuged for 30s at 11,000g. The column was washed twice with NT3 wash buffer by centrifugation for 30s at 11,000g, and then dried by centrifugation for 2min at 11,000g. 15-30µl (depending on fragment amount isolated) of prewarmed NE Elution Buffer (50°C) was added to the dried column, which was incubated for 3min and centrifuged for 1min at 11,000g. The concentration of the eluted DNA was determined by a UV/Vis spectrophotometer (NanoDrop 2000™, Thermo Fisher Scientific Inc., Waltham, US).

2.2.1.5 DNA ligation

In order to obtain circular plasmids, a ligation reaction was set up, containing the digested and cleaned DNA fragment, backbone and T4 ligase (New England Biolabs GmbH, Frankfurt am Main, Germany) in the appropriate buffer (**Table 4**). The molar ratio of backbone to insert used was 1:5, with 100ng of backbone. The reaction was incubated for 1h at room temperature. In addition, for each ligation setup also a backbone only ligation (without insert) was performed, which allowed the estimation of incomplete backbone digestion.

Table 4: Formulation of ligation mix.

Component	Volume
T4 ligase (New England Biolabs GmbH, Frankfurt am Main, Germany)	1µl
10X T4 ligase buffer (New England Biolabs GmbH, Frankfurt am Main, Germany	2µl
DNA insert)	Xµl
DNA backbone (100ng)	Xµl
add nuclease free H_2O to final volume of	20µl

2.2.1.6 Transformation

Amplification of plasmids was performed using One Shot™ Stbl3™ Chemically Competent *E. coli*. A 50µl aliquot/transformation was thawed on ice, and 2µl ligation mixture or 0.5µg plasmid was added. This mixture was incubated on ice for 30min, heat-shocked at 42°C for 25s, and incubated on ice for 2min. 500µl prewarmed super optimal broth with catabolite repression (SOC) medium (PEI media kitchen) was added, the mixture was gently shaken at 37°C for 1h, and 100µl of bacteria solution plated on LB agar plates containing 100µg/ml Ampicillin and 25µg/ml Zeocin™ (PEI media kitchen). The plates were incubated at 37°C overnight, and single colonies were picked.

2.2.1.7 Plasmid amplification

Single colonies of transformed *E. coli* were picked and inoculated in 8ml LB medium (containing the selecting antibiotics). Those single colony cultures are hereinafter referred to as precultures. Precultures were cultivated under gentle shaking at 37°C overnight. To isolate small volumes of plasmid, as for sequencing purposes, 3ml of preculture was harvested, and plasmids were isolated with the QIAprep Spin Miniprep Kit (QIAGEN, Hilden, Germany) according to the manufacturer's protocol. To isolate large volumes of plasmid, as for transfection and lentiviral particle production, 5ml of preculture was added to 200ml of LB medium containing the selecting antibiotics and cultivated under gentle shaking at 37°C overnight, and plasmids were isolated by NucleoBond® Xtra Midi Kit (Macherey-Nagel GmbH & Co. KG, Düren, Germany) according to the manufacturer's protocol. Isolated plasmids were dissolved in TE buffer, and DNA concentration was determined by a UV/Vis spectrophotometer.

2.2.2 qPCR and associated techniques

2.2.2.1 Isolation of nucleic acids

2.2.2.1.1 RNA isolation and DNase digestion

In order to determine knockdown efficiency of host factors or the reversal of latency in J-Lat clones and U1 cells reverse transcriptase quantitative PCR (RT-qPCR) was performed. For this, RNA was isolated with the NucleoSpin® RNA Plus (Macherey-Nagel GmbH & Co. KG, Düren, Germany) according to the manufacturer's protocol. In short, samples were collected,

the supernatant discarded, and cells resuspended in 200µl of LBP lysis buffer per well of a 96 well format. RNA isolation was either directly continued or samples stored at -80°C. The lysed cells were loaded onto genomic DNA (gDNA) removal column, centrifuged at 11,000g for 30s. The flow-through was mixed with Binding Solution, loaded to on the RNA binding column, washed with WB1, centrifuged at 11,000g for 30s. The column was transferred into a new tube and washed with WB2 twice and column dried by centrifugation at 11,000g for 2min. The column with bound RNA was transferred into a new tube, 15µl of H_2O was added onto the column, incubated for 1min and centrifuged at 11,000g for 1min. The elution step was repeated, yielding 30µl purified RNA.

For quantification of *gag* or *gfp* mRNA from J-Lat clones or U1 cells, samples were DNase treated to avoid amplification from genomic DNA. For this 30µl of RNA were digested with the TURBO DNA-*free*™ kit (Invitrogen™, brand of Thermo Fisher Scientific Inc., Waltham, US) according to **Table 5**. In short, RNA samples were mixed with Turbo DNase in the appropriate buffer, including recombinant RNasin® Ribonuclease inhibitor (Promega Corporation, Fitchburg, US). The mixture was incubated for 20min at 37°C, then inactivated by adding 3.5µl inactivation reagent, incubated for 5min at RT and centrifuged at full speed for 5min. The supernatant containing the DNA-free RNA was transferred into a new tube and either used directly for RT-qPCR or stored at -80°C.

Table 5: Formulation of DNase digest for RNA samples.

Component	Volume
RNA sample	30.0µl
Turbo DNase buffer 10x	3.5µl
recombinant RNasin® Ribonuclease inhibitor	0.5µl
add DNase free H_2O to a final volume of	35.0µl

2.2.2.1.2 Genomic DNA isolation from primary HIV-1 positive PBMCs

Genomic DNA (gDNA) was isolated using the QIAamp DNA Mini Kit (51304, Qiagen, Hilden, Germany) following the instructions of the manufacturer, all solutions used were provided with the kit. In short, one million PBMCs were diluted in PBS up to a final volume of 200µl. 20µl Proteinase K solution was added, followed by 200µl AL buffer. The samples were pulse vortexed and incubated at 56°C for 10min. 200µl 100% ethanol was added, the mixture applied to a spin column and centrifuged at 6,000g for 1min. The spin column was placed into a new collection tube and 500µl AW1 buffer was added, followed by centrifugation at 6,000g for 1min. The flow-through with the collection tube was discarded. The spin column was placed into a

new collection tube and washed with 500µl AW2 buffer, followed by centrifugation at full speed for 3min. The spin column was placed into a 1.5ml elution tube and 100µl of AE buffer was added. After 3min of incubation the DNA was eluted by centrifugation at 6,000g for 1min. The genomic DNA was stored at -20°C until further used for HIV copies determination.

2.2.2.2 qPCR

2.2.2.2.1 HIV copy number determination by qPCR on gDNA

To determine the absolute numbers of HIV integrates per million PBMCs, a duplex qPCR was performed amplifying a HIV-1 fragment and a CCR5 gene fragment in parallel (the experimental conditions follow a publication for HIV-1 viral load quantification (Malnati et al., 2008). The qPCR was set up with the Agilent Brilliant II MM (Agilent Technologies, Inc., Santa Clara, US) according to the manufacturer's protocol. In short, a master mix was set up (**Table 6**) excluding the DNA template and 17µl/well distributed to the designated wells. Afterwards 8µl of DNA or H_2O, serving as non-template control, were added. The qPCR was performed on the Mx3000P® qPCR system (Agilent Technologies, Inc., Santa Clara, US) in a 96 well format, each sample was run in five replicates and the plasmid standard dilution series in triplicates. The cycling conditions were according to **Table 7**. Analysis of the raw data was performed using MxPro QPCR Software (Agilent Technologies, Inc., Santa Clara, US). Absolute copy numbers were determined with the help of the plasmid standard dilution series with known copy numbers of both reference plasmids. Further, CCR5 results were used to determine the number of tested cells in order to calculate the number of HIV-1 integrates per one million PBMCs (Malnati et al., 2008).

Table 6: Formulation of qPCR mix for HIV-1 provirus quantification.

Component	Volume
2x Agilent Brilliant II MM	12.5µl
HIV-1 forward primer (10µM)	0.75µl
HIV-1 reverse primer (10µM)	0.75µl
HIV-1 probe FAM (10µM)	0.3µl
CCR5 forward primer (10µM)	0.5µl
CCR5 reverse primer (10µM)	0.5µl
CCR5 probe HEX (10µM)	0.5µl
ROX dye (2µM)	0.375µl
template DNA	8.0µl
add DNase free H2O to a final volume of	25.0µl

Table 7: Cycling conditions for qPCR on HIV-1 provirus quantification.

Step	Temperature	Time	
Polymerase activation	95°C	10min	
Denaturation	95°C	30s	repeat 45x
Annealing and extension	60°C	1min	
On hold	4°C	∞	

2.2.2.2.2 One-step RT-qPCR relative quantification of mRNA levels

To determine the relative mRNA levels of genes of interest RT-qPCR was performed. For this, the isolated samples were measured by an UV/Vis spectrophotometer and equal concentrations of total RNA (usually 20ng/well) were tested. The RT-qPCR was set up with the QuantiTect® SYBR® Green RT-PCR kit (Qiagen, Hilden, Germany) according to the manufacturer's protocol. In short, a master mix was set up excluding the RNA template (**Table 8**) and distributed in to the designated wells. Afterwards the RNA samples were added to the wells. A no template control was included which allowed primer dimer detection. For DNase-digested samples, a no RT control for each sample was included which gave a signal if DNA digestion was incomplete. The RT-qPCR was performed on the 7900HT Fast Real-Time PCR System cycler (Applied Biosystems, brand of Thermo Fisher Scientific Inc., Waltham, US) in a 384 well plate format, each sample was run in technical triplicates. The cycling conditions were according to **Table 9**. Analysis of the raw data was performed using SDS2.4 software. For this, the threshold of each primer pair was set, the CT values extrapolated and the relative expression levels determined by 2^-(CT 'gene of interest' – CT 'reference gene').

Table 8: Formulation of one-step RT-qPCR mix for relative RNA quantification.

Component	Volume
2X QuantiTect SYBR Green RT-PCR Master Mix	5.0µl
QuantiTect RT Mix	0.1µl
Template RNA (30ng)	3.0µl
primer fw (5mM)	0.1µl
primer rev (5mM)	0.1µl
add RNase free H_2O to a final volume of	10.0µl

Table 9: Cycling conditions for one-step RT-qPCR on RNA samples.

Step	Time	Temperature	
Reverse transcription	30min	50°C	
Polymerase activation	15min	95°C	
Denaturation	15s	94°C	repeat 45x
Annealing	30s	56°C	
Extension	30s	72°C	
denaturation	15s	95°C	
annealing	15s	60°C	

2.2.3 Cell-associated techniques

2.2.3.1 Culture of cell lines

All cells were grown at 37°C, 95% humidity and 5% CO_2 in T75 cell culture flasks, if not stated otherwise. All procedures were performed under sterile conditions and cells regularly checked for being mycoplasma negative. Cell lines were cultivated up to passage number 40, and then discarded and a new vial thawed.

Suspension cells were cultured in supplemented RPMI1640 (Sigma Aldrich Corporation, St. Louis, US) (10% heat inactivated FCS (Biowest, Nuaillé, France), 1% L-glutamine (Biochrom GmbH, Berlin, Germany)) and split 1:5 for J-Lat cells and 1:10 for U1 cells three times a week.

Adherent cells as HEK293T and HIVluc HEK293T were grown in supplemented Dulbecco's modified eagle medium (DMEM) (Lonza Group AG, Basel, Switzerland) (10% heat inactivated FCS and 1% L-glutamine). Cells were split 1:12 twice a week. For this, medium was discarded, cells were rinsed once with PBS, 2ml trypsin solution was added and incubated until cells detached from the flask. 10ml of supplemented DMEM was added, the cells singularized by pipetting up and down several times. 1ml was used for continuous culturing.

2.2.3.2 Cell counting

In order to determine to cell number, a Neubauer chamber was used. For this 10µl of cell suspension was mixed with 90µl of 0.1% Trypan blue solution (in PBS, PEI media kitchen) and 10µl transferred to the counting chamber. Four squares were counted, the mean was formed, multiplied by 10,000 and by 10 (dilution with Trypan blue), resulting in the number of cells per ml.

Primary cells were counted using an automated cell counter (Coulter® Counter Z2™, Beckman Coulter, Inc., Indianapolis, US). For this 100µl cell suspension was added to 10ml degassed Casey ton (OLS® OMNI Life Science, Bremen, Germany) and measured with the appropriate settings.

2.2.3.3 Cell thawing and freezing

Frozen cells were stored for short-term storage at -80°C and for long-term storage in liquid nitrogen. Cells were thawed by warming the cryovial until cell suspension liquefied. Cells were transferred to a 50ml Falcon tube and 4ml of medium added. Cells were centrifuged at 100g for 5min, the supernatant was discarded, and the cells carefully resuspended in 5ml of medium and transferred to a T25 flask. For the different assays, cells were expanded in T75 flasks.

For freezing cells, the cells were counted and a minimum of two million cells/cryovial frozen. The cells were centrifuged at 100g for 5min, the supernatant was discarded, and cells resuspended in 1ml of cold freezing medium (90% FCS, 10% DMSO (Sigma Aldrich Corporation, St. Louis, US)). The cryovials were transferred into a freezing container, Nalgene® Mr. Frosty (Sigma Aldrich Corporation, St. Louis, US), and stored at -80°C for 24h before being transferred into liquid nitrogen.

2.2.3.4 Transfection of adherent cells (siRNA)

For transient knockdown of host factors in adherent cells, Lipofectamine™ RNAiMAX Transfection Reagent (Thermo Fisher Scientific Inc., Waltham, US) was used to transfer siRNA into cells. A reverse transfection approach was chosen and performed according to the manufacturer's protocol. All surfaces and equipment were cleaned with RNase AWAY beforehand. In short, the siRNA stock was diluted in fresh OPTI-MEM™ to a final concentration of 0.1pmol/µl (for details refer to **Table 10**) and added to the wells. Lipofectamine™ RNAiMAX Transfection Reagent was prediluted in OPTI-MEM™ and added to the diluted siRNA and incubated for 20min at room temperature. Meanwhile, the cells were counted and diluted to a final concentration of one million cells/6ml medium containing 20% FCS and then seeded onto the transfection mix. The cells were incubated at 37°C ≤72h before harvest or read-out was performed.

Table 10: Ratio of siRNA to transfection reagent to cell number in dependence of well format.

	µl/well (96 well)	µl/well (384 well)
siRNA in OPTI-MEM™ (0.1pmol/µl)	30µl	10µl
1:200 diluted Lipofectamine™ RNAiMAX in OPTI-MEM™	30µl	10µl
cells/well seeded	3333/20µl	10000/60µl

2.2.3.5 Transfection of suspension cells (siRNA)

For transient knockdown of host factors in suspension cells, transfection by electroporation was chosen to transfer siRNA into cells. For this, the cell specific electroporation kits, i.e. Cell Line Nucleofector® Kit V for J-Lat clones and Cell Line Nucleofector® Kit C for U1 (both Lonza Group AG, Basel, Switzerland), were used, and the instruction of the manufacturer followed. In short, cells were counted and centrifuged at 100g for 10min, the supernatant was completely discarded and two million cells per sample were resuspended in nucleofector solution and 2µl of 20µM siRNA was added. The suspension was transferred into a cuvette. The cells were electroporated with the appropriate program with a Nucleofector™ 2b device (Lonza Group AG, Basel, Switzerland). The cells were transferred into a well of a 12 well plate, containing 1ml of prewarmed RPMI1640. If electroporated cells were further stimulated, the cells were split over three wells and a stimulus was added for 24h.

2.2.3.6 Lentiviral particle production

Lentiviral particles were produced in HEK293T/17 cells, seeded at 0.75 million cells well in a 6 well plate. 24h post seeding, the medium was replaced with 1ml OPTI-MEM™. The DNA mix was prepared (according to **Table 11**) in 500µl OPTI-MEM™ and 5µl Lipofectamine® 2000 Transfection Reagent (Thermo Fisher Scientific Inc., Waltham, US) prediluted in 500µl OPTI-MEM™ were added to the DNA, followed by incubation for 20min at room temperature. The plasmid DNA transfection mix was added drop wise to the cells followed by overnight incubation. The next day, medium was replaced by supplemented DMEM. On the two following days, the lentiviral particle containing supernatant was collected on ice, filtered through a 0.42µm filter, aliquoted in 1ml aliquots and stored at -80°C.

Table 11: Formulation of DNA ratios for lentiviral particle production.

Component	Amount
pAX2	1.0µg
pCMV-VSV-G	0.5µg
shRNA containing plasmid	2.0µg
filled up with OPTI-MEM™ to final volume of	500.0µl

2.2.3.7 Transduction of adherent cells (stable cell lines)

Production of stable HEK293T cells, expressing luciferase from HIV promoter, was performed by transducing cells with lentiviral particles containing a modified version of pNL4.3 (pNL4.3 *env* deleted by frameshift mutation, *nef* replaced by firefly luciferase) in a ratio of one particle per cell. The cells were seeded and allowed to attach before viral particles were added. The next day, medium was changed, and cells cultivated over twenty passages before being checked for expression of luciferase and testing. Those produced cells were denoted HIVluc HEK293T in all further experiments.

2.2.3.8 Transduction of suspension cells (stable cell lines)

Production of stable suspension cell lines was achieved by transduction of target cells with lentiviral particles. For this, 0.75 million cells/well were seeded in 1.5ml supplemented RPMI1640 in a 6 well plate format. 1ml of lentiviral particles was added to the cells and then spin occulated at 300g for 90min at 30°C. The next day, medium was exchanged with supplemented RPMI1640. Two days after spin occulation, puromycin (InvivoGen, San Diego, US) was added to the medium at a final concentration of 1µg/ml to start the selection process. For each round of transduction, a non-transduced control was taken along. During the first week of puromycin selection the cells and the non-transduced control were closely monitored, and medium was regularly changed. One week after selection, cells were expanded and experimentally tested. For suspension cells containing pTRIPZ derived integrates a further induction of shRNA by doxycycline (InvivoGen, San Diego, US) was initiated before these cells were tested.

2.2.4 Primary cells

2.2.4.1 Origin of patient material

Primary material was obtained from follow-up blood samples of participants of the 'seroconverter' study (RKI - HIV-Serokonverterstudie). This study is ongoing in Germany since 1997 and collects data on the long-term disease progression and the overall survival time within the study cohort as well as observes trends in HIV mutations and subtypes. Study participants included are ≥18 years, HIV-1 positive with an acute or documented seroconversion (<3 years) and provided written consent. The Robert Koch Institute is conducting this study and receives 20ml of EDTA blood at least once per year from each participant. The blood plasma is used for further analysis and the remainders, which are not used for any further testing, were used for the isolation of $CD4^+$ T cells. All experiments on primary $CD4^+$ T cells were conducted at the Robert Koch Institute within a 2.5-month period.

2.2.4.2 PBMC isolation from HIV-1 positive study participants

HIV-1 positive full blood was diluted with two parts of PBS and carefully layered on 11ml Histopaque®-1077 (Sigma Aldrich Corporation, St.Louis, US) in a 50ml tube. The sample was centrifuged for 25min at 900g without brake and acceleration. The formed lymphocyte ring was carefully aspirated and transferred into a new tube, which was filled up to a final volume of 50ml with PBS and then centrifuged at 600g for 10min with brake and acceleration, as all centrifugation steps from here on. The supernatant was discarded, and the cell pellet resuspended in 10ml 0.87% NH_4CL for 5min under occasional swirling to allow lysis of remaining erythrocytes. After incubation, PBS was added to a final volume of 50ml and centrifuged at 300g for 10min. The supernatant was discarded, and the cell pellet was resuspended twice more in PBS and centrifuged at 300g for 10min. The supernatant was discarded, and the cell pellet was resuspended in 5ml PBS and cell numbers determined.

2.2.4.3 Isolation of $CD4^+$ T cells from PBMCs

For the further isolation of $CD4^+$ T cells from the PBMCs, the $CD4^+$ T Cell Isolation Kit (Miltenyi Biotec, Bergisch Gladbach, Germany) was used and the instructions of the manufacturer followed. For all washing and resuspension steps, sterile-filtered PBS with 5% BSA and 2mM EDTA was used, which is in the following assigned as MACS buffer. All steps were performed with pre-cooled solutions. Volumes of MACS buffer, antibodies and microbeads used were

calculated based on the cell numbers. All centrifugation steps were carried out at 300g for 10min, unless stated differently.

In short, cells were centrifuged, the supernatant was discarded, and cells resuspended in 40µl MACS buffer per $1x10^7$ cells. All non-$CD4^+$ T cells were labeled by addition of 10µl of biotin-antibody cocktail (containing antibodies against the following surface markers: CD8, CD14, CD15, CD16, CD19, CD36, CD56, CD123, TCR γ/δ, and CD235a) per $1x10^7$ cells total and incubated for 5min in the fridge. Another 30µl MACS buffer was added to the cells followed by 20µl microbead cocktail (microbeads conjugated to anti-biotin antibodies) per $1x10^7$ cells total. The mixture was incubated for another 10min in the fridge, before applied onto LS columns set under a strong magnetic field (Midi MACS separator and MACS Multistand, both Miltenyi Biotec, Bergisch Gladbach, Germany). The cell suspension was applied to the column and the flow-through containing the unlabeled $CD4^+$ T cells was collected, while the labeled unwanted cells were retained in the magnetic field. The cell number was determined with the Coulter Counter Z2.

2.2.4.4 Isolation of non-activated $CD4^+$ T cells from $CD4^+$ T cells

In a final isolation step, untouched $CD4^+$ T cells were isolated for non-activated $CD4^+$ T cells, i.e. cells that do not express the activation markers HLA-DR, CD69, and CD25 on the cell surface. For this, cells were centrifuged and resuspended in 100µl MACS buffer per $1x10^7$ cells. The $CD4^+$ T cell population was mixed with 10µl of each PE-coupled antibody solution directed against HLA-DR, CD69 and CD25 per $1x10^7$ cells and cells incubated for 10min in the fridge. After addition of 1ml MACS buffer, the cell suspension was centrifuged, and the supernatant discarded. The cells were resuspended in 80µl MACS buffer per $1x10^7$ cells and 20µl anti-PE conjugated microbead solution (Miltenyi Biotec, Bergisch Gladbach, Germany) was added. The mixture was incubated for 15min in the fridge, 1ml MACS buffer was added and the cells centrifuged. The supernatant was discarded, the cells resuspended in 500µl MACS buffer and then applied to a LD column (Miltenyi Biotec, Bergisch Gladbach, Germany) set under a strong magnetic field. The flow-through was collected containing the unlabeled and non-activated $CD4^+$ T cells. The cell number was determined with the CASY cell counter.

2.2.4.5 Primary T cell stimulation

For stimulation of primary $CD4^+$ T cells, $5x10^5$ cells per condition were seeded in RPMI1640 supplemented with 20% FCS and 1% L-glutamine in a 48 well plate in a final volume of 500µl

per well. Cells were treated with compound, LRAs, a combination of both, antiCD3/antiCD28 (both Miltenyi Biotec, Bergisch Gladbach, Germany) as positive control or with only medium as negative control. Cells were treated for initially six days, with treatment replacement on day three (and later onwards treated for three days only). Cells were transferred into a 1.5ml collection tube and centrifuged at 300g for 10min. 110µl of supernatant was collected for p24 ELISA and the leftover kept for optional RT-qPCR of viral RNA. The cell pellet was resuspended in 0.5ml of TRIzol™ reagent (Thermo Fisher Scientific Inc., Waltham, US) and stored for subsequent isolation of RNA and DNA at -20°C.

2.2.5 Protein associated techniques

2.2.5.1 p24 ELISA on cell line supernatant

In order to determine p24 levels, the HIV-1 $p24^{CA}$ antigen capture assay (via the material transfer agreement from Frederick National Laboratory for Cancer Research) was acquired and performed according to the manufacturer's protocol. 200µl of supernatant of treated U1 cells was collected and mixed with 20µl of lysis buffer (10% Triton X-100 (Sigma Aldrich Corporation, St.Louis, US) in H_2O), incubated for 2h at 37°C before being stored at -80°C until further used.

The ELISA was performed in a 96-flat well plate and all incubations were performed at room temperature unless stated differently. 24h prior to the ELISA, the capture antibody was diluted 1:1440 in PBS and 100µl per well distributed. The coated wells were sealed and stored overnight at 4°C. The next day, the capture antibody solution was discarded, and the wells were blocked with 300µl blocking solution (1% BSA in PBS) for 30min at room temperature. The wells were washed five times with 1X wash buffer (1:10 diluted ELISA plate wash 10X (Perkin Elmer, Inc., Waltham, US)). 100µl of lysed supernatant or standard dilution series was added and incubated for 2h. The wells were washed five times with 1X wash buffer. 100µl of primary antibody solution (sterile filtered 10% FCS, 2% NMS in RPMI1640 + primary antibody anti-HIV-1 p24) was added and incubated for 1h. The wells were washed five times with 1X wash buffer. 100µl of secondary antibody solution (sterile filtered 2% NMS, 5% NGS, 0.01% Tween 20 in RPMI1640 + 1:100,000 diluted HRP-conjugated goat-anti-rabbit) was added and incubated for 1h. The plates were washed five times with 1X wash buffer. 100µl of TMB Peroxidase substrate was added and incubated for 30min. The reaction was stopped by the addition of 100µl 1M HCl. The wells were read with a microplate reader (PHERAstar FSX,

BMG Labtech, Ortenberg, Germany) at 450nm and 650nm background wavelength. The background results were subtracted from the raw data. A sigmoidal fit was performed (GraphPad Prism 7) using the values given by the standard dilution series and the pg/ml p24 calculated from it.

2.2.5.2 Sensitive p24 ELISA on primary cells

In order to detect reactivation of latent HIV-1 provirus on protein level a highly sensitive and commercially available p24 ELISA (Innotest® HIV antigen mAb kit 80564, Fujirebio, Inc., Malvern, US) was chosen, which allows the detection of small amounts of p24 of all HIV strains within short time. The instructions of manufacturer were followed. In short, 100µl conjugate working solution I was mixed with 100µl supernatant, added to the pre-coated 8-well strips and incubated at 37°C for 1h. The supernatant was discarded, and the wells washed five times with 300µl of 1X washing solution by addition and removal via inversion and gentle tapping on absorbing cloth. 200µl of conjugate working solution II was added to the wells, incubated at 37°C for 30min. After incubation the wells were washed five times as before. 200µl of substrate working solution was added to the wells and incubated at RT for 30min and the strips gently tapped to allow mixing. Then 50µl of 25% sulfuric acid were added to the wells, incubated for 5min and the wells read at 450/620nm (Spark® TECAN Group Ltd., Mannedorf, Switzerland) absorbance with a plate reader. A standard dilution series of was run along with the samples, a sigmoidal curve fit was applied to the standard dilution series allowing the extrapolation of p24 concentrations of the tested supernatants.

2.2.5.3 Protein lysate preparation

Protein lysate of treated J-Lat 8.4 cells or U1 cells was prepared from ≥0.5 million cells. For this, cells were transferred to a 1.5ml collection tube and centrifuged in a precooled centrifuge (4°C) at 300g for 5min. The supernatant was discarded, the cells washed once with 1ml cooled PBS, and centrifuged as before. The supernatant was completely discarded, the cell pellet resuspended in 30µl RIPA buffer containing protease inhibitor (cOmplete Protease Inhibitor Cocktail, Roche Holding AG, Basel, Switzerland), and incubated for 30min on ice. The lysed cells were centrifuged in a precooled (4°C) centrifuge at full speed for 30min. Afterwards the supernatant was transferred to a new collection tube and either stored at -20°C or directly used to further determine the protein concentration.

2.2.5.4 Protein concentration determination by Bradford

The protein concentration of the lysates was determined with the Bradford Protein Assay (Bio-Rad Laboratories, Inc., Hercules, US), based on a color change of Coomassie brilliant blue G-250 dye due to its binding affinity to basic and aromatic residues present on other proteins (Bradford, 1976).

The Bradford reagent was diluted 1:5 in H_2O and transferred into a cuvette, 5µl of 1:5 diluted lysates or BSA standard was added, mixed well, incubated for 5min, and the absorption measured in a UV/VIS-spectrometer. Due to the known concentration of the standard and the measured absorbance, a standard curved was compiled, and the concentration of the samples was calculated.

2.2.5.5 Polyacrylamide gel electrophoresis

To separate proteins according to their size SDS polyacrylamide gel electrophoresis (SDS-PAGE) was applied. The gel chamber was assembled, the inner and outer chamber were filled with MOPS running buffer. 500µl Antioxidant (Life Technologies™, brand of Thermo Fisher Scientific Inc., Waltham, US) was added to the inner chamber in addition. The samples were prepared according to **Table 12**, incubated at 70°C for 10min and loaded on a pre-cast 15 well 4% - 12% NuPAGE® Bis-Tris gradient gel (Life Technologies™, brand of Thermo Fisher Scientific Inc., Waltham, US) along with 5µl protein marker/ladder XXL DeLuxe (GeneON GmbH, Ludwigshafen, Germany). 160V were applied to the samples for 110min.

Table 12: Formulation of protein samples for SDS-PAGE.

Component	Volume
Protein lysate (20µg)	Xµl
4X NuPAGE® Sample buffer	6.0µl
10X NuPAGE® Sample Reducing Agent	2.4µl
add H_2O to a final volume of	24.0µl

2.2.5.6 Protein blotting and detection

The size-separated proteins were transferred onto Amersham Hybond P 0.45 PVDF membrane (GE Healthcare GmbH, Solingen, Germany) using the Semi-Wet-Blotting Module Novex® (Life Technologies™, brand of Thermo Fisher Scientific Inc., Waltham, US). For this, 500ml transfer buffer was prepared (NuPAGE® Transfer buffer 20X (Life Technologies™,

brand of Thermo Fisher Scientific Inc., Waltham, US), 20% methanol, 500µl Antioxidant (Life Technologies™, brand of Thermo Fisher Scientific Inc., Waltham, US) in H_2O). The blotting chamber, the cut to size Whatman papers and sponges were soaked in transfer buffer. The cut to size PVDF membrane was incubated first in methanol for 20s, in H_2O for 20s before also soaked in transfer buffer. The blotting chamber was assembled with sponges and Whatman paper sandwiching the gel and the membrane. 35V were applied for 1h. After blotting the membrane was blocked in blocking buffer (5% BSA solved in 1X TBS-T) for ≥1h at room temperature under gentle shaking. In addition, the gel was stained with Coomassie staining solution for 1h and destained in Coomassie de-staining solution. This served as quality control for successful protein separation. After blocking, the membrane was incubated with the first antibody in blocking buffer overnight at 4°C. The membrane was washed three times in 1X TBS-T for 10min, followed by incubation with the secondary HRP-labeled antibody in blocking buffer for 1h at room temperature. The membrane washed three times as before. The membrane was incubated with ECL Prime (GE Healthcare GmbH, Solingen, Germany) according to the manufacturer instructions for 5min and transferred into a light tight film cassette. Autoradiography films were exposed to the membrane and developed with an autoradiography film developer (Agfa Healthcare N.V., Mortsel, Belgium).

2.2.6 Compound preparation and read-out associated techniques

2.2.6.1 Flow cytometric sample preparation

J-Lat and U1 cells were analyzed by flow cytometry for viability (and GFP) after treatment. For this, a minimum of 80,000 cells per sample was used. Cells were pelleted by centrifugation at 300g for 5min. The supernatant was discarded, and cells washed twice with 200µl PBS. The cells were resuspended in Fixable Viability Dye eFluor® 450 (eBioscience, brand of Thermo Fisher Scientific Inc., Waltham, US) diluted 1:2000 in PBS and incubated at 4°C for 30min in the dark. Then cells were washed twice in 200µl PBS and fixed in 2% PFA for 30min. Samples were measured using the MACSQuant® Analyzer 10 (Miltenyi Biotec, Bergisch Gladbach, Germany) or the BD™ LSR II SORP (BD Biosciences, Franklin Lakes, US) and analyzed using FCS Express V4 software.

Primary cells were analyzed by flow cytometry for purity and viability. A minimum of 30,000 cells was stained. The cells were transferred into a 96 U well plate, centrifuged at 300g for 10min and the supernatant discarded. The cell pellet was resuspended in 200µl PBS and again

centrifuged at 300g for 10min. The supernatant was discarded, and the cells resuspended in 50µl of 1:11 diluted anti-HLA-DR, anti-CD69, anti-CD25 or in 1:20 diluted anti-CD4. Samples were incubated at 4°C in the dark for 15min. 150µl of PBS was added to the samples, centrifuged at 300g for 10min and the supernatant discarded. The washing step was repeated. The samples were finally resuspended in 80µl of PBS.

Determination of viability in primary was done as stated above using the Fixable Viability Dye eFluor ®780 (eBioscience, brand of Thermo Fisher Scientific Inc., Waltham, US). Samples were measured with the BD FACSCalibur™ (BD Biosciences, Franklin Lakes, US) flow cytometer. Analysis of data was done with FCS Express 4.0 software.

2.2.6.2 Gating strategy

For flow cytometric analysis, the cells were first gated for the cell population, excluding cell debris, followed by exclusion of duplets. Then the singlets were gated for viable cells excluding stained dead cells. In the case of J-Lat cells, singlets were also gated for GFP positivity, which as a measure to determine the level of latency reversal. In case of stable suspension cell lines containing pTRIPZ or pRIPZ derived shRNA integrates, RFP was measured in addition, whereas RFP served as measure for shRNA-derived knockdown of host factors tested.

2.2.6.3 Luminescence read-out

Luciferase activity in HEK293T cells after treatment was assessed by adding Britelite™ substrate (Perkin Elmer, Inc., Waltham, US) to the cells and incubation for 5min at room temperature. Luciferase activity was determined using a microplate reader (PHERAstar FSX, BMG Labtech, Ortenberg, Germany).

Viability of adherent HEK293T cells after treatment was assessed by adding ATPlite™ 1 step substrate (Perkin Elmer, Inc., Waltham, US) to the cells followed by 5min of incubation at room temperature and read with a microplate reader (PHERAstar FSX, BMG Labtech, Ortenberg, Germany).

2.2.7 Statistical analysis

For the statistical analysis of compounds with LRA in comparison to LRA only a Kruskal-Wallis test was chosen. This test is non-parametric one and allows comparing more than two groups (Daniel, 1990). The choice of test was in accordance with the bioinformatic department of the Paul-Ehrlich-Institut. Statistical significance was calculated by GraphPad Prism software and is indicated by * on the group itself in comparison to the control group, whereas * indicates the p-value (also known as probability value) < 0.05, **<0.01, ***<0.001, ****<0.0001.

3 Results

3.1 The initial screening - starting point

In the following, the initial screening setup will be explained. The primary hits of a genome-wide siRNA screen served as starting point to choose and follow-up candidate factors, whereas the screen itself, its execution, analysis and primary hit discrimination are not part of this scientific work.

A genome-wide siRNA screen was performed in HEK293T, which had been transduced with an HIV-1 derived reporter virus (pNL4.3 expressing luciferase instead of *nef*, *env* deleted by frameshift mutation and VSV-G pseudotyped). After transduction, the cells were cultured over several weeks and expressed baseline luciferase levels from the HIV -1 LTR promoter. As *env* was deleted neither complete viral particles could form nor could be released. This transduced cell line was then used for a genome-wide siRNA screen. The screen was performed in a 384 well format, using two siRNAs per target in a pooled approach, i.e. both siRNAs were applied simultaneously in the same well, and two wells per target were transfected. The luciferase read-out was performed 72h post siRNA transfection. Upon substrate addition the production of luciferin was measured (a graphical overview of the experimental procedure is shown in **Figure 5**). The Z-score was calculated for all values and served as a measure on how far a specific value deviates from the normal distribution. Hits were considered if their Z-score was either ≤ -2 or ≥ +2, reflecting either a decreased or an increased luciferase signal beyond the baseline luciferase signal derived from negative (non-targeting) controls. Increased luciferase values point towards a restrictive ability of the given factor, whereas decreased luciferase values point towards a supportive role of the factor on HIV-1 transcription.

The identified primary hits (**Table S1**, Appendix) potentially play a role in HIV-1 transcriptional processes. Further, those primary hits may also play a role in HIV-1 latency. This assumption is supported by two published examples, namely BRD4 and CYLD (Manganaro et al., 2014; Zhu et al., 2012), both host factors support latency maintenance and have been identified by the primary screening as restrictive hits, i.e. increased luciferase signal upon their knockdown. This also underlines the suitability of the primary screening hits as a starting point to (chose and) validate follow-up hits.

Nevertheless, some general considerations concerning the initial screening need to be kept in mind. The usage of VSV-G pseudotyped viral particles allows for one or more infections per cell. In this regard, the infected cell line is non-homogenous for the number of proviruses

present per cell and also in regard to diverse integration sites. Further, the cells express a luciferase baseline level; therefore, this model is strictly speaking not a latency cell model.

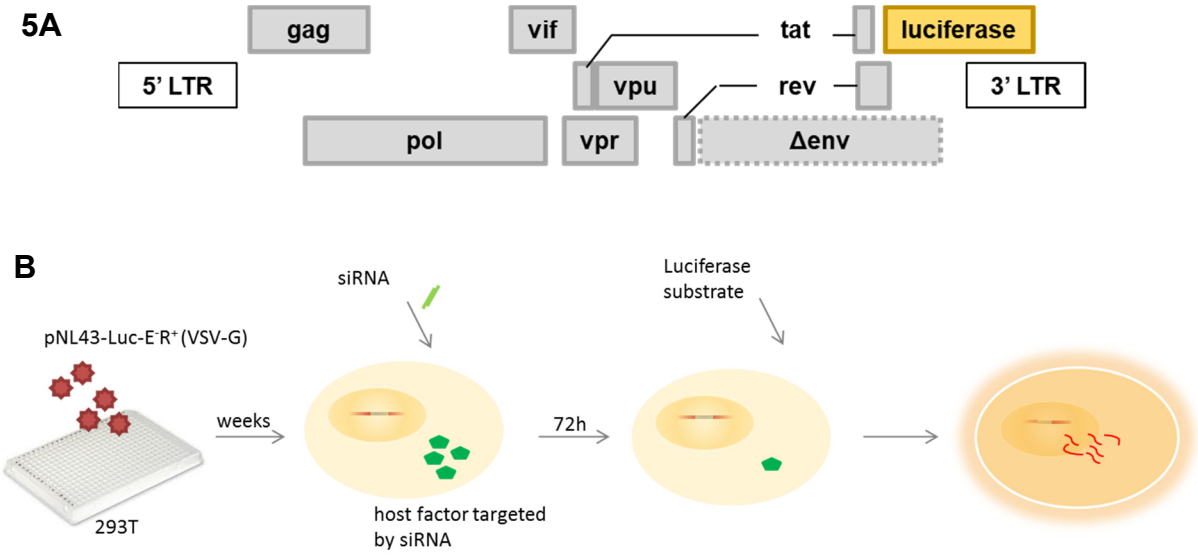

Figure 5: Graphical overview on the HIV-1 derived reporter virus and the initial screening setup. **A)** Genomic organization of the HIV-1 reporter virus used for the initial screening and for the re-testing of follow-up candidates. The reporter construct was derived from pNL4.3 being *env* deleted by frameshift mutation and possessing luciferase gene in place of *nef*. **B)** HEK293T cells were transduced with an HIV-1 reporter construct (genomic composition described in **A**). Transduced cells were cultured several weeks before host-factors were knocked down by siRNA. 72h post knockdown luciferase substrate was added and luciferin production was assessed. Increases or decreases in luciferase signal beyond baseline can be correlated to a potential supportive or restrictive effect of the host factor on HIV transcriptional processes.

3.2 Two differential approaches to identify novel LRAs

The hits of a genome-wide siRNA screen, as detailed in 3.1, served as basis for the selection of follow-up hits to be tested for their impact on latency reversal. A schematic overview of the initial screening is shown in **Figure 5B**. For the follow-up hit selection two differential strategies were applied and a graphical scheme is shown in **Figure 6**. For the approach I (left arm), the selection of follow-up hits was based on their potential to bind and/or modify chromatin. The selected candidates were then retested in the initial screening test system, followed by validation in a latency cell line model. A follow-up on validated factors would be done in primary HIV-1 cells. For the approach II, follow-up hits were based on their property to be druggable and are known targets of available compounds, here referred to as druggability. The idea behind this approach is to repurpose licensed drugs for new medical indications, also known as ‘drug repurposing’. Chosen compounds were directly tested in different latency cell lines, followed by siRNA knockdown of host factor to verify the compound target and finally testing potential compounds in primary HIV-1 cells.

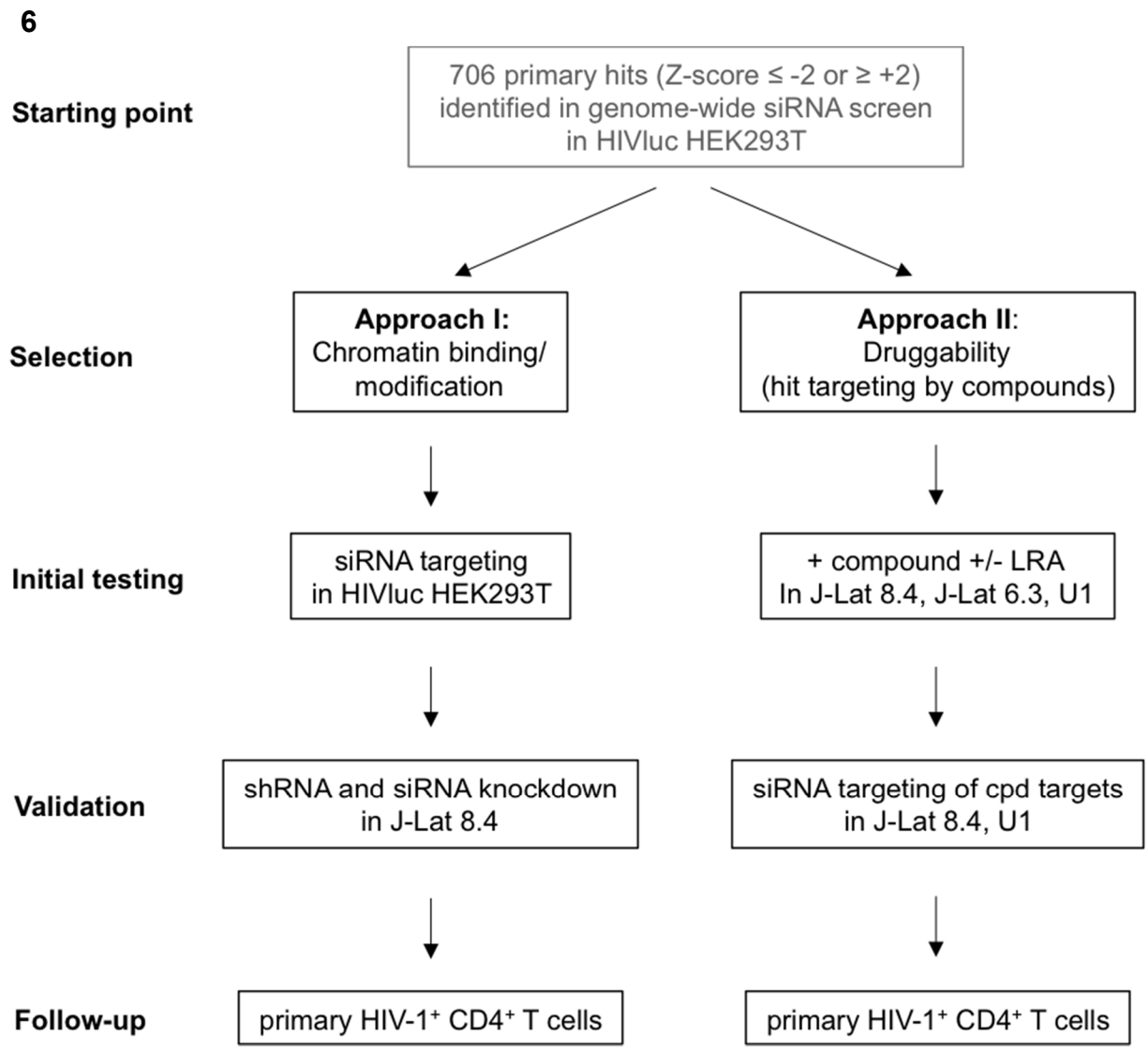

Figure 6: Graphical scheme on hit selection and follow-up strategies to identify novel candidates. Left arm) Selection of hits based on the presence of chromatin binding/modifying domains and their verification strategy. **Right arm)** Selection of hits based on their druggability (here referred to as hits, which can be inhibited by available compounds) and their verification strategy.

3.3 Approach I: Chromatin targets

3.3.1 Test of target hits in the initial screening system

For the first approach, the initial 706 primary screening hits were checked against publications listing chromatin associated proteins (Arrowsmith et al., 2012; Bottomley, 2004; de la Cruz et al., 2005; Patel and Wang, 2013; Talbert and Henikoff, 2010). The selection criteria for the first approach followed the assumption that chromatin modifications and involved factors can influence proviral latency. 10 hits were found to possess domains known to interact with chromatin, as shown in **Table 13**, even though this number likely underestimated the actual number of hits meeting these criteria. The selected hits were followed up on. The experimental setup followed the initial screening setup with the difference that four independent siRNAs per candidate host factor were tested individually. Staying in line with the initial screening, an increase in luciferase signal as derived from increased luciferase expression from the HIV-1 LTR promotor upon knockdown of a host factor would point towards its potential restrictive capacity on HIV-1 transcriptional processes. The results are shown in **Figure 7**.

Table 13: Screening hits identified to possess chromatin binding and/or modification properties.

Z-score	NCBI-official symbol	NCBI-official full name	Protein domains	reported HIV interactions
4.588	BRD4	bromodomain containing 4	bromo	among others Li et al., 2013; Mbonye et al., 2013; Taube & Peterlin, 2013
4.4118	MSH6	mutS homolog 6	PWWP	not announced
4.2379	SMYD2	SET and MYND domain containing 2	HMT	not announced
2.8281	SETD3	SET domain containing 3	HMT	not announced
2.4388	TRRAP	transformation/transcription domain-associated protein	others	Brès et al., 2009; Gautier et al., 2009
2.3053	CXXC1	CXXC finger protein 1	PHD	Gautier et al., 2009
2.2635	CBX6	chromobox homolog 6	chromo	not announced
2.1472	KAT6B	lysine acetyltransferase 6B	HAT	Gautier et al., 2009
2.058	ASXL3	additional sex combs like 3 (Drosophila)	PHD	Zhou et al., 2008
2.0267	USP22	ubiquitin specific peptidase 22	others	not announced

bromo: bromodomain, chromo: chromodomain, HAT: histone acetyltransferase, HMT: histone methyltransferase, PHD: plant homeodomain, PWWP: proline-tryptophan-tryptophan-proline containing domain.

Luciferase signal was measured in HIVluc HEK293T (*env* deleted by frameshift mutation, luciferase in place of *nef*) 72h post-knockdown, determining the potential influence of the host factor on HIV-1 transcription processes **Figure 7A**). A panel of non-targeting siRNAs was transfected, the luciferase counts were set to 100% for the negative controls and the results of all other siRNAs were normalized to them. As an internal control, a siRNA targeting luciferase was transfected (designated si luciferase), leading to a decrease in signal by ~90% and thereby validating the assay functionality. As positive controls, siRNAs targeting either BRD4 or CYLD were used, leading to an increase of luciferase signal beyond the negative control. Of note, CYLD is not chromatin associated but evokes its effect by indirectly regulating NFκB. An increase in luciferase signal, comparable to the results for the BRD4 knockdown, was detected upon silencing of the transformation/transcription domain-associated protein (TRRAP) (**Figure 7A**). This result led to further testing of TRRAP regarding its potential influence in HIV-1 latency.

In order to validate the luciferase results, the same panel of siRNAs was transfected simultaneously in HEK293T cells. This allowed the identification of a potential effect on cell viability (**Figure 7B**) measured by ATPlite. The panel of non-targeting siRNAs was set to 100% and all other results normalized to it. As internal control, validating the assay functionality, a siRNA targeting the ribosomal protein 27 (designated as 'si tox control'), which is essential for cell survival, was transfected. The knockdown of this internal control resulted in a decrease of viability by around 90%. All other tested siRNAs resulted in a decrease of maximally 30%, suggesting that RNAi silencing only minimally influenced cell viability (except siCYLD #2).

In a final setting, the knockdown efficiency of each tested siRNA was determined by RT-qPCR (**Figure 7C**). For this, HEK293T cells were transfected with siRNA, samples were harvested after 48h and total RNA was isolated for each sample. Each gene of interest was internally normalized to GAPDH, serving as housekeeping gene. Furthermore, a fold change for each tested host factor was determined with the averaged non-targeting controls. Most siRNAs efficiently silenced their targets.

In summary, silencing of host factors by siRNA has led in some cases to an increase in luciferase signal. This increase was specific for the knockdown of the given factor. This was further confirmed by viability testing, in which no tested siRNA led to a toxic effect, which could bias the luciferase read-out. In addition, the specific targeting of host factor by siRNA was confirmed on mRNA level. TRRAP was confirmed as hit and chosen for further testing in J-Lat clone 8.4 latency model.

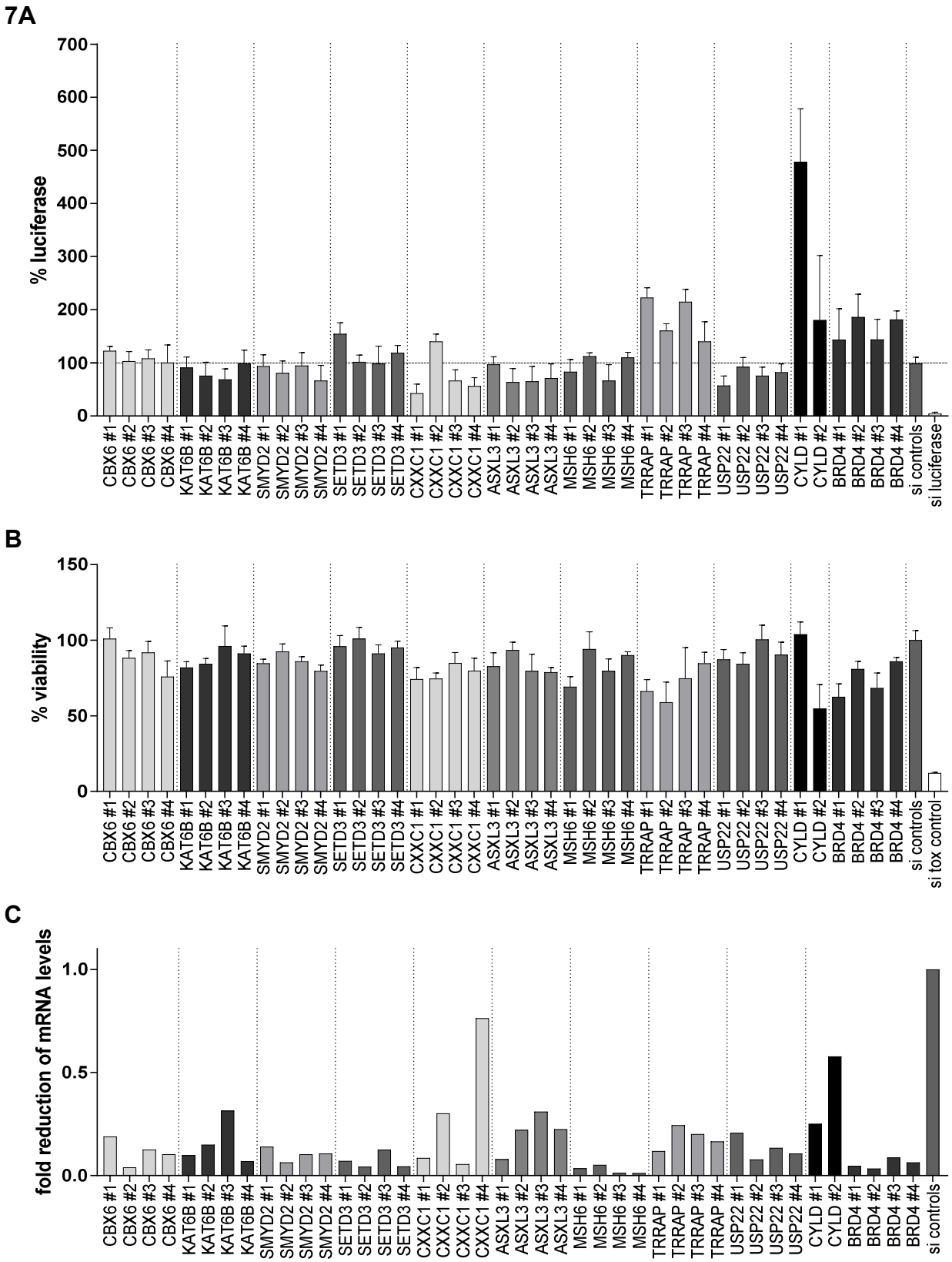

Figure 7: siRNA knockdown results of chosen hits. A) Luciferase read-out in HIVluc HEK293T cells and **(B)** viability read-out in HEK293T cells 72h post siRNA transfection. Four individual siRNA per host factor were tested individually and in quadruplicates in a 384 well plate setting. The results for all applied non-targeting siRNA controls were averaged, set to 100% and all other values normalized to the control. The combined results of three independent experiments are shown including standard deviation.

C) Fold change of host factor knockdown on mRNA level tested in HEK293T cells 48h post siRNA transfection as measured by RT-qPCR. Each siRNA was tested individually in triplicates in a 96 well plate setting.

3.3.2 Establishment of J-Lat 8.4 induction

In order to determine the optimal stimulus concentration and time point of read-out, J-Lat (clone 8.4) cells were treated with four different LRAs, i.e. TNFα, prostratin, SAHA or sodium butyrate. The LRAs were applied at different concentration for either 24h or 48h followed by flow cytometric analysis for viable cells and GFP positive cells, to determine the optimal concentration to induce reversal of latency (as measured by GFP positive cells) without inducing cell toxicity. The results are shown in **Figure 8** and a scheme on how J-Lat cells were generated (Jordan et al., 2003) and work is provided in **Figure 4**.

High concentrations (up to 270ng/ml) of TNFα, a T cell activating LRA, did not negatively affect cell viability. TNFα concentration, as low as 1.11ng/ml, could induce minimal GFP expression. J-Lat 8.4 cells showed up to 20% of GFP positive cells after 24h of stimulation, which increased up to 30% of GFP positive cells after 48h at the highest concentration applied (**Figure 8A**).

Prostratin (also a T cell activating LRA) treatment showed 20% reduction in viability when the highest concentration of 135μM was applied. This decrease in viability was even more drastic upon 48h of treatment leading to a cell death greater than 50%. The minimum concentration to induce GFP positive cells in this assay system was determined to be at 1.67μM. The highest concentration of prostratin could induce almost 30% of GFP positive cells after 24h, and less after 48h that was accounted to the high toxicity of prolonged prostratin exposure (**Figure 8B**).

SAHA (an HDACi and non-T cell activating LRA) treatment resulted in 20% reduction of viability after 24h when used at high concentrations. Prolonged treatment for 48h showed high toxicity. 2.5μM SAHA was seen to induce minimal GFP expression. The highest percentage of GFP, of almost 20%, was induced at a concentration of 22.5μM after 24h, which did not increase further after 48h of treatment (**Figure 8C**).

The results for sodium butyrate were comparable to the results of SAHA, the other tested HDACi. 125mM, the highest concentration tested, of sodium butyrate led to a drastic decrease (up to 40%) in cell viability after 24h and to almost 100% after 48h. At 15mM the maximum of 30% GFP induction was reached after 24h. Prolonged sodium butyrate treatment did not lead

to an increase in GFP positive cells, which was accounted to its high toxicity. A concentration of 1.667mM was determined to induce minimal GFP expression (**Figure 8D**).

In summary, all tested stimuli could induce GFP expression in J-Lat 8.4 cells to a various degree. The influence on cell viability was more pronounced after 48h of LRA treatment, while less after 24h. Due to this, the assay duration was set to 24h for all further experiments. The concentrations were chosen to be 10ng/ml TNFα, 5μM prostratin, 2.5μM SAHA, and 5mM sodium butyrate. Those concentrations led to GFP induction without reaching the maximum, which allows the detection of additional effects. In addition, the concentrations are in line with publications using the same model (Blazkova et al., 2009; Zhu et al., 2012).

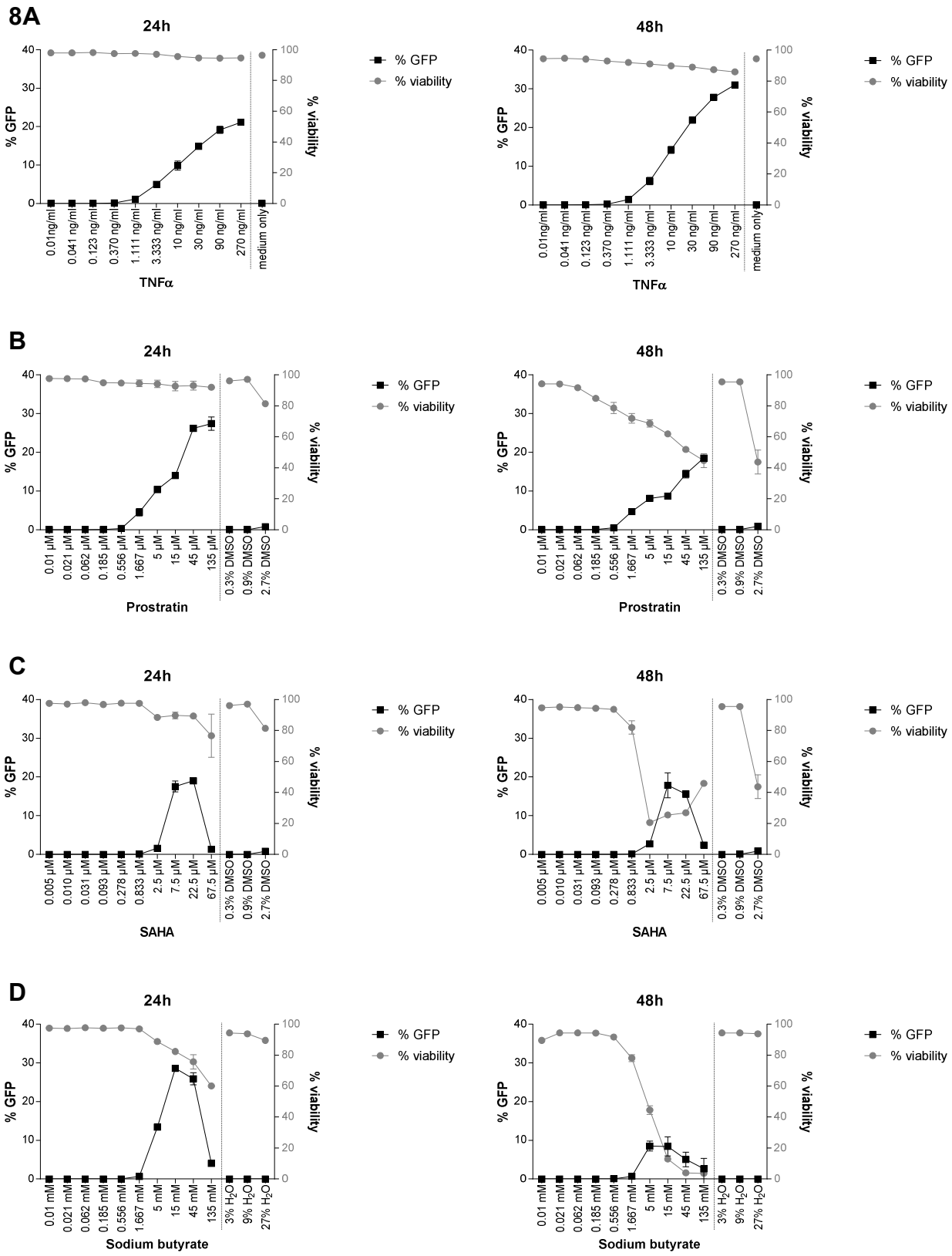

Figure 8: Reversal of latency in J-Lat 8.4 cells in dependence of stimulus concentration. J-Lat 8.4 cells were treated with different concentrations of TNFα **(A)**, prostratin **(B)**, SAHA **(C)** or sodium butyrate **(D)** for 24h and 48h. % Viability (right y-axis) in grey and %GFP positive cells (left y-axis) in black were assessed by flow cytometry. Each point was measured in technical duplicates and standard deviation was indicated.

3.3.3 Inducible shRNA encoding J-Lat 8.4 cells - establishment of experimental system

TRRAP is a highly conserved adapter protein, which is found in multiprotein complexes with HAT activity without possessing HAT activity on its own. It recruits HATs to facilitate acetylation of histones and by this supports transcription. TRRAP is further involved in cell cycle progression and DNA repair (Ard et al., 2002; Ikura et al., 2000; McMahon et al., 1998, 2000).

To verify TRRAP involvement in latency reversal, stable J-Lat 8.4 cells were generated that contained vectors where TRRAP silencing could be elicited including negative and positive control cells, i.e. encoding shRNAs against no cellular target or against BRD4, respectively. For this, the so-called TRIPZ system was chosen, i.e. those vectors encode an shRNA against a cellular target, along with a *rfp* gene under a tetracycline depend promoter. Knockdown of host factors is only achieved in the presence of doxycycline and can be monitored by RFP expression, while reversal of latency in J-Lat cells can be measured by expression of GFP. This test system allowed for determination of double positive cells. For this, cells were transduced with lentiviral particles, then selected with puromycin over five days, followed by doxycycline induction of the shRNA along with RFP (being expressed from the same tetracycline-dependent promoter). The doxycycline induction was tested in two control cell lines encoding either a non-silencing shRNA or no shRNA. Two different concentration of doxycycline, either 1µg/ml or 2µg/ml, respectively, were tested for induction of shRNA along with RFP. Doxycycline was replenished every 24h. As seen in **Figure 9A**, 1µg/ml doxycycline treatment for 96h led to the same level of RFP induction as 2µg/ml, the maximum level of RFP expression was found to be around 60%. For all further experiments, 1µg/ml of doxycycline was applied for induction of the TRIPZ constructs.

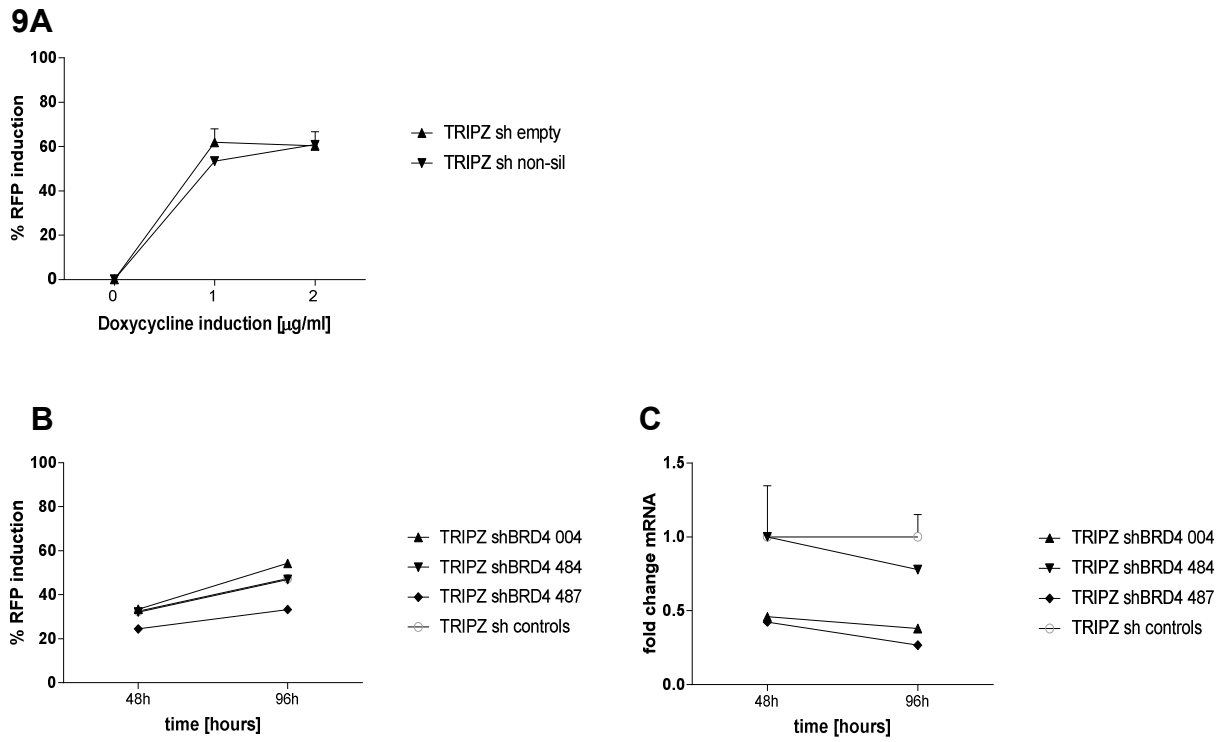

Figure 9: Establishment of TRIPZ derived stable J-Lat cells. A) RFP induction in dependence of doxycycline concentration determined by flow cytometry after 96h of induction. **B)** Determination of RFP levels in dependence of doxycycline duration measured after 48h and 96h. **C)** Determination of knockdown on mRNA level by RT-qPCR (same samples as in (**B**), standard deviation derived from the two negative controls which were averaged and set to one, and all other values normalized to those.

In the next step, the optimal duration of doxycycline induction was tested. For this, the control cell lines as well as the three generated cell lines containing different shRNA targeting BRD4 (as positive control) were tested for RFP induction by flow cytometry and for knockdown of BRD4 by qRT-PCR at either 48h or 96h after induction. The results are shown in **Figure 9B** and **C**. A prolonged doxycycline treatment resulted in higher RFP levels (**Figure 9B**) and led to a better knockdown (**Figure 9C**). Of note, even though all stable cell lines could be induced with doxycycline to a varying degree, the knockdown capacity of each shRNA varied greatly.

In a final experiment, the doxycycline induced stable cell lines were exposed to prostratin stimulation for 24h and the cells analyzed for double positive cells, whereas RFP correlated to the knockdown of host factor targeted and GFP correlated to reactivation of latency (as determined by flow cytometry). The results are shown in **Figure 10**. Medium treatment led to average 5% of double positive cells. The stable cell line encoding TRIPZ shBRD4 004 showed even around 10% of double positive cells without additional stimulation. Upon treatment with prostratin, an increase in double positive cells was seen for all tested cell lines. The induction

capacity was greatest for the control cell line. The TRIPZ shBRD4 004 cell line showed a slight increase in double positive cells over the negative control cell line, whereas TRIPZ shBRD4 484 and 487 did not. The results did not well correlate to the knockdown results (determined in **Figure 9C** at 96h), as the knockdown with TRIPZ shBRD4 484 was not as efficient as the knockdown for TRIPZ shBRD4 487, but both showed comparable numbers of double positive cells with and without stimulation.

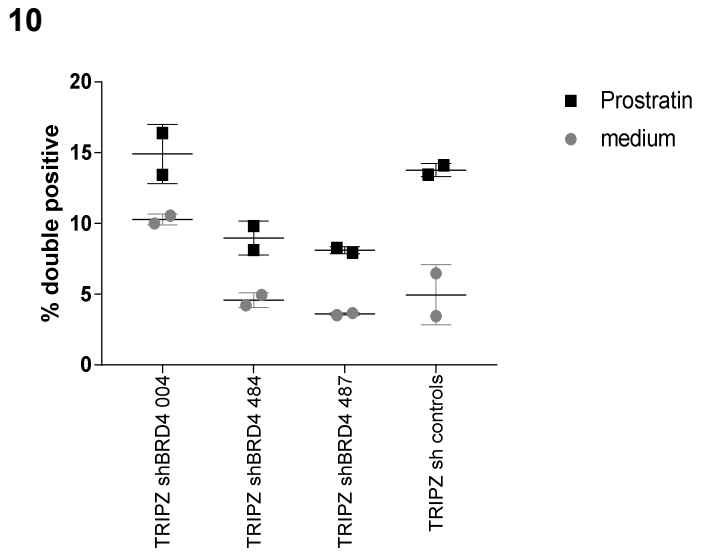

Figure 10: Determination of double positive J-Lat cells upon induction and stimulation. Stable inducible J-Lat 8.4 cells containing either shRNA encoding against the cellular target BRD4 or non-target encoding (controls) were stimulated for 24h with prostratin (dark squares) or medium (grey circles). Percentage of double positive cells was determined by flow cytometry. GFP determined the level of latency reversal and RFP served as measure for targeted knockdown. The experiment was measured in technical duplicates and standard deviation was indicated.

In summary, the TRIPZ knockdown approach led to a reduction of host factor of about 2.5-fold on mRNA level and to maximum RFP expression of 60%. This approach needs induction of shRNA and RFP by doxycycline for prolonged period including the replenishment of the antibiotic due to its short half-life. In addition, the background reactivation was considered rather high. Due to this, we decided to change to a more efficient system. The RIPZ approach, as from here on referred to, allowed the expression of shRNA and RFP from a constant active promoter.

3.3.4 RIPZ plasmid generation - cloning of non-inducible shRNAs

Since the induction of pTRIPZ stable cell lines did not result in high percentage of RFP positive cells, an approach was chosen without the need for doxycycline induction. For this, the GFP gene from the pGIPZ backbone was replaced with the RFP gene from the pTRIPZ backbone, resulting in a construct, which expresses the shRNA and RFP gene under a constant active promoter, the new construct was designated pRIPZ.

As there were no compatible restriction sites present in both constructs, a fusion PCR approach was chosen, which is illustrated in **Figure 11**. For this, three fragments were amplified by PCR. Two fragments from the pGIPZ backbone were amplified, resulting in a 634bp fragment (referred to as fragment I, primer P1 and P2, annealing temperature 52°C) with an XbaI restriction site and an overhang identical to the beginning of the RFP gene and a 695bp fragment (referred to as fragment III, primer P3 and P4, annealing temperature 54°C) containing an XhoI site and an end identical to the end of the RFP gene. Additionally, one fragment was amplified from the pTRIPZ backbone, spanning the 1308bp long RFP gene (referred to as fragment II, primer P5 and P6, annealing temperature 53°C) including overhangs identical to the sequence shortly before and after the GFP gene. Successful PCR amplification was confirmed by the presence of bands at the specific height on an agarose gel (**Figure 11E**). In a next step 5µl of PCR product from II and I were mixed, and a PCR was run (for the first 10 cycles without primers, followed by the addition of primer P1 and P6 for further 30 cycles). The resulting fragment IV was the joint product of fragments II and I with an overall length of 1,378bp (**Figure 11E**). Mixing of 5µl PCR product IV and III, followed by PCR (for the first 10 cycles without primers, followed by the addition of primer P1 and P4 for further 30 cycles), led to the production of the final 2,686bp fragment (**Figure 11F**). This fragment was gel purified and via restriction digestion with XbaI and XhoI cloned into the pGIPZ backbone. The correct sequence of the newly produced pRIPZ backbone was confirmed by sequencing.

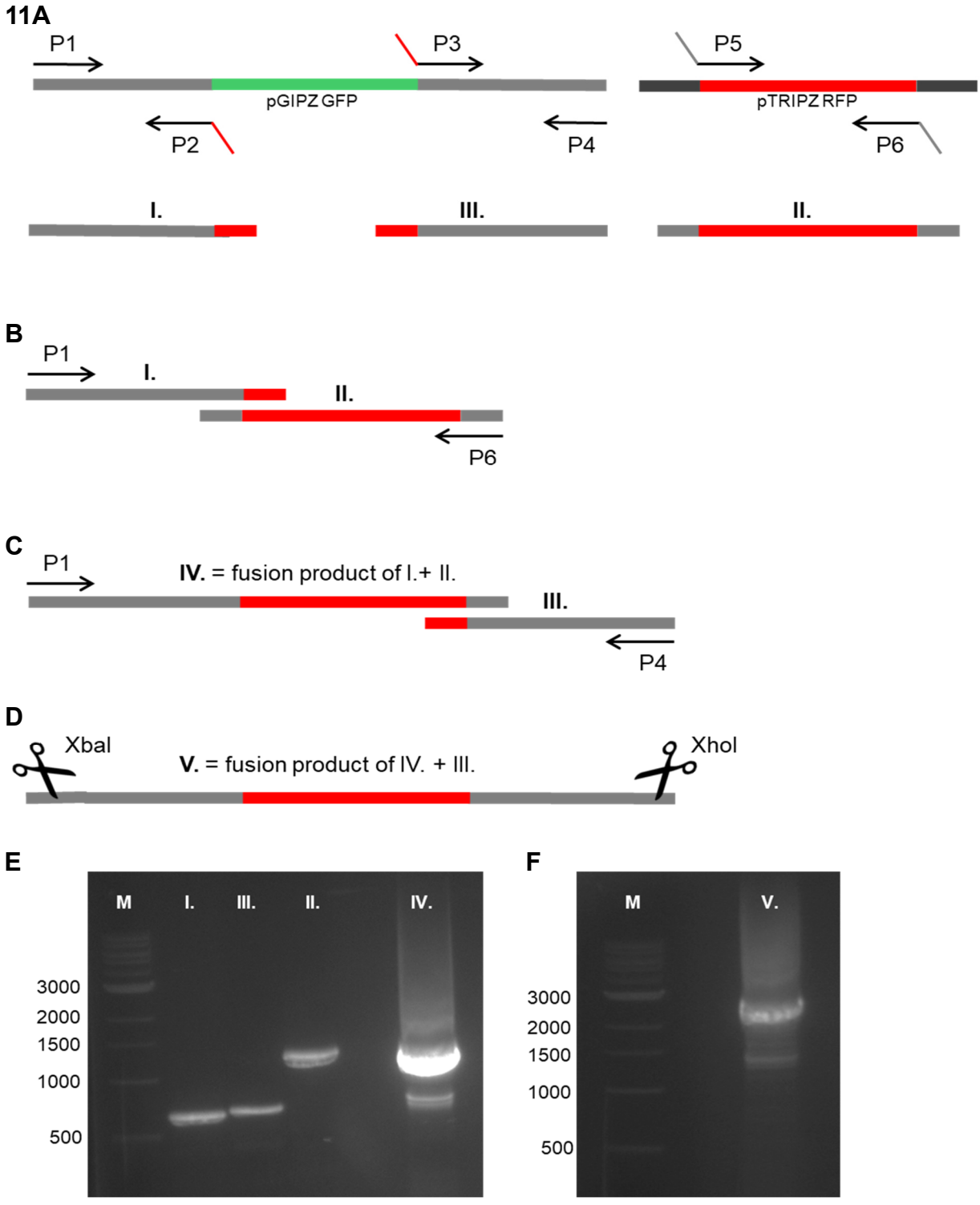

Figure 11: Generation of a pRIPZ plasmid. Scheme of the PCR-based strategy executed to generate a plasmid containing the RFP gene under a constant active promoter **(A-D)**. Verification of PCR amplified fragments by agarose gel electrophoresis **(E, F)**. Expected fragment size: Fragment I 634bp, fragment II 1,308bp, fragment III 695bp, fragment IV 1,378bp, fragment V 2,686bp. M= marker.

Further, the generated pRIPZ plasmid was tested for its functionality. For this, HEK293T cells were transfected and expression of RFP was checked by fluorescent microscope. As seen in **Figure 12**, RFP expression can be readily detected after 48h post transfection without the addition of doxycycline. Thus, the generation of a non-inducible RFP expression plasmid was successful.

12

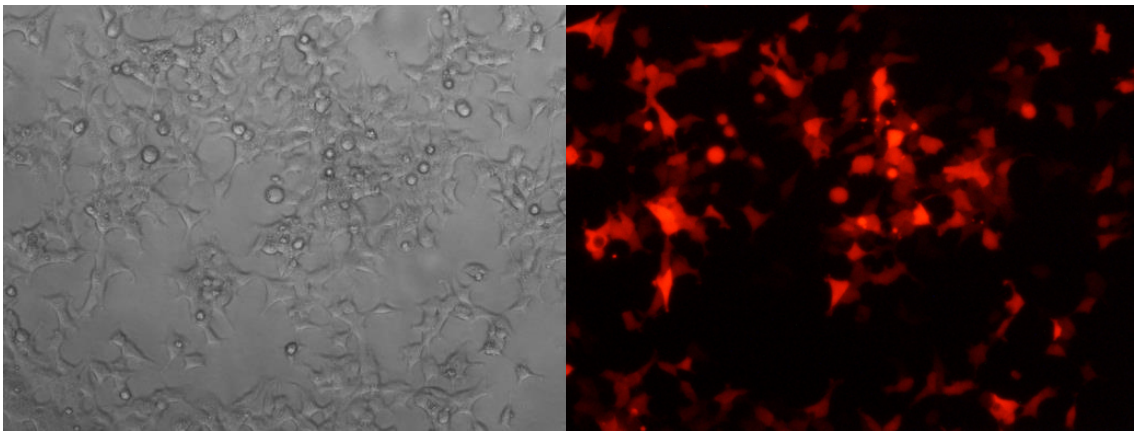

Figure 12: Confirmation of pRIPZ generation. HEK293T cells were transfected with newly generated pRIPZ plasmid, presence of RFP was checked microscopically 48h post-transfection.

In a final set of experiments, the different shRNA in the pTRIPZ backbone were cloned via restriction digest into the pRIPZ backbone. Successful cloning was confirmed by plasmid sequencing.

3.3.5 Non-inducible shRNA encoding J-Lat 8.4 cells - establishment of experimental system

In order to test the effect of host factor knockdown in J-Lat 8.4 cells, lentiviral particles for all pRIPZ constructs were produced and used to transduce J-Lat 8.4 cells. The transduced cells were selected with puromycin for at least a week. The percentage of RFP expressing cells of the different stable cell lines was evaluated by flow cytometry and the knockdown efficiency was determined by RT-qPCR. As a positive control shCYLD was used instead of shBRD4, as the effect of CYLD knockdown was assumed to be greater (as seen in **Figure 7A** for the luciferase results in HIVluc HEK293T) and due to this easier to determine. The results are shown in **Figure 13** (for CYLD **Figure 13A** and **B**, for TRRAP **Figure 13C** and **D**, respectively). The RFP results (**Figure 13A** and **C**) clearly showed that stable cell lines encoding a non-inducible shRNA produced on average 90% of RFP positive cells. This being around 30% more when compared to the RFP results produced from inducible TRIPZ transduced cells (see **Figure 9B**). The knockdown efficiency, as seen in **Figure 13B** and **D**, showed a mRNA decrease to a varying degree, ranging from around 10-fold reduction, as seen for the best shRNA (RIPZ shCYLD 89) to less than 2-fold reduction (RIPZ shTRRAP 543).

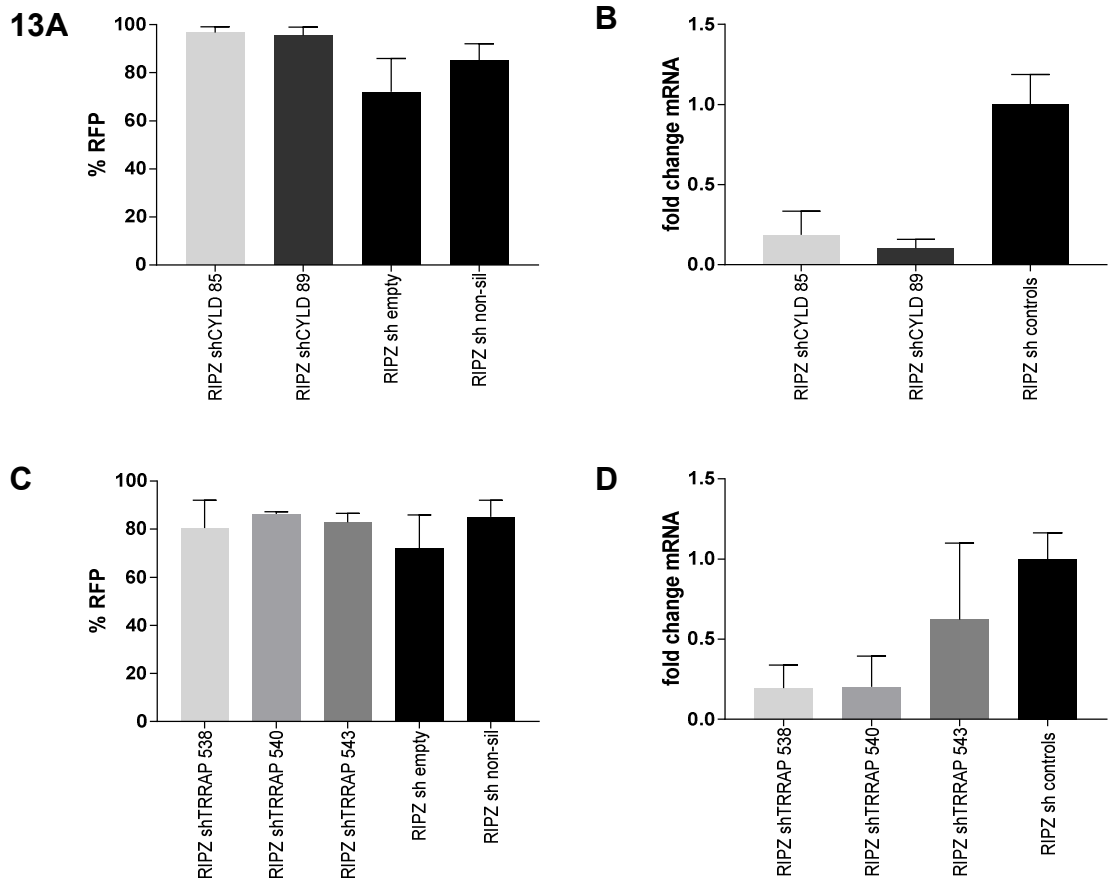

Figure 13: Correlation of RFP expression and host factor knockdown. Stable pRIPZ J-Lat 8.4 cells were generated and tested for the expression of RFP as determined by flow cytometry and for the level

of host factor knockdown as determined by RT-qPCR. Results for CYLD used as positive control **(A, B)**, results for TRRAP as factor of interest **(C, D)**. The experiment was performed in technical duplicates and standard deviation was indicated.

Further, the RFP expression and host factor knockdown level were determined under continued puromycin selection pressure, as seen in **Figure 14A** for the different stable shTRRAP containing cell lines. Even though, an additional week of puromycin treatment could increase the number of RFP expressing cells further, the knockdown efficiency for all tested cell lines was halved (**Figure 14B**). In an additional experiment, the knockdown stability over one freeze-thaw cycle was tested. As seen in **Figure 14C**, the cells expressed RFP to high levels after thawing but the knockdown (**Figure 14D**) was completely lost.

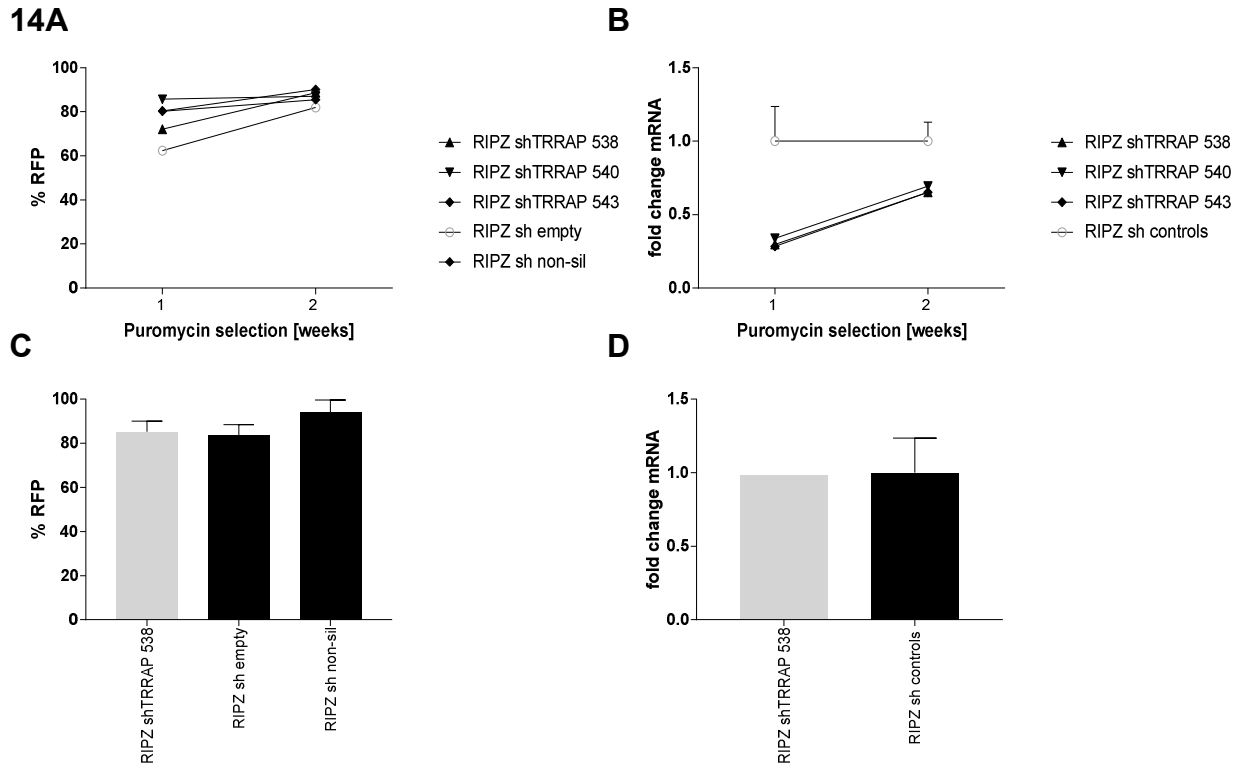

Figure 14: Prolonged puromycin selection of stable RIPZ cells in correlation to knockdown levels. Stable pRIPZ derived knockdown J-Lat 8.4 cells were checked for % RFP expression **(A)** by flow cytometry (single measurements only) and for knockdown **(B)** on mRNA level by RT-qPCR after one week and two weeks under continued puromycin selection. Negative control cell lines were averaged, and the other values normalized to the control. **C)** Generated knockdown cell lines were exposed to one freeze-thaw cycle and % RFP expression was checked via flow cytometry and for knockdown of host factor **(D)** by RT-qPCR on mRNA level.

In summary, the RIPZ approach led to high numbers of stable RFP expressing cells. The knockdown efficiency was initially robust but was gradually lost. The test period of the stable cell needed to be kept short.

3.3.6 pRIPZ knockdown of TRRAP

In a final set of experiments, stable shRNA encoding J-Lat 8.4 cell lines were stimulated or medium treated for 24h and analyzed by flow cytometry for double positive cells, expressing RFP and GFP for the shRNA mediated knockdown and the reversal of latency, respectively. The results are shown in **Figure 15**. Two stable cells lines encoding for a non-silencing shRNA or no shRNA served as negative controls, representing the level of double positive cells which can be attributed to the stimulus itself. Further, two stable cell lines were included targeting CYLD serving as positive control. For the host factor of interest, TRRAP, three cell lines were tested. For this, stable knockdown cell lines were exposed to a stimulus or medium and analyzed by flow cytometry for an increase in double positive cells 24h post treatment.

Treatment of stable knockdown cell lines with medium only (**Figure 15A**) did not lead to more than 3% of double positive cells and was not considered significant. Upon treatment with TNFα (**Figure 15B**) a clear increase in double positive cells was seen only for shCYLD89. Treatment with prostratin (**Figure 15C**) led to a marked increase in double positive cells as seen for both positive controls, whereas no effect was seen in cell lines targeting TRRAP. Upon treatment with either SAHA (**Figure 15D**) or sodium butyrate (**Figure 15E**), an increase in double positive cells was only seen for the positive controls, but not for the TRRAP knockdown cell lines. Successful knockdown on mRNA level was determined by RT-qPCR as shown before (**Figure 13B** and **D**).

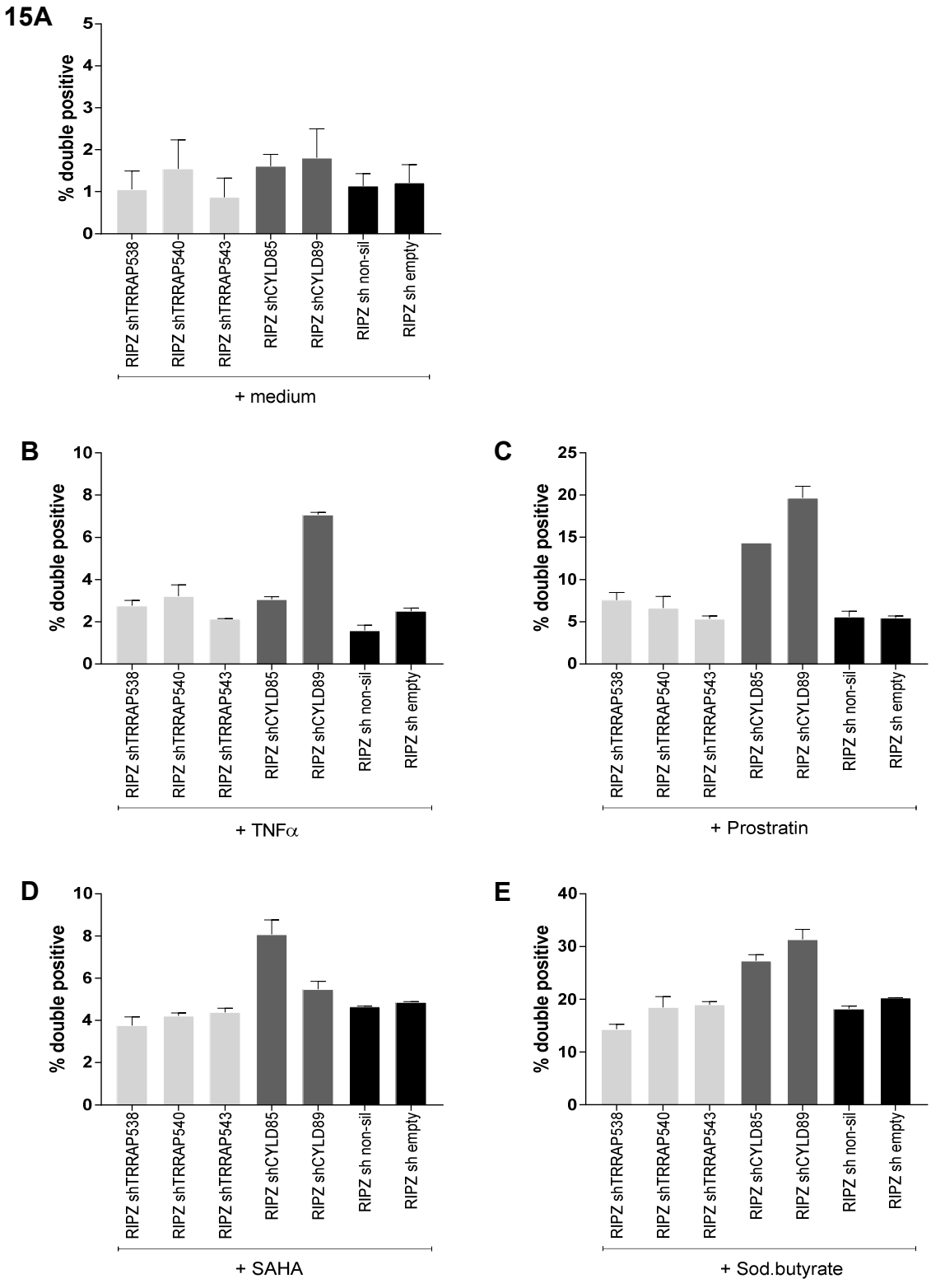

Figure 15: Effect of host factor knockdown in combination with different LRAs. Stable pRIPZ derived knockdown J-Lat 8.4 knockdown cells were generated and treated with either medium **(A)**, TNFα **(B)**, prostratin **(C)**, SAHA **(D)** or sodium butyrate **(E)** for 24h. % Double positive cells (RFP and GFP) were assessed by flow cytometry. The experiment was performed twice and in technical duplicates, the result of one representative experiment was shown and standard deviation is indicated.

In summary, different stable cell lines were generated and exposed to medium or stimuli. The stimulation of knockdown cell lines targeting TRRAP did not lead to an increase in number of double positive cells beyond the numbers achieved with the negative controls whereas targeting of CYLD, used as positive control, did.

3.3.7 Transient knockdown of host factors by siRNA - establishment of experimental system

In order to confirm the results generated with the stable shRNA knockdown approach, a transient knockdown approach was chosen utilizing electroporation of siRNAs. This approach allowed detection of increased GFP positive cells by flow cytometry. In an initial experiment, four individual siRNAs either against CYLD (as positive control) or against TRRAP were tested for their potential in decreasing host factor mRNA levels as determined by RT-qPCR. Successful electroporation was confirmed by electroporating pMax EGFP (provided by the manufacturer) and GFP expression was microscopically checked after 24h (**Figure 16A**). The knockdown results for electroporated J-Lat 8.4 cells are shown in **Figure 16B** and **C** for CYLD and TRRAP, respectively. Knockdown of host factors by different siRNAs proved successful to a varying degree and only the best siRNAs were chosen for all further experiments, i.e. siCYLD #3 and siTRRAP #3. Of note, the proof of CYLD and TRRAP knockdown was only confirmed on mRNA level but not on protein level. In addition, electroporated cells were checked by fluorescence microscope to exclude GFP induction upon electroporation, which was not observed.

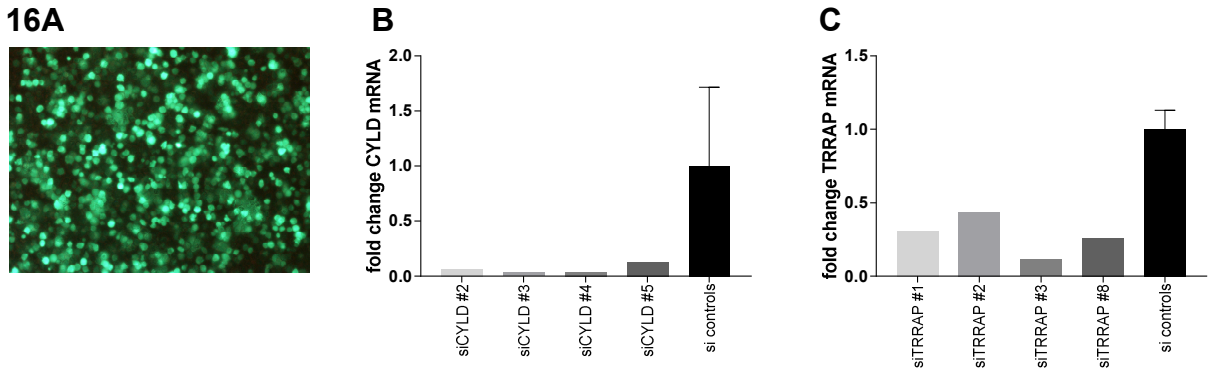

Figure 16: Establishment of siRNA mediated knockdown of host factors by electroporation. J-Lat 8.4 cells were electroporated with pMAX EGFP plasmid and microscopically checked for the presence of GFP **(A)** after 24h. Determination of CYLD knockdown levels **(B)** and TRRAP knockdown levels **(C)** in electroporated cells, as determined on mRNA level by RT-qPCR for four individual siRNAs per target. Samples were taken 24h post electroporation, two non-targeting controls were averaged, and the other values normalized to it.

3.3.8 Transient knockdown of TRRAP

In a final set of experiments, the effect of transient TRRAP knockdown plus stimulation on the percentage of GFP positive cells was evaluated, to elucidate a potential effect of TRRAP on HIV-1 latency. For this, J-Lat 8.4 cells were electroporated with siRNA and incubated for 24h, then split into equal portions for stimulation or medium treatment for 24h before being analyzed by flow cytometry. Of note, due to cell number limitation for electroporation cuvettes along with the need for enough cells to allow for differential analysis afterwards, it was decided to reduce the number of LRAs from four to two, i.e. including only prostratin and sodium butyrate next to medium for all further experiments.

Treatment of electroporated cells (**Figure 17A**) with medium did not lead to an induction of GFP (**A**, first block), whereas prostratin treatment (**A**, middle block) led to around 6% GFP positive cells for the negative controls used (black column) serving as reference for the stimulus activation capacity. A clear increase, up to 14% in GFP positive cells, was only seen upon knockdown of CYLD (dark grey column) but not for the TRRAP knockdown results (**A**, middle block, light grey column). The increase in GFP positive cells with sodium butyrate treatment (**A**, last block) was less pronounced for all tested targets. Baseline activation was found to be around 8%, upon knockdown of CYLD a slight increase of around 12% was seen and for TRRAP an increase of around 11% was found.

Further, the viability was determined in this experiment (**Figure 17B**), showing that electroporation did not negatively affect cell viability. Addition of prostratin or sodium butyrate led to a slight reduction in viability of maximally 10%, an effect already observed earlier. The knockdown (**Figure 17C**) was confirmed for the positive control CYLD and the host factor of interest, i.e. TRRAP on mRNA level as determined by RT-qPCR.

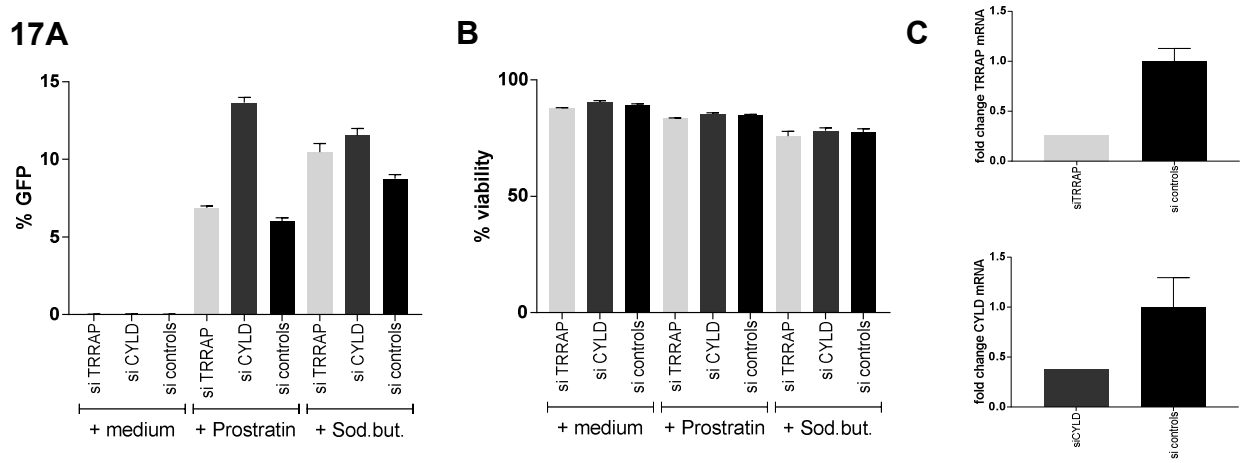

Figure 17: Effect of transient host factor knockdown in combination with two different LRAs. J-Lat 8.4 cells were electroporated with siRNA followed by stimulation with either medium, prostratin or sodium butyrate. % GFP positive cells **(A)** and % viability **(B)** were assessed by flow cytometry. In addition, knockdown on mRNA level **(C)** was determined by RT-qPCR. Results for TRRAP were indicated in light grey, for CYLD in dark grey and for the averaged negative controls in black. Samples were measured in technical duplicates and standard deviation was indicated.

In summary, the siRNA knockdown approach was successfully established and influence of host factor knockdown plus stimulation was tested. Electroporation led to a robust knockdown of both factors on mRNA level, did not reactivate the cells per se and did not negatively impact cell viability. The drastic increase in GFP positive cells upon CYLD knockdown along with prostratin treatment confirmed published results (Manganaro et al., 2014), while knockdown of TRRAP led to a slight increase over the negative control.

3.4 Approach II: Druggability

3.4.1 Compound selection

In a second approach, hits from the primary RNAi screen were selected based on their property to be druggable and are known targets of available compounds. The idea behind is so-called “drug repurposing”, a drug development strategy predicated on the reuse of existing licensed drugs for new medical indications. In this thesis, the aim was to identify compounds for known targets within the hit list that could reverse latency on its own or would elicit latency reversal in combination or in synergy with LRAs. Importantly, the combinational application has been proven advantageous over single compound application, as several pathways have to be targeted to grant latency reversal of the complete reservoir. First, the compounds were identified, then tested for their optimal working concentration and further tested for their effect on latency reversal alone or in combination with an LRA.

To identify potential compounds targeting primary hits two independent databases were employed, i.e. the Drug-Gene Interaction database (DGIbd) (Cotto et al., 2018) and the proprietary Genego database. The DGIbd combines multiple other databases, which allow mining for targets or compounds without restriction to one database only. This database is freely available, whereas the Genego database is proprietary. From the initial 706 primary hits (see **Table S1**, Appendix) only the hits with a Z-score ≥ +2, i.e. being potential restrictive host factors, were considered. This choice was made due to the published positive controls, being restrictive to latency reversal and possessing a +Z-score. The remaining 562 hits were run through both databases revealing 73 hits to be targetable according to the DGIbd and 82 hits according to the Genego database. The hits from both databases were merged and only hits further selected which are targetable according to both databases, leading to 42 hits. The remaining hits were checked for their expression levels with the help of ‘The Human Protein Atlas’ (Uhlén et al., 2015). Inclusion criteria for follow-up hit selection included their expression levels to be ≥ ‘low’ in the category ‘bone marrow and immune system’ and data reliability needed to be consistent according to ‘The Human Protein Atlas’. Upon this final selection step 24 hits remained. Out of the 24 hits 7 hits were randomly chosen, the compounds purchased and tested in J-Lat 8.4 cells. A scheme of the selection strategy is shown in **Figure 18** including the compounds tested and their potential targets.

18

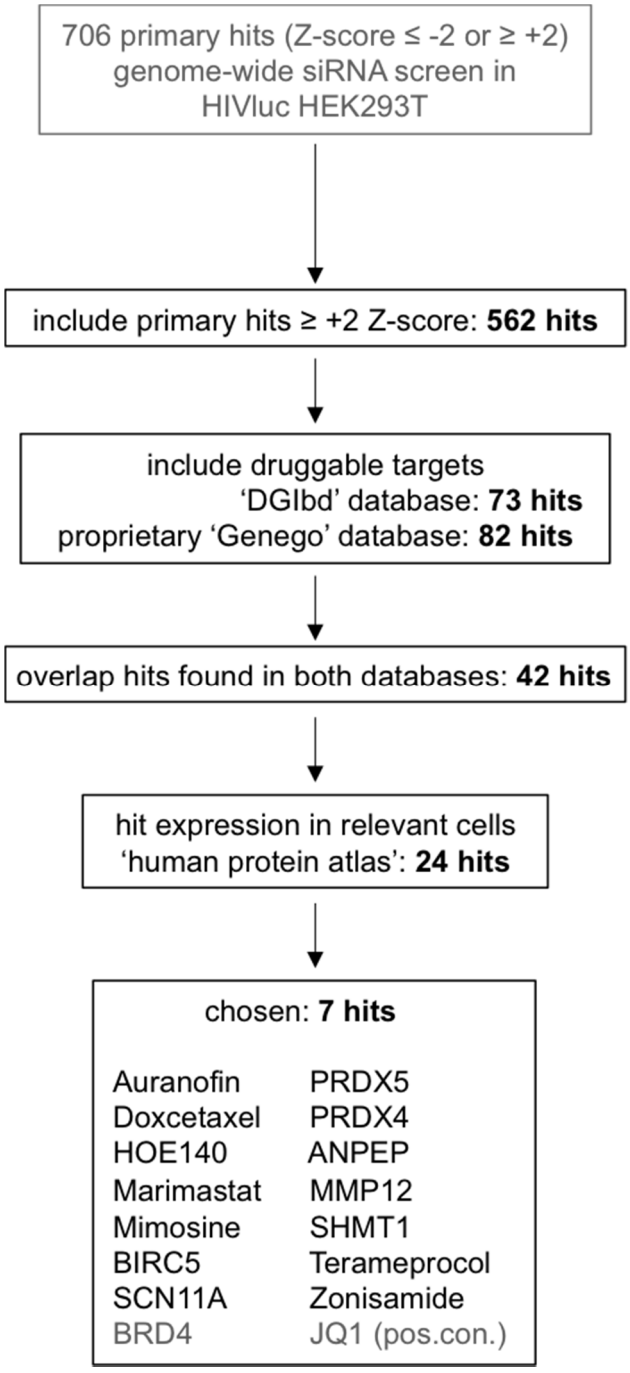

Figure 18: Detailed presentation of compound selection strategy. Selection of compounds was based on the overlap of two different databases (DGIbd (Li et al., 2018) and proprietary Genego database) and further on expression levels of host factors according to 'The Human Protein Atlas' (Uhlén et al., 2015) (inclusion criteria: expression level ≥ low; exclusion criteria: inconsistent data). 7 hits were finally selected plus JQ1 inhibiting BRD4, which served as positive control in further experiments. ANPEP= alanyl aminopeptidase, BIRC5= baculoviral IAP repeat containing 5, MMP= matrix metallopeptidase, PRDX4/5= peroxiredoxin 4/5, SCN11A= sodium voltage-gated channel alpha subunit 11, SHMT1= serine hydroxymethyltransferase 1, BRD4= bromodomain containing protein 4.

3.4.2 Compound titration and test in combination with LRAs

In order to determine the optimal working concentration for the different compounds, a dilution series was prepared for each compound. J-Lat 8.4 cells were treated with the respective compound dilution or with the appropriate solvent controls for 24h. The results are shown in **Figure 19** and the working concentration for all following assays was determined to be 0.2µM for auranofin (**Figure 19A**), 12.5µM for docetaxel (**Figure 19B**), 20µM for HOE140 (**Figure 19C**), 10µM for marimastat (**Figure 19D**), 32µM for mimosine (**Figure 19E**), 2µM for terameprocol (**Figure 19F**), 20µM for zonisamide (**Figure 19G**), and 0.25µM for JQ1 (**Figure 19H**). JQ1 served as positive control as it inhibits the host factor BRD4 and will be used in all further experiments. None of the tested compounds showed induction of GFP greater than 0.2%, and thereby none of the tested compounds could induce reversal of latency on its own.

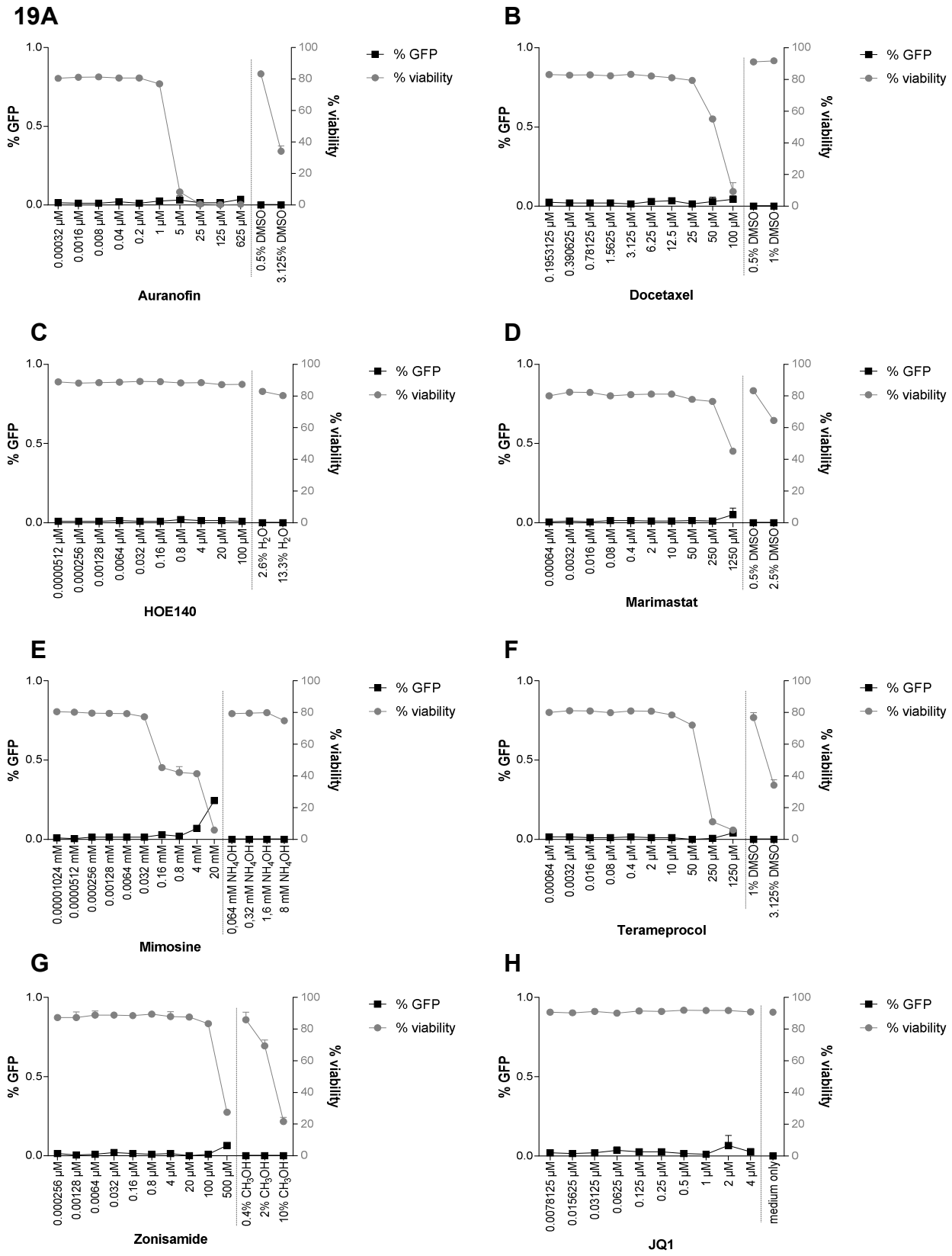

Figure 19: Optimal concentration determination of selected compounds. J-Lat 8.4 cells were treated with different concentrations of auranofin **(A)**, docetaxel **(B)**, HOE140 **(C)**, marimastat **(D)**, mimosine **(E)**, terameprocol **(F)**, zonisamide **(G)** or JQ1 **(H)** as positive control for 24h. % Viable cells (right y-axis) and % GFP induction (left y-axis) were assessed by flow cytometry. Each condition was measured in technical duplicates and standard deviation was indicated.

Next, the compounds were tested along with LRAs to address whether they would elicit latency reversal in combination/synergy (**Figure 20**). JQ1, an inhibitor of BRD4, on its own could not reverse latency in J-Lat 8.4 cells, but with addition of either TNFα or prostratin (both T cell activating LRAs), the number of GFP positive cells almost doubled when compared to stimulus only treatment (**Figure 20H**). Interestingly, only auranofin was found to have a positive effect on latency reversal (**Figure 20A**). Auranofin, supposedly targeting the peroxiredoxin 5 (PRDX5), enhanced reversal of latency in combination with all applied stimuli even though the increase in GFP positive cells was not as outstanding as for the positive control JQ1. Interestingly, mimosine was found to hinder reversal of latency, leading to a decrease in GFP positive cell numbers applied with any LRA (**Figure 20E**).

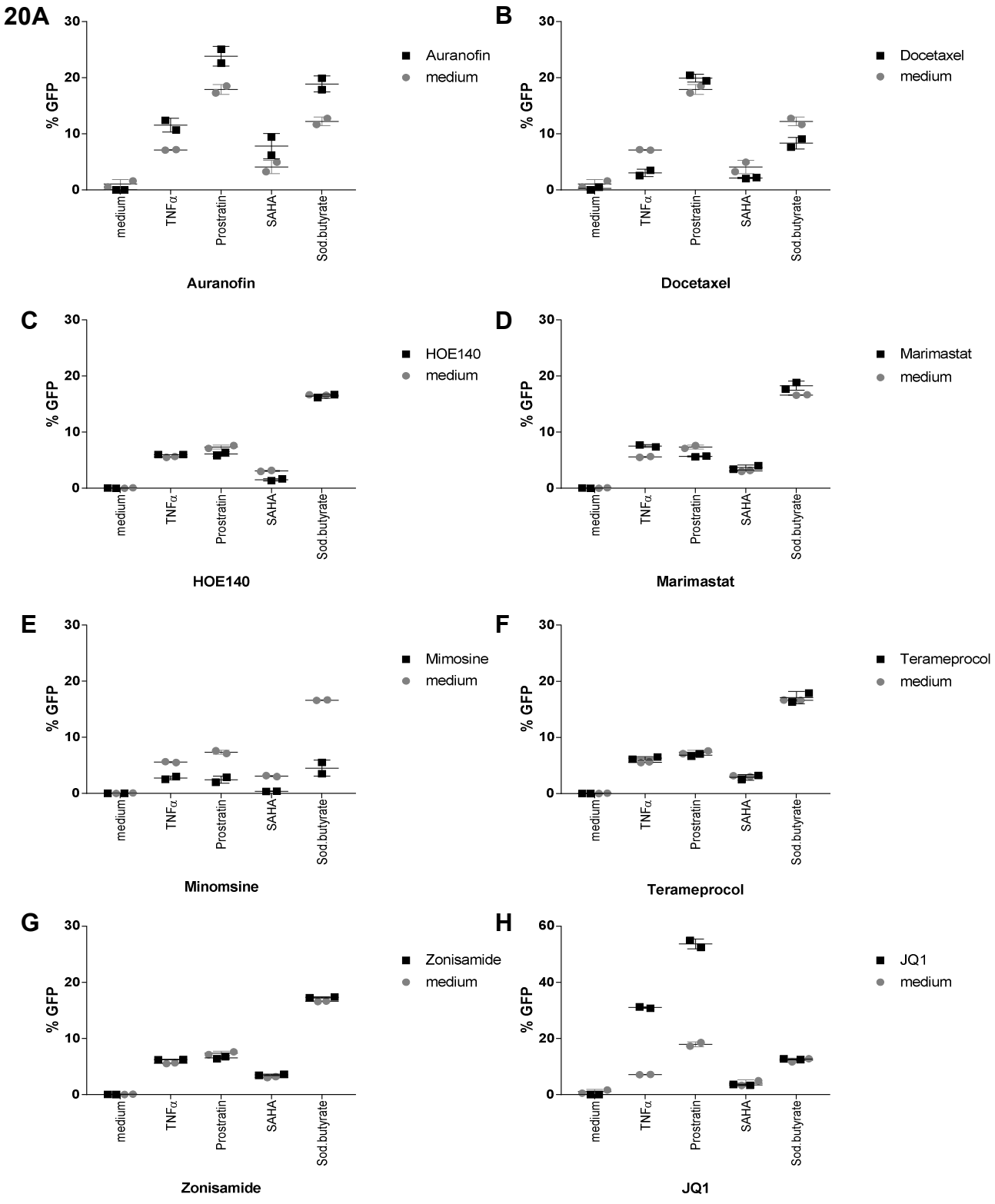

Figure 20: Effect of compounds in combination with different LRAs. J-Lat 8.4 cells were treated with auranofin **(A)**, docetaxel **(B)**, HOE140 **(C)**, marimastat **(D)**, mimosine **(E)**, terameprocol **(F)**, zonisamide **(G)** or JQ1 **(H)** as positive control in combination with either medium, TNFα, prostratin, SAHA or sodium butyrate for 24h. % GFP positive cells were assessed by flow cytometry. Each condition was measured in technical duplicates and standard deviation was indicated.

3.4.3 Targeting PRDX5 by different compounds

Auranofin, as stated by the DrugBank database (Law et al., 2014), targets the primary screening hit PRDX5 and was found to have a positive effect on the reversal of latency in J-Lat 8.4 cells when applied in combination with any stimulus tested. To validate the target of auranofin, three different databases (proprietary Genego database and freely accessible Therapeutic Target Database (Li et al., 2018) and DrugBank database) were researched for additional compounds described to target PRDX5, a host factor involved in detoxification of reactive oxygen species. A graphical overview is shown in **Figure 21**. As further candidate compounds benzoic acid, diminazene and 4hydroxynonenal were identified and tested for their potential to induce the reversal of latency. The Therapeutic Target Database did not list PRDX5 to be targetable by any compound.

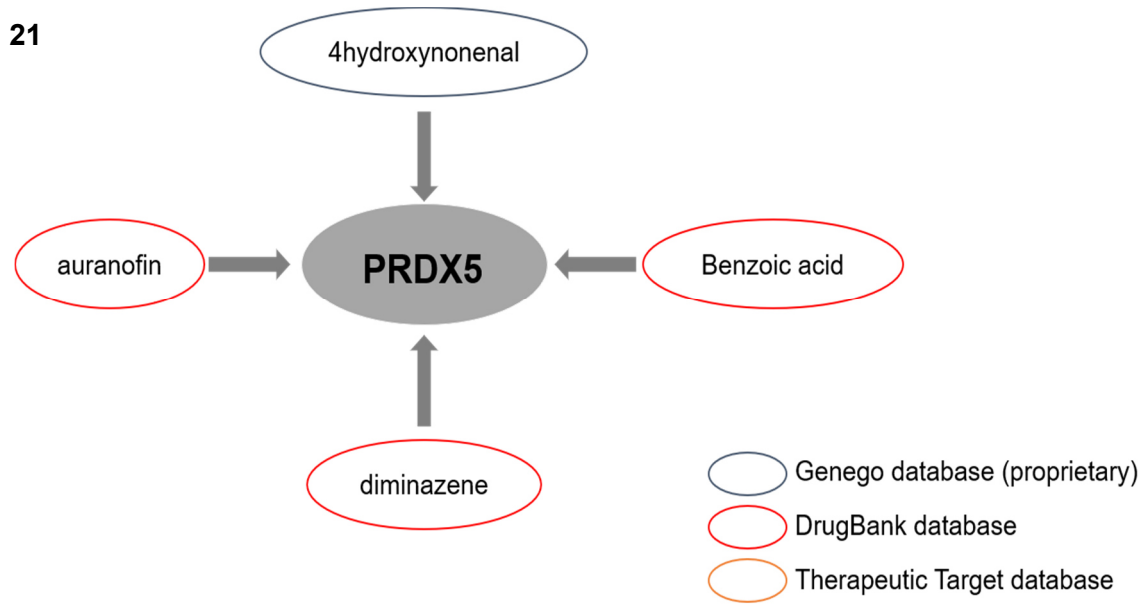

Figure 21: Graphical presentation of compounds targeting the host factor PRDX5. Three different databases were used (proprietary Genego, DrugBank (Law et al., 2014), and TTD (Li et al., 2018) as indicated by colored frames, to identify compounds targeting PRDX5. The TTD database did not list a specific compound to target PRDX5. PRDX5= peroxiredoxin 5

In addition, an inverse search was performed on all compounds to identify all further known cellular targets. **Figure 22** shows all known cellular targets for the different compounds tested as derived from three different databases. Interestingly, but not surprisingly, only very few compounds had only one specific cellular target, most of the compounds targeted several. Of note, 4hydroxynonenal was not listed by the DrugBank database and also not by the

Therapeutic Target Database. Further, the different databases revealed hardly any overlap in target for the different compounds and PRDX5 was not claimed as target of auranofin by any other database. Of importance, auranofin was listed to be inhibiting thioredoxin reductase (TXNRD) family members by two independent databases, a factor situated upstream of the PRDX family. The potential action of auranofin against TXNRDs was also described in several publications (Becker et al., 2000; Hwang-Bo et al., 2017). Due to this, inhibition of TXNRDs by fotemustine (Schallreuter et al., 1990), a specific inhibitor, was included in all further experiments.

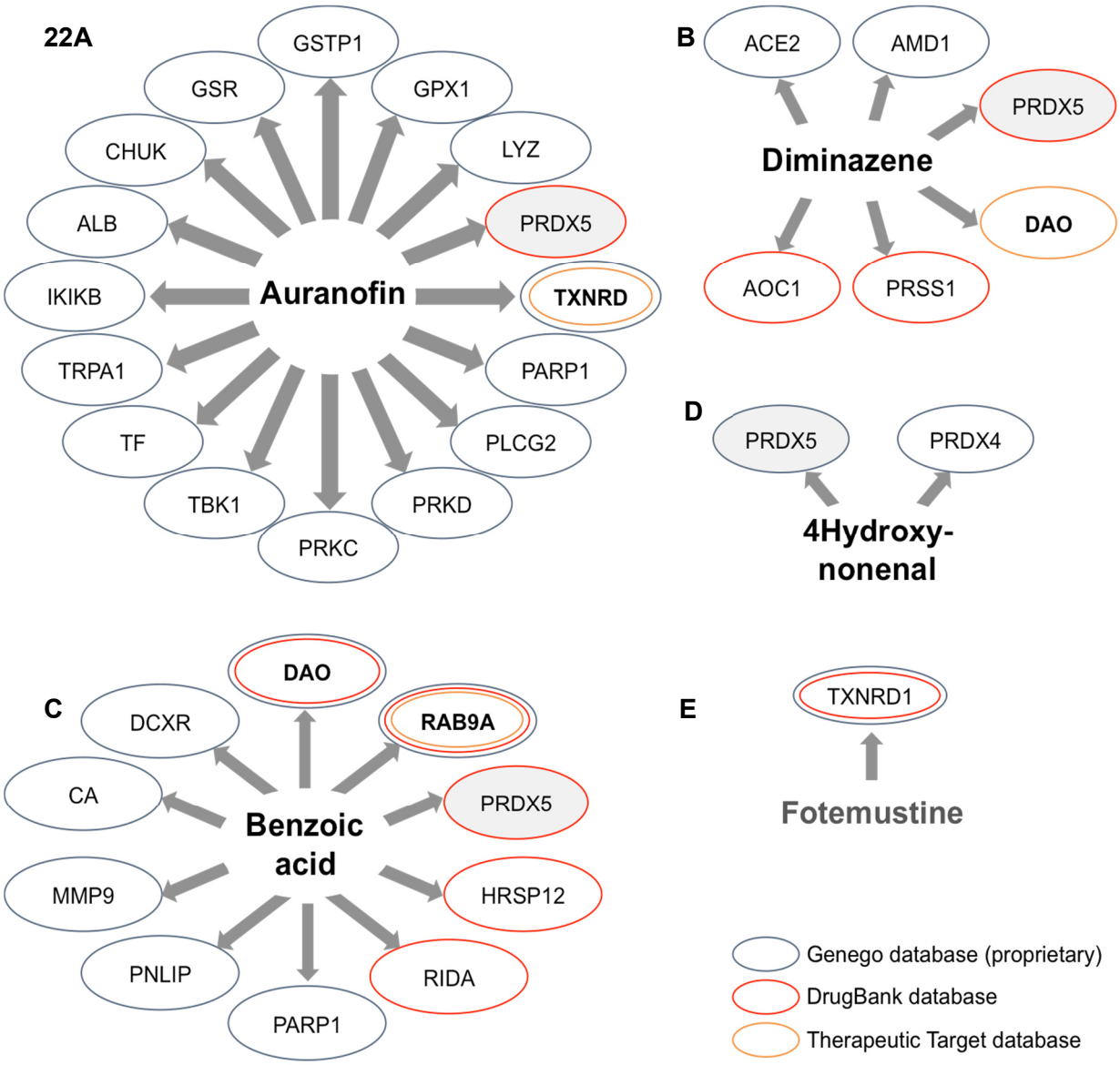

Figure 22: Graphical presentation of compounds tested and their potential host factor targets. Three different databases were used, as indicated by colored frame, to identify all possible cellular targets of auranofin **(A)**, diminazene **(B)**, benzoic acid **(C)**, 4hydroxynonenal and **(D)** fotemustine.

3.4.4 Titration of compounds targeting PRDX5 and upstream pathway

In order to determine the optimal working concentration for the different compounds described to target PRDX5 or upstream pathway, a dilution series was prepared, and J-Lat 8.4 cells were treated with respective compound dilutions or solvent controls for 24h and analyzed by flow cytometry. The results are shown in **Figure 23**. The working concentration for all following assays was determined to be 2.5mM for benzoic acid (**Figure 23A**), 100µg/ml for diminazene (**Figure 23B**), 1.5µM for 4hydroxynonenal (**Figure 23C**) and 15µM for fotemustine (**Figure 23D**). None of the compounds negatively influenced cell viability except for 4hydroxynonenal. Also, none of the compounds tested could reverse latency.

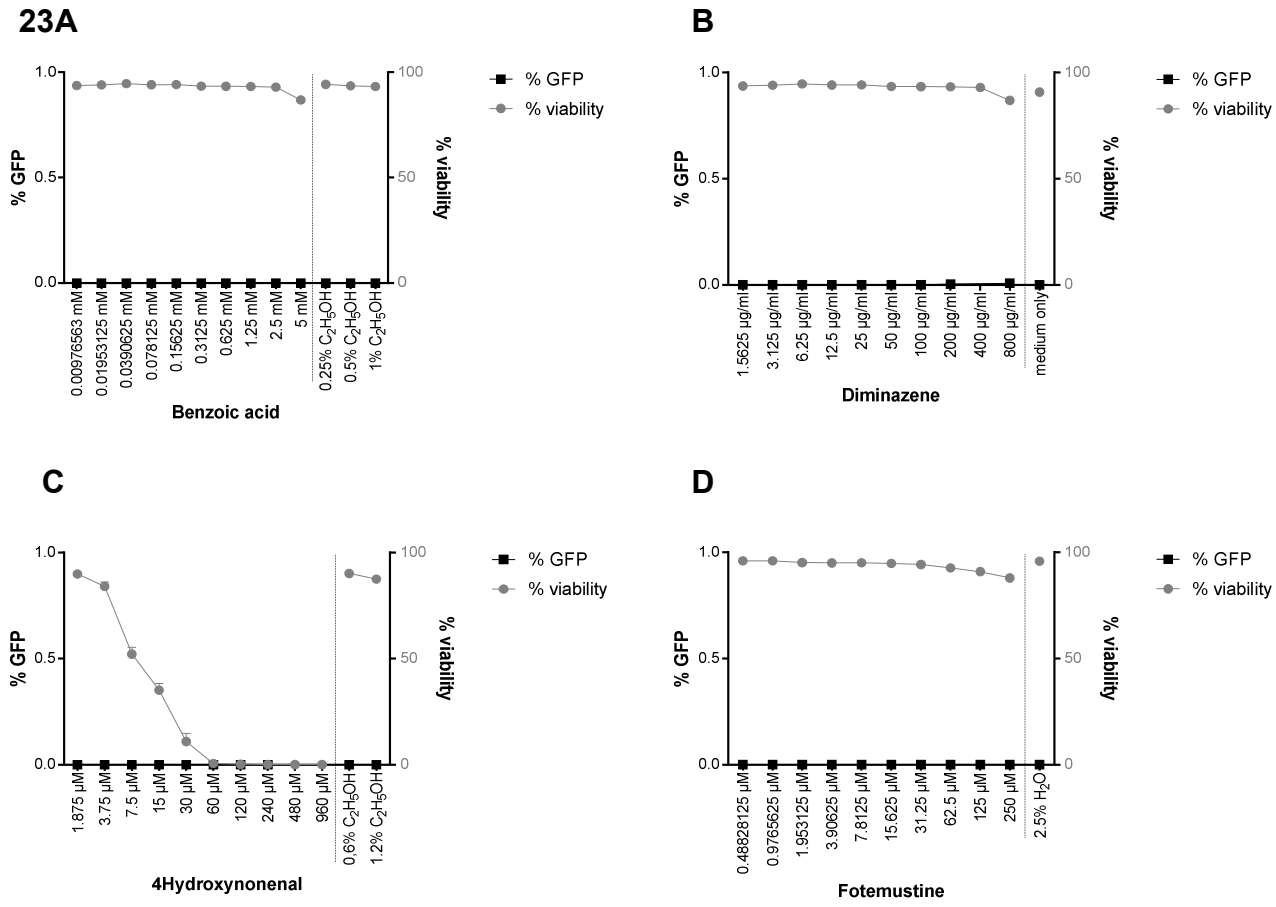

Figure 23: Optimal concentration determination of selected compounds. J-Lat 8.4 cells were treated with different concentrations of benzoic acid **(A)**, diminazene **(B)**, 4hydroxynonenal **(C)** or fotemustine **(D)** for 24h. % Viability (right y-axis) and %GFP positive cells (left y-axis) were assessed by flow cytometry. Each condition was measured in technical duplicates and standard deviation was indicated. Compound solvent controls were included.

Next, the compounds were tested along with an LRA to check for increased reversal of latency and JQ1 was used as positive control. The results are shown in **Figure 24** for each LRA separately. As seen in **Figure 24A** again, none of the compounds could reverse latency on its own. Upon addition of TNFα (**Figure 24B**) to the compounds, only auranofin and diminazene along with the positive control JQ1 showed significant increase in GFP positive cell numbers above the level of TNFα only treatment (last column). Upon prostratin treatment (**Figure 24C**), only diminazene along with the positive control significantly enhanced the number of GFP positive cells beyond the levels of prostratin only treatment, whereas for auranofin only a slight, non-significant increase was determined. SAHA addition (**Figure 24D**) to auranofin, diminazene, fotemustine or JQ1 led to a statistically significant increase in GFP positive cell numbers. The same compounds showed increased numbers in GFP positive when applied in combination with sodium butyrate (**Figure 24E**). In addition, neither benzoic acid nor 4hydroxynonenal could increase the number of GFP positive cells with any LRA applied.

Moreover, along with the flow cytometry results on GFP expression, provirus induction on mRNA level was determined by RT-qPCR. For this, samples were tested for elevated levels of *gag* and *gfp* mRNA. The results are shown in **Figure 25** (*gag* levels left column, *gfp* levels right column, respectively). The results for compound only treatment without any additional stimuli are not shown, since none of the compounds on its own induced *gfp* mRNA levels that could be reliably detected by RT-qPCR, i.e. ct values ≤ 35. In general, the results for *gag* induction (left) showed the same trend as seen for *gfp* induction (right). The slight fold change increase for auranofin along with TNFα (**Figure 25A**) and the more pronounced fold change increase for diminazene along with TNFα (**Figure 25A**) and diminazene along with prostratin (**Figure 25B**) verified the flow cytometry results. Nevertheless, the RT-qPCR results for the different compounds treated with either of the two HDACi (**Figure 25C** and **D**, respectively) did not confirm the observed enhancement of GFP signal as measured in **Figure 24**.

In summary, certain combinations of LRA with auranofin or diminazene led to latency reversal suggesting that the PRDX5 pathway might be the common target of these compounds.

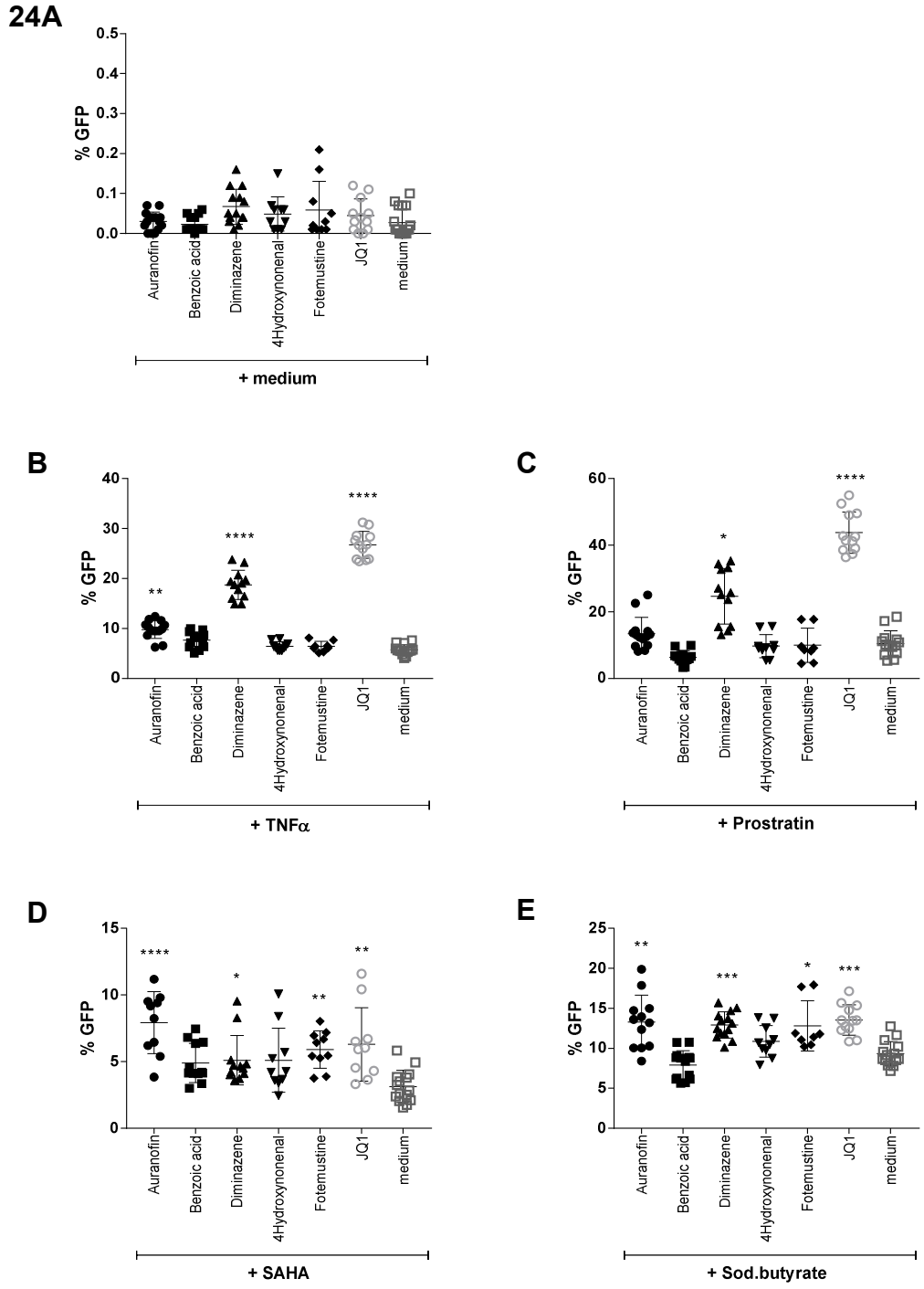

Figure 24: J-Lat 8.4 cells were treated with candidate compounds and different LRAs. J-Lat 8.4 cells were treated for 24h with different compounds alone **(A)**, or in combination with TNFα **(B)**, prostratin **(C)**, SAHA **(D)** or Sodium butyrate **(E)**. % GFP positive cells were assessed by flow cytometry. A minimum of four independent experiments is shown. Standard deviation was indicated, and statistical significance was tested with non-parametric Kruskal-Wallis test in comparison to the control group, i.e. LRA treatment only.

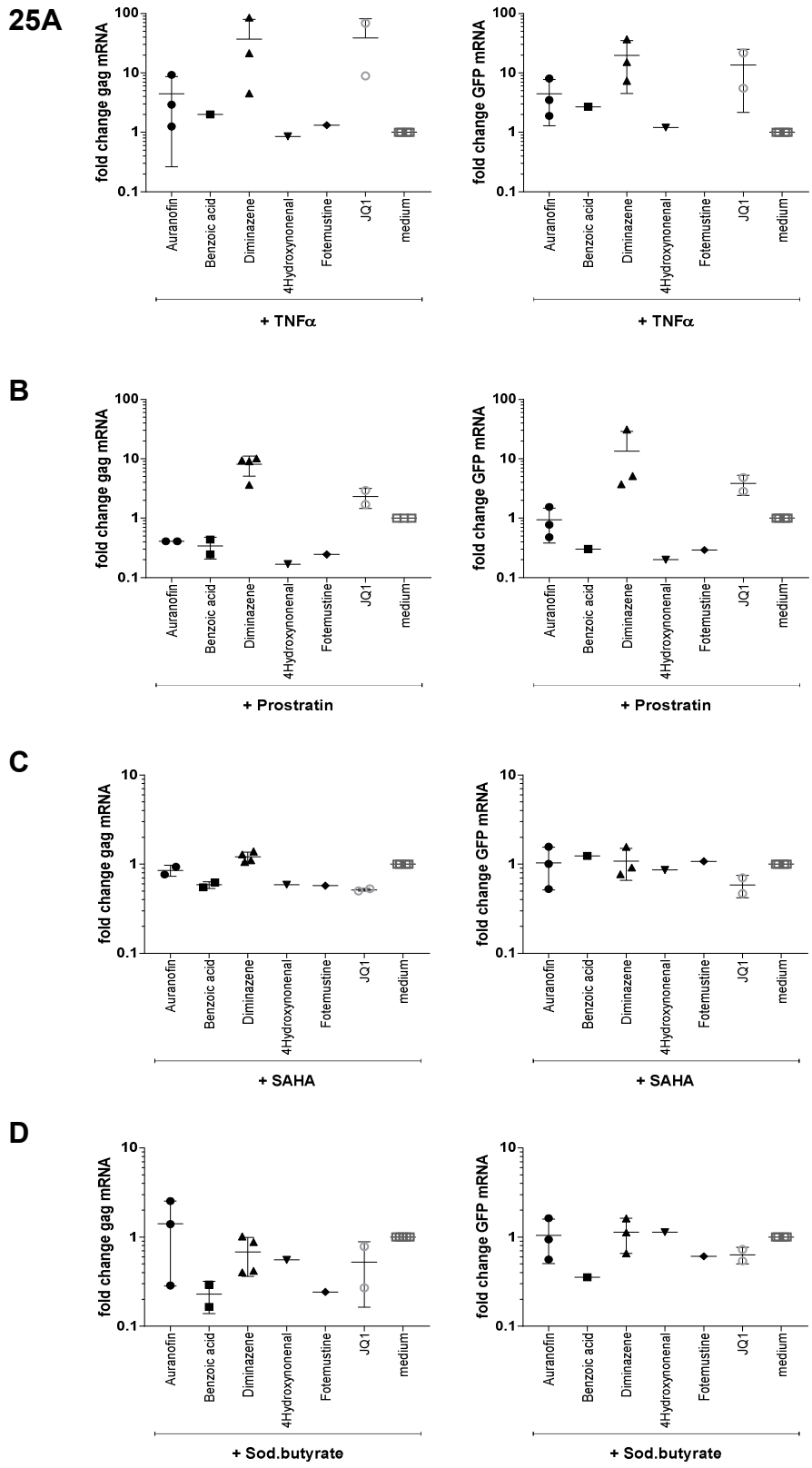

Figure 25: Provirus induction by compound treatment along with different LRAs as determined on mRNA level by RT-qPCR. J-Lat 8.4 cells were treated with candidate compounds and TNFα **(A)**, prostratin **(B)**, SAHA **(C)** or sodium butyrate **(D)** for 24h. *Gag* (left) and *gfp* (right) mRNA levels were determined by RT-qPCR. Each data point represents an independent experiment and standard deviation was indicated.

In a final experiment, the best compound candidates i.e. auranofin and diminazene, along with the positive control JQ1, were tested for their induction of intracellular Gag levels (unspliced Gag around 56kDa) by Western blot. As loading control GAPDH was used (around 37kDa). The results are shown in **Figure 26**. J-Lat 8.4 cells did not express Gag protein without stimulation and also not upon treatment of either auranofin or diminazene, verifying the previous flow cytometry and RT-qPCR results. Auranofin induced Gag expression in J-Lat 8.4 cells with all tested stimuli above the level of stimulus only. Diminazene in comparison showed a much stronger Gag induction with TNFα or prostratin but showed no additive effect when used in combination with either SAHA or sodium butyrate confirming the RT-qPCR results. The Gag protein levels resulting from diminazene treatment were comparable to the results of the positive control JQ1.

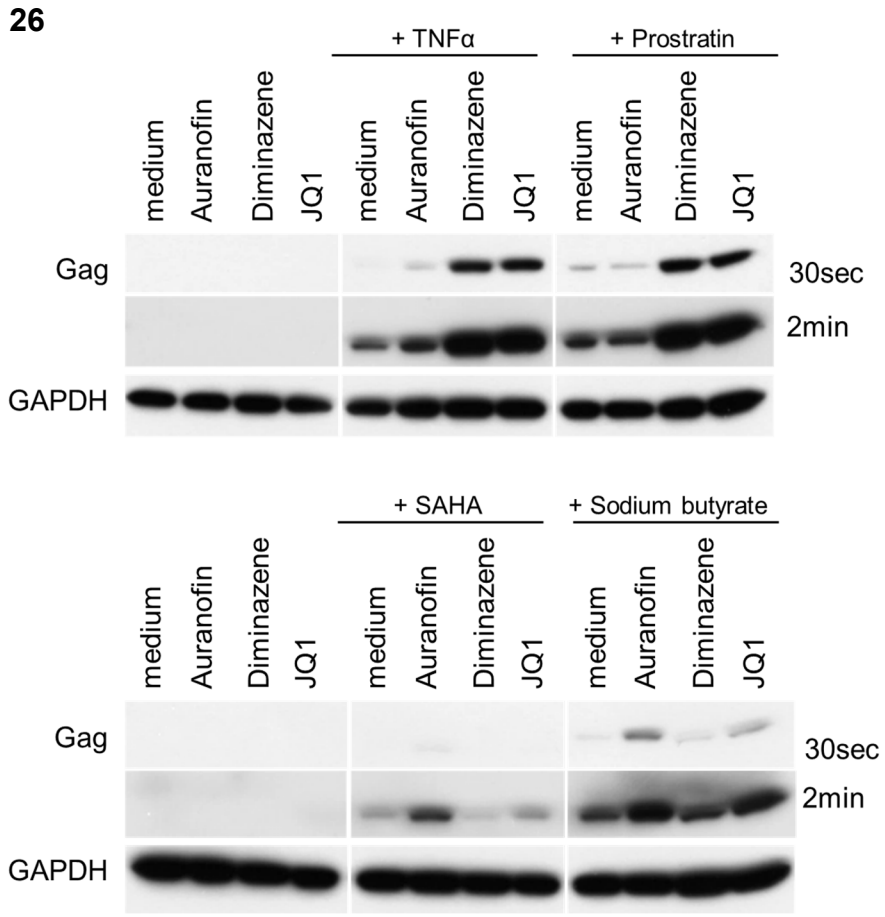

Figure 26: Verification of candidate compounds on protein level by Western blot. J-Lat 8.4 cells were treated with medium, candidate compounds (auranofin or diminazene) or JQ1 as positive control, alone or in combination with TNFα, prostratin (upper blot), SAHA or sodium butyrate (lower blot) for 24h. Gag levels were visualized by Western blot; GAPDH was used as loading control. Two different exposure times for Gag are shown.

Altogether the results obtained by various methods in J-Lat 8.4 cells showed that auranofin enhanced the level of latency reversal with any applied stimulus. Further, diminazene was identified to have a positive influence on latency reversal when applied along with T cell activating LRAs, i.e. TNFα or prostratin.

3.4.5 Verification of compound effects in different J-Lat clones

In a next step, the compounds of interest, i.e. auranofin as well as diminazene, were tested in the same experimental settings using J-Lat 6.3 cells instead (another J-Lat clone) to confirm the results derived from the J-Lat 8.4 cells. The reactivation pattern as measured by percentage of GFP positive cells (**Figure 27**) was highly comparable (see **Figure 24**). But the overall reactivation potential of this J-Lat 6.3 clone was slightly lower when compared to J-Lat 8.4. Auranofin could enhance reversal of latency when applied in combination with all tested LRAs, whereas diminazene only in combination with TNFα or prostratin led to a marked increase in GFP positive cells. The results for compound treatment with either SAHA (**Figure 27D**) or sodium butyrate (**Figure 27E**) showed some variance, which was attributed to the loss of activity of the LRA.

In addition, the *gfp* and *gag* mRNA levels were determined (**Figure 28**, left or right column, respectively) by RT-qPCR to verify the flow cytometry results. The results for compound only treatment without any additional stimuli are not shown, since none of the compounds on its own induced GFP mRNA levels that could be reliably detected by RT-qPCR, i.e. ct values ≤ 35. The results for compounds used in combination with either TNFα (**Figure 28A**) or prostratin (**Figure 28B**) were comparable to the results obtained from flow cytometry. Auranofin, diminazene and JQ1 induced robust mRNA transcription. The results achieved in combination with either SAHA (**Figure 28C**) or sodium butyrate (**Figure 28D**) showed greater deviation and were not in line with the flow cytometry results, this was especially seen for JQ1.

In summary, the results obtained from J-Lat 6.3 cells are highly comparable to the results from the J-Lat 8.4 cells, thus confirming the latency reversing capacity of auranofin and diminazene in combination with certain LRAs.

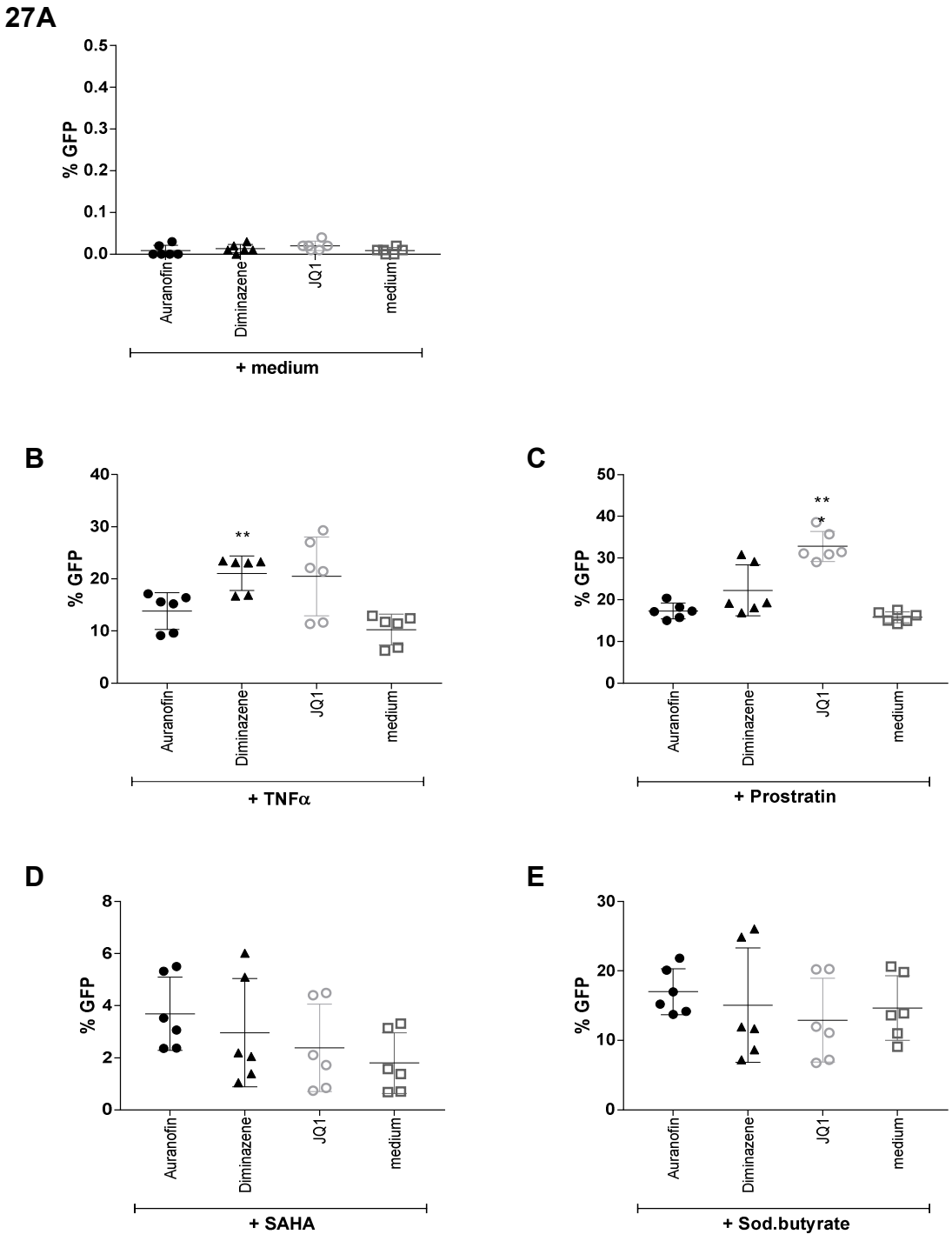

Figure 27: Verification of candidate compounds in in J-Lat 6.3 cells. J-Lat 6.3 cells were treated with candidate compounds along with medium **(A)**, TNFα **(B)**, prostratin **(C)**, SAHA **(D)** or sodium butyrate **(E)** for 24h. % GFP positive cells were assessed by flow cytometry. The results of three independent experiments are shown and standard deviation was indicated. Standard deviation was indicated, and statistical significance was tested with non-parametric Kruskal-Wallis test in comparison to the control group, i.e. LRA treatment only.

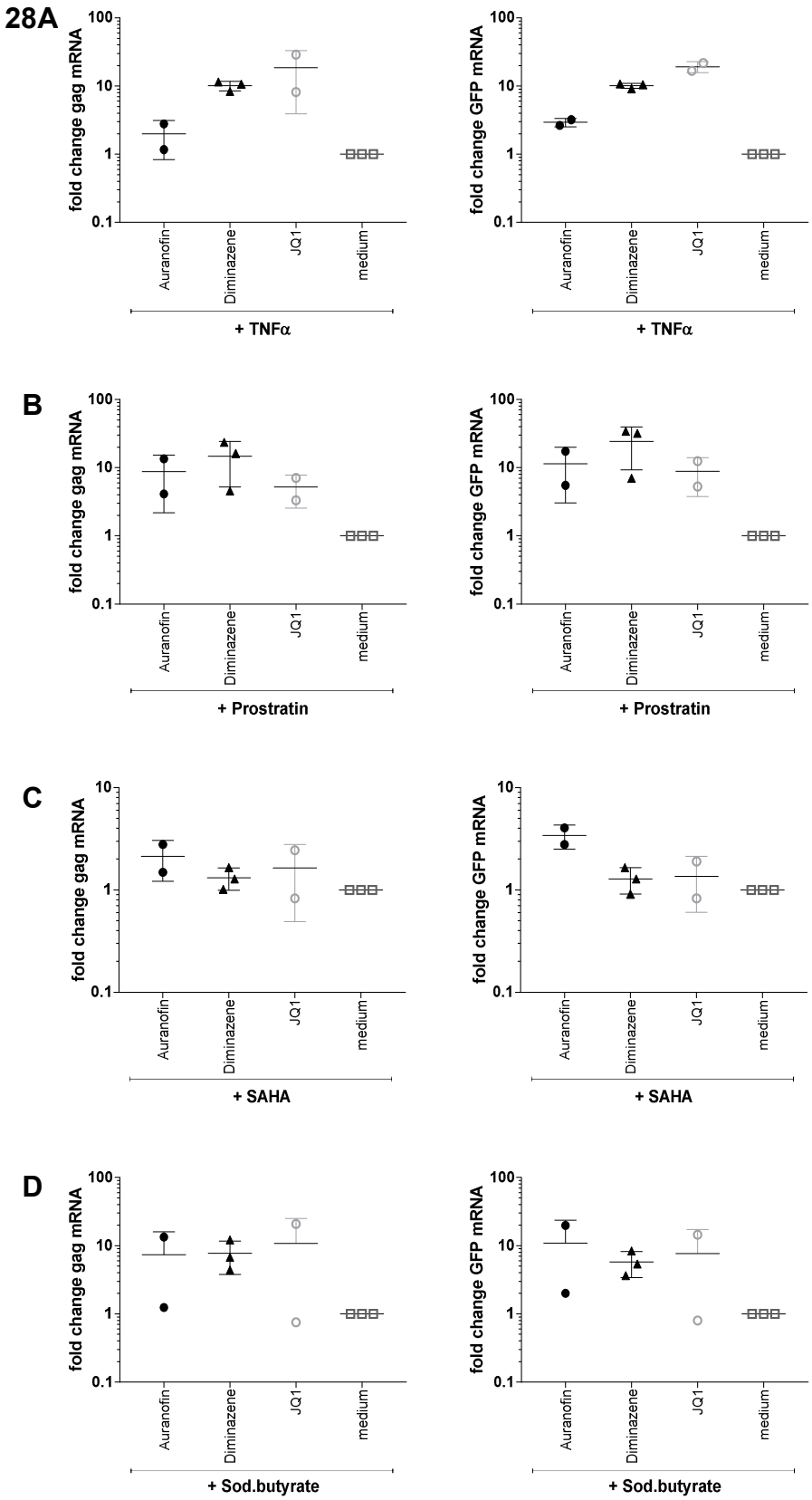

Figure 28: Provirus induction by compound treatment along with different LRAs as determined on mRNA level by RT-qPCR. J-Lat 6.3 cells were treated with candidate compounds and TNFα **(A)**, prostratin **(B)**, SAHA **(C)** or sodium butyrate **(D)** for 24h. *Gag* (left) and *gfp* (right) mRNA levels were determined by RT-qPCR. Each data point represents an independent experiment and standard deviation was indicated.

3.4.6 Verification of compound effects in a different latency cell line

To verify the reactivation pattern of the different compounds in a latency cell model with a different cellular origin, U1 cells derived from monocytic U937 cells were tested. This latency cell model possesses two integrated copies of HIV-1 with no reporter gene, therefore a p24 ELISA was chosen as read-out. The stimulation was performed as described for J-Lat 8.4 cells and the p24 ELISA was performed on the undiluted supernatant. As seen in **Figure 29A**, U1 cells treated with compounds or medium only showed p24 levels close to the detection limit of 100pg/ml. Treatment of compounds along with TNFα (**Figure 29B**) showed no increase in p24 levels except for JQ1. Treatment with prostratin (**Figure 29C**) without additional compound led to a tremendous production of p24, a further increase was only seen upon addition of JQ1 but neither with auranofin nor with diminazene. The addition of SAHA (**Figure 29D**) on its own did not lead to a significant increase in p24 levels, but in combination of either auranofin or JQ1 showed increased p24 levels. The same tendency was seen upon stimulation with sodium butyrate (**Figure 29E**).

In summary, auranofin could support reactivation when applied in combination with either SAHA or sodium butyrate (i.e. HDACi, non-T cell activating LRA) but did not lead to an effect when used in combination with either TNFα or prostratin (i.e. T cell activating LRAs via NFκB pathway). Diminazene in combination with any stimulus tested did not lead to an effect. Of note, the reactivation pattern in U1 cells differed from J-Lat cells. Neither TNFα, SAHA or sodium butyrate alone did induce reactivation to a robust level beyond the minimum detection limit of the used p24 ELISA.

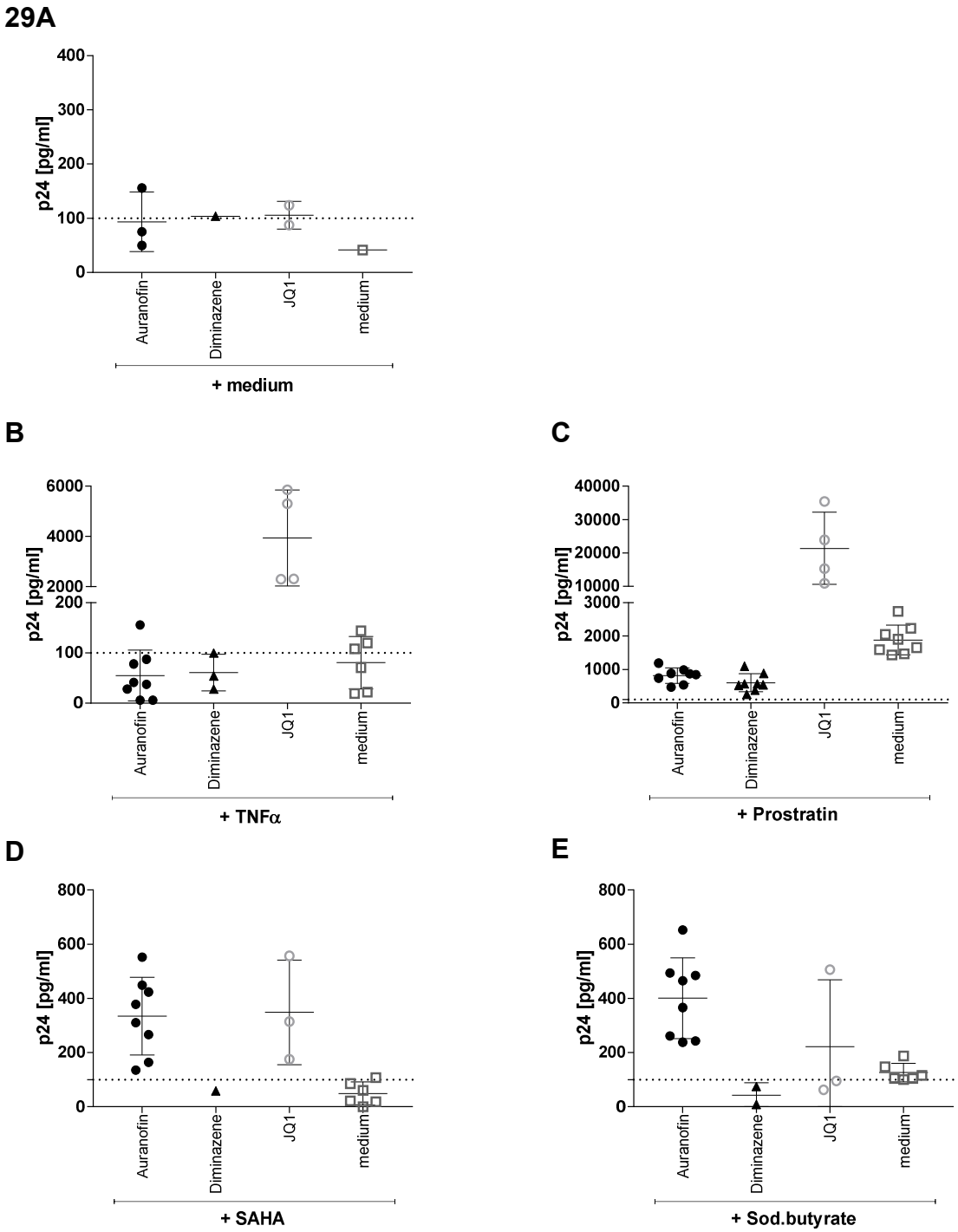

Figure 29: Verification of candidate compounds in U1 cells. U1 cells were treated with candidate compounds and medium **(A)**, TNFα **(B)**, prostratin **(C)**, SAHA **(D)** or sodium butyrate **(E)** for 24h. Provirus induction was measured by p24 production in the supernatant. A minimum of two individual experiments is shown, for each experiment measurements were done technical duplicates and standard deviation was indicated. Dotted lines represent the lower level of detection as denoted by the manufacturer.

RT-qPCR was performed on HIV-1 *gag* mRNA levels on compound and LRA treated U1 cells to verify the results obtained by p24 ELISA. The results are shown in **Figure 30**. Treatment with compound only (**Figure 30A**) led to an induction of *gag* mRNA for JQ1 and for diminazene. Upon additional stimulation with either TNFα (**Figure 30B**) or prostratin (**Figure 30C**), only JQ1 showed increased levels of *gag* mRNA, which was not seen for either auranofin or diminazene. Treatment in combination with either SAHA (**Figure 30D**) did lead to increased induction when applied along with auranofin, while diminazene did not show an effect. The results for JQ1 showed a high variation between the samples tested and were therefore inconclusive. Treatment of compounds along with sodium butyrate (**Figure 30E**) showed no effect with diminazene or JQ1. The results for auranofin were inconclusive due to high variability between samples tested.

Overall, the results of *gag* mRNA levels followed the results determined by p24 ELISA even though a direct correlation was not possible due to a high variability. Furthermore, the fold change increases seen did not correlate with the p24 levels obtained.

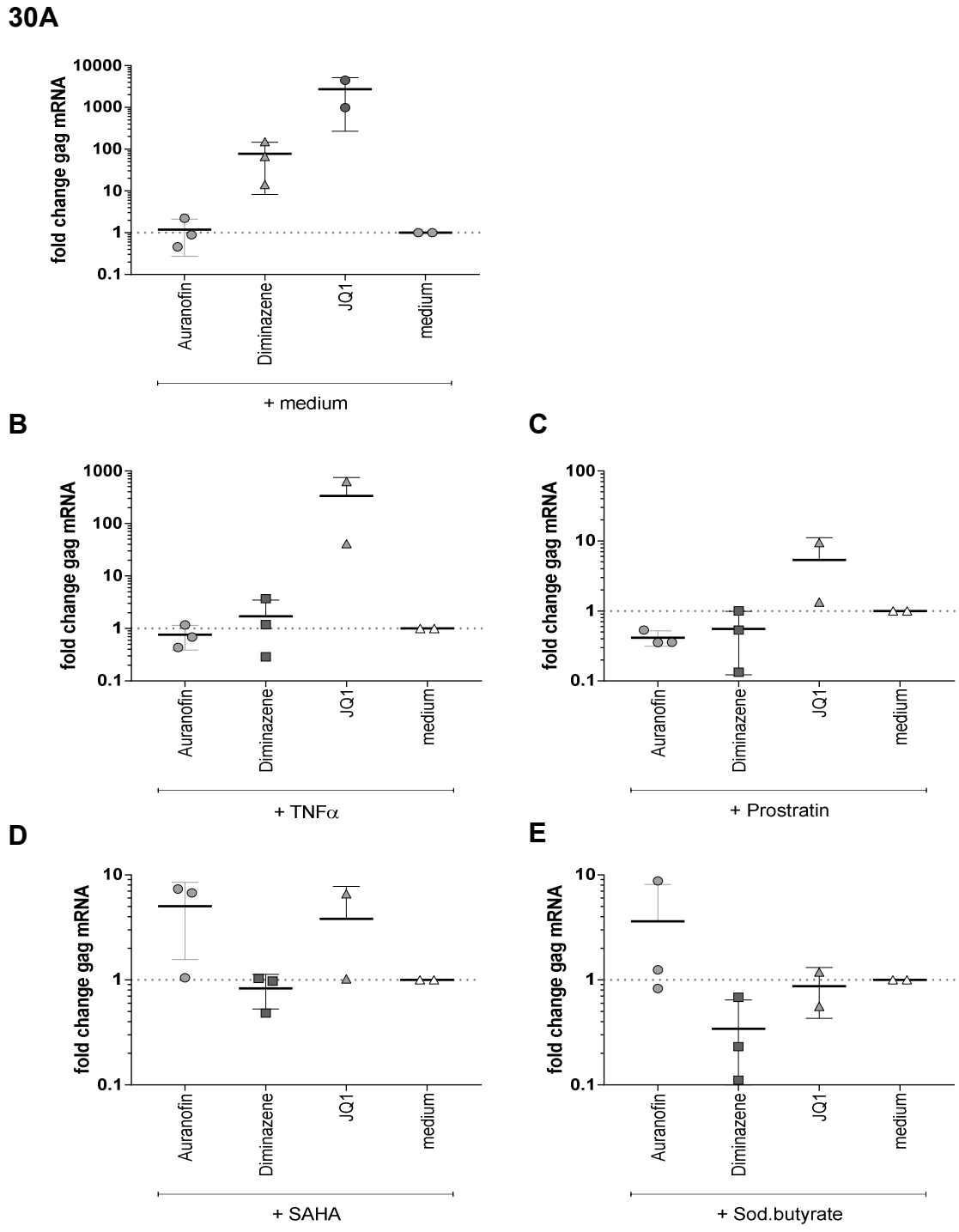

Figure 30: Verification of candidate compounds on mRNA level in U1 cells. U1 cells were treated with candidate compounds alone **(A)**, or with TNFα **(B)**, prostratin **(C),** SAHA **(D),** or sodium butyrate **(E)** for 24h. *Gag* mRNA levels were determined by RT-qPCR. Each data point presents an independent experiment and standard deviation was indicated.

In a final experiment, the effect of auranofin and diminazene on intracellular Gag levels was tested by Western blot. The results are shown in **Figure 31**. Unequal loading of samples was observed, as seen by the tubulin bands (around 50kDa). Due to this, only a tendency of p24 (around 24kDa) induction could be deduced. Treatment with compounds alone led to an induction of p24 only in the case of JQ1. Treatment with compounds along with TNFα or prostratin led to a reliable p24 induction only in combination with JQ1. An additional effect was neither seen for auranofin, nor for diminazene. Further, upon treatment along with SAHA or sodium butyrate only Auranofin showed a clear increase, whereas diminazene did not show an additional effect.

Taking together the results obtained for U1 cells with different methods, increased reactivation was found for auranofin only in combination with SAHA and sodium butyrate. Diminazene was not found to have a potential effect on latency reversal in this latency cell model.

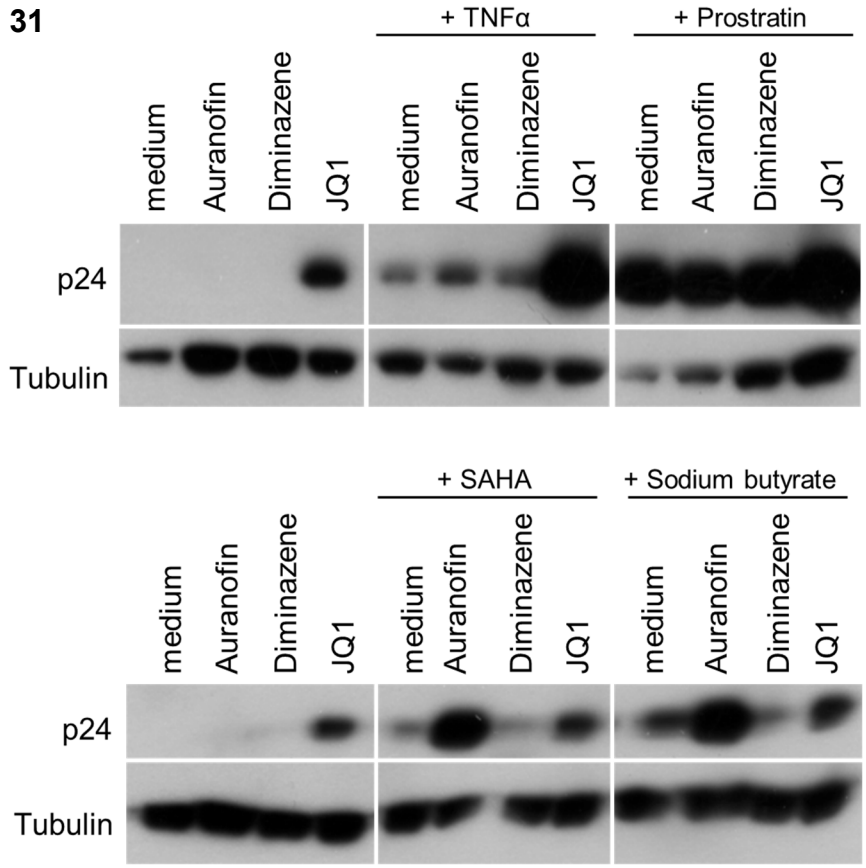

Figure 31: Verification of candidate compounds on protein level by Western blot. U1 cells were treated with medium or candidate compounds (Auranofin, Diminazene or JQ1) and TNFα, prostratin (upper blot), SAHA or sodium butyrate (lower blot) for 24h. p24 levels were visualized by Western blot, tubulin was used as loading control.

3.4.7 Summary compounds

In summary, auranofin was validated as compound with the potential to drive reversal of latency when applied in combination with an LRA (see **Table 14**, upper part). The effect was robust when tested in combination with one of the used HDACi in all applied latency cell models and with various methods. An effect of auranofin with either TNFα or prostratin was only seen for the J-Lat latency cell model.

Diminazene application, on the other hand, led to a sound induction of GFP on protein and mRNA level when applied along with either TNFα or prostratin, a potential which outranged the one of auranofin (see **Table 14**, lower part). The reactivation pattern of diminazene was comparable to the one seen for JQ1. This effect was seen for both J-Lat clones tested but was not found in U1 cells.

None of the tested compounds, chosen on basis to target either PRDX5 or TXNRD family members, recapitulated the exact reactivation pattern than the one seen for auranofin. 4hydroxynonenal and benzoic acid showed no effect in the tested J-Lat 8.4 cell model. Fotemustine showed a slight additive effect when applied in combination with either of the HDACi. Those compounds were not further tested.

Taken together, auranofin and diminazene proved to have an additive effect on the reversal of latency (under selected conditions); but the potential host target(s) still need to be identified by further experiments.

Table 14: Overview over effect of either auranofin or diminazene alone or in combination with different LRAs in all latency cell models.

		medium + auranofin	TNFα + auranofin	prostratin + auranofin	SAHA + auranofin	sod. but. + auranofin
J-Lat 8.4	RT-qPCR *gag* & *gfp*	b.d.	↑	-	-	-
	FACS GFP	-	↑	↑	↑↑	↑
	WB Gag	-	↑	-	↑	↑
J-Lat 6.3	RT-qPCR *gag* & *gfp*	b.d.	↑	↑	↑	↑
	FACS GFP	-	↑	-	↑	↑
	WB Gag	n.t.	n.t.	n.t.	n.t.	n.t.
U1	RT-qPCR *gag*	-	-	-	↑	↑
	ELISA p24	-	-	-	↑	↑
	WB Gag	-	↑	↑	↑↑	↑↑

		medium + diminazene	TNFα + diminazene	prostratin + diminazene	SAHA + diminazene	sod. but. + diminazene
J-Lat 8.4	RT-qPCR *gag* & *gfp*	b.d.	↑↑	↑	-	-
	FACS GFP	-	↑↑	↑↑	↑	↑
	WB Gag	-	↑↑	↑↑	-	-
J-Lat 6.3	RT-qPCR *gag* & *gfp*	b.d.	↑	↑	-	↑
	FACS GFP	-	↑↑	↑	↑	↑
	WB Gag	n.t.	n.t.	n.t.	n.t.	n.t.
U1	RT-qPCR *gag*	↑	-	-	-	-
	ELISA p24	-	-	-	-	-
	WB P24	-	-	-	-	-

b.d.= below detection, n.t.= not tested; for qRT-PCR results : ↑ ≤ 10 fold increase to LRA only, ↑↑ ≤ 100 fold increase to LRA only ; for GFP results : ↑ ≤ 5% increase to LRA only, ↑↑ ≥ doubling of GFP % to LRA only ; for p24 ELISA results : ↑ ≤ 5 times increase to LRA only ; for WB results : ↑ ≥ visbile increase on protein level above LRA only, ↑↑ ≥ increase on protein level comparable to/or greater than positive control JQ1. Grey shaded cells: increase in reactivation seen, non-robust results linked to reduced activity of SAHA and sodium butyrate.

3.4.8 Validation of host factors by genetic manipulation

3.4.8.1 Choosing optimal siRNAs and knockdown time points

In order to attribute the compound effects to specific host factors, i.e. PRDX5, TXNRD1 and TXNRD2, a direct knockdown of host factor by siRNA electroporation was performed. For this, four individual siRNAs per host factor were tested for their knockdown potential in either J-Lat 8.4 cells (**Figure 32A**-**C**) or U1 cells (**Figure 32D**-**F**) as determined by RT-qPCR. The knockdown of *prdx5* was most efficient when targeted by siPRDX5#5 for both J-Lat and U1 cells, as seen **Figure 32A** and **D**, respectively. Further, the knockdown of *txnrd1* was most efficient when targeted by siTXNRD1#3 for both cell lines as seen in **Figure 32B** and **E**. The knockdown of *txndr2* was most efficient when targeted by siTXNRD2#6 in J-Lat 8.4 cells (**Figure 32C**) and in U1 cells (**Figure 32F**). These siRNAs were used for all further experiments.

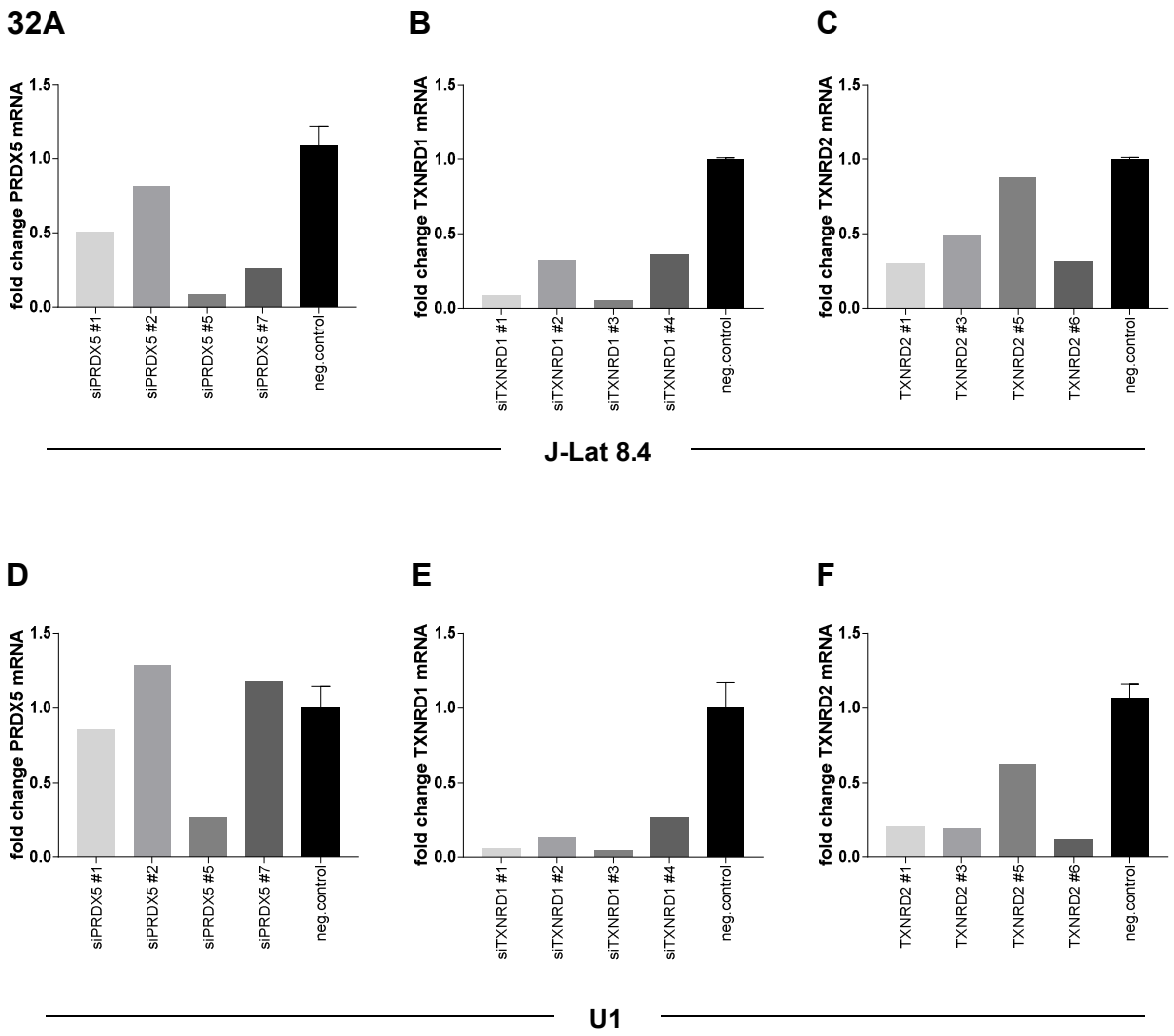

Figure 32: Determination of best siRNAs for J-Lat and U1 cells. Four individual siRNAs against a host factor of interest were individually tested. For this, either J-Lat 8.4 cells **(A, B, C)** or U1 cells **(D, E, F)** cells were checked for reduction on mRNA level by RT-qPCR 24h post electroporation of the indicated siRNAs. Knockdown results are shown for PRDX5 (**A** and **D**), TXNRD1 (**B** and **E**) and for TXNRD2 (**C** and **F**).

In a next set of experiments, the time course of knockdown for each host factor was determined on mRNA level by RT-qPCR as well as on protein level by Western blot. The results are shown for J-Lat 8.4 cells **Figure 33A**-**C** and for U1 cells **Figure 33E**-**F**. The knockdown of PRDX5 (**Figure 33A**) showed a drastic decrease on mRNA level after 24h, which was gradually lost over 72h. The knockdown on protein level was readily detected after 48h and lost upon 72h. PRDX5 knockdown in U1 cells (**Figure 33D**) showed a reduction on the mRNA level after 24h, which lasted up to 72h. The RT-qPCR results were confirmed by Western blot, which showed a pronounced decrease in PRDX5 protein levels for up to 48h and a slight increase upon 72h post-knockdown.

The knockdown results for TXNRD1 in J-Lat 8.4 cells on mRNA level showed a distinct reduction for up to 72h (**Figure 33B**), whereas an effect on protein level gradually increased upon time. Comparable results were also found in U1 cells (**Figure 33E**).

The knockdown of TXNRD2 in J-Lat 8.4 cells (**Figure 33C**) showed a gradual decrease on mRNA level for all time points determined. The knockdown on mRNA level was found to be low already upon 24h post-siRNA electroporation. This effect seemed to last up to 72h even though the loading control for the 72h value showed reduced loading. The knockdown of TXNRD2 in U1 cells (**Figure 33F**) showed reduction on mRNA level already upon 24h, which persisted until 48h and was lost after 72h. Those results were in line with the Western blot results even though a slightly decreased loading was observed for 24h.

In summary, the knockdown of different host factors could be reliably detected on protein level 48h post-electroporation in J-Lat 8.4 and U1 cells. Nevertheless, it has to be taken into account that knockdown efficiency as well as duration varied for the different host factors and between the cell lines.

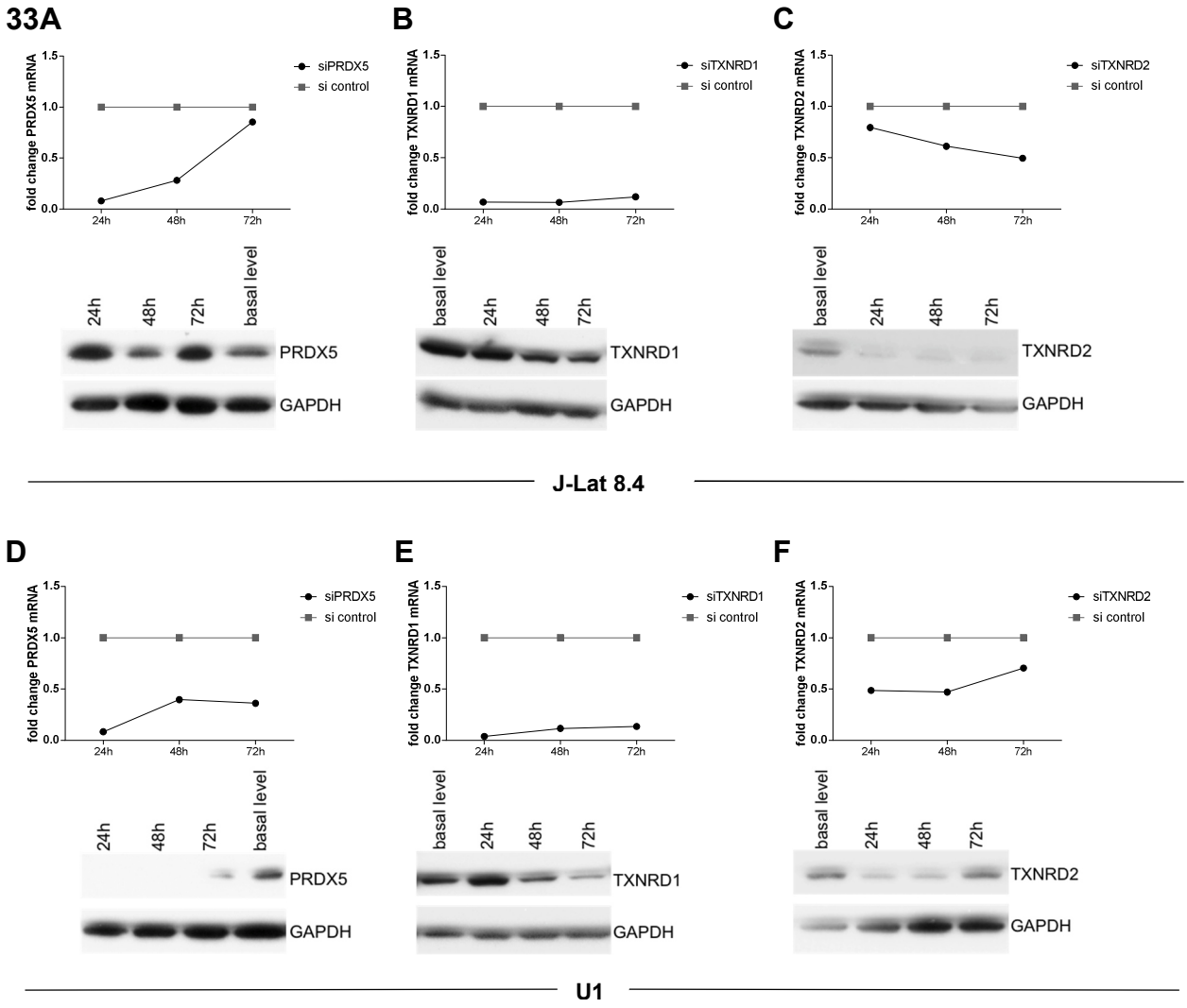

Figure 33: Determination of optimal time point for host factor knockdown on mRNA and protein level. siRNAs were electroporated and samples harvested at 24h, 48h and 72h to determine knockdown efficiency on mRNA level (upper graphs) and on protein level (lower Western blot images) for J-Lat 8.4 cells **(A, B, C)** and U1 cells **(D, E, F)**. Knockdown results are shown for PRDX5 (**A** and **D**), TXNRD1 (**B** and **E**) and for TXNRD2 (**C** and **F**).

3.4.9 siRNA knockdown followed by LRA treatment

In a final step, the potential role of direct host factor knockdown on reversal of latency was determined. For this, J-Lat 8.4 and U1 cells were electroporated with siRNA, after 36h the cells were split into four equal portions. One portion was taken to prepare Western blot samples to confirm successful knockdown. The remaining three portions were either treated with medium or stimulated with prostratin or sodium butyrate for another 24h.

J-Lat 8.4 cells were analyzed for increased numbers of GFP positive cells by flow cytometry (**Figure 34**), and U1 cells were analyzed for increased p24 levels determined by ELISA (**Figure 35**). As positive control, CYLD knockdown was included and as negative controls non-target siRNAs (referred to as 'si control') were used. Of note, CYLD knockdown was not confirmed on protein level. The results for the knockdown of PRDX5, TXNRD1 alone or in combination for J-Lat 8.4 cells are shown in **Figure 34**. siRNA knockdown followed by medium treatment did not lead to any GFP induction for any tested target (**Figure 34A**, first block), which was in line with former results. Knockdown followed by stimulation with prostratin (**Figure 34A**, middle block) led to an induction of GFP up to 6% for the negative control. The knockdown of either PRDX5, TXNRD1 or in combination did not lead to an additional increase in GFP positive cells above the level of the negative control. Only the knockdown of the positive control CYLD followed by prostratin stimulation led to an enhanced number of GFP positive cells of around 13%. The effect of knockdown in addition with sodium butyrate stimulation led to around 9% of GFP positive cells for the negative control. A slight increase in GFP positive cells, upon TXNRD1 knockdown compared to the negative control was seen in combination with sodium butyrate same as with the positive control CYLD, hinting towards the involvement of the pathway for latency reversal in this particular cell system (**Figure 34A**, last block).

The knockdown on protein level as determined by Western blot (**Figure 34B**) was successful for PRDX5, TXNRD1 and the double knockdown of both host factors, even though the joint knockdown of PRDX5 and TXNRD1 was less efficient than the single ones. It needs to be kept in mind that the decreased knockdown efficiency for both host factors together might have masked an effect on latency reversal. In addition, the viability after treatment was determined, as shown in **Figure 34C**. None of the siRNAs tested led to a significant decrease in viability, additional stimulation led to a slight decrease in viability.

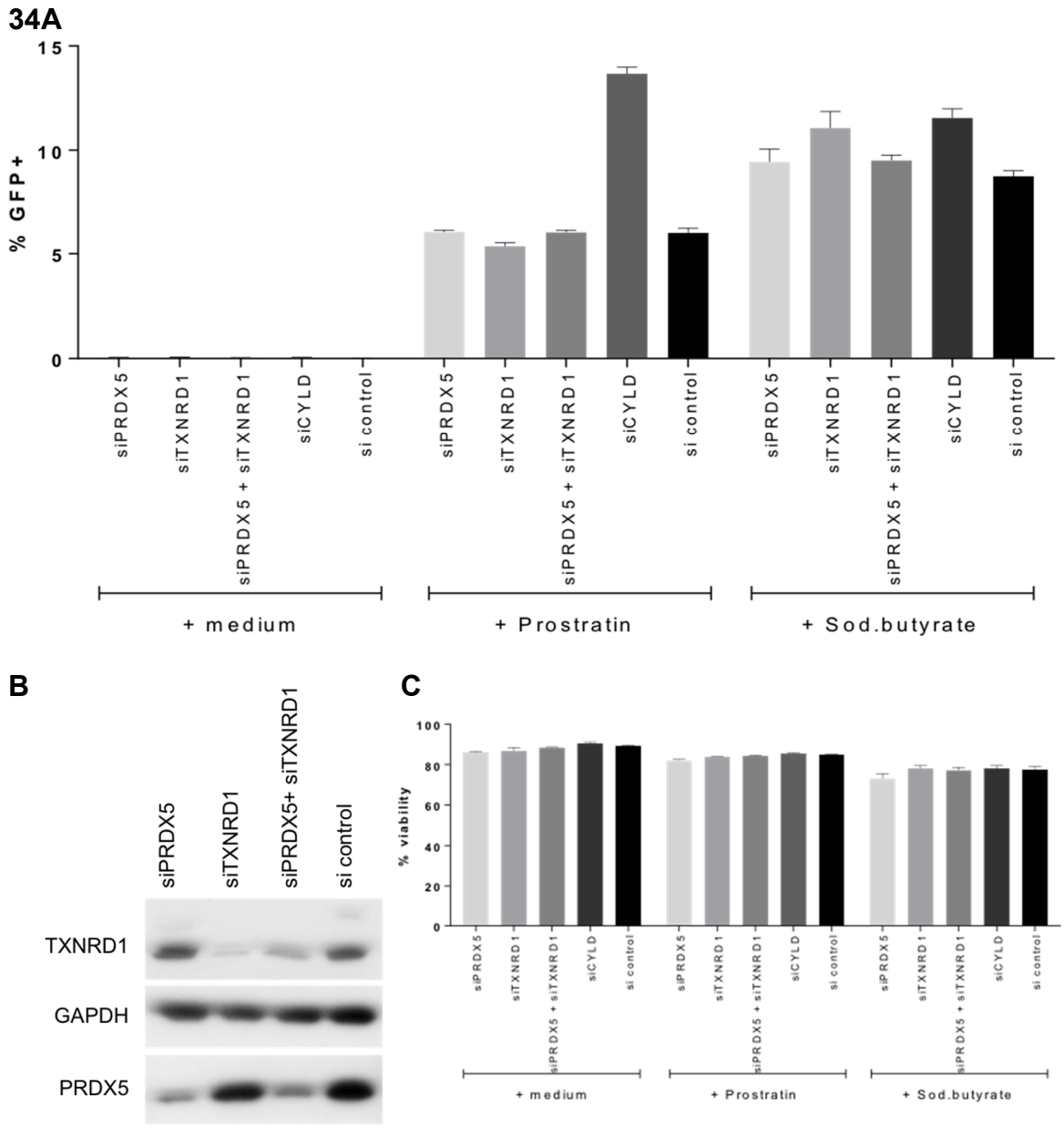

Figure 34: siRNA knockdown of host factors in combination with LRA stimulation in J-Lat 8.4 cells. PRDX5, TXNRD1 alone or in combination were knocked down in J-Lat 8.4 cells followed by stimulation with either prostratin or sodium butyrate for 24h. **A)** % GFP positive cells as determined by flow cytometry. **B)** Verification of knockdown on protein level by Western blot. **C)** Influence of knockdown and stimulation on cell viability.

The results for the single and double knockdown in U1 cells are shown in **Figure 35**. Knockdown on its own, without additional stimulation, did not lead to a statistically significant p24 induction, still slight induction above the negative control (**Figure 35A**, first graph) was detected. Interestingly, prostratin and sodium butyrate treatment did increase p24 levels compared to the negative control for the double knockdown of PRDX5 and TXNRD1, whereas

the respective single knockdowns did not show an effect. Of interest, knockdown of CYLD did not lead to significantly increased p24 levels in U1 cells (**Figure 35A**, second and third graph).

The knockdown on protein level for the single and double knockdown was successful as seen in **Figure 35B**. And viability was not negatively affected by electroporation and LRA treatment (**Figure 35C**).

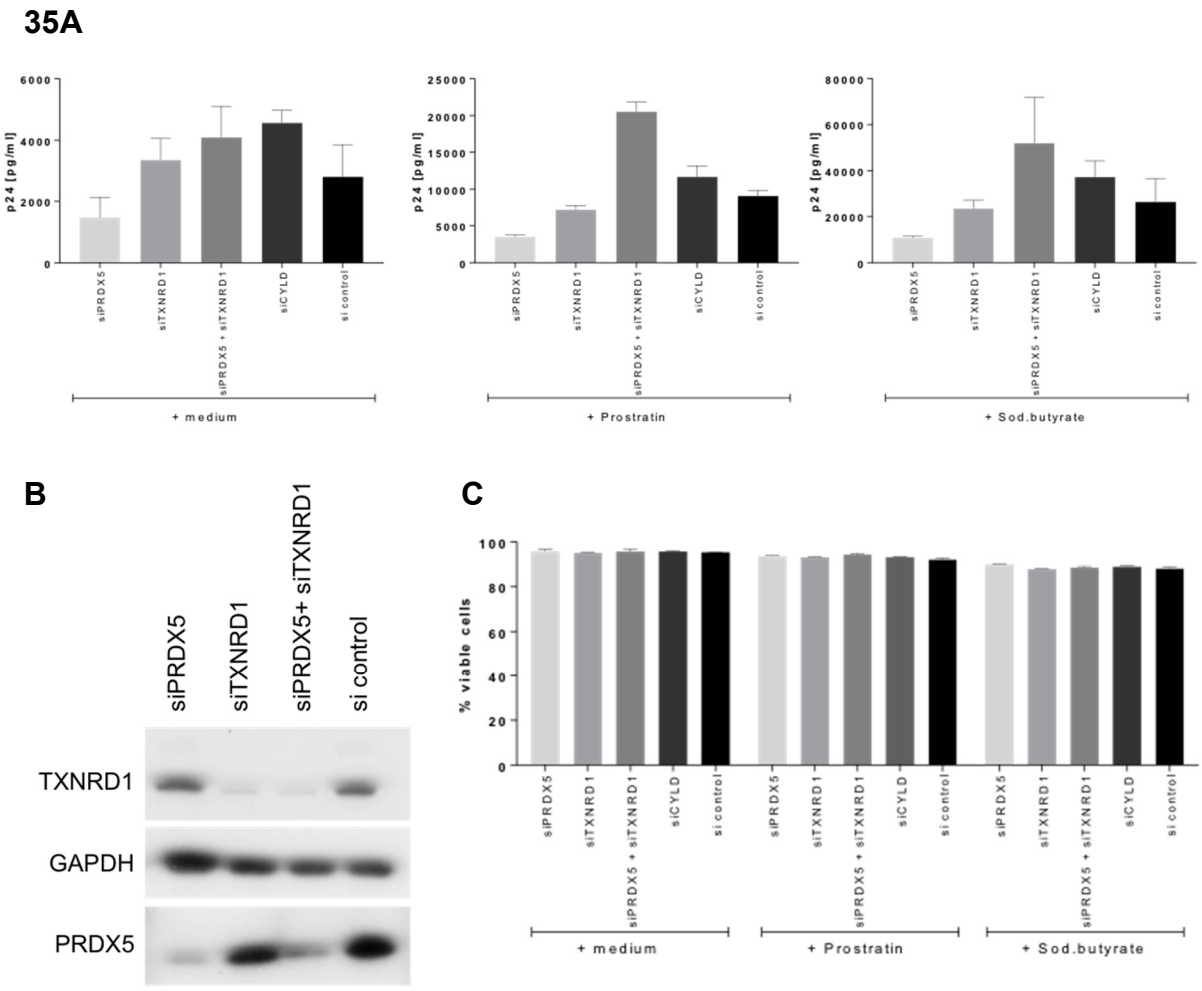

Figure 35: siRNA knockdown of host factors in combination with LRA stimulation in U1 cells. PRDX5, TXNRD1 alone or in combination were knocked down in U1 cells followed by stimulation with either prostratin or sodium butyrate for 24h. **A)** Level of reactivation determined by p24 ELISA on culture supernatant. **B)** Verification of knockdown on protein level by Western blot. **C)** Influence of knockdown and stimulation on cell viability.

In summary, silencing of PRDX5 and TXNRD1 was successful in J-Lat 8.4 and U1 cells as indicated by Western blot results on the expression levels of the respective genes. In the J-Lat 8.4 cell system, in TXNRD1 silenced cells upon sodium butyrate treatment, a marginal

increase in latency reversal measured by percentage of GFP positive cells compared to control cells was detected, similar to the positive control CYLD silenced cells. However, in the U1 cell system, in double knockdown PRDX5 and TXNRD1 cells, upon LRA treatment, i.e. prostratin or sodium butyrate, a successful latency reversal was detected compared to negative control cells suggesting an involvement of this pathway in latency reversal.

3.4.10 Results on HIV-1 positive primary cells

3.4.10.1 Setup of methods

3.4.10.1.1 Experimental design

As described in the present study, both identified compounds (auranofin and diminazene) showed (differential) increases in latency reversal in the tested latency models, i.e. J-Lat clones and U1 cells. To test whether those compounds would also show this effect in long term HIV-1 infected primary cells, resting $CD4^+$ T cells were isolated from HIV-1 positive patient blood and reactivation of the latent reservoir was tested.

An overview of the initial procedure is shown in **Figure 36**, which was adapted from experimental procedures previously published (Darcis et al., 2015). PBMCs were isolated from HIV-1 positive full blood and one million cells were used for DNA extraction followed by analysis for proviral integrates by qPCR. The remaining PBMCs were further used to isolate $CD4^+$ T cells followed by final isolation of non-activated $CD4^+$ T cells, i.e. cells not expressing activation markers and therefore considered resting. Those cells were treated with compound, stimuli, a combination of those, medium (negative control) or antiCD3/antiCD28 antibodies (positive control). After three days, the supernatant was collected for p24 ELISA and the treatment conditions refreshed. At day six, the cells were collected for the potential analysis of viral RNA and the supernatant for p24 ELISA.

36

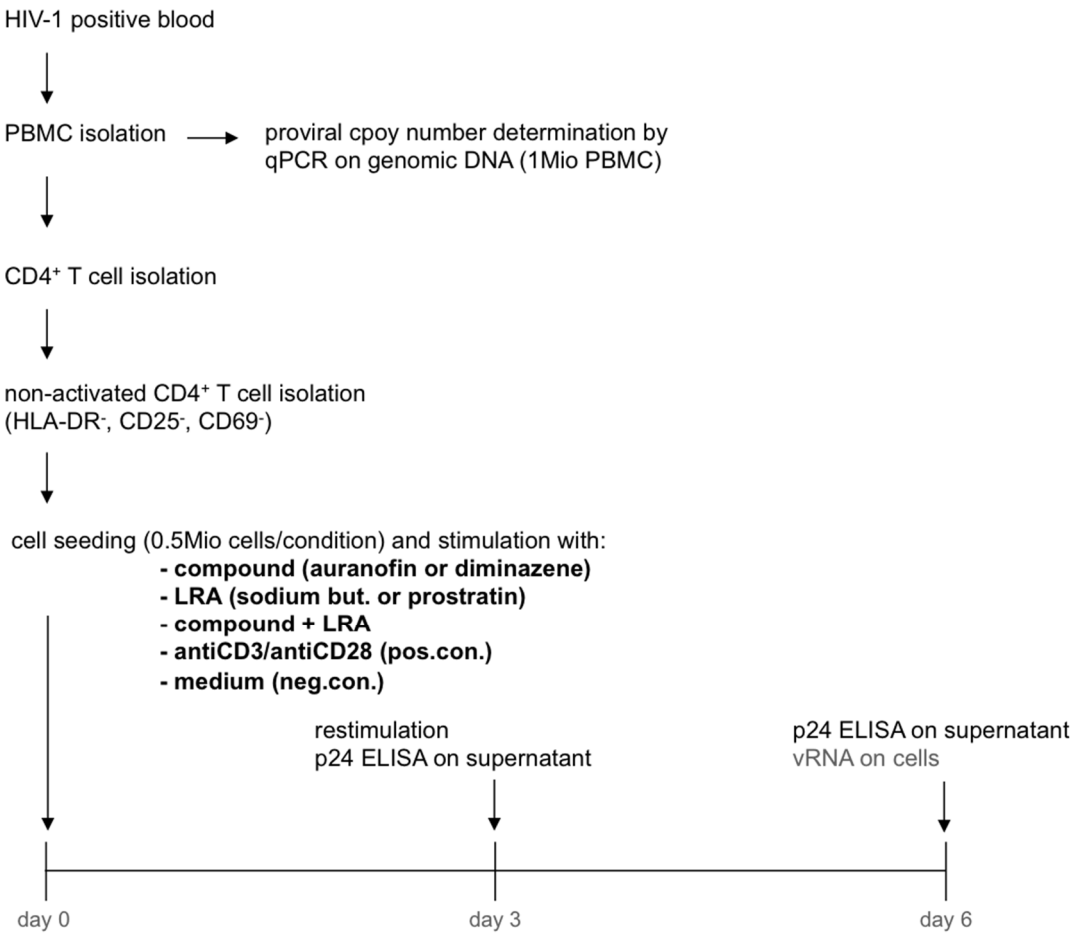

Figure 36: Overview on the experimental workflow on primary HIV-1 positive cell isolation and their reactivation. Stepwise isolation of non-activated CD4+ T cells from PBMCs, followed by stimulation with candidate compounds: LRAs and positive control or medium to reactivate the latent reservoir. Treatment refreshment after three days, cell collection for viral RNA (vRNA) isolation and supernatant collection for p24 ELISA testing on day six.

3.4.10.1.2 Establishment and verification of target cell isolation

In an initial setup experiment, the purity of the isolated cells was checked by flow cytometry. The results are shown in **Figure 37A**. Isolated resting CD4+ T cells from one representative donor were analyzed for viability, purity (presence of CD4) and for activation status (absence of activation markers HLA-DR, CD25 and CD69). Isolated cells were highly viable; around 94% of isolated cells were CD4+ and resting, due to the absence of activation marker expression (**Figure 37A**). The isolation of resting CD4+ T cells was successfully established.

Figure 37B shows the decrease in cell numbers during the isolation process for 8 donors. Between 22 - 37 million PBMCs were isolated from the obtained patient full blood. In a next isolation step, untouched $CD4^+$ T cells were purified from PBMCs, on average six million cells were obtained in this isolation step. In a final isolation, the untouched $CD4^+$ T cells were further purified for non-activated $CD4^+$ T cells. The removal of activated cells resulted in averaged 0.9 million non-activated $CD4^+$ T cells. This cell number drastically limited the experimental conditions, which could be tested. In case the overall $CD4^+$ T cell number was ≤ 3 million, the cells were not further isolated but used directly for reactivation testing.

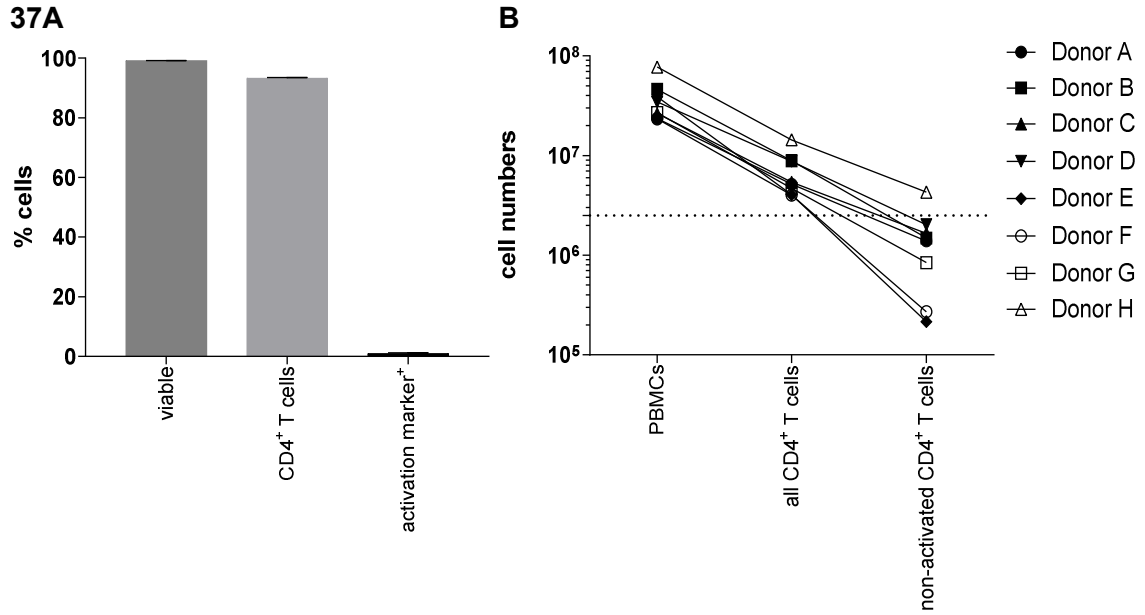

Figure 37: Determination of purity of isolated cells and reduction of cell counts during the isolation process. A) Isolated non-activated $CD4^+$ T cells from one respective donor were stained for viability, CD4 and activation marker (HLA-DR, CD69, and CD25) expression after isolation. **B**) Reduction in cell numbers over stepwise isolation of target cells for eight donors.

3.4.10.1.3 Confirmation of viability after treatment

To determine the optimal compound and LRA concentration, primary $CD4^+$ T cells from two healthy donors were treated for 24h and viability was analyzed by flow cytometry (**Figure 38**). Auranofin (**Figure 38A**) and prostratin (**Figure 38D**) treatment led to a massive decrease in viability when applied at high concentration. Sodium butyrate treatment (**Figure 38B**) was less toxic even at high concentrations. Diminazene treatment (**Figure 38C**) did not negatively influence viability even at high concentrations.

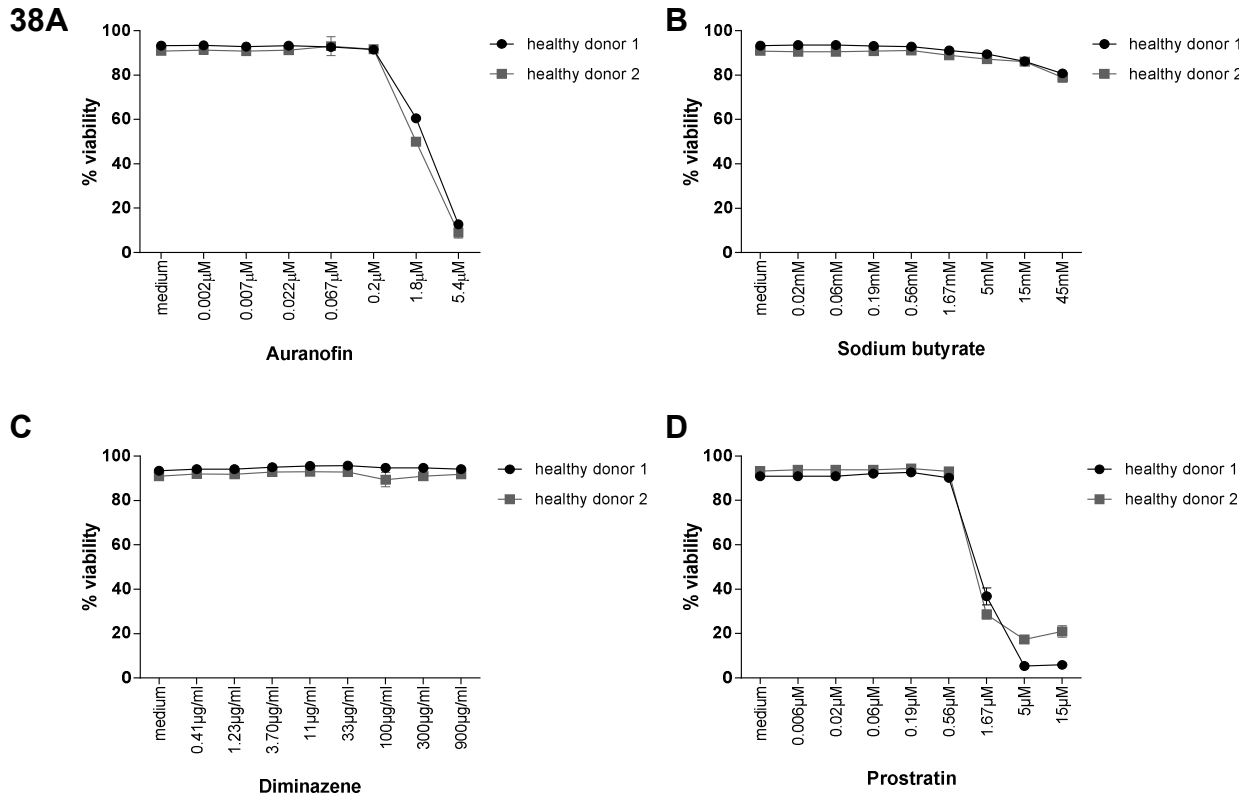

Figure 38: Effect on viability of candidate compounds or LRAs on primary CD4⁺ T cells. Primary CD4⁺ T cells were isolated from PBMCs (from two healthy donors) and treated with auranofin **(A)**, sodium butyrate **(B)**, diminazene **(C)**, or prostratin **(D)** dilution series and viability was assessed by flow cytometry after 24h of treatment.

In a next step, the effect of LRAs in combination with the respective compound on cell viability was determined after three and six days for CD4⁺ T cells from two healthy donors (**Figure 39**). It was decided to test auranofin in combination with sodium butyrate, as auranofin treatment led to an enhanced reversal when applied in combination with non-T cell activating LRAs. Further, diminazene was tested in combination with prostratin. Two different concentrations of LRAs were tested along with a constant concentration of the respective compound. The stimuli and compounds were replenished at day three. Here, prolonged combined treatment with auranofin and sodium butyrate led to a significant decrease in viability (**Figure 39A**). Sodium butyrate, however, showed high toxicity over six days of treatment on its own. It was decided to use 1mM sodium butyrate in combination with 0.2µM auranofin. The results for combined prostratin treatment along with diminazene (**Figure 39B**) showed a less toxic effect even over a prolonged period of treatment. It was decided to use 0.5µM prostratin with 100µg/ml diminazene for further experiments.

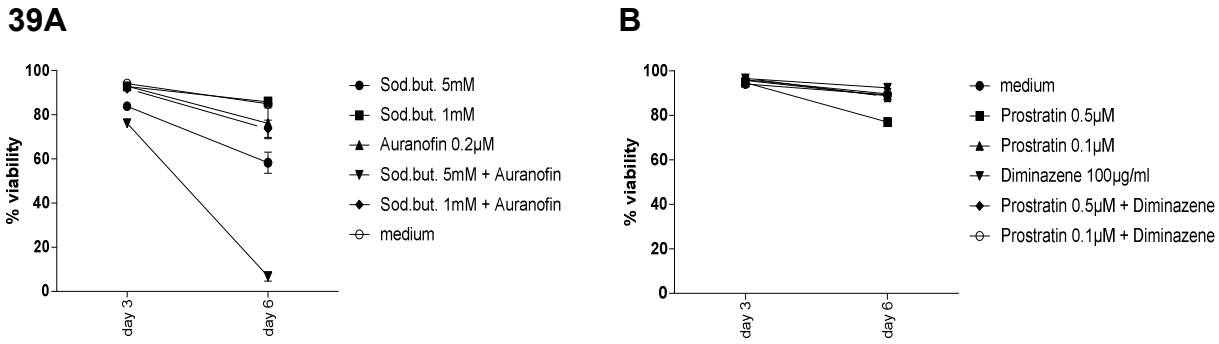

Figure 39: Effect on viability of candidate compounds in combination with LRAs on primary CD4⁺ T cells. Primary CD4⁺ T cells were isolated from PBMCs (from two healthy donors) and treated with two different concentrations of sodium butyrate alone or in combination with auranofin **(A)**, or with two different concentrations of prostratin with diminazene **(B)**. % Cell viability was determined by flow cytometry after three and six days.

In a final set of experiments, cell viability of non-activated CD4⁺ T (HIV-1 positive) cells was determined after treatment (**Figure 40**). In general, non-activated CD4⁺ T cells showed an overall decrease in viability over six days of culture (**Figure 40A**). The presence of prostratin in the medium led to a decrease in viability, whereas sodium butyrate treatment led to an even stronger decrease in viability. For the compounds tested, diminazene did not affect cell viability, whereas auranofin treatment led to over 90% of dead cells. Next, the viability after three days of compound treatment was determined (**Figure 40B**). The non-activated CD4⁺ T cells survived the treatment for a shortened period with a decrease in viability that was acceptable. Due to time limitations, it was decided to shorten the experimental procedure to three days.

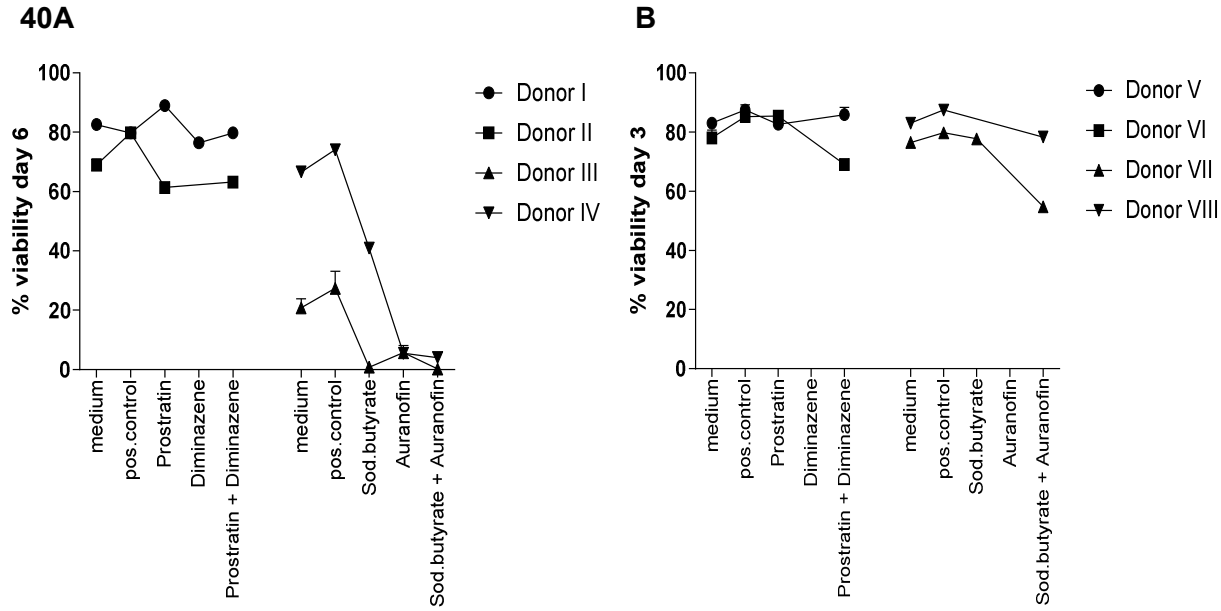

Figure 40: Effect on viability of candidate compounds in combination with LRAs on non-activated CD4$^+$ T cells from HIV-1 positive donors. Determination of cell viability after six days **(A)** and three days **(B)** of treatment with the indicated compounds, LRAs, combinations of those, positive control (antiCD3/antiCD28) or medium. Data is derived from 8 different donors; due to low cell numbers not all experimental conditions could be tested.

3.4.11 Increasing chances - Copy number PCR

In addition, a qPCR was performed on genomic DNA from HIV-1 positive PBMCs, which allowed determining the HIV-1 copies per genome equivalents of PBMCs (Malnati et al., 2008). For this, the *CCR5* gene and a conserved region of the HIV-1 LTR-*gag* were PCR amplified. The number of HIV-1 copies was determined by amplification of a plasmid standard with known numbers of copies and corrected for the *CCR5* copy number input. An example of PCR amplified HIV-1 and CCR5 fragments run on agarose gel is shown in **Figure 41**. For donor 8 a faint band (285bp) was seen above CCR5 fragment (81bp), indicating the presence of HIV-1 integrates in this donor, whereas in donor 12 only the CCR5 fragment amplification was seen after PCR. One standard dilution was run on gel serving as positive control.

41

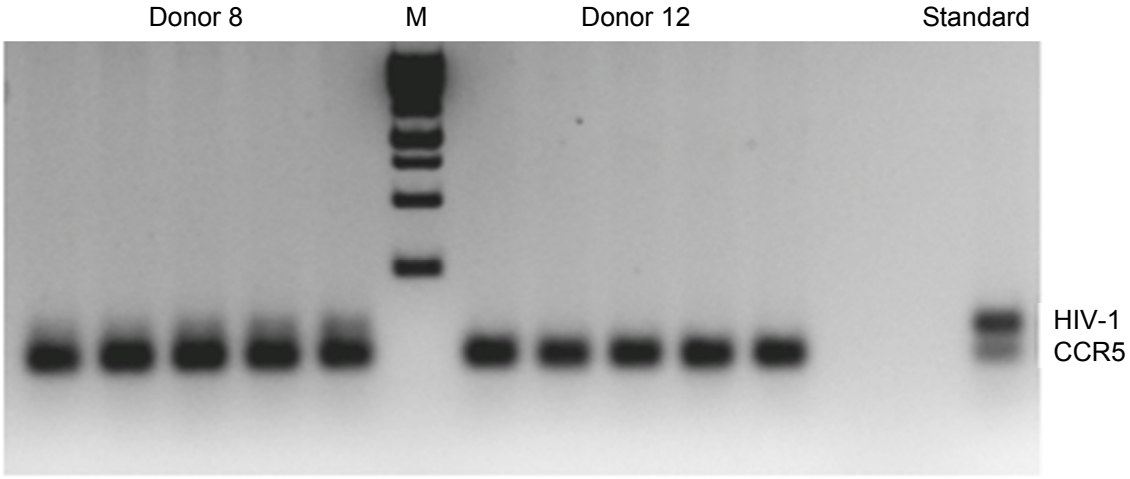

Figure 41: Representative result from two donors tested for the presence of HIV-1 provirus. Duplex qPCR was run to amplify a fragment specific for the CCR5 gene (81bp) and a fragment specific for HIV-1 LTR-*gag* (285bp). The qPCR was run on a 1% agarose gel for size separation followed by visualization. As control one standard dilution (containing known numbers of CCR5 and HIV-1 copies) was taken along. M= marker.

Table 15 shows the extrapolated numbers of extracted HIV-1 genomes from all isolated donors. Out of 19 donors, 13 were found positive for HIV-1 integrates. PBMCs, which were tested positive for HIV-1 integrates, varied greatly in numbers, ranging from 1 to around 360,000 HIV-1 genome equivalents found in one million PBMCs. Whereas in PBMCs from donors 5, 9, 10 and 12, no HIV-1 integrates could be determined. Furthermore, in donor 15 and 17 only two integrates per 100 million cells could be determined, which was considered below detection limit of the PCR. Only if proviruses were detected in donor PBMCs, cells were further isolated and tested. In total, 13 donors were isolated of which 7 donors were isolated for non-activated $CD4^+$ T cells and 6 donors were only isolated for $CD4^+$ T cells. Those cells were tested for reactivation of latent provirus after three days of treatment. It is important to highlight that a positive qPCR on genomic DNA does not specify whether the provirus is intact.

Table 15: Overview over primary donors isolated and HIV-1 genome equivalents determined by qPCR on genomic DNA. Indicated in light grey (donors 1-8, respectively) are donors isolated for non-activated $CD4^+$ T cells, whereas non-highlighted (donors 9-19, respectively) donors were isolated for (overall) $CD4^+$ T cells only, due to low cell cumbers. Marked in red are donors with HIV-1 integrates below detection limit of the assay. Those donors were excluded from further testing.

Donor number	HIV-1 copies/million genome equivalents in PBMCs
1	63.10
2	173632.17
3	2.64
4	3036.78
5	0.00
6	288.90
7	31.35
8	518.25
9	0.00
10	0.00
11	1.28
12	0.00
13	6.87
14	4.96
15	0.02
16	1.52
17	0.02
18	40.64
19	360268.23

3.4.12 p24 ELISA results from primary $CD4^+$ T cells after reactivation

To measure reactivation of latent provirus, the supernatant was collected at day 3 post-stimulation and tested for the presence of p24 capsid protein by a high sensitivity and commercially available ELISA (tested in singlets). Out of 13 donors tested under various conditions, only donor 19 was positive for p24 as shown in **Figure 42**. Prostratin treatment led to around 20pg/ml of p24 in the supernatant, whereas diminazene treatment alone led to around 11pg/ml. The combinational treatment led to around 20pg/ml. There was no synergistic or additive effect on reactivation when compound and LRA were applied together. The medium treatment led to a 7pg/ml of p24, an amount slightly smaller than the one seen for diminazene treatment. The highest amount of p24 was seen for the positive control using antiCD3/antiCD28 for overall T cell activation. Of note, the results were obtained from overall isolated $CD4^+$ T cells. This donor also showed highest number of HIV-1 copies per genome

equivalent. Since only one donor was positive tested for p24, the sample number was too small to draw adequate conclusions from this experiment.

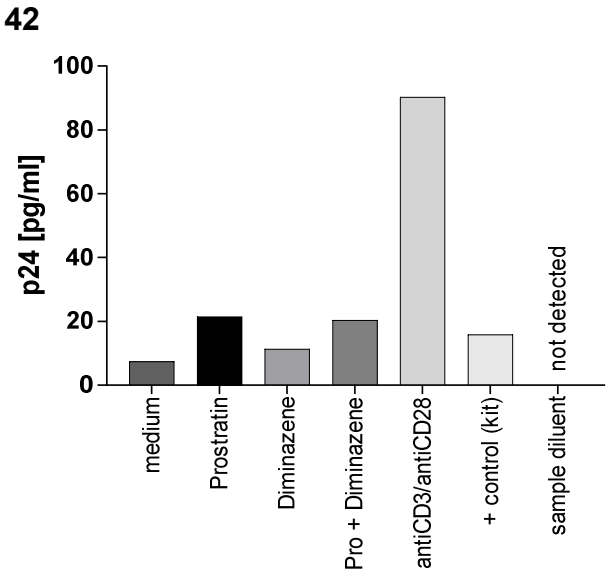

Figure 42: p24 ELISA results of donor 19. p24 ELISA was performed on culture supernatant of all isolated donors; 13 donors in total. Here the results of donor 19 are shown, the only donor in which reactivation of latent HIV-1 could be detected. Results are derived from treatment with prostratin, diminazene, a combination of both, medium or antiCD3/antiCD28 as positive control for three days.

4 Discussion

In this scientific work, two differential approaches were followed to validate candidates involved in HIV-1 latency. The candidate factors were derived from a genome-wide siRNA screen performed in HIVluc HEK293T cells, which were transduced with a HIVluc reporter construct, cultivated over several weeks before effect of host factor knockdown on HIV driven luciferase expression was determined (graphical presentation **Figure 5**, details on the screening setup described in section 3.1). A graphical scheme of the two approaches taken is shown in **Figure 6**. The results of the two approaches will be separately discussed in the following sections.

4.1 Approach I: Chromatin targets

4.1.1 Summary of TRRAP results

A graphical scheme is shown in **Figure 43** and represents the consecutive steps taken in this work to choose follow-up hits and the validation approach to identify a potential influence on HIV-1 latency.

The initial hits from a genome-wide siRNA screen were searched for host factors involved in chromatin binding and/or modification, as the chromatin environment along with the presence or availability of transcription and co-factors plays a crucial role in overall gene expression and also impacts HIV-1 transcriptional processes. It is assumed that a subset of factors involved in HIV-1 transcription might also impact HIV-1 latency. This assumption is supported by the two positive controls BRD4 and CYLD, which increased luciferase signal upon their knockdown in HIVluc HEK293 cells (**Figure 7A**), i.e. model for HIV-1 transcriptional influences (overview scheme **Figure 5B**), but were also found to support reversal of latency upon their knockdown (Manganaro et al., 2014; Zhu et al., 2012). The chosen set of host factors was tested under the same experimental conditions and transient knockdown of TRRAP by four individual siRNAs led to a robust increase in luciferase signal in HIVluc-infected HEK293T cells (**Figure 7A**), verifying TRRAP as a hit in this model system on HIV-1 transcriptional processes. The increase in luciferase signal in this system points towards a restrictive action of TRRAP

on HIV-1 transcription. In a consecutive step, stable TRRAP knockdown J-Lat cells were generated and tested with medium or in combination with different LRAs for a potential increase in latency reactivation (**Figure 15**). The results in J-Lat cells did not support an influence of TRRAP in this latency test system. In a final step, the stable knockdown results were confirmed by transient TRRAP knockdown via siRNA (**Figure 17A**) and again no effect of TRRAP knockdown on latency reversal was observed. In summary, the results of the conducted experiments point towards a restrictive involvement of TRRAP on HIV-1 transcriptional processes, whereas an involvement of TRRAP in HIV-1 latency could not be definitely determined. Potential experimental effects will be discussed separately (see section 4.1.4).

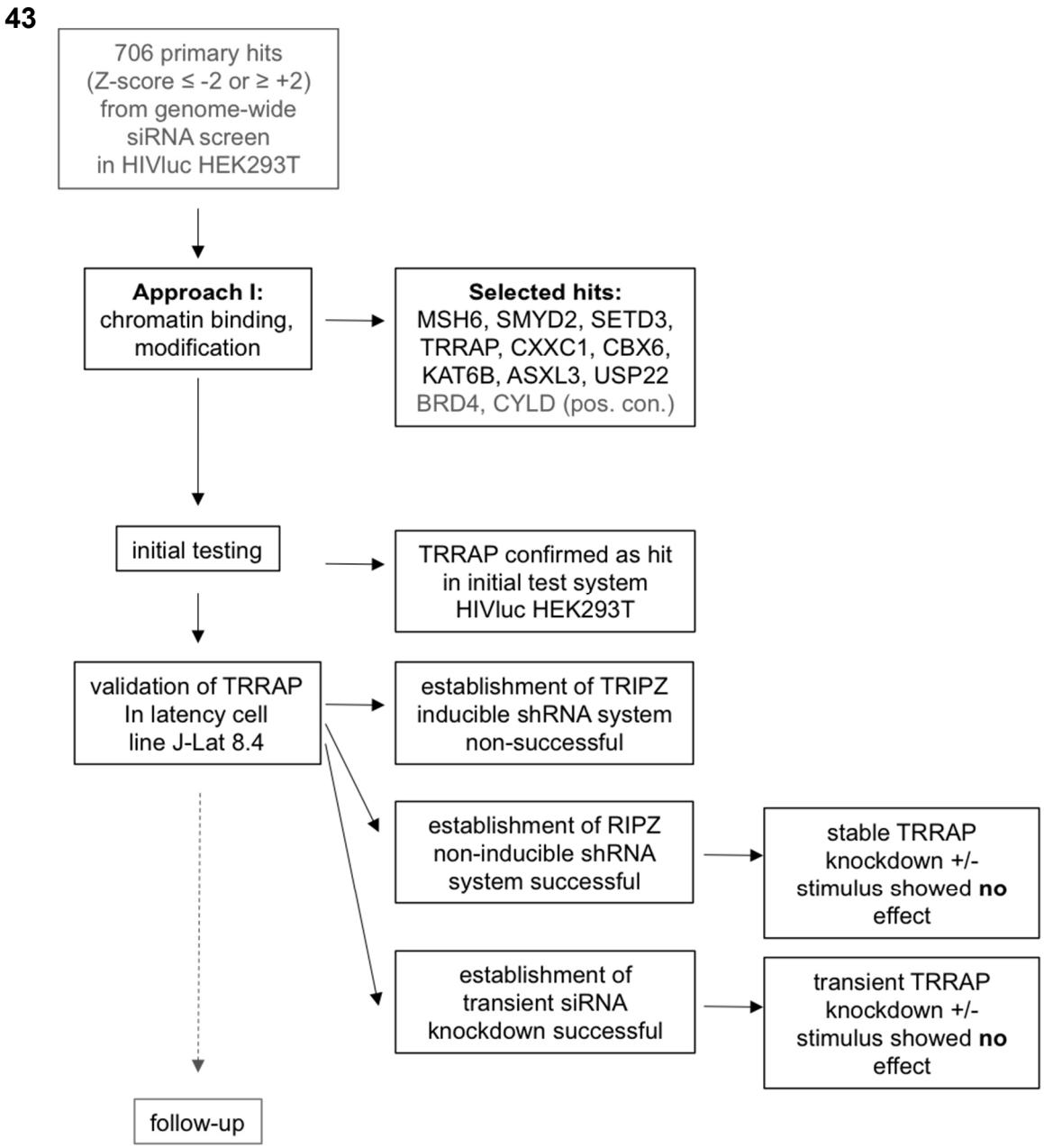

Figure 43: Graphical overview of approach I: Chromatin targets – *Identification of potential* latency reversing factors with chromatin binding and/or modification properties. Initial target selection was followed by validation in HIVluc HEK293T cells. TRRAP was confirmed as hit in HIV-1 transcriptional processes. Several methodologies were established to generate stable and transient knockdown J-Lat 8.4 cells. Stable knockdown of TRRAP in combination with various LRAs did not result in reversal of latency. Also, transient knockdown of TRRAP did not lead to a reversal of latency.

4.1.2 TRRAP involvement in HIV-1 transcriptional processes

TRRAP is conserved among many species (McMahon et al., 1998) and possesses an essential function during embryonic development, as mutations or gene disruptions lead to embryonic lethality (Herceg et al., 2001; Saleh et al., 1998). TRRAP itself is a huge protein with a molecular mass of >400kDa, therefore offers many binding sites for e.g. Skp1, c-Myc, p53 as well as E2F among others, and it is found in large complexes localized in the nucleus. Those TRRAP containing multi-protein complexes possess HAT activity, i.e. catalyzing the addition of acetyl groups to histone tails and thereby allowing spatial accessibility of DNA to transcription factors. It is noteworthy, that TRRAP itself does not possess HAT activity on its own. The composition of HAT complexes greatly varies by its subunit composition, while TRRAP remains the shared element between different complexes (Murr et al., 2007). It is assumed that HAT composition is dictating its substrate specificity. Therefore, TRRAP knockdown can have different effects on various pathways. The fact that TRRAP is of importance for the cell is underlined by its expression in all tissues (acc.to 'The Human Protein Atlas for TRRAP (Uhlén et al., 2015)).

There is also a report on TRRAP being an interaction partner of HIV-1 Tat, as TRRAP was identified in an affinity chromatography coupled to mass spectrometry approach from cellular extracts of Jurkat cells (Gautier et al., 2009). In this experimental setting, Tat binding of TRRAP could also be mediated by an intermediary protein and not by direct interaction. Moreover, in this study, the potential effect of Tat's interaction with TRRAP was assumed on TRRAP's role as being a transcriptional activator (by literature) but not further tested.

Another study proposed c-Myc along with TRRAP to be of importance for Tat transactivation downstream of P-TEFb engagement (Brès et al., 2009). The authors proposed that Tat recruits P-TEFb followed by c-Ski-interacting protein (SKIP) to the viral promoter (Brès et al., 2005), which consecutively leads to the recruitment of c-Myc and TRRAP and to the specific methylation of histones by HMT and viral gene transcription. The requirement of those factors was changed upon stress (as seen by UV induction) (Brès et al., 2009). This as well supports TRRAP as a candidate involved in HIV-1 transcriptional processes, but rather as a supportive factor, which would be in direct contrast to what was observed in the initial genome-wide siRNA screen and in the confirmation experiments performed in this study (**Figure 7A**) where TRRAP was found to be a restrictive factor. The difference might arise from divergent test systems used in both studies: On the one hand, Brès et al. transfected Hela LTR-luciferase cells with (varying) concentrations of Tat protein or with plasmid, from which Tat was expressed, whereas in the genome-wide siRNA screen HEK293T cells were transduced with an HIV-1 derived reporter virus (pNL4.3 expressing luciferase instead of *nef*, *env* deleted by frameshift

mutation and VSV-G pseudotyped, see **Figure 5A**). This already encompasses a big difference, as on one hand in the first approach Tat was additionally supplemented by transfection (Brès et al., 2009) whereas in the other case Tat needed to be produced from the integrate before it could push viral transcription. In addition to this, the pNL4.3-derived vector transcribed for additional viral proteins, which can also influence the results. Further, the usage of lentiviral particles leads to an integration of transgene/provirus into the host genome, whereas plasmid transfection will have only a transient but strong effect, as the cell will produce huge amounts of gene product from transfected plasmid, whereas the production from the integrated transgene might be lower, due to the usage of the viral LTR as promoter. The difference in test systems might account for the different results concerning the involvement of TRRAP in HIV-1 transcription.

Further, one could also argue that TRRAP-containing HAT complexes are supportive to transcription by acetylating histone tails and releasing the DNA from tightly bond nucleosomes. This would point towards a supportive role of TRRAP for HIV-1 transcription and that the results from the genome-wide siRNA screen are derived from an accumulation of aberrant processes which also affect, on the second line and not by a direct effect, the HIV-1 promoter. More experiments will be needed to determine under which conditions TRRAP functions as a supportive or a restrictive factor in HIV-1 transcription.

4.1.3 TRRAP involvement in HIV-1 latency reversal

Further, there was no significant effect after TRRAP knockdown on HIV-1 latency reversal neither on its own nor in combination with an LRA as determined in J-Lat 8.4 cells (**Figure 15**, **Figure 17A**). Therefore, one might argue against a role of TRRAP in HIV latency and reactivation from it. It is possible that TRRAP containing complexes might be differentially presented in a latency setting and by this evoke a different effect on latency than under ‘normal’ transcription, i.e. transcriptional processes in resting versus activated $CD4^+$ T cells. However, this potential difference cannot be elucidated by the usage of immortal cell lines.

Nevertheless, it could be possible that TRRAP elicits differential effects on HIV-1 transcription and latency as, for example, described for c-Myc: On the one hand, c-Myc supports Tat transactivation needed for HIV-1 transcription processes, but on the other hand acts restrictive in HIV-1 latency reactivation (Jiang et al., 2007). As TRRAP associates with c-Myc (McMahon et al., 1998), it is daring to argue for a differential role of TRRAP as well. But it is likely that the

restrictive effect of c-Myc in latency cell lines is due to its higher expression (de la Fuente et al., 2002; Stojanova et al., 2004), forming a repressive complex at the viral promoter and the recruitment of HDAC1 (Satou et al., 2001). This repressive mark would likely outrange the capacity of co-activators and chromatin remodelers without additional stimulation. Whether TRRAP plays a role in HIV-1 latency could not be definitely determined (also due to some technical considerations, discussed below). Further, TRRAP expression as well as its half-life might differ in J-Lat cells, i.e. actively dividing cells, from resting $CD4^+$ T cells, masking a direct or second line effect of TRRAP on latency due to its abundance or stability. Unfortunately, there are no reports on TRRAP half-life and stability in non-dividing cells and further no reports exist on TRRAP and HIV latency.

4.1.4 Experimental aspects

There are several technical considerations regarding the experimental settings and the techniques used. As first point, TRRAP knockdown was only confirmed on mRNA level in all experiments since the confirmation on protein level failed twice by Western blot. Adaption of the Western blot test system should have included low percentage polyacrylamide gels plus a size-suitable protein marker, which would confirm successful migration into the gel and successful transfer to the membrane after blotting. Further, as also a dot blot with protein extracts failed, an extraction of nuclear extracts followed by DNase digest could support detection of ‘freed’ TRRAP in the supernatant. Since knockdown with siRNA/shRNA only affects newly produced mRNA but does not affect the level of produced protein, it is impossible to conclude that knockdown was achieved and/or maintained. In addition, TRRAP protein abundance peaks in S phase while is lowest in G0/G1 phase, demonstrating its involvement in cell cycle-progression (Ichim et al., 2014). Its mRNA levels, however, stay constant during different cell cycle-phases, pointing towards a post-transcriptional regulation of TRRAP in which e.g. binding partners will impact its protein half-life (Ichim et al., 2014). Therefore, to elucidate an effect of TRRAP in resting (HIV-1 positive) $CD4^+$ T cells, the usage of cycling cells might not result in a reliable result.

Further, the production of stable inducible knockdown cells was complicated as seen for the results of inducible shBRD4 knockdown J-Lat 8.4 cells (serving as positive control). The inducible knockdown did result in averaged 60% knockdown degree on mRNA level (**Figure 9C**) with correlatable RFP expression levels (**Figure 9B**) but no effect on increased reversal of latency was observed when tested along with an LRA (**Figure 10**) which is in

contrast to the results in HIVluc HEK293T (**Figure 7A**) and published data (as mentioned above), suggesting the inducible shRNA test system not being sensitive enough to detect small changes. And this low sensitivity probably stems from the low induction capacity of shRNA. Neither selection with puromycin to allow only transduced cells to survive or higher concentrations of doxycycline or prolonged exposure did result in a better knockdown result. The consequent change towards a non-inducible system (RIPZ derived shTRRAP and shCYLD) led to slightly better knockdown results along with increased RFP expression (**Figure 13**), even though a correlation of mRNA knockdown and RFP expression was less robust. An explanation for this could be the high multiplicity of infection used for the transduction process leading to multiple transductions and a potential loss of transgene over time. Further, it is also possible that TRRAP, since it participates in cell cycle progression, is of importance for cellular integrity and survival with a different turnover time than the positive control CYLD. In this case, the puromycin selection process could select on cells, which can outgrow the knockdown effect of TRRAP, and this could explain why RFP expression stayed high while mRNA knockdown was gradually lost over time and after freezing (**Figure 14**).

4.1.5 TRRAP outlook

For the elucidation of a potential role of TRRAP in HIV-1 latency, the protein expression levels need to be determined in target, i.e. resting, cells. It is likely that TRRAP levels are reduced in resting cells as compared to cycling cells, since the lack of proliferation. In a consecutive step, TRRAP knockdown (by shRNA/siRNA, CRISPR or other means) would need to be achieved and proven on protein level in a time dependent manner, to allow a predication on protein half-life and the elucidation of a potential direct effect on the cellular viability. In addition, the status of transcription factors known to also initiate HIV transcription could be quantitated after TRRAP knockdown, which could support TRRAP's potential role in affecting gene expression. The next step would aim at identifying TRRAP's involvement in HIV-1 latency alone or in combination with an LRA, while this will be experimentally challenging, due to the low number of circulating resting $CD4^+$ T cells, which carry an intact provirus. Leukapheresis could be an option to obtain high numbers of resting cells from patients, while a potential influence of TRRAP knockdown on HIV-1 latency could be easily masked by the bulk of non-infected ones and would need highly sensitive techniques or propagation of reactivated virus as by a quantitative viral outgrow assay. As a possible alternative direct infection of non-activated $CD4^+$ T cells would allow the isolation cells from HIV-1 negative donors and infection with a

characterized virus without considering the presence of quasi species. Even though direct infection of resting cells is possible, it only leads to low number of infected cells (Lassen et al., 2012; Swiggard et al., 2005). Of course, also the usage of other primary models (using activated T cells for infection and allowing the cells to return to a resting state) could be used to test for a potential effect of TRRAP on latency.

4.2 Approach II: Druggability

4.2.1 Auranofin, diminazene summary

In the second approach, the follow-up hits were chosen based on the availability of compounds, which are documented to inhibit the respective host factors. **Figure 44** summarizes the steps taken to identify and validate compounds, which possibly influence HIV-1 latency: The chosen compounds were titrated on J-Lat 8.4 cells to determine the optimal concentration and tested along with different LRAs to determine potential effects on latency reversal. Auranofin was found to have a positive effect on latency reversal tested in combination with any LRA in J-Lat clones tested but not its own (**Figure 20**), whereas in U1 cells auranofin robustly reversed latency only in combination with the tested HDACi (**Figure 29**). In a consecutive step, the effect of auranofin on latency reversal was mimicked by other compounds, which were proposed to inhibit auranofin's target PRDX5 and its upstream pathway. None of the mimicking compounds showed the exact effect than auranofin **(Figure 24).**

However, diminazene was identified to impact latency reversal in J-Lat cells when applied in combination with either TNFα or prostratin, to a level, which was even greater than what was seen for auranofin. This could point towards a certain overlap in target(s) of auranofin and diminazene. However, diminazene's effect was cell line specific and was only detected in J-Lat clones but not in U1 cells. Target validation by siRNA knockdown followed by stimulation in specific combinations and cell systems showed slight induction in HIV-1 latency reversal (**Figure 34A, Figure 35A**), supporting this pathway to be the target of auranofin and potentially also of diminazene (see following sections). In a final step, the methodology of testing auranofin or diminazene in combination with an LRA was established in primary HIV-1^+ $CD4^+$ T cells. In the following sections, auranofin, diminazene and primary HIV-1^+ $CD4^+$ T cell results will be discussed separately.

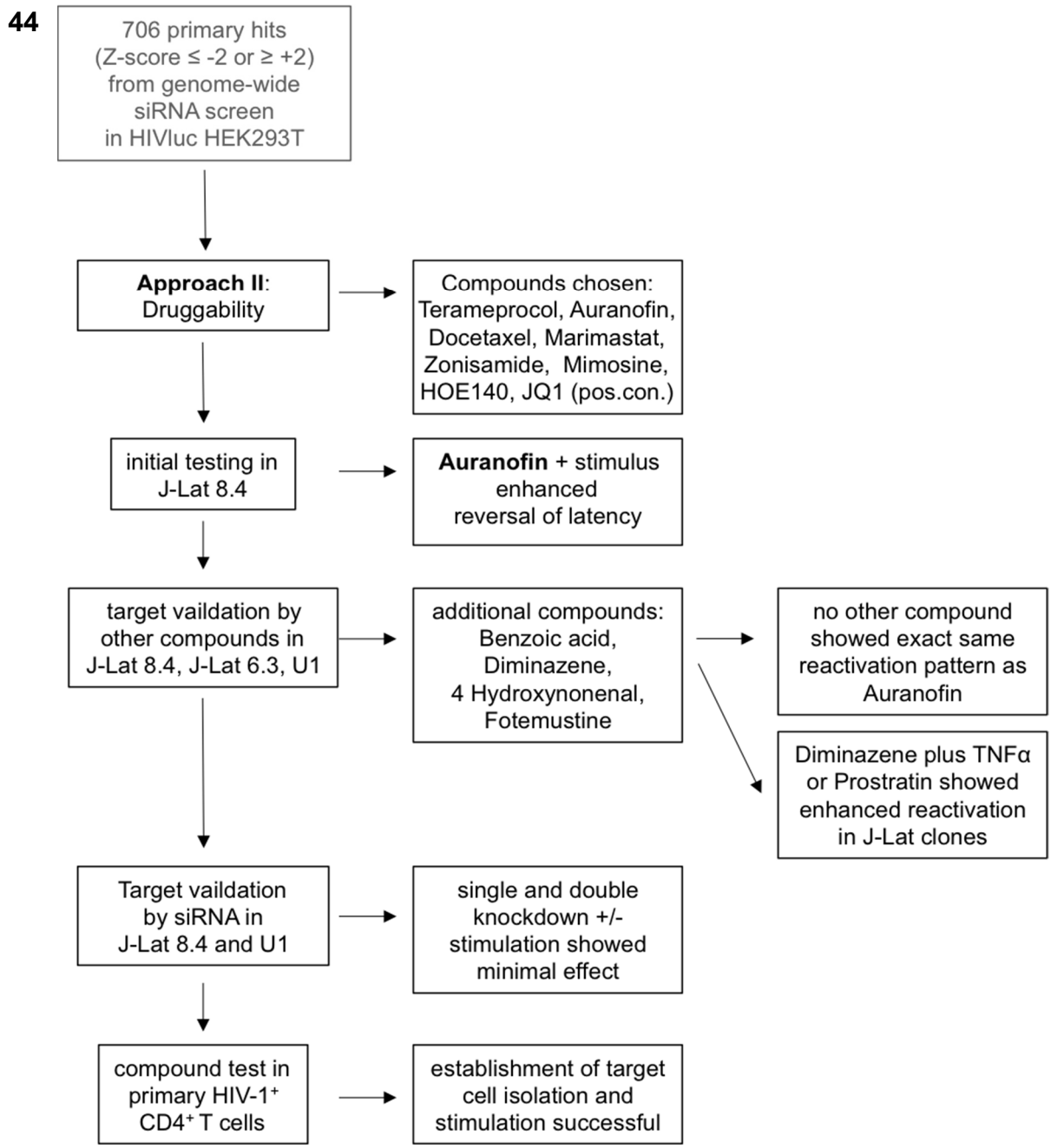

Figure 44: Graphical overview of approach II - Druggability. The initial selection of compounds was chosen and tested in J-Lat 8.4 cells. Auranofin was identified to enhance the reactivation of latency when applied in combination with any of the tested LRAs, i.e. TNFα, prostratin, SAHA or sodium butyrate. As consecutive step, compounds were identified which were stated to target the same host factor, i.e. PRDX5 and its upstream pathway member TXNRD. The subsequent testing of the additional compounds identified diminazene to enhance reactivation, an effect which differed from auranofin and which was cell line specific. Target validation was performed by siRNA, which could slightly recapitulate the effect of auranofin (and diminazene). As a final step the methodology of testing the identified compounds in primary HIV-1$^+$ CD4$^+$ T cells was established.

4.2.2 Auranofin and its mechanisms of action

4.2.2.1 Auranofin and the thioredoxin system

Auranofin is an organo-gold compound, which is approved for the treatment of rheumatoid arthritis, although its exact mechanisms of action is not yet fully elucidated (Tejman-Yarden et al., 2013). Auranofin gained interest as it might also be useful in treatment of cancer (Chen et al., 2014; Fiskus et al., 2014; Marzano et al., 2007), bacterial (Hokai et al., 2014; Jackson-Rosario and Self, 2009; Jackson-Rosario et al., 2009) as well as parasite infections (Ilari et al., 2012; Lobanov et al., 2006; Sharlow et al., 2014) and potentially even in neurodegenerative diseases (Madeira et al., 2013, 2014). There is cumulating evidence that auranofin evokes its effect by the thioredoxin system. This system, with its contributing partners thioredoxin reductase (TXNRD), thioredoxin (TRX) and the reduced form of nicotinamide adenine dinucleotide phosphate (NADPH), supports the cellular redox homeostasis by scavenging reactive oxygen species (ROS) species and oxidized proteins (Arnér and Holmgren, 2011; Holmgren and Björnstedt, 1995). ROS species, as H_2O_2 and OH, are instable, highly reactive and continuously produced as by-product from essential metabolic processes, like oxidative phosphorylation in the mitochondria, but can also be derived from pollutants, chemicals, and radiation, among others (Lobo et al., 2010). An imbalance in the redox regulation, by an excess of ROS or an inadequacy of redox proteins, leads to oxidative stress, which compromises the integrity of DNA, lipids and proteins and can ultimately lead to apoptosis (Du et al., 2012). An imbalanced redox homeostasis is also associated with aging and cancer (Kruk and Aboul-Enein, 2017; Liochev, 2013). However, it is important to mention that ROS not only has detrimental effects but also serves as a crucial second messenger in various signaling cascades. Further, ROS are also implemented in NFκB signaling, whereas it can have both activating and inhibiting effects, which is dependent on the kind of ROS, its exposure time/intensity and the cell type (Hirota et al., 1999; Morgan and Liu, 2011).

TXNRD (cytosolic TXNRD1 and mitochondrial TXNRD2) uses NADPH to reduce oxidized TRX (cytosolic TRX1 and mitochondrial TXR2) and also other targets. Reduced TRX is a powerful protein disulfide reductase, which serves as electron donor for ribonucleotide reductase (Holmgren and Björnstedt, 1995), influences the DNA-binding of transcription factors such as NFκB and activator protein 1 (AP-1), and reduces PRDX, which in turn reduces H_2O_2 (Du et al., 2012; Halliwell and Gutteridge, 2015; Matthews et al., 1992; Zhang et al., 2014). The oxidized forms of PRDX and TRX are recycled to its reduced form by electron donation from TRX and TXNRD, respectively. A graphical presentation of the thioredoxin system is shown in **Figure 45**.

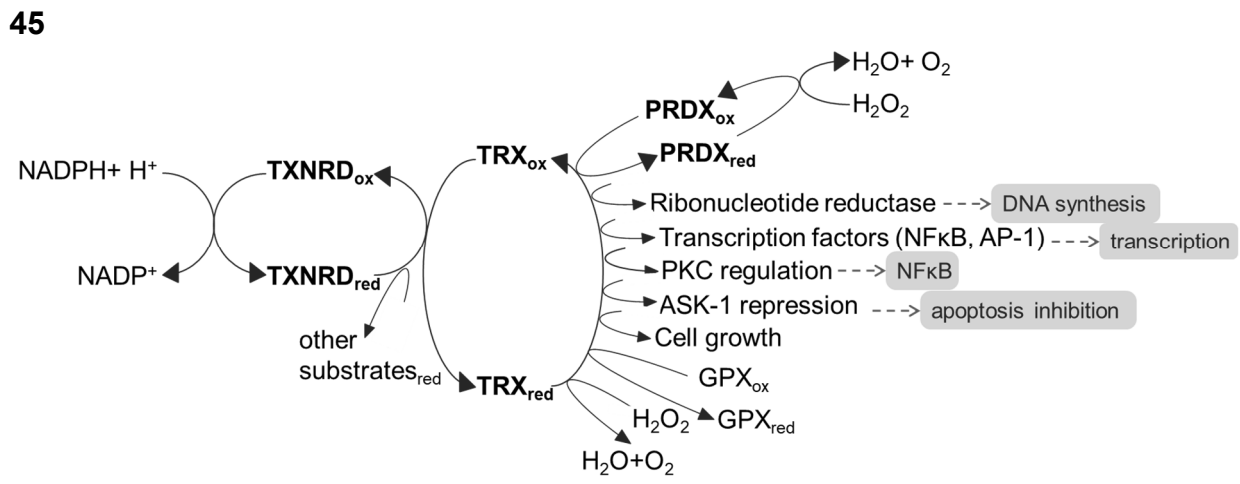

Figure 45: Schematic representation of the thioredoxin system. Reduced TXNRD serves as electron donor for oxidized TXR and other substrates. Reduced TRX serves as electron donor for PRDX, ROS directly and other substrates. Further, TRX can influence binding of transcription factors, suppress apoptosis, stimulate cell growth among many other functions. AP-1= activator protein 1, ASK-1= apoptosis signal-regulating kinase 1, $NADP^+$= nicotinamide adenine dinucleotide phosphate, NADPH= reduced form of nicotinamide adenine dinucleotide phosphate, GPX= glutathione peroxidase, ox= oxidized, PRDX= peroxiredoxin, PKC= protein kinase family C, red= reduced, TRX= thioredoxin, TXNRD= thioredoxin reductase.

Auranofin's proposed mode of action is by inhibiting TXNRD (TXNRD2 more potently than TXNRD1 (Rigobello et al., 2005)) and by this, it induces apoptosis via the mitochondrial pathway (Cox et al., 2008; Rigobello et al., 2005, 2008). It does not increase H_2O_2 levels directly but indirectly by its irreversible binding to TXNRD (Fan et al., 2014), leading to an oxidized status and a decreased mitochondrial membrane potential. Of note, the cellular redox homeostasis involves several pathways with various antioxidant enzymes, which can partially account for each other (Du et al., 2012; Zhang et al., 2014).

It is a possible explanation that auranofin-induced apoptosis leads to a reversal of latency in the tested latency cell models. This was shown to be the case for several cytotoxic drugs, which induced apoptosis-derived latency reversal in a dose-dependent manner in ACH-2 and U1 cells (Khan et al., 2015). On the other hand, the auranofin concentration applied was tested for its effect on cell viability and no negative influence was determined for the duration tested. Therefore, reversal of latency in our experiments cannot be satisfiably explained by a sole apoptosis induction capacity of auranofin. This is also further supported by other publications, which tested auranofin as cytotoxic drug on various cell lines without observing cell death at comparable low concentration (≤0.5μM) but at doses 2μM and higher, which also resulted of inhibition of other redox enzymes (Du et al., 2012; Fan et al., 2014; Park and Kim, 2005;

Varghese and Büsselberg, 2014). Of note, in various cancers and cancer cell lines the thioredoxin system is expressed at higher levels, which allows better response to ROS and contributes to cell survival and proliferation (Arnér and Holmgren, 2006; Gopalakrishna et al., 2018; Lincoln et al.; Yoo et al., 2007). This might also bias the usage of those cell lines. The proposed effect of auranofin on the thioredoxin system is shown in **Figure 46** on the left side.

4.2.2.2 Auranofin and PKC

Despite TXNRD, also the protein kinase (PKC) family is described by some publications (published around 1990) to be targeted by auranofin (Froscio et al., 1989; Parente et al., 1989; Wong et al., 1990). Even though other publications clearly claim PKC not being a target of auranofin (Hashimoto et al., 1992), the discrepancy might be derived from the different types of cell used, as PKC inhibition was seen in neutrophils, but not in Jurkat cells or by the different test systems applied. This kinase family comprises 15 enzymes, which are further grouped according to their cofactor dependency (Mellor and Parker, 1998) into conventional, novel and atypical isoenzymes. The PKC family is of importance in signal transduction and in cellular survival, proliferation, migration, as well as apoptosis (Dempsey et al., 2000). PKC activation has been linked to latency reversal, as seen for prostratin, a PKC agonist (Jiang and Dandekar, 2015) which leads to NFKB activation (Jeon et al., 2000). The potential inhibition of PKC by auranofin is in clear contrast to our results, as treatment of J-Lat cells with both T cell activating LRAs led to increased reversal of latency (**Figure 20A**), whereas the opposite would be expected due to their opposed action, i.e. PKC agonist versus inhibition. The difference might be explained by the auranofin concentration applied, as PKC inhibition was observed upon 5µM, whereas our experiments were conducted at 0.2µM- a concentration 25 times lower. It is likely that the concentration applied is too low to efficiently block PKC, which would need to be experimentally determined. Nevertheless, the synergistic effect of auranofin and prostratin on latency reversal is unlikely derived from auranofin's sole action on PKC.

Interestingly, there is a link of PKCs, the thioredoxin system and ROS. On the one hand, PKC proteins possess a catalytic and a regulatory domain, both domains being cysteine-rich and are therefore also prone to oxidation by ROS (Gopalakrishna et al., 2018). It has been shown that low levels of ROS can activate PKC, independent of its cofactor, while high levels of ROS inactivate PKC (Gopalakrishna and Jaken, 2000). On the other hand, the thiol redoxin system is responsible for the reduction of oxidized PKC and further TRX is binding PKC with high affinity at its catalytic domain, preventing its autophosphorylation and by this keeping PKC inactive (Watson et al., 1999). If auranofin does not directly target PKC, it would still indirectly

affect it. So would the inhibition of TXNRD lead to a decrease of reducing capacity of the cell and the resulting increase in ROS could activate PKC signaling while oxidized TRX could also not occupy its catalytic domain and therefore also not inhibit its (auto-) phosphorylation. PKC as potential target of auranofin is shown in **Figure 46** middle part.

4.2.2.3 Auranofin and IKK

One further host factor described in literature to be targeted by auranofin is IKKβ – a member of the IKK complex, which is a major player in NFκB activation (Jeon et al., 2003, 2000). The inhibition of IKK is used to explain the beneficial effect of auranofin in rheumatoid arthritis patients, as it leads to reduction of inflammatory NFκB-signaling. The IKK complex consists of IKKα, IKKβ and two molecules of IKKγ (also known as NEMO) for the canonical NFκB activation or of two molecules IKKα without IKKγ for the non-canonical pathway. Activation of the IKK complex by e.g. proinflammatory cytokines as TNFα or receptor stimulation (canonical pathway) will lead to phosphorylation of IKK complex and this will in turn lead to phosphorylation of IκBα, which is associated with NFκB (p50/p65) heterodimers, masking the nuclear localization signal (NLS). Upon phosphorylation at specific residues, IκBα is marked for proteasomal degradation, unmasking the NLS allowing NFκB to translocate to the nucleus and induce target gene transcription (Luo et al., 2005; Moynagh, 2005; Scheidereit, 2006). If auranofin would block IKK, then NFκB activation followed by nuclear translocation and transcription would be inhibited and no reversal of latency would be expected. This contrasts with our results, as auranofin together with TNFα (an inflammatory cytokine) or prostratin leads to increased reversal as compared to LRA treatment alone (**Figure 20A**) and not to a decrease. The inhibition of IKK by auranofin (as reported by the above-mentioned references) was tested in several cell lines at higher concentrations for shorter time points than our presented experiments. It is possible that IKK inhibition of auranofin is concentration dependent, whereas at low doses no inhibition occurs. It is also possible that IKK inhibition is time dependent and is overcome by the cell. Those possibilities have to be experimentally confirmed. Further, there is also evidence that NFκB can be activated by ROS independent of IKK phosphorylation, even though this is highly dependent on the ROS species, concentration, exposure time and cell type (Gloire et al., 2006; Lingappan, 2018). An integrated scheme of IKK as potential target for auranofin and the overlap in pathways is shown in **Figure 46** on the right side.

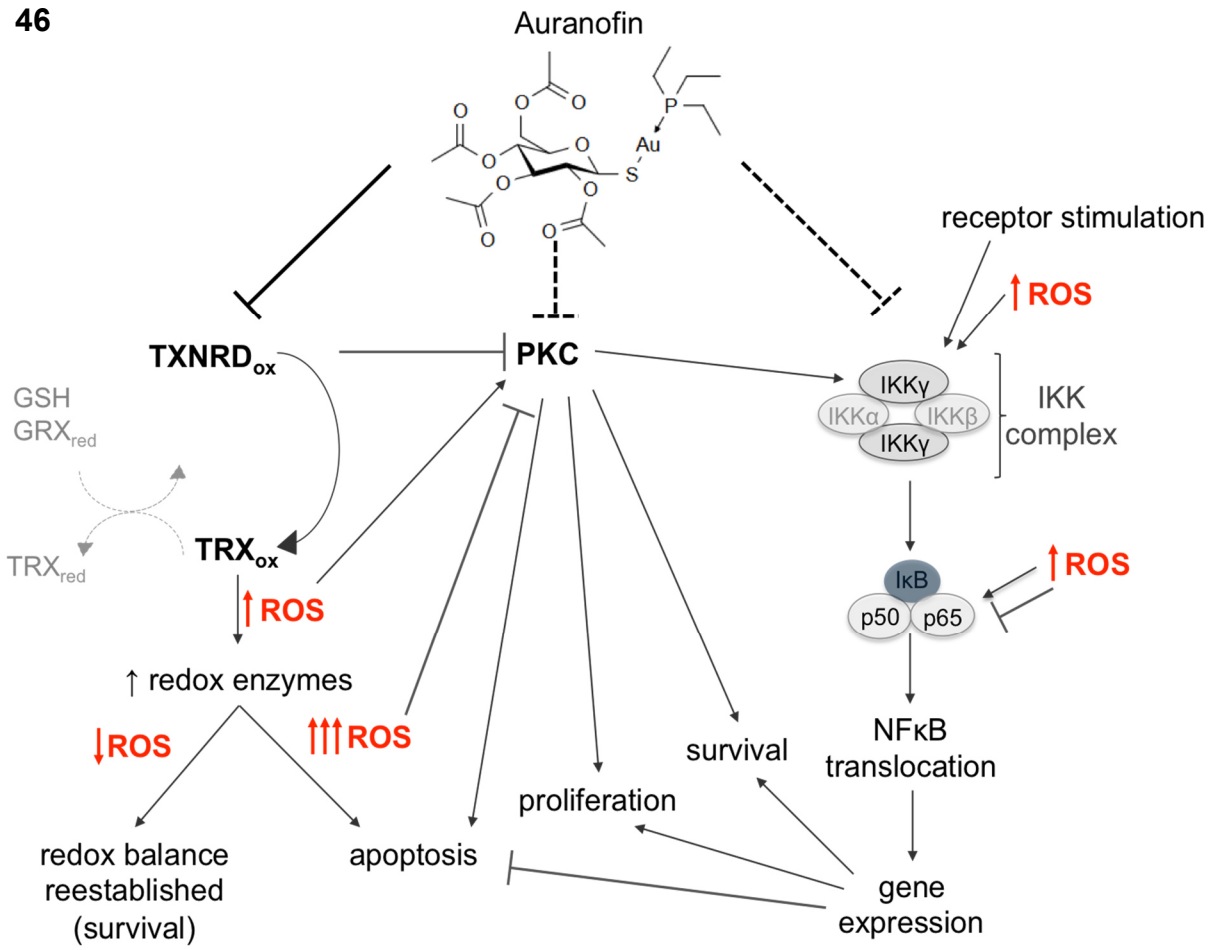

Figure 46: Graphical presentation of auranofin's (potential) targets and its effect. **Left side)** TXNRD as potential target of auranofin: TNNRD is blocked by auranofin and cannot reduce its targets as TRX. Partly, this will lead to increases in oxidized substrates and susceptibility towards ROS. Reduced glutaredoxin as well as glutathione are indicated as backup system and can reduce oxidized thioredoxin. Increased levels of ROS will lead to increased redox enzyme transcription, whereas prolonged exposure to ROS will lead to the induction of apoptosis. **Middle part)** PKC as potential target of auranofin: PKC can activate various signaling pathways involved in survival, proliferation and apoptosis. It can also activate the NFκB pathway. Further, thioredoxin can inhibit PKC activation and also ROS can activate and inhibit PKC, dependent on the kind of ROS, exposure time and target cell. **Right side)** IKK as potential target of auranofin: IKK inhibition can inhibit canonical NFκB signaling, even though the non-canonical pathway might be unaffected. Further, ROS can induce but also block NFκB activation dependent on the kind of ROS, exposure time and target cell. GSH= glutathione (an antioxidant), GRX= glutaredoxin, IKK= IκB kinase complex, IκB= inhibitor of kappa B, ox= oxidized, p50/p65= NFκB heterodimer, PKC= protein kinase C family, red= reduced, ROS= reactive oxygen species, TRX= thioredoxin, TXNRD= thioredoxin reductase.

4.2.3 Auranofin and its involvement in latency reversal

Auranofin‘s effect on the latent reservoir has been reported before as tested on a non-human primate model (SIVmac251-infected rhesus macaques) and on *ex vivo* tested HIV-1$^+$ CD4$^+$ T cell populations (Chirullo et al., 2013; Lewis et al., 2011). The mode of action was not determined in both studies, but an increase of annexin V positive cells, i.e. marker for apoptosis, which went along with a downregulation of CD27 and CD28 surface markers, i.e. markers recognized for memory or survival (Hendriks et al., 2000; Mir and Mir, 2015), was observed. The authors claim that a lower oxidative status of the memory T cell compartment renders those cells more susceptible to auranofin treatment, which subsequently leads to the induction of apoptosis, while auranofin treatment did not induce proviral transcription.

Our primary cell results point towards a higher susceptibility of resting CD4$^+$ T cells to auranofin than overall CD4$^+$ T cells (compare **Figure 39A** and **Figure 40**). This clearly indicates the higher sensitivity of this cell population to auranofin (and sodium butyrate). But whether this effect on cell viability is due to lower levels of antioxidant enzymes in non-activated CD4$^+$ T cells could not be determined by the experimental setup and read-out. Sorting of different CD4$^+$ T cell populations could elucidate the differential susceptibility of these populations to auranofin.

4.2.4 Auranofin conclusion and outlook

Auranofin robustly increases latency reversal in J-Lat cells when tested with various LRAs, whereas its mechanism of action remains to be determined. Auranofin also induced reversal of latency in U1 cells when treated with HDACi. Supported by literature, auranofin might primarily evoke its effect via the redox system and an imbalance leading to an overall effect on the cell, due to a change in the redox homeostasis towards more oxidized products, a change in binding affinity of transcription factors to DNA and also to a change in NFκB signaling, among others. Since redox enzymes can partially account for each other, it is not surprising that conducted siRNA knockdown experiments did not fully recapitulate the effect of auranofin. Also, other (additional) targets of auranofin cannot be excluded. In addition, the experimental possibilities of measuring specific redox processes within a cell are limited and reflect in many cases only the overall redox state, complicating the elucidation of auranofin’s specific effect on the thioredoxin system. Further, special attention needs to be given to the cells tested, as cancer cell lines generally possess higher levels of redox enzymes and might cope differential

with redox stress than primary cells. Despite all those considerations and hurdles, auranofin is an interesting compound, which is worth to be further tested. A major benefit is that auranofin is approved for use in humans and due to this good data on safety, dosing, and side effect among others already exist. The results of a currently ongoing clinical trial, testing for an effect on the reservoir size under intensified HAART applied in combination with auranofin, are eagerly awaited (clinical trial number: NCT02961829).

4.2.5 Diminazene and its mechanisms of action

4.2.5.1 Diminazene and its trypanocidal action

Diminazene is a synthetic diamidine used since the 1950s as trypanocidal agent, protecting cattle and also other ruminants against protozoal species of the genus *Trypsanosoma*, *Babesia* and *Leishmania*, among others (Jean-Moreno et al., 2006; Nehrbass-Stuedli et al., 2011; Nnadi et al., 2019). Even though diminazene usage is limited to the treatment of domestic life stocks, there are also some reports on treatment of African Trypanosomiasis in humans, which led to side effects as vomiting, diarrhea and rash among others, but without long-term effects once treatment was stopped (Abaru et al., 1984). Its mechanism of action is not well understood but there is evidence that it exhibits its effect by binding to AT rich regions and due to this inhibiting replication of kinetoplast DNA (kDNA) of *Trypsanosoma* species and potentially also host DNA (Mikek et al., 2018; Tuvshintulga et al., 2017; Valenzuela et al., 2017), including the blocking of protozoal DNA topoisomerase (Shapiro, 1993) and potentially mammalian DNA topoisomerase I (Chen et al., 1993; Portugal, 1994). Since diminazene research focused (for a long time) mainly on protozoal research, there is a lack of cumulative evidence on diminazene's effect on host DNA and topoisomerases.

4.2.5.2 Diminazene and angiotensin converting enzyme 2 (ACE2)

Further, diminazene gained interest in the last two decades, as it might be also beneficial in treatment of neurological disorders like Alzheimer's disease (Kamel et al., 2018) and might also protect from myocardial infarcts (Castardeli et al., 2018; Chen et al., 2017) as well as ischemic strokes (Bennion et al., 2015). The protective effect of diminazene can be explained by diminazene-mediated increase in angiotensin converting enzyme 2 (ACE2) activity, which is involved in the regulation of cardiovascular, renal, pulmonary and central nervous systems (Guang et al., 2012). Whether diminazene is a direct activator of ACE2 (Bruce et al., 2018; De

Maria et al., 2016; Tao et al., 2016) or an indirect one is still a matter of debate (Haber et al., 2014; Rajapaksha et al., 2018). Nevertheless, the direct or indirect effect of diminazene on the ACE2 cannot explain the reversal of latency as seen in the J-Lat cell model as the expression of ACE2 is highly organ/tissue specific and not expressed in lymphocytes (acc. to 'The Human Protein Atlas' for ACE2 (Uhlén et al., 2015)).

4.2.5.3 Diminazene reduces proinflammatory response

Diminazene's action has been also linked to reduced phosphorylation of the mitogen-activated protein kinases (MAPK) pathway, signal transducer and activator of transcription (STAT) and NFκB subunit p65 in protozoa challenged- or lipopolysaccharide (LPS)-treated macrophages, leading to reduced proinflammatory cytokine production (Kuriakose and Uzonna, 2014; Kuriakose et al., 2012, 2014). Considering a reduction in cytokine production and signaling, this might explain why there was no effect seen in U1 cells when treated with diminazene in combination with the tested T cell activating LRAs. However, it would not explain the reversing effect seen in J-Lat cells (compare **Figure 24** and **Figure 29**).

4.2.5.4 Diminazene and its influence on polyamines

Other described targets of diminazene include, for instance, the human diamine oxidase (DAO) (also known as amine oxidase copper containing 1 (AOC1)), which is an enzyme serving in the oxidation of histamines and other polyamines as putrescine or spermidine (Finney et al., 2014; Jänne et al., 1985; McGrath et al., 2009). Further, adenosylmethionine decarboxylase (AMD1) (also known as AdoMedDC) has been stated to be irreversibly blocked by diminazene (Karvonen et al., 1985). Interestingly, both enzymes are linked to polyamines, with AMD1 being a key enzyme in the polyamine biosynthesis.

Polyamines are small carbon chains containing at least two amino-groups, are positively charged (at neutral pH) and abundantly present in all living cells. In mammalian cells, three endogenous polyamines are produced, namely putrescine (diamine), spermidine (triamine) and spermine (tetraamine), which are consecutively synthesized (Michael, 2016). In a first step, putrescine is formed by ornithine decarboxylation. This enzymatic reaction is performed by ornithine decarboxylase (ODC), an enzyme with a short half-life, tightly regulated on various levels and transcriptionally initiated by c-Myc (Peña et al., 1993). Another enzyme of major importance is the above-mentioned AMD1, which catalyzes the reaction of decarboxylated S-adenosylmethioninamine (dcSAM) from S-adenosyl methionine (SAM). The availability of

dcSAM is the rate-limiting step in the synthesis of spermidine and spermine, as dcSAM provides the aminopropyl group for the spermidine and spermine conversion by their respective synthases (Pegg, 2016). The catabolism of those two polyamines is executed by the spermidine/spermine-N^1-acetyltransferase (SSAT). The acetylated product is then further oxidized by the acetylpolyamine oxidase (APAO) to form spermidine (from spermine) or putrescine (from spermidine) (Pegg, 2008). Of note, also spermidine/spermine-N^1-acetyltransferase was mentioned to be a target of diminazene (Neidhart et al., 2014). An overview scheme on polyamine synthesis and catabolism is shown in **Figure 47**.

47

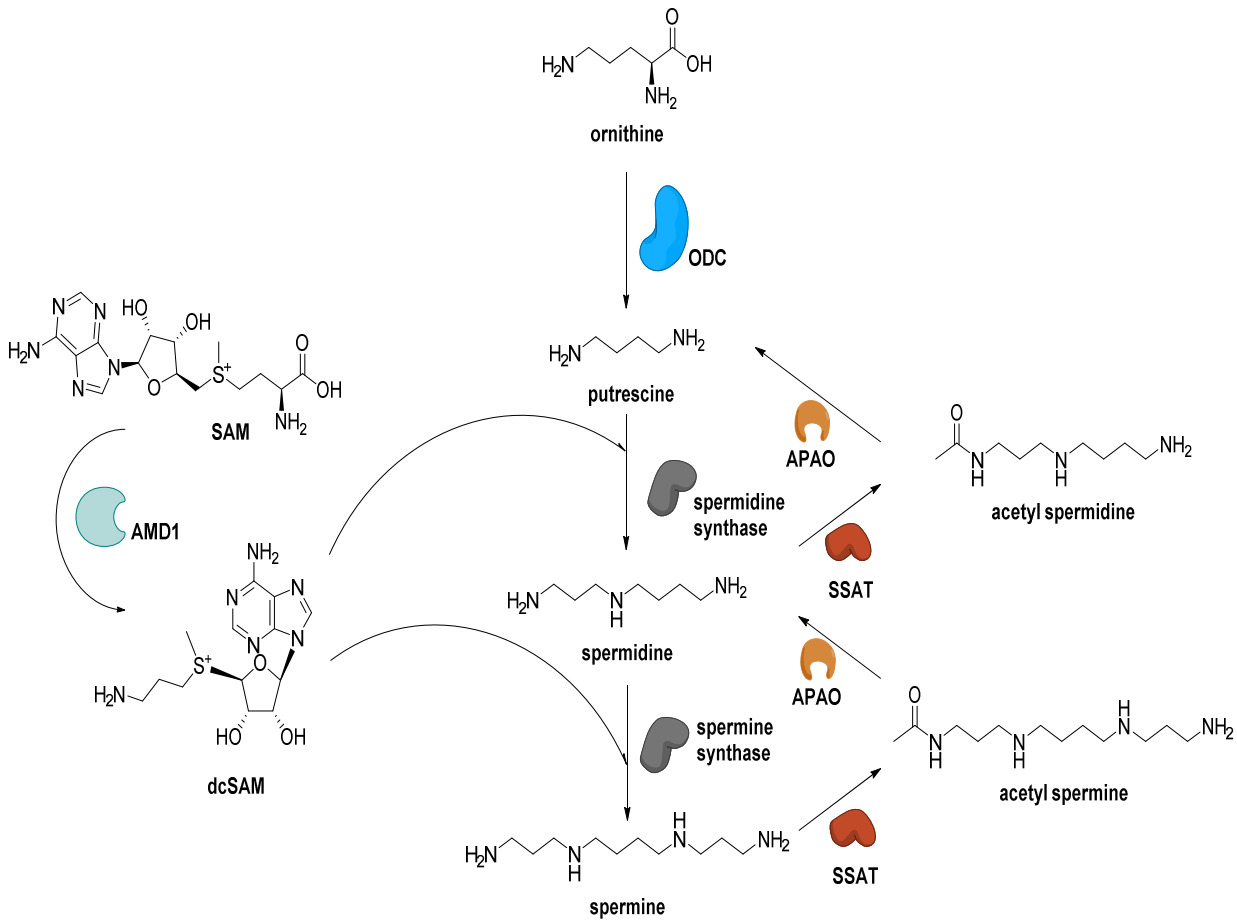

Figure 47: Scheme of polyamine synthesis and catabolism. Putrescine is formed from ornithine by ODC and further processed to spermidine and spermine by spermidine and spermine synthase, respectively under the consumption of dcSAM, which is produced from SAM by AMD1. Spermine and spermidine are catabolized into spermidine and putrescine respectively by SSAT and APOA. AMD1= adenosylmethionine decarboxylase, APAO= acetylpolyamine oxidase, dcSAM= decarboxylated S-adenosylmethioninamine, ODC= ornithine decarboxylase, SAM= S-adenosyl methionine, SSAT= spermidine/spermine-N^1-acetyltransferase. Adapted from Huang et al., 2009.

The importance of polyamines is reflected in the plethora of cellular functions they support (schematically summarized in **Figure 48**): It was shown that polyamines stabilize DNA by direct binding, support DNA bending and protect DNA from oxidation by ROS. Further, polyamines also bind RNA (as mRNA, tRNA) and can thereby directly (but also indirectly) influence translation (Igarashi and Kashiwagi, 2010). A well-documented example for an indirect effect of polyamines on protein synthesis was described for spermidine, as it provides an aminobutyl group to modify the eukaryotic translation initiation factor 5A (eIF5A) (Igarashi and Kashiwagi, 2010; Park et al., 1981). This post-translational modification of eIF5A is needed to assist paused ribosomes at mRNA encoding proline-rich sequences to complete translation and also to successfully terminate translation. In addition, polyamines also modulate ion channels and receptor-ligand interactions, serve directly as ROS scavengers (even though their catabolism also leads to ROS formation (Murray Stewart et al., 2018)) and are involved in growth, proliferation and apoptosis. In line with the mentioned examples, it is unsurprising that polyamine synthesis and homeostasis are tightly regulated on various levels and by different mechanisms: For instance, specific inhibitors of ODC, i.e. antizymes, regulate ODC activity. Whereas the antizymes itself are regulated by their own inhibitors, i.e. inhibitor of antizymes (Mangold and Leberer, 2005). Further, transcription of e.g. AMD1 and SSAT can be induced in response to the cellular polyamine content or by other (upstream) enzymes (Gamble et al., 2012). In addition, polyamines can be also imported and exported by the cell (Huang et al., 2009).

Worthwhile to mention is that polyamines also play a role in the viral life cycle. So has been has been found that polyamine synthesis can be differently affected by different viruses (Li and MacDonald, 2016; Mounce et al., 2017). Furthermore, it is also known that polyamines condense viral genomes which supports the packaging of these into newly produced viruses (Sun et al., 2010). A schematic overview on polyamine functions and interactions is shown in **Figure 48**. Regarding HIV-1, evidence exists that inhibition of AMD1 by different compounds will negatively impact the viral life cycle (Jin et al., 2015, Schäfer et al., 2006). This also clearly shows the importance of polyamines for HIV-1.

Further, early reports stated that diminazene inhibited AMD1 *in vivo* and *ex vivo* and replaced DNA-bound spermidine (Da'dara et al., 1998; Karvonen et al., 1985). Inhibition of AMD1 by methylglyoxal-bis-guanylhydrazone (MGBG), a polyamine analogue as well as a structural analogue of diminazene (Marques et al., 2008; Pegg and McCann, 1992), led to a depletion of spermidine and spermine pools, while elevating the levels of ODC (in line with the increased putrescine levels observed) (Regenass et al., 1992). The usage of another AMD1 inhibitor, i.e. 5'-(((Z)-4-amino-2-butenyl)methylamino)-5'-deoxyadenosine (AbeAdo), led also to a decrease

in spermidine and spermine levels associated with a decrease in certain transcription factors as c-Fos and c-Jun (Desiderio et al., 1996), an increase in putrescine levels (Byers et al., 1994a) and to unmodified eIF5A as secondary effect of spermidine depletion (Byers et al., 1994b). Further, AMD1 inhibition influences the cellular SAM to dcSAM ratio, with higher rates of SAM being present. SAM also serves as methyl-group donor for DNA methyltransferases (DNMT) as well as HMTs, as a consequence it can affect the DNA and histone methylation status, thereby influencing gene transcription in an either supporting or silencing fashion (Hashimoto et al., 2010; Poomipark et al., 2016). This is supported by the finding that dcSAM blocks the activity of DNMTs (Yamamoto et al., 2010). Further, an (age related) decline of spermidine was found to increase HAT activity (Eisenberg et al., 2009). The mentioned examples will affect transcription and translation, alter cell proliferation and can induce apoptosis. Further, it is also likely that depleted polyamines are lacking as ROS scavengers and stabilizers for DNA and RNA, which further influence the cell and its fate. The wide-ranging consequences of a disturbed polyamine homeostasis will most likely also the latent state of the provirus.

Additionally, a single publication states that diminazene inhibits SSAT, leading to increased putrescine and reduced AMD1 levels in primary fibroblasts from rheumatoid arthritis patients (Neidhart et al., 2014). Despite the differential target, the results are comparable to the above-mentioned examples. Also, ODC inhibition by its specific inhibitor, i.e. α-D,L-difluoromethylornithine hydrochloride (DFMO), led to the described results, including changed DNA methylation, halted cell proliferation (Mamont et al., 1976) and apoptosis induction via the mitochondrial pathway (Mandal et al., 2015).

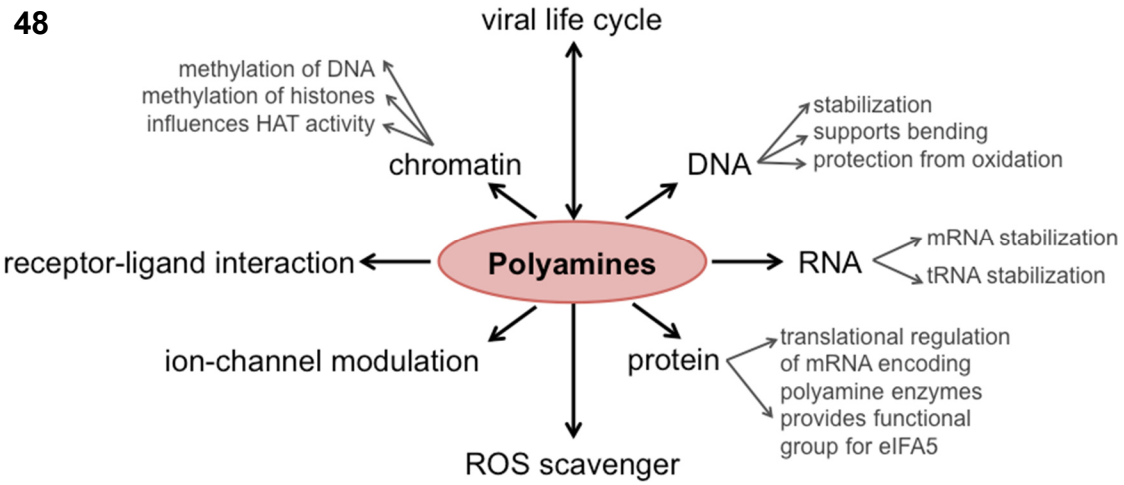

Figure 48: Simplified scheme on the influence of polyamines. Polyamines participate in various processes and interact with a wide range of cellular molecules; due to this polyamines affect cellular proliferation and apoptosis. In addition, polyamines homeostasis can be differently affected by viral infections. Adapted from Mounce et al., 2017.

4.2.6 Diminazene conclusion and outlook

Diminazene was identified to have a positive effect on latency reversal in J-Lat cells when applied in combination with different LRAs, with the effect being most prominent with TNFα or prostratin. U1 cells on the other hand did not recapitulate this effect. There are several literature reports linking diminazene to the polyamine synthesis/catabolism, specifically to AMD1, whereas no evidence exists that link diminazene and the thioredoxin system, i.e. the proposed target of auranofin. Therefore one could assume that auranofin and diminazene do not target the same pathway and that the observed reversal of latency is induced by mechanisms different from the proposed inhibition of the thioredoxin system. On the other hand, one could argue that diminazene's effect on polyamine content leads as a secondary effect to an imbalance in the overall redox state of the cell, as depleted/non-converted polyamines could not serve as direct ROS scavengers. This in turn could have a wide range of effects and would link the polyamine system to the redox state of the cell, which could serve as possible explanation for the comparable effect of auranofin and diminazene on latency reversal. On the other hand, polyamines are essential for the cell and participate in many more cellular processes than just as ROS scavenger. It is therefore likely that the effect of diminazene cannot be only linked to its potential influence on redox state. But that the effect on latency reversal might be also evoked by a potential destabilization of DNA and RNA, by an influence on protein translation, or by effects on the chromatin state. Whether latency reversal is evoked by disturbance of one of the mentioned examples or by the accumulation of cellular pertubations derived from various mechanisms need to be experimentally tested. The usage of other known specific inhibitors of the polyamine synthesis and catabolism will help to verify diminazene's target (pathway).

Even though the target (pathway) of diminazene still needs to be fully elucidated, we found robust reversal of latency in the J-Lat cell system. This effect has never been documented so far while diminazene's proposed influence on the polyamine synthesis is seizable. Therefore polyamine synthesis and catabolism might present a yet underinvestigated target pathway in regard to latency, in which polyamine disturbances lead to cellular pertubations affecting also the the provirus

4.2.7 Primary human results

In order to test auranofin's and diminazene's potential effect on latency reversal in primary cells, overall $CD4^+$ T cells or non-activated $CD4^+$ T cells were isolated from HIV-1 positive patient blood. The isolation of $CD4^+$ T cells (overall and non-activated) was successfully established and the optimal compound (and LRA) concentration for a 3-day treatment was determined. Reversal of latency, though, could not be successfully confirmed, except for one donor out of 13 tested. This example supports the general experimental setup but does not allow overall conclusions for the tested compounds. Further, testing and fine-tuning would be needed to definitely allow a conclusion of auranofin's and diminazene's action on latency reversal.

A major limitation of the primary experiments was the overall time limitation, i.e. as primary experiments were conducted at the Robert Koch Institute for a period of 2.5 months. The initial experimental duration was reduced from six days to three days (graphical overview on the initial experimental setup **Figure 36**). This, on the one hand, shortened the assay duration and allowed for acceptable cell viability results (see **Figure 40**). But this shortening, on the other hand, might have also taken time needed to produce sufficient levels of progeny viruses to a detectable level in the supernatant. So further experiments might be conducted with the initially planned duration, while retitrating compounds and LRA concentrations to allow for cell survival. Another aspect to consider was the overall low cell numbers isolated, which were due to the low amount of starting material provided. A greater quantity of patient blood would allow to isolate higher numbers of resting cells and therefore to test all experimental conditions initially planned and also allow for an increase in cell number per experimental condition, since higher cell numbers would also increase the probability of isolating cells carrying a replication-competent provirus. Considering the overall cell needs due to the low numbers of cells harboring a provirus (assumed one resting cells out of one million cells (Eriksson et al., 2013)), leukapheresis might be the best suitable option to guarantee enough cells. Further, the implementation of a qVOA, which is considered the gold standard to measure reactivation of latent primary cells, could be considered, as it would allow an amplification of the p24 signal due to propagation of the of reactivated virus, which in turn could facilitate the read-out.

Despite the difficulties mentioned, it would be of interest to continue testing both compounds in a primary setting and to elucidate whether I) auranofin has an effect on latency reversal or evokes its effect primarily by the higher sensitivity of resting cells and further II) whether diminazene application proves advantageous for latency reversal.

4.3 Overall conclusion

HTS have been proven a valuable tool for accelerated hit identification for various research areas, and so has also the validation of the primary hits from a genome-wide siRNA screen performed in HIVluc HEK293T cells involved in HIV-1 latency, as assayed in this scientific work, led to interesting results and pointed towards the involvement of so far under-investigated pathways. Following two differential approaches to choose and validate primary hits, the chromatin-binding protein TRRAP (= approach I) as well as the compounds auranofin and diminazene (= approach II) were identified and tested. While TRRAP knockdown recapitulated the results of the genome-wide siRNA screen, a latency involvement could not be definitely defined. Further, the compounds auranofin and diminazene were identified and successfully tested in J-Lat cells, even though their effect was different and cell line specific. The proposed initial target, i.e. PRDX5 and upstream pathway, could not be absolutely verified. Interestingly, there is a huge discrepancy between publications and databases considering the cellular targets of compounds, which needs to be kept in mind while working with those databases as DrugBank (Law et al., 2014). According to literature it is highly likely that auranofin evokes its effect via the inhibition of the thioredoxin system, while diminazene evokes its effect via its influence on the polyamine homeostasis. Though, the host factors associated with the two systems, namely TXNRD and TRX for auranofin and AMD1 (and potentially SSAT) for diminazene have not been identified as primary hit. Nevertheless, both systems are of crucial importance for the cell and have been implied in HIV-1 infection (Couret and Chang, 2016; Jin et al., 2015; Porter and Sutliff, 2012; Schäfer et al., 2006), but have not been recognized for their importance in HIV-1 latency. Further experiments are needed to determine the cellular target(s) of those compounds and to prove their involvement in HIV-1 latency.

In summary, the choice of primary hits to follow-up on had led to the identification of two compounds, which proved supportive in latency reversal, whereas their mechanism of action and their targets remain to be determined. The proposed influence of those compounds on either the redox or the polyamine system, as well as a possible interconnection of those systems, needs to be experimentally tested. It is possible that resting cells are more sensitive for disturbances of those systems and that application of those compounds might support reversal of latency. Those compounds could then support the ‘shock step’ in the ‘shock and kill’ approach. Further, it is also possible that the application of those compounds leads to a depletion of the viral reservoir by inducing apoptosis without reversing latency. If this possibility proves true, specific depletion of resting cells could support an HIV-1 cure by depleting the

more sensitize resting cells along with the latent reservoir without the need to first induce proviral transcription followed by killing of the virus producing cell.

5 References

Abaru, D.E., Liwo, D.A., Isakina, D., and Okori, E.E. (1984). Retrospective long-term study of effects of berenil by follow-up of patients treated since 1965. Tropenmed. Parasitol. *35*, 148–150.

Abdel-Mohsen, M., Kuri-Cervantes, L., Grau-Exposito, J., Spivak, A.M., Nell, R.A., Tomescu, C., Vadrevu, S.K., Giron, L.B., Serra-Peinado, C., Genescà, M., et al. (2018). CD32 is expressed on cells with transcriptionally active HIV but doesnot enrich for HIV DNA in resting T cells. Sci. Transl. Med. *10*.

Ahluwalia, J.K., Khan, S., Soni, K., Rawat, P., Gupta, A., Hariharan, M., Scaria, V., Lalwani, M., Pillai, B., Mitra, D., et al. (2008). Human cellular microRNA hsa-miR-29a interferes with viral nef protein expression and HIV-1 replication. Retrovirology *5*, 117.

Alberts, B., Johnson, A., Lewis, J., Raff, M., Roberts, K., and Walter, P. (2002). Chromosomal DNA and Its Packaging in the Chromatin Fiber.

Allers, K., Hütter, G., Hofmann, J., Loddenkemper, C., Rieger, K., Thiel, E., and Schneider, T. (2011). Evidence for the cure of HIV infection by CCR5Δ32/Δ32 stem cell transplantation. Blood *117*, 2791–2799.

Archin, N.M., Sung, J.M., Garrido, C., Soriano-Sarabia, N., and Margolis, D.M. (2014). Eradicating HIV-1 infection: seeking to clear a persistent pathogen. Nat. Rev. Microbiol. *12*, 750–764.

Ard, P.G., Chatterjee, C., Kunjibettu, S., Adside, L.R., Gralinski, L.E., and McMahon, S.B. (2002). Transcriptional regulation of the mdm2 oncogene by p53 requires TRRAP acetyltransferase complexes. Mol. Cell. Biol. *22*, 5650–5661.

Arnér, E.S.J., and Holmgren, A. (2006). The thioredoxin system in cancer. Semin. Cancer Biol. *16*, 420–426.

Arnér, E.S.J., and Holmgren, A. (2011). Thioredoxin System. In Encyclopedia of Cancer, (Berlin, Heidelberg: Springer Berlin Heidelberg), pp. 3670–3671.

Arrowsmith, C.H., Bountra, C., Fish, P. V., Lee, K., and Schapira, M. (2012). Epigenetic protein families: a new frontier for drug discovery. Nat. Rev. Drug Discov. *11*, 384–400.

Badia, R., Ballana, E., Castellví, M., García-Vidal, E., Pujantell, M., Clotet, B., Prado, J.G., Puig, J., Martínez, M.A., Riveira-Muñoz, E., et al. (2018). CD32 expression is associated to T-cell activation and is not a marker of the HIV-1 reservoir. Nat. Commun. *9*, 2739.

Baeten, J.M., and Overbaugh, J. (2003). Measuring the infectiousness of persons with HIV-1: opportunities for preventing sexual HIV-1 transmission. Curr. HIV Res. *1*, 69–86.

Baldauf, H.-M., Pan, X., Erikson, E., Schmidt, S., Daddacha, W., Burggraf, M., Schenkova, K., Ambiel, I., Wabnitz, G., Gramberg, T., et al. (2012). SAMHD1 restricts HIV-1 infection in resting CD4(+) T cells. Nat. Med. *18*, 1682–1687.

Becker, K., Gromer, S., Schirmer, R.H., and Müller, S. (2000). Thioredoxin reductase as a pathophysiological factor and drug target. Eur. J. Biochem. *267*, 6118–6125.

Bennion, D.M., Haltigan, E.A., Irwin, A.J., Donnangelo, L.L., Regenhardt, R.W., Pioquinto, D.J., Purich, D.L., and Sumners, C. (2015). Activation of the Neuroprotective Angiotensin-Converting Enzyme 2 in Rat Ischemic Stroke. Hypertens. (Dallas, Tex. 1979) *66*, 141–148.

Berry, N., Jaffar, S., Schim van der Loeff, M., Ariyoshi, K., Harding, E., N'Gom, P.T., Dias, F., Wilkins, A., Ricard, D., Aaby, P., et al. (2002). Low level viremia and high CD4% predict normal survival in a cohort of HIV type-2-infected villagers. AIDS Res. Hum. Retroviruses *18*, 1167–1173.

Bisgrove, D.A., Mahmoudi, T., Henklein, P., and Verdin, E. (2007). Conserved P-TEFb-interacting domain of BRD4 inhibits HIV transcription. Proc. Natl. Acad. Sci. U. S. A. *104*, 13690–13695.

Blazkova, J., Trejbalova, K., Gondois-Rey, F., Halfon, P., Philibert, P., Guiguen, A., Verdin, E., Olive, D., Van Lint, C., Hejnar, J., et al. (2009). CpG Methylation Controls Reactivation of HIV from Latency. PLoS Pathog. *5*, e1000554.

Blazkova, J., Murray, D., Justement, J.S., Funk, E.K., Nelson, A.K., Moir, S., Chun, T.-W., and Fauci, A.S. (2012). Paucity of HIV DNA Methylation in Latently Infected, Resting CD4+ T Cells from Infected Individuals Receiving Antiretroviral Therapy. J. Virol. *86*, 5390–5392.

Bonczkowski, P., De Scheerder, M.A., Malatinkova, E., Borch, A., Melkova, Z., Koenig, R., De Spiegelaere, W., and Vandekerckhove, L. (2016). Protein expression from unintegrated HIV-1 DNA introduces bias in primary in vitro post-integration latency models. Sci. Rep. *6*, 38329.

Bottomley, M.J. (2004). Structures of protein domains that create or recognize histone modifications. EMBO Rep. *5*, 464–469.

Bourgeois, C.F., Kim, Y.K., Churcher, M.J., West, M.J., and Karn, J. (2002). Spt5 cooperates with human immunodeficiency virus type 1 Tat by preventing premature RNA release at terminator sequences. Mol. Cell. Biol. *22*, 1079–1093.

Bradford, M.M. (1976). A rapid and sensitive method for the quantitation of microgram quantities of protein utilizing the principle of protein-dye binding. Anal. Biochem. *72*, 248–254.

Brès, V., Gomes, N., Pickle, L., and Jones, K.A. (2005). A human splicing factor, SKIP, associates with P-TEFb and enhances transcription elongation by HIV-1 Tat. Genes Dev. *19*, 1211–1226.

Brès, V., Yoshida, T., Pickle, L., and Jones, K.A. (2009). SKIP Interacts with c-Myc and Menin to Promote HIV-1 Tat Transactivation. Mol. Cell *36*, 75–87.

Brooks, D.G., Hamer, D.H., Arlen, P.A., Gao, L., Bristol, G., Kitchen, C.M.R., Berger, E.A., and Zack, J.A. (2003). Molecular characterization, reactivation, and depletion of latent HIV. Immunity *19*, 413–423.

Bruce, E.B., Sakarya, Y., Kirichenko, N., Toklu, H.Z., Sumners, C., Morgan, D., Tümer, N., Scarpace, P.J., and Carter, C.S. (2018). ACE2 activator diminazene aceturate reduces adiposity but preserves lean mass in young and old rats. Exp. Gerontol. *111*, 133–140.

Bruner, K.M., Murray, A.J., Pollack, R.A., Soliman, M.G., Laskey, S.B., Capoferri, A.A., Lai, J., Strain, M.C., Lada, S.M., Hoh, R., et al. (2016). Defective proviruses rapidly accumulate during acute HIV-1 infection. Nat. Med. *22*, 1043–1049.

Bruner, K.M., Wang, Z., Simonetti, F.R., Bender, A.M., Kwon, K.J., Sengupta, S., Fray, E.J., Beg, S.A., Antar, A.A.R., Jenike, K.M., et al. (2019). A quantitative approach for measuring the reservoir of latent HIV-1 proviruses. Nature *566*, 120–125.

Byers, T.L., Wechter, R.S., Hu, R.H., and Pegg, A.E. (1994a). Effects of the S-adenosylmethionine decarboxylase inhibitor, 5'-([(Z)-4-amino-2-butenyl]methylamino)-5'-deoxyadenosine, on cell growth and polyamine metabolism and transport in Chinese hamster ovary cell cultures. Biochem. J. *303 (Pt 1)*, 89–96.

Byers, T.L., Lakanen, J.R., Coward, J.K., and Pegg, A.E. (1994b). The role of hypusine depletion in cytostasis induced by S-adenosyl-L-methionine decarboxylase inhibition: new evidence provided by 1-methylspermidine and 1,12-dimethylspermine. Biochem. J. *303 (Pt 2)*, 363–368.

Campeau, E., and Gobeil, S. (2011). RNA interference in mammals: behind the screen. Brief. Funct. Genomics *10*, 215–226.

Caraus, I., Alsuwailem, A.A., Nadon, R., and Makarenkov, V. (2015). Detecting and overcoming systematic bias in high-throughput screening technologies: a comprehensive review of practical issues and methodological solutions. Brief. Bioinform. *16*, 974–986.

Castardeli, C., Sartório, C.L., Pimentel, E.B., Forechi, L., and Mill, J.G. (2018). The ACE 2 activator diminazene aceturate (DIZE) improves left ventricular diastolic dysfunction following myocardial infarction in rats. Biomed. Pharmacother. *107*, 212–218.

Chen, A.Y., Yu, C., Gatto, B., and Liu, L.F. (1993). DNA minor groove-binding ligands: a different class of mammalian DNA topoisomerase I inhibitors. Proc. Natl. Acad. Sci. U. S. A. *90*, 8131–8135.

Chen, J., Cui, L., Yuan, J., Zhang, S., Ma, R., Sang, H., Liu, Q., and Shan, L. (2017). Protective effect of diminazene attenuates myocardial infarction in rats via increased inflammation and ACE2 activity. Mol. Med. Rep. *16*, 4791–4796.

Chen, X., Shi, X., Zhao, C., Li, X., Lan, X., Liu, S., Huang, H., Liu, N., Liao, S., Zang, D., et al. (2014). Anti-rheumatic agent auranofin induced apoptosis in chronic myeloid leukemia cells resistant to imatinib through both Bcr/Abl-dependent and -independent mechanisms. Oncotarget *5*, 9118–9132.

du Chéné, I., Basyuk, E., Lin, Y.-L., Triboulet, R., Knezevich, A., Chable-Bessia, C., Mettling, C., Baillat, V., Reynes, J., Corbeau, P., et al. (2007). Suv39H1 and HP1gamma are responsible for chromatin-mediated HIV-1 transcriptional silencing and post-integration latency. EMBO J. *26*, 424–435.

Chirullo, B., Sgarbanti, R., Limongi, D., Shytaj, I.L., Alvarez, D., Das, B., Boe, A., DaFonseca, S., Chomont, N., Liotta, L., et al. (2013). A candidate anti-HIV reservoir compound, auranofin, exerts a selective “anti-memory” effect by exploiting the baseline oxidative status of lymphocytes. Cell Death Dis. *4*, e944.

Chomont, N., El-Far, M., Ancuta, P., Trautmann, L., Procopio, F.A., Yassine-Diab, B., Boucher, G., Boulassel, M.-R., Ghattas, G., Brenchley, J.M., et al. (2009). HIV reservoir size and persistence are driven by T cell survival and homeostatic proliferation. Nat. Med. *15*, 893–900.

Chun, T.W., Stuyver, L., Mizell, S.B., Ehler, L.A., Mican, J.A., Baseler, M., Lloyd, A.L., Nowak, M.A., and Fauci, A.S. (1997). Presence of an inducible HIV-1 latent reservoir during highly active antiretroviral therapy. Proc. Natl. Acad. Sci. U. S. A. *94*, 13193–13197.

Chun, T.W., Engel, D., Berrey, M.M., Shea, T., Corey, L., and Fauci, A.S. (1998). Early establishment of a pool of latently infected, resting CD4(+) T cells during primary HIV-1 infection. Proc. Natl. Acad. Sci. U. S. A. *95*, 8869–8873.

Clutton, G., Xu, Y., Baldoni, P.L., Mollan, K.R., Kirchherr, J., Newhard, W., Cox, K., Kuruc, J.D., Kashuba, A., Barnard, R., et al. (2016). The differential short- and long-term effects of HIV-1 latency-reversing agents on T cell function. Sci. Rep. *6*, 30749.

Coiras, M., Bermejo,M., Descours, B., Mateos, E., García-Pérez, J., López-Huertas, MR., Lederman, M.M., Benkirane, M., and Alcamí, J. (2016). IL-7 Induces SAMHD1 Phosphorylation in CD4+ T Lymphocytes, Improving Early Steps of HIV-1 Life Cycle. Cell Rep. *14*, 2100–2107.

Core, L.J., and Lis, J.T. (2008). Transcription Regulation Through Promoter-Proximal Pausing of RNA Polymerase II. Science (80-.). *319*, 1791–1792.

Cotto, K.C., Wagner, A.H., Feng, Y.-Y., Kiwala, S., Coffman, A.C., Spies, G., Wollam, A., Spies, N.C., Griffith, O.L., and Griffith, M. (2018). DGIdb 3.0: a redesign and expansion of the drug–gene interaction database. Nucleic Acids Res. *46*, D1068–D1073.

Couret, J., and Chang, T.L. (2016). Reactive Oxygen Species in HIV Infection. EC Microbiol. *3*, 597–604.

Cox, A.G., Brown, K.K., Arner, E.S.J., and Hampton, M.B. (2008). The thioredoxin reductase inhibitor auranofin triggers apoptosis through a Bax/Bak-dependent process that involves peroxiredoxin 3 oxidation. Biochem. Pharmacol. *76*, 1097–1109.

Craigie, R., and Bushman, F.D. (2012). HIV DNA integration. Cold Spring Harb. Perspect. Med. *2*, a006890.

de la Cruz, X., Lois, S., Sánchez-Molina, S., and Martínez-Balbás, M.A. (2005). Do protein motifs read the histone code? BioEssays *27*, 164–175.

Da'dara, A.A., Mett, H., and Walter, R.D. (1998). MGBG analogues as potent inhibitors of S-adenosylmethionine decarboxylase of Onchocerca volvulus. Mol. Biochem. Parasitol. *97*, 13–19.

Daniel, W.W. (1990). Applied nonparametric statistics (PWS-KENT Pub).

Darcis, G., Kula, A., Bouchat, S., Fujinaga, K., Corazza, F., Ait-Ammar, A., Delacourt, N., Melard, A., Kabeya, K., Vanhulle, C., et al. (2015). An In-Depth Comparison of Latency-Reversing Agent Combinations in Various In Vitro and Ex Vivo HIV-1 Latency Models Identified Bryostatin-1+JQ1 and Ingenol-B+JQ1 to Potently Reactivate Viral Gene Expression. PLOS Pathog. *11*, e1005063.

Das, A.T., Harwig, A., and Berkhout, B. (2011). The HIV-1 Tat Protein Has a Versatile Role in Activating Viral Transcription. J. Virol. *85*, 9506–9516.

Davey, R.T., Bhat, N., Yoder, C., Chun, T.W., Metcalf, J.A., Dewar, R., Natarajan, V., Lempicki, R.A., Adelsberger, J.W., Miller, K.D., et al. (1999). HIV-1 and T cell dynamics after interruption of highly active antiretroviral therapy (HAART) in patients with a history of sustained viral suppression. Proc. Natl. Acad. Sci. U. S. A. *96*, 15109–15114.

Dempsey, E.C., Newton, A.C., Mochly-Rosen, D., Fields, A.P., Reyland, M.E., Insel, P.A., and Messing, R.O. (2000). Protein kinase C isozymes and the regulation of diverse cell responses. Am. J. Physiol. Lung Cell. Mol. Physiol. *279*, L429-38.

Descours, B., Petitjean, G., López-Zaragoza, J.-L., Bruel, T., Raffel, R., Psomas, C., Reynes, J., Lacabaratz, C., Levy, Y., Schwartz, O., et al. (2017). CD32a is a marker of a CD4 T-cell HIV reservoir harbouring replication-competent proviruses. Nature *543*, 564–567.

Desiderio, M.A., Tacchini, L., Anzon, E., Pogliaghi, G., Radice, L., and Bernelli-Zazzera, A. (1996). Effects of polyamine imbalance on the induction of stress genes in hepatocarcinoma cells exposed to heat shock. Hepatology *24*, 150–156.

Dey, A., Chitsaz, F., Abbasi, A., Misteli, T., and Ozato, K. (2003). The double bromodomain protein Brd4 binds to acetylated chromatin during interphase and mitosis. Proc. Natl. Acad. Sci. *100*, 8758–8763.

Dokmanovic, M., Clarke, C., and Marks, P.A. (2007). Histone deacetylase inhibitors: overview and perspectives. Mol. Cancer Res. *5*, 981–989.

Du, Y., Zhang, H., Lu, J., and Holmgren, A. (2012). Glutathione and glutaredoxin act as a backup of human thioredoxin reductase 1 to reduce thioredoxin 1 preventing cell death by aurothioglucose. J. Biol. Chem. *287*, 38210–38219.

DuBridge, R.B., Tang, P., Hsia, H.C., Leong, P.M., Miller, J.H., and Calos, M.P. (1987). Analysis of mutation in human cells by using an Epstein-Barr virus shuttle system. Mol. Cell. Biol. *7*, 379–387.

Egger, M., Hirschel, B., Francioli, P., Sudre, P., Wirz, M., Flepp, M., Rickenbach, M., Malinverni, R., Vernazza, P., and Battegay, M. (1997). Impact of new antiretroviral combination therapies in HIV infected patients in Switzerland: prospective multicentre study. Swiss HIV Cohort Study. BMJ *315*, 1194–1199.

Eisenberg, T., Knauer, H., Schauer, A., Büttner, S., Ruckenstuhl, C., Carmona-Gutierrez, D., Ring, J., Schroeder, S., Magnes, C., Antonacci, L., et al. (2009). Induction of autophagy by spermidine promotes longevity. Nat. Cell Biol. *11*, 1305–1314.

Emiliani, S., Fischle, W., Ott, M., Van Lint, C., Amella, C.A., and Verdin, E. (1998). Mutations in the tat gene are responsible for human immunodeficiency virus type 1 postintegration latency in the U1 cell line. J. Virol. *72*, 1666–1670.

Eriksson, S., Graf, E.H., Dahl, V., Strain, M.C., Yukl, S.A., Lysenko, E.S., Bosch, R.J., Lai, J., Chioma, S., Emad, F., et al. (2013). Comparative analysis of measures of viral reservoirs in HIV-1 eradication studies. PLoS Pathog. *9*, e1003174.

Estes, J.D., Wong, S.W., and Brenchley, J.M. (2018). Nonhuman primate models of human viral infections. Nat. Rev. Immunol. *18*, 390–404.

Evans, D.T., and Silvestri, G. (2013). Nonhuman primate models in AIDS research. Curr. Opin. HIV AIDS *8*, 255–261.

Fan, C., Zheng, W., Fu, X., Li, X., Wong, Y.-S., and Chen, T. (2014). Enhancement of auranofin-induced lung cancer cell apoptosis by selenocystine, a natural inhibitor of TrxR1 in vitro and in vivo. Cell Death Dis. *5*, e1191.

Finney, J., Moon, H.-J., Ronnebaum, T., Lantz, M., and Mure, M. (2014). Human copper-dependent amine oxidases. Arch. Biochem. Biophys. *546*, 19–32.

Finzi, D., Hermankova, M., Pierson, T., Carruth, L.M., Buck, C., Chaisson, R.E., Quinn, T.C., Chadwick, K., Margolick, J., Brookmeyer, R., et al. (1997). Identification of a reservoir for HIV-1 in patients on highly active antiretroviral therapy. Science *278*, 1295–1300.

Finzi, D., Blankson, J., Siliciano, J.D., Margolick, J.B., Chadwick, K., Pierson, T., Smith, K., Lisziewicz, J., Lori, F., Flexner, C., et al. (1999). Latent infection of CD4+ T cells provides a mechanism for lifelong persistence of HIV-1, even in patients on effective combination therapy. Nat. Med. *5*, 512–517.

Fiskus, W., Saba, N., Shen, M., Ghias, M., Liu, J., Gupta, S. Das, Chauhan, L., Rao, R., Gunewardena, S., Schorno, K., et al. (2014). Auranofin induces lethal oxidative and endoplasmic reticulum stress and exerts potent preclinical activity against chronic lymphocytic leukemia. Cancer Res. *74*, 2520–2532.

Folks, T.M., Justement, J., Kinter, A., Dinarello, C.A., and Fauci, A.S. (1987). Cytokine-induced expression of HIV-1 in a chronically infected promonocyte cell line. Science *238*, 800–802.

Friedman, J., Cho, W.-K., Chu, C.K., Keedy, K.S., Archin, N.M., Margolis, D.M., and Karn, J. (2011). Epigenetic Silencing of HIV-1 by the Histone H3 Lysine 27 Methyltransferase Enhancer of Zeste 2. J. Virol. *85*, 9078–9089.

Froscio, M., Murray, A.W., and Hurst, N.P. (1989). Inhibition of protein kinase C activity by the antirheumatic drug auranofin. Biochem. Pharmacol. *38*, 2087–2089.

de la Fuente, C., Santiago, F., Deng, L., Eadie, C., Zilberman, I., Kehn, K., Maddukuri, A., Baylor, S., Wu, K., Lee, C.G., et al. (2002). Gene expression profile of HIV-1 Tat expressing cells: a close interplay between proliferative and differentiation signals. BMC Biochem. *3*, 14.

Gamble, L.D., Hogarty, M.D., Liu, X., Ziegler, D.S., Marshall, G., Norris, M.D., and Haber, M. (2012). Polyamine pathway inhibition as a novel therapeutic approach to treating neuroblastoma. Front. Oncol. *2*, 162.

Gao, F., Bailes, E., Robertson, D.L., Chen, Y., Rodenburg, C.M., Michael, S.F., Cummins, L.B., Arthur, L.O., Peeters, M., Shaw, G.M., et al. (1999). Origin of HIV-1 in the chimpanzee Pan troglodytes troglodytes. Nature *397*, 436–441.

Gautier, V.W., Gu, L., O'Donoghue, N., Pennington, S., Sheehy, N., and Hall, W.W. (2009). In vitro nuclear interactome of the HIV-1 Tat protein. Retrovirology *6*, 47.

Germain, R.N. (2002). T-cell development and the CD4-CD8 lineage decision. Nat. Rev. Immunol. *2*, 309–322.

Gerritsen, M.E., Williams, A.J., Neish, A.S., Moore, S., Shi, Y., and Collins, T. (1997). CREB-binding protein/p300 are transcriptional coactivators of p65. Proc. Natl. Acad. Sci. U. S. A. *94*, 2927–2932.

Gloire, G., Legrand-Poels, S., and Piette, J. (2006). NF-kappaB activation by reactive oxygen species: fifteen years later. Biochem. Pharmacol. *72*, 1493–1505.

Goldstone, D.C., Ennis-Adeniran, V., Hedden, J.J., Groom, H.C.T., Rice, G.I., Christodoulou, E., Walker, P.A., Kelly, G., Haire, L.F., Yap, M.W., et al. (2011). HIV-1 restriction factor SAMHD1 is a deoxynucleoside triphosphate triphosphohydrolase. Nature *480*, 379–382.

Gopalakrishna, R., and Jaken, S. (2000). Protein kinase C signaling and oxidative stress. Free Radic. Biol. Med. *28*, 1349–1361.

Gopalakrishna, R., Gundimeda, U., Zhou, S., Bui, H., and Holmgren, A. (2018). Redox regulation of protein kinase C by selenometabolites and selenoprotein thioredoxin reductase limits cancer prevention by selenium. Free Radic. Biol. Med. *127*, 55–61.

Greene, W.C. (2007). A history of AIDS: looking back to see ahead. Eur. J. Immunol. *37 Suppl 1*, S94-102.

Greger, I.H., Demarchi, F., Giacca, M., and Proudfoot, N.J. (1998). Transcriptional interference perturbs the binding of Sp1 to the HIV-1 promoter. Nucleic Acids Res. *26*, 1294–1301.

Guang, C., Phillips, R.D., Jiang, B., and Milani, F. (2012). Three key proteases--angiotensin-I-converting enzyme (ACE), ACE2 and renin--within and beyond the renin-angiotensin system. Arch. Cardiovasc. Dis. *105*, 373–385.

Gupta, R.K., Abdul-Jawad, S., McCoy, L.E., Mok, H.P., Peppa, D., Salgado, M., Martinez-Picado, J., Nijhuis, M., Wensing, A.M.J., Lee, H., et al. (2019). HIV-1 remission following CCR5Δ32/Δ32 haematopoietic stem-cell transplantation. Nature *568*, 244–248.

Gustafson, K.R., Cardellina, J.H., McMahon, J.B., Gulakowski, R.J., Ishitoya, J., Szallasi, Z., Lewin, N.E., Blumberg, P.M., and Weislow, O.S. (1992). A nonpromoting phorbol from the Samoan medicinal plant Homalanthus nutans inhibits cell killing by HIV-1. J. Med. Chem. *35*, 1978–1986.

Haber, P.K., Ye, M., Wysocki, J., Maier, C., Haque, S.K., and Batlle, D. (2014). Angiotensin-converting enzyme 2-independent action of presumed angiotensin-converting enzyme 2 activators: studies in vivo, ex vivo, and in vitro. Hypertens. (Dallas, Tex. 1979) *63*, 774–782.

Halliwell, B., and Gutteridge, J.M.C. (2015). Free Radicals in Biology and Medicine (Oxford University Press).

Han, Y., Lassen, K., Monie, D., Sedaghat, A.R., Shimoji, S., Liu, X., Pierson, T.C., Margolick, J.B., Siliciano, R.F., and Siliciano, J.D. (2004). Resting CD4+ T cells from human immunodeficiency virus type 1 (HIV-1)-infected individuals carry integrated HIV-1 genomes within actively transcribed host genes. J. Virol. *78*, 6122–6133.

Han, Y., Wind-Rotolo, M., Yang, H.-C., Siliciano, J.D., and Siliciano, R.F. (2007). Experimental approaches to the study of HIV-1 latency. Nat. Rev. Microbiol. *5*, 95–106.

Han, Y., Lin, Y.B., An, W., Xu, J., Yang, H.-C., O'Connell, K., Dordai, D., Boeke, J.D., Siliciano, J.D., and Siliciano, R.F. (2008). Orientation-dependent regulation of integrated HIV-1 expression by host gene transcriptional readthrough. Cell Host Microbe *4*, 134–146.

Hashimoto, H., Vertino, P.M., and Cheng, X. (2010). Molecular coupling of DNA methylation and histone methylation. Epigenomics *2*, 657–669.

Hashimoto, K., Whitehurst, C.E., Matsubara, T., Hirohata, K., and Lipsky, P.E. (1992). Immunomodulatory effects of therapeutic gold compounds. Gold sodium thiomalate inhibits the activity of T cell protein kinase C. J. Clin. Invest. *89*, 1839–1848.

Heby, O., Persson, L., and Rentala, M. (2007). Targeting the polyamine biosynthetic enzymes: a promising approach to therapy of African sleeping sickness, Chagas' disease, and leishmaniasis. Amino Acids *33*, 359–366.

Hendriks, J., Gravestein, L.A., Tesselaar, K., van Lier, R.A., Schumacher, T.N., and Borst, J. (2000). CD27 is required for generation and long-term maintenance of T cell immunity. Nat. Immunol. *1*, 433–440.

Henrich, T.J., Hanhauser, E., Marty, F.M., Sirignano, M.N., Keating, S., Lee, T.-H., Robles, Y.P., Davis, B.T., Li, J.Z., Heisey, A., et al. (2014). Antiretroviral-free HIV-1 remission and viral rebound after allogeneic stem cell transplantation: report of 2 cases. Ann. Intern. Med. *161*, 319–327.

Henrich, T.J., Deeks, S.G., and Pillai, S.K. (2017). Measuring the Size of the Latent Human Immunodeficiency Virus Reservoir: The Present and Future of Evaluating Eradication Strategies. J. Infect. Dis. *215*, S134–S141.

Herceg, Z., Hulla, W., Gell, D., Cuenin, C., Lleonart, M., Jackson, S., and Wang, Z.-Q. (2001). Disruption of Trrap causes early embryonic lethality and defects in cell cycle progression. Nat. Genet. *29*, 206–211.

Hirota, K., Murata, M., Sachi, Y., Nakamura, H., Takeuchi, J., Mori, K., and Yodoi, J. (1999). Distinct roles of thioredoxin in the cytoplasm and in the nucleus. A two-step mechanism of redox regulation of transcription factor NF-kappaB. J. Biol. Chem. *274*, 27891–27897.

Hiscott, J., Kwon, H., and Génin, P. (2001). Hostile takeovers: viral appropriation of the NF-kappaB pathway. J. Clin. Invest. *107*, 143–151.

Ho, Y.-C., Shan, L., Hosmane, N.N., Wang, J., Laskey, S.B., Rosenbloom, D.I.S., Lai, J., Blankson, J.N., Siliciano, J.D., and Siliciano, R.F. (2013). Replication-competent noninduced proviruses in the latent reservoir increase barrier to HIV-1 cure. Cell *155*, 540–551.

Hokai, Y., Jurkowicz, B., Fernández-Gallardo, J., Zakirkhodjaev, N., Sanaú, M., Muth, T.R., and Contel, M. (2014). Auranofin and related heterometallic gold(I)-thiolates as potent inhibitors of methicillin-resistant Staphylococcus aureus bacterial strains. J. Inorg. Biochem. *138*, 81–88.

Holmgren, A., and Björnstedt, M. (1995). Thioredoxin and thioredoxin reductase. Methods Enzymol. *252*, 199–208.

Hu, W.-S., and Hughes, S.H. (2012). HIV-1 reverse transcription. Cold Spring Harb. Perspect. Med. *2*.

Huang, J., Wang, F., Argyris, E., Chen, K., Liang, Z., Tian, H., Huang, W., Squires, K., Verlinghieri, G., and Zhang, H. (2007). Cellular microRNAs contribute to HIV-1 latency in resting primary CD4+ T lymphocytes. Nat. Med. *13*, 1241–1247.

Huang, Y., Marton, L.J., Woster, P.M., Casero, R.A., and Jr (2009). Polyamine analogues targeting epigenetic gene regulation. Essays Biochem. *46*, 95–110.

Hütter, G., Nowak, D., Mossner, M., Ganepola, S., Müssig, A., Allers, K., Schneider, T., Hofmann, J., Kücherer, C., Blau, O., et al. (2009). Long-term control of HIV by CCR5 Delta32/Delta32 stem-cell transplantation. N. Engl. J. Med. *360*, 692–698.

Hwang-Bo, H., Jeong, J.-W., Han, M.H., Park, C., Hong, S.-H., Kim, G.-Y., Moon, S.-K., Cheong, J., Kim, W.-J., Yoo, Y.H., et al. (2017). Auranofin, an inhibitor of thioredoxin reductase, induces apoptosis in hepatocellular carcinoma Hep3B cells by generation of reactive oxygen species. Gen. Physiol. Biophys. *36*, 117–128.

Ichim, G., Mola, M., Finkbeiner, M.G., Cros, M.-P., Herceg, Z., and Hernandez-Vargas, H. (2014). The histone acetyltransferase component TRRAP is targeted for destruction during the cell cycle. Oncogene *33*, 181–192.

Igarashi, K., and Kashiwagi, K. (2010). Modulation of cellular function by polyamines. Int. J. Biochem. Cell Biol. *42*, 39–51.

Ikura, T., Ogryzko, V. V, Grigoriev, M., Groisman, R., Wang, J., Horikoshi, M., Scully, R., Qin, J., and Nakatani, Y. (2000). Involvement of the TIP60 histone acetylase complex in DNA repair and apoptosis. Cell *102*, 463–473.

Ilari, A., Baiocco, P., Messori, L., Fiorillo, A., Boffi, A., Gramiccia, M., Di Muccio, T., and Colotti, G. (2012). A gold-containing drug against parasitic polyamine metabolism: the X-ray structure of trypanothione reductase from Leishmania infantum in complex with auranofin reveals a dual mechanism of enzyme inhibition. Amino Acids *42*, 803–811.

Imai, K., Togami, H., and Okamoto, T. (2010). Involvement of Histone H3 Lysine 9 (H3K9) Methyltransferase G9a in the Maintenance of HIV-1 Latency and Its Reactivation by BIX01294. J. Biol. Chem. *285*, 16538–16545.

Inglese, J., and Auld, D.S. (2008). High Throughput Screening (HTS) Techniques: Applications in Chemical Biology. In Wiley Encyclopedia of Chemical Biology, (Hoboken, NJ, USA: John Wiley & Sons, Inc.), pp. 1–15.

Jackson-Rosario, S., and Self, W.T. (2009). Inhibition of selenium metabolism in the oral pathogen Treponema denticola. J. Bacteriol. *191*, 4035–4040.

Jackson-Rosario, S., Cowart, D., Myers, A., Tarrien, R., Levine, R.L., Scott, R.A., and Self, W.T. (2009). Auranofin disrupts selenium metabolism in Clostridium difficile by forming a stable Au-Se adduct. J. Biol. Inorg. Chem. *14*, 507–519.

Jang, M.K., Mochizuki, K., Zhou, M., Jeong, H.-S., Brady, J.N., and Ozato, K. (2005). The bromodomain protein Brd4 is a positive regulatory component of P-TEFb and stimulates RNA polymerase II-dependent transcription. Mol. Cell *19*, 523–534.

Jänne, J., Alhonen-Hongisto, L., Nikula, P., and Elo, H. (1985). S-adenosylmethionine decarboxylase as target of chemotherapy. Adv. Enzyme Regul. *24*, 125–139.

Jean-Moreno, V., Rojas, R., Goyeneche, D., Coombs, G.H., and Walker, J. (2006). Leishmania donovani: differential activities of classical topoisomerase inhibitors and antileishmanials against parasite and host cells at the level of DNA topoisomerase I and in cytotoxicity assays. Exp. Parasitol. *112*, 21–30.

Jeon, K.-I., Byun, M.-S., and Jue, D.-M. (2003). Gold compound auranofin inhibits IkappaB kinase (IKK) by modifying Cys-179 of IKKbeta subunit. Exp. Mol. Med. *35*, 61–66.

Jeon, K.I., Jeong, J.Y., and Jue, D.M. (2000). Thiol-reactive metal compounds inhibit NF-kappa B activation by blocking I kappa B kinase. J. Immunol. *164*, 5981–5989.

Jiang, G., and Dandekar, S. (2015). Targeting NF-κB signaling with protein kinase C agonists as an emerging strategy for combating HIV latency. AIDS Res. Hum. Retroviruses *31*, 4–12.

Jiang, G., Espeseth, A., Hazuda, D.J., and Margolis, D.M. (2007). c-Myc and Sp1 contribute to proviral latency by recruiting histone deacetylase 1 to the human immunodeficiency virus type 1 promoter. J. Virol. *81*, 10914–10923.

Jin, X., McGrath, M.S., and Xu, H. (2015). Inhibition of HIV Expression and Integration in Macrophages by Methylglyoxal-Bis-Guanylhydrazone. J. Virol. *89*, 11176–11189.

Jones, R.B., O'Connor, R., Mueller, S., Foley, M., Szeto, G.L., Karel, D., Lichterfeld, M., Kovacs, C., Ostrowski, M.A., Trocha, A., et al. (2014). Histone deacetylase inhibitors impair the elimination of HIV-infected cells by cytotoxic T-lymphocytes. PLoS Pathog. *10*, e1004287.

Jordan, A., Bisgrove, D., and Verdin, E. (2003). HIV reproducibly establishes a latent infection after acute infection of T cells in vitro. EMBO J. *22*, 1868.

Kamel, A.S., Abdelkader, N.F., Abd El-Rahman, S.S., Emara, M., Zaki, H.F., and Khattab, M.M. (2018). Stimulation of ACE2/ANG(1-7)/Mas Axis by Diminazene Ameliorates Alzheimer's Disease in the D-Galactose-Ovariectomized Rat Model: Role of PI3K/Akt Pathway. Mol. Neurobiol. *55*, 8188–8202.

Karvonen, E., Kauppinen, L., Partanen, T., and Pösö, H. (1985). Irreversible inhibition of putrescine-stimulated S-adenosyl-L-methionine decarboxylase by berenil and pentamidine. Biochem. J. *231*, 165–169.

Khan, S.Z., Hand, N., and Zeichner, S.L. (2015). Apoptosis-induced activation of HIV-1 in latently infected cell lines. Retrovirology *12*, 42.

Kinoshita, S., Su, L., Amano, M., Timmerman, L.A., Kaneshima, H., and Nolan, G.P. (1997). The T cell activation factor NF-ATc positively regulates HIV-1 replication and gene expression in T cells. Immunity *6*, 235–244.

König, R., Zhou, Y., Elleder, D., Diamond, T.L., Bonamy, G.M.C., Irelan, J.T., Chiang, C.-Y., Tu, B.P., De Jesus, P.D., Lilley, C.E., et al. (2008). Global analysis of host-pathogen interactions that regulate early-stage HIV-1 replication. Cell *135*, 49–60.

Kruk, J., and Aboul-Enein, H.Y. (2017). Reactive Oxygen and Nitrogen Species in Carcinogenesis: Implications of Oxidative Stress on the Progression and Development of Several Cancer Types. Mini Rev. Med. Chem. *17*, 904–919.

Kuhlmann, A.-S., Peterson, C.W., and Kiem, H.-P. (2018). Chimeric antigen receptor T-cell approaches to HIV cure. Curr. Opin. HIV AIDS *13*, 1.

Kulkosky, J., Nunnari, G., Otero, M., Calarota, S., Dornadula, G., Zhang, H., Malin, A., Sullivan, J., Xu, Y., DeSimone, J., et al. (2002). Intensification and Stimulation Therapy for Human Immunodeficiency Virus Type 1 Reservoirs in Infected Persons Receiving Virally Suppressive Highly Active Antiretroviral Therapy. J. Infect. Dis. *186*, 1403–1411.

Kuriakose, S., and Uzonna, J.E. (2014). Diminazene aceturate (Berenil), a new use for an old compound? Int. Immunopharmacol. *21*, 342–345.

Kuriakose, S., Muleme, H.M., Onyilagha, C., Singh, R., Jia, P., and Uzonna, J.E. (2012). Diminazene aceturate (Berenil) modulates the host cellular and inflammatory responses to Trypanosoma congolense infection. PLoS One *7*, e48696.

Kuriakose, S., Muleme, H., Onyilagha, C., Okeke, E., and Uzonna, J.E. (2014). Diminazene aceturate (Berenil) modulates LPS induced pro-inflammatory cytokine production by inhibiting phosphorylation of MAPKs and STAT proteins. Innate Immun. *20*, 760–773.

Lassen, K.G., Hebbeler, A.M., Bhattacharyya, D., Lobritz, M.A., and Greene, W.C. (2012). A Flexible Model of HIV-1 Latency Permitting Evaluation of Many Primary CD4 T-Cell Reservoirs. PLoS One *7*, e30176.

Law, V., Knox, C., Djoumbou, Y., Jewison, T., Guo, A.C., Liu, Y., Maciejewski, A., Arndt, D., Wilson, M., Neveu, V., et al. (2014). DrugBank 4.0: shedding new light on drug metabolism. Nucleic Acids Res. *42*, D1091-7.

Lee, W.S., Kristensen, A.B., Rasmussen, T.A., Tolstrup, M., Østergaard, L., Søgaard, O.S., Wines, B.D., Hogarth, P.M., Reynaldi, A., Davenport, M.P., et al. (2017). Anti-HIV-1 ADCC Antibodies following Latency Reversal and Treatment Interruption. J. Virol. *91*.

Lewinski, M.K., Bisgrove, D., Shinn, P., Chen, H., Hoffmann, C., Hannenhalli, S., Verdin, E., Berry, C.C., Ecker, J.R., and Bushman, F.D. (2005). Genome-wide analysis of chromosomal features repressing human immunodeficiency virus transcription. J. Virol. *79*, 6610–6619.

Lewis, M.G., DaFonseca, S., Chomont, N., Palamara, A.T., Tardugno, M., Mai, A., Collins, M., Wagner, W.L., Yalley-Ogunro, J., Greenhouse, J., et al. (2011). Gold drug auranofin restricts the viral reservoir in the monkey AIDS model and induces containment of viral load following ART suspension. AIDS *25*, 1347–1356.

Li, M.M.H., and MacDonald, M.R. (2016). Polyamines: Small Molecules with a Big Role in Promoting Virus Infection. Cell Host Microbe *20*, 123–124.

Li, H., Gao, Z., Zhang, J., Ye, X., Xu, A., Ye, J., and Jia, W. (2012). Sodium butyrate stimulates expression of fibroblast growth factor 21 in liver by inhibition of histone deacetylase 3. Diabetes *61*, 797–806.

Li, Y.H., Yu, C.Y., Li, X.X., Zhang, P., Tang, J., Yang, Q., Fu, T., Zhang, X., Cui, X., Tu, G., et al. (2018). Therapeutic target database update 2018: enriched resource for facilitating bench-to-clinic research of targeted therapeutics. Nucleic Acids Res. *46*, D1121–D1127.

Li, Z., Guo, J., Wu, Y., and Zhou, Q. (2013). The BET bromodomain inhibitor JQ1 activates HIV latency through antagonizing Brd4 inhibition of Tat-transactivation. Nucleic Acids Res. *41*, 277–287.

Lincoln, D.T., Ali Emadi, E.M., Tonissen, K.F., and Clarke, F.M. The thioredoxin-thioredoxin reductase system: over-expression in human cancer. Anticancer Res. *23*, 2425–2433.

Lingappan, K. (2018). NF-κB in Oxidative Stress. Curr. Opin. Toxicol. *7*, 81–86.

Van Lint, C., Bouchat, S., and Marcello, A. (2013). HIV-1 transcription and latency: an update. Retrovirology *10*, 67.

Liochev, S.I. (2013). Reactive oxygen species and the free radical theory of aging. Free Radic. Biol. Med. *60*, 1–4.

Liu, L., Patel, B., Ghanem, M.H., Bundoc, V., Zheng, Z., Morgan, R.A., Rosenberg, S.A., Dey, B., and Berger, E.A. (2015). Novel CD4-Based Bispecific Chimeric Antigen Receptor Designed for Enhanced Anti-HIV Potency and Absence of HIV Entry Receptor Activity. J. Virol. *89*, 6685–6694.

Lobanov, A. V, Gromer, S., Salinas, G., and Gladyshev, V.N. (2006). Selenium metabolism in Trypanosoma: characterization of selenoproteomes and identification of a Kinetoplastida-specific selenoprotein. Nucleic Acids Res. *34*, 4012–4024.

Lobo, V., Patil, A., Phatak, A., and Chandra, N. (2010). Free radicals, antioxidants and functional foods: Impact on human health. Pharmacogn. Rev. *4*, 118–126.

Luger, K., and Richmond, T.J. (1998). DNA binding within the nucleosome core. Curr. Opin. Struct. Biol. *8*, 33–40.

Luger, K., Mäder, A.W., Richmond, R.K., Sargent, D.F., and Richmond, T.J. (1997). Crystal structure of the nucleosome core particle at 2.8 Å resolution. Nature *389*, 251–260.

Luo, J.-L., Kamata, H., and Karin, M. (2005). IKK/NF-kappaB signaling: balancing life and death--a new approach to cancer therapy. J. Clin. Invest. *115*, 2625–2632.

MacLeod, M.K.L., Kappler, J.W., and Marrack, P. (2010). Memory CD4 T cells: generation, reactivation and re-assignment. Immunology *130*, 10–15.

Madeira, J.M., Renschler, C.J., Mueller, B., Hashioka, S., Gibson, D.L., and Klegeris, A. (2013). Novel protective properties of auranofin: inhibition of human astrocyte cytotoxic secretions and direct neuroprotection. Life Sci. *92*, 1072–1080.

Madeira, J.M., Bajwa, E., Stuart, M.J., Hashioka, S., and Klegeris, A. (2014). Gold drug auranofin could reduce neuroinflammation by inhibiting microglia cytotoxic secretions and primed respiratory burst. J. Neuroimmunol. *276*, 71–79.

Mahnke, Y.D., Brodie, T.M., Sallusto, F., Roederer, M., and Lugli, E. (2013). The who's who of T-cell differentiation: human memory T-cell subsets. Eur. J. Immunol. *43*, 2797–2809.

Malnati, M.S., Scarlatti, G., Gatto, F., Salvatori, F., Cassina, G., Rutigliano, T., Volpi, R., and Lusso, P. (2008). A universal real-time PCR assay for the quantification of group-M HIV-1 proviral load. Nat. Protoc. *3*, 1240–1248.

Mamont, P.S., Bohlen, P., McCann, P.P., Bey, P., Schuber, F., and Tardif, C. (1976). α -Methyl Ornithine, a Potent Competitive Inhibitor of Ornithine Decarboxylase, Blocks Proliferation of Rat Hepatoma Cells in Culture. Proc. Natl. Acad. Sci. U. S. A. *73*, 1626–1630.

Mandal, S., Mandal, A., and Park, M.H. (2015). Depletion of the polyamines spermidine and spermine by overexpression of spermidine/spermine N^1-acetyltransferase 1 (SAT1) leads to mitochondria-mediated apoptosis in mammalian cells. Biochem. J. *468*, 435–447.

Manganaro, L., Lusic, M., Gutierrez, M.I., Cereseto, A., Del Sal, G., and Giacca, M. (2010). Concerted action of cellular JNK and Pin1 restricts HIV-1 genome integration to activated CD4+ T lymphocytes. Nat. Med. *16*, 329–333.

Manganaro, L., Pache, L., Herrmann, T., Marlett, J., Hwang, Y., Murry, J., Miorin, L., Ting, A.T., König, R., García-Sastre, A., et al. (2014). Tumor suppressor cylindromatosis (CYLD) controls HIV transcription in an NF-κB-dependent manner. J. Virol. *88*, 7528–7540.

Mangold, U., and Leberer, E. (2005). Regulation of all members of the antizyme family by antizyme inhibitor. Biochem. J. *385*, 21.

Margolis, D.M. (2010). Mechanisms of HIV Latency: an Emerging Picture of Complexity. Curr. HIV/AIDS Rep. *7*, 37–43.

De Maria, M.L.A., Araújo, L.D., Fraga-Silva, R.A., Pereira, L.A.S., Ribeiro, H.J., Menezes, G.B., Shenoy, V., Raizada, M.K., and Ferreira, A.J. (2016). Anti-hypertensive Effects of Diminazene Aceturate: An Angiotensin- Converting Enzyme 2 Activator in Rats. Protein Pept. Lett. *23*, 9–16.

Marini, B., Kertesz-Farkas, A., Ali, H., Lucic, B., Lisek, K., Manganaro, L., Pongor, S., Luzzati, R., Recchia, A., Mavilio, F., et al. (2015). Nuclear architecture dictates HIV-1 integration site selection. Nature *521*, 227–231.

Marks, P.A. (2007). Discovery and development of SAHA as an anticancer agent. Oncogene *26*, 1351–1356.

Marques, M.P.M., Gil, F.P.S.C., Calheiros, R., Battaglia, V., Brunati, A.M., Agostinelli, E., and Toninello, A. (2008). Biological activity of antitumoural MGBG: the structural variable. Amino Acids *34*, 555–564.

Marzano, C., Gandin, V., Folda, A., Scutari, G., Bindoli, A., and Rigobello, M.P. (2007). Inhibition of thioredoxin reductase by auranofin induces apoptosis in cisplatin-resistant human ovarian cancer cells. Free Radic. Biol. Med. *42*, 872–881.

Mathis, B.J., Lai, Y., Qu, C., Janicki, J.S., and Cui, T. (2015). CYLD-mediated signaling and diseases. Curr. Drug Targets *16*, 284–294.

Matthews, J.R., Wakasugi, N., Virelizier, J.L., Yodoi, J., and Hay, R.T. (1992). Thioredoxin regulates the DNA binding activity of NF-kappa B by reduction of a disulphide bond involving cysteine 62. Nucleic Acids Res. *20*, 3821–3830.

Mbonye, U.R., Gokulrangan, G., Datt, M., Dobrowolski, C., Cooper, M., Chance, M.R., and Karn, J. (2013). Phosphorylation of CDK9 at Ser175 Enhances HIV Transcription and Is a Marker of Activated P-TEFb in CD4+ T Lymphocytes. PLoS Pathog. *9*, e1003338.

McGrath, A.P., Hilmer, K.M., Collyer, C.A., Shepard, E.M., Elmore, B.O., Brown, D.E., Dooley, D.M., and Guss, J.M. (2009). Structure and Inhibition of Human Diamine Oxidase. Biochemistry *48*, 9810–9822.

McKernan, L.N., Momjian, D., and Kulkosky, J. (2012). Protein Kinase C: One Pathway towards the Eradication of Latent HIV-1 Reservoirs. Adv. Virol. *2012*, 1–8.

McMahon, S.B., Van Buskirk, H.A., Dugan, K.A., Copeland, T.D., and Cole, M.D. (1998). The novel ATM-related protein TRRAP is an essential cofactor for the c-Myc and E2F oncoproteins. Cell *94*, 363–374.

McMahon, S.B., Wood, M.A., and Cole, M.D. (2000). The essential cofactor TRRAP recruits the histone acetyltransferase hGCN5 to c-Myc. Mol. Cell. Biol. *20*, 556–562.

Mellor, H., and Parker, P.J. (1998). The extended protein kinase C superfamily. Biochem. J. *332 (Pt 2)*, 281–292.

Michael, A.J. (2016). Polyamines in Eukaryotes, Bacteria, and Archaea. J. Biol. Chem. *291*, 14896–14903.

Mikek, C.G., West, S.J., Gwin, J.C., Dayal, N., Sintim, H.O., and Lewis, E.A. (2018). Berenil Binds Tightly to Parallel and Mixed Parallel/Antiparallel G-Quadruplex Motifs with Varied Thermodynamic Signatures. ACS Omega *3*, 11582–11591.

Mir, M.A., and Mir, M.A. (2015). Introduction to Costimulation and Costimulatory Molecules. Dev. Costimulatory Mol. Immunother. Dis. 1–43.

Mitsuya, H., Weinhold, K.J., Furman, P.A., St Clair, M.H., Lehrman, S.N., Gallo, R.C., Bolognesi, D., Barry, D.W., and Broder, S. (1985). 3'-Azido-3'-deoxythymidine (BW A509U): an antiviral agent that inhibits the infectivity and cytopathic effect of human T-lymphotropic virus type III/lymphadenopathy-associated virus in vitro. Proc. Natl. Acad. Sci. U. S. A. *82*, 7096–7100.

Morgan, M.J., and Liu, Z. (2011). Crosstalk of reactive oxygen species and NF-κB signaling. Cell Res. *21*, 103–115.

Mounce, B.C., Olsen, M.E., Vignuzzi, M., and Connor, J.H. (2017). Polyamines and Their Role in Virus Infection. Microbiol. Mol. Biol. Rev. *81*.

Moynagh, P.N. (2005). The NF-kappaB pathway. J. Cell Sci. *118*, 4589–4592.

Murr, R., Vaissière, T., Sawan, C., Shukla, V., and Herceg, Z. (2007). Orchestration of chromatin-based processes: mind the TRRAP. Oncogene *26*, 5358–5372.

Murray Stewart, T., Dunston, T.T., Woster, P.M., and Casero, R.A. (2018). Polyamine catabolism and oxidative damage. J. Biol. Chem. *293*, 18736–18745.

Nabel, G., and Baltimore, D. (1987). An inducible transcription factor activates expression of human immunodeficiency virus in T cells. Nature *326*, 711–713.

Nehrbass-Stuedli, A., Boykin, D., Tidwell, R.R., and Brun, R. (2011). Novel diamidines with activity against Babesia divergens in vitro and Babesia microti in vivo. Antimicrob. Agents Chemother. *55*, 3439–3445.

Neidhart, M., Karouzakis, E., Jüngel, A., Gay, R.E., and Gay, S. (2014). Inhibition of spermidine/spermine N1-acetyltransferase activity: a new therapeutic concept in rheumatoid arthritis. Arthritis Rheumatol. (Hoboken, N.J.) *66*, 1723–1733.

Nilson, K.A., and Price, D.H. (2011). The Role of RNA Polymerase II Elongation Control in HIV-1 Gene Expression, Replication, and Latency. Genet. Res. Int. *2011*, 726901.

Nnadi, C.O., Ebiloma, G.U., Black, J.A., Nwodo, N.J., Lemgruber, L., Schmidt, T.J., and de Koning, H.P. (2019). Potent Antitrypanosomal Activities of 3-Aminosteroids against African Trypanosomes: Investigation of Cellular Effects and of Cross-Resistance with Existing Drugs. Molecules *24*, 268.

Norton, N.J., Fun, A., Bandara, M., Wills, M.R., Mok, H.P., and Lever, A.M.L. (2017). Innovations in the quantitative virus outgrowth assay and its use in clinical trials. Retrovirology *14*, 58.

Pace, M.J., Agosto, L., Graf, E.H., and O'Doherty, U. (2011). HIV reservoirs and latency models. Virology *411*, 344–354.

Pagano, J.M., Kwak, H., Waters, C.T., Sprouse, R.O., White, B.S., Ozer, A., Szeto, K., Shalloway, D., Craighead, H.G., and Lis, J.T. (2014). Defining NELF-E RNA binding in HIV-1 and promoter-proximal pause regions. PLoS Genet. *10*, e1004090.

Palacios, J.A., Pérez-Piñar, T., Toro, C., Sanz-Minguela, B., Moreno, V., Valencia, E., Gómez-Hernando, C., and Rodés, B. (2012). Long-term nonprogressor and elite controller patients who control viremia have a higher percentage of methylation in their HIV-1 proviral promoters than aviremic patients receiving highly active antiretroviral therapy. J. Virol. *86*, 13081–13084.

Palella, F.J., Delaney, K.M., Moorman, A.C., Loveless, M.O., Fuhrer, J., Satten, G.A., Aschman, D.J., and Holmberg, S.D. (1998). Declining morbidity and mortality among patients with advanced human immunodeficiency virus infection. HIV Outpatient Study Investigators. N. Engl. J. Med. *338*, 853–860.

Panfil, A.R., London, J.A., Green, P.L., and Yoder, K.E. (2018). CRISPR/Cas9 Genome Editing to Disable the Latent HIV-1 Provirus. Front. Microbiol. *9*, 3107.

Pantaleo, G., Graziosi, C., Fauci, A.S., and Fauci, A.S. (1993). The immunopathogenesis of human immunodeficiency virus infection. N. Engl. J. Med. *328*, 327–335.

Parente, J.E., Walsh, M.P., Girard, P.R., Kuo, J.F., Ng, D.S., and Wong, K. (1989). Effects of gold coordination complexes on neutrophil function are mediated via inhibition of protein kinase C. Mol. Pharmacol. *35*, 26–33.

Park, S.-J., and Kim, I.-S. (2005). The role of p38 MAPK activation in auranofin-induced apoptosis of human promyelocytic leukaemia HL-60 cells. Br. J. Pharmacol. *146*, 506–513.

Park, M.H., Cooper, H.L., and Folk, J.E. (1981). Identification of hypusine, an unusual amino acid, in a protein from human lymphocytes and of spermidine as its biosynthetic precursor. Proc. Natl. Acad. Sci. U. S. A. *78*, 2869–2873.

Patel, D.J., and Wang, Z. (2013). Readout of Epigenetic Modifications. Annu. Rev. Biochem. *82*, 81–118.

Pear, W.S., Nolan, G.P., Scott, M.L., and Baltimore, D. (1993). Production of high-titer helper-free retroviruses by transient transfection. Proc. Natl. Acad. Sci. U. S. A. *90*, 8392–8396.

Pearson, R., Kim, Y.K., Hokello, J., Lassen, K., Friedman, J., Tyagi, M., and Karn, J. (2008). Epigenetic silencing of human immunodeficiency virus (HIV) transcription by formation of restrictive chromatin structures at the viral long terminal repeat drives the progressive entry of HIV into latency. J. Virol. *82*, 12291–12303.

Pegg, A.E. (2008). Spermidine/spermine-N(1)-acetyltransferase: a key metabolic regulator. Am. J. Physiol. Endocrinol. Metab. *294*, E995-1010.

Pegg, A.E. (2016). Functions of Polyamines in Mammals. J. Biol. Chem. *291*, 14904–14912.

Pegg, A.E., and McCann, P.P. (1992). S-adenosylmenthionine decarboxylase as an enzyme target for therapy. Pharmacol. Ther. *56*, 359–377.

Peña, A., Reddy, C.D., Wu, S., Hickok, N.J., Reddy, E.P., Yumet, G., Soprano, D.R., and Soprano, K.J. (1993). Regulation of human ornithine decarboxylase expression by the c-Myc.Max protein complex. J. Biol. Chem. *268*, 27277–27285.

Perelson, A.S., Essunger, P., Cao, Y., Vesanen, M., Hurley, A., Saksela, K., Markowitz, M., and Ho, D.D. (1997). Decay characteristics of HIV-1-infected compartments during combination therapy. Nature *387*, 188–191.

Perkins, K.J., Lusic, M., Mitar, I., Giacca, M., and Proudfoot, N.J. (2008). Transcription-dependent gene looping of the HIV-1 provirus is dictated by recognition of pre-mRNA processing signals. Mol. Cell *29*, 56–68.

Perkins, N.D., Felzien, L.K., Betts, J.C., Leung, K., Beach, D.H., and Nabel, G.J. (1997). Regulation of NF-kappaB by cyclin-dependent kinases associated with the p300 coactivator. Science *275*, 523–527.

Pierson, T., Hoffman, T.L., Blankson, J., Finzi, D., Chadwick, K., Margolick, J.B., Buck, C., Siliciano, J.D., Doms, R.W., and Siliciano, R.F. (2000). Characterization of chemokine receptor utilization of viruses in the latent reservoir for human immunodeficiency virus type 1. J. Virol. *74*, 7824–7833.

Policicchio, B.B., Pandrea, I., and Apetrei, C. (2016). Animal Models for HIV Cure Research. Front. Immunol. *7*, 12.

Poomipark, N., Flatley, J.E., Hill, M.H., Mangnall, B., Azar, E., Grabowski, P., and Powers, H.J. (2016). Methyl Donor Status Influences DNMT Expression and Global DNA Methylation in Cervical Cancer Cells. Asian Pac. J. Cancer Prev. *17*, 3213–3222.

Popper, S.J., Sarr, A.D., Guèye-Ndiaye, A., Mboup, S., Essex, M.E., and Kanki, P.J. (2000). Low plasma human immunodeficiency virus type 2 viral load is independent of proviral load: low virus production in vivo. J. Virol. *74*, 1554–1557.

Porter, K.M., and Sutliff, R.L. (2012). HIV-1, reactive oxygen species, and vascular complications. Free Radic. Biol. Med. *53*, 143–159.

Portugal, J. (1994). Berenil acts as a poison of eukaryotic topoisomerase II. FEBS Lett. *344*, 136–138.

Prins, J.M., Jurriaans, S., van Praag, R.M., Blaak, H., van Rij, R., Schellekens, P.T., ten Berge, I.J., Yong, S.L., Fox, C.H., Roos, M.T., et al. (1999). Immuno-activation with anti-CD3 and recombinant human IL-2 in HIV-1-infected patients on potent antiretroviral therapy. AIDS *13*, 2405–2410.

Rajapaksha, I.G., Mak, K.Y., Huang, P., Burrell, L.M., Angus, P.W., and Herath, C.B. (2018). The small molecule drug diminazene aceturate inhibits liver injury and biliary fibrosis in mice. Sci. Rep. *8*, 10175.

Rasmussen, T.A., and Søgaard, O.S. (2018). Clinical Interventions in HIV Cure Research. In Advances in Experimental Medicine and Biology, pp. 285–318.

Rayet, B., and Gélinas, C. (1999). Aberrant rel/nfkb genes and activity in human cancer. Oncogene *18*, 6938–6947.

Regenass, U., Caravatti, G., Mett, H., Stanek, J., Schneider, P., Müller, M., Matter, A., Vertino, P., and Porter, C.W. (1992). New S-adenosylmethionine decarboxylase inhibitors with potent antitumor activity. Cancer Res. *52*, 4712–4718.

Richman, D.D. (1990). Susceptibility to nucleoside analogues of zidovudine-resistant isolates of human immunodeficiency virus. Am. J. Med. *88*, 8S-10S.

Rigobello, M.P., Folda, A., Baldoin, M.C., Scutari, G., and Bindoli, A. (2005). Effect of auranofin on the mitochondrial generation of hydrogen peroxide. Role of thioredoxin reductase. Free Radic. Res. *39*, 687–695.

Rigobello, M.P., Folda, A., Dani, B., Menabò, R., Scutari, G., and Bindoli, A. (2008). Gold(I) complexes determine apoptosis with limited oxidative stress in Jurkat T cells. Eur. J. Pharmacol. *582*, 26–34.

RKI - HIV-Serokonverterstudie. https://www.rki.de/DE/Content/InfAZ/H/HIVAIDS/Studien/SeroKon/SeroKon_node.html (access date: 28 January 2018).

RKI- RKI Ratgeber - HIV- Infektion/AIDS. https://www.rki.de/DE/Content/Infekt/EpidBull/Merkblaetter/Ratgeber_HIV_AIDS.html (access date: 29 April 2018)

Roebuck, K.A., and Saifuddin, M. (1999). Regulation of HIV-1 transcription. Gene Expr. *8*, 67–84.

Sahu, G.K., Lee, K., Ji, J., Braciale, V., Baron, S. and Cloyd, M.W. (2006). A novel in vitro system to generate and study latently HIV-infected long-lived normal $CD4^+$ T-lymphocytes. Virology *355*, 127-37.

Saleh, A., Schieltz, D., Ting, N., McMahon, S.B., Litchfield, D.W., Yates, J.R., Lees-Miller, S.P., Cole, M.D., and Brandl, C.J. (1998). Tra1p is a component of the yeast Ada.Spt transcriptional regulatory complexes. J. Biol. Chem. *273*, 26559–26565.

Saliou, J.-M., Bourgeois, C.F., Ayadi-Ben Mena, L., Ropers, D., Jacquenet, S., Marchand, V., Stevenin, J., and Branlant, C. (2009). Role of RNA structure and protein factors in the control of HIV-1 splicing. Front. Biosci. (Landmark Ed. *14*, 2714–2729.

Sallusto, F., Geginat, J., and Lanzavecchia, A. (2004). Central memory and effector memory T cell subsets: function, generation, and maintenance. Annu. Rev. Immunol. *22*, 745–763.

Satou, A., Taira, T., Iguchi-Ariga, S.M., and Ariga, H. (2001). A novel transrepression pathway of c-Myc. Recruitment of a transcriptional corepressor complex to c-Myc by MM-1, a c-Myc-binding protein. J. Biol. Chem. *276*, 46562–46567.

Schäfer, B., Hauber, I., Bunk, A., Heukeshoven, J., Düsedau, A., Bevec, D., and Hauber, J. (2006). Inhibition of multidrug-resistant HIV-1 by interference with cellular S-adenosylmethionine decarboxylase activity. J. Infect. Dis. *194*, 740–750.

Schallreuter, K.U., Gleason, F.K., and Wood, J.M. (1990). The mechanism of action of the nitrosourea anti-tumor drugs on thioredoxin reductase, glutathione reductase and ribonucleotide reductase. Biochim. Biophys. Acta *1054*, 14–20.

Scheidereit, C. (2006). IkappaB kinase complexes: gateways to NF-kappaB activation and transcription. Oncogene *25*, 6685–6705.

Schröder, A.R.W., Shinn, P., Chen, H., Berry, C., Ecker, J.R., and Bushman, F. (2002). HIV-1 integration in the human genome favors active genes and local hotspots. Cell *110*, 521–529.

Sedger, L.M., and McDermott, M.F. (2014). TNF and TNF-receptors: From mediators of cell death and inflammation to therapeutic giants – past, present and future. Cytokine Growth Factor Rev. *25*, 453–472.

Selliah, N., Zhang, M., DeSimone, D., Kim, H., Brunner, M., Ittenbach, R.F., Rui, H., Cron, R.Q., and Finkel, T.H. (2006). The gammac-cytokine regulated transcription factor, STAT5, increases HIV-1 production in primary CD4 T cells. Virology *344*, 283–291.

Shan, L., Deng, K., Shroff, N.S., Durand, C.M., Rabi, S.A., Yang, H.-C., Zhang, H., Margolick, J.B., Blankson, J.N., and Siliciano, R.F. (2012). Stimulation of HIV-1-specific cytolytic T lymphocytes facilitates elimination of latent viral reservoir after virus reactivation. Immunity *36*, 491–501.

Shapiro, T.A. (1993). Inhibition of topoisomerases in African trypanosomes. Acta Trop. *54*, 251–260.

Sharlow, E.R., Leimgruber, S., Murray, S., Lira, A., Sciotti, R.J., Hickman, M., Hudson, T., Leed, S., Caridha, D., Barrios, A.M., et al. (2014). Auranofin is an apoptosis-simulating agent with in vitro and in vivo anti-leishmanial activity. ACS Chem. Biol. *9*, 663–672.

Sharp, P.M., and Hahn, B.H. (2011). Origins of HIV and the AIDS Pandemic. Cold Spring Harb. Perspect. Med. *1*, a006841–a006841.

Sheppard, K.A., Rose, D.W., Haque, Z.K., Kurokawa, R., McInerney, E., Westin, S., Thanos, D., Rosenfeld, M.G., Glass, C.K., and Collins, T. (1999). Transcriptional activation by NF-kappaB requires multiple coactivators. Mol. Cell. Biol. *19*, 6367–6378.

Shirakawa, K., Chavez, L., Hakre, S., Calvanese, V., and Verdin, E. (2013). Reactivation of latent HIV by histone deacetylase inhibitors. Trends Microbiol. *21*, 277–285.

Sok, D., and Burton, D.R. (2018). Recent progress in broadly neutralizing antibodies to HIV. Nat. Immunol. *19*, 1179–1188.

Spivak, A.M., and Planelles, V. (2018). Novel Latency Reversal Agents for HIV-1 Cure. Annu. Rev. Med. *69*, 421–436.

Stojanova, A., Caro, C., Jarjour, R.J. V, Oster, S.K., Penn, L.Z., and Germinario, R.J. (2004). Repression of the human immunodeficiency virus type-1 long terminal repeat by the c-Myc oncoprotein. J. Cell. Biochem. *92*, 400–413.

Strain, M.C., Little, S.J., Daar, E.S., Havlir, D.V., Günthard, H.F., Lam, R.Y., Daly, O.A., Nguyen, J., Ignacio, C.C., Spina, C.A., et al. (2005). Effect of Treatment, during Primary Infection, on Establishment and Clearance of Cellular Reservoirs of HIV-1. J. Infect. Dis. *191*, 1410–1418.

Sun, S.-C. (2010). CYLD: a tumor suppressor deubiquitinase regulating NF-κB activation and diverse biological processes. Cell Death Differ. *17*, 25–34.

Sun, S., Rao, V.B., and Rossmann, M.G. (2010). Genome packaging in viruses. Curr. Opin. Struct. Biol. *20*, 114–120.

Swiggard, W.J., Baytop, C., Yu, J.J., Dai, J., Li, C., Schretzenmair, R., Theodosopoulos, T., and O'Doherty, U. (2005). Human immunodeficiency virus type 1 can establish latent infection in resting CD4+ T cells in the absence of activating stimuli. J. Virol. *79*, 14179–14188.

Talbert, P.B., and Henikoff, S. (2010). Histone variants — ancient wrap artists of the epigenome. Nat. Rev. Mol. Cell Biol. *11*, 264–275.

Tao, L., Qiu, Y., Fu, X., Lin, R., Lei, C., Wang, J., and Lei, B. (2016). Angiotensin-converting enzyme 2 activator diminazene aceturate prevents lipopolysaccharide-induced inflammation by inhibiting MAPK and NF-κB pathways in human retinal pigment epithelium. J. Neuroinflammation *13*, 35.

Taube, R., and Peterlin, M. (2013). Lost in Transcription: Molecular Mechanisms that Control HIV Latency. Viruses *5*, 902–927.

Tebas, P., Stein, D., Tang, W.W., Frank, I., Wang, S.Q., Lee, G., Spratt, S.K., Surosky, R.T., Giedlin, M.A., Nichol, G., et al. (2014). Gene editing of CCR5 in autologous CD4 T cells of persons infected with HIV. N. Engl. J. Med. *370*, 901–910.

Tejman-Yarden, N., Miyamoto, Y., Leitsch, D., Santini, J., Debnath, A., Gut, J., McKerrow, J.H., Reed, S.L., and Eckmann, L. (2013). A reprofiled drug, auranofin, is effective against metronidazole-resistant Giardia lamblia. Antimicrob. Agents Chemother. *57*, 2029–2035.

Thompson, J.E., Phillips, R.J., Erdjument-Bromage, H., Tempst, P., and Ghosh, S. (1995). IκB-β regulates the persistent response in a biphasic activation of NF-κB. Cell *80*, 573–582.

Tuvshintulga, B., AbouLaila, M., Sivakumar, T., Tayebwa, D.S., Gantuya, S., Naranbaatar, K., Ishiyama, A., Iwatsuki, M., Otoguro, K., Ōmura, S., et al. (2017). Chemotherapeutic efficacies of a clofazimine and diminazene aceturate combination against piroplasm parasites and their AT-rich DNA-binding activity on Babesia bovis. Sci. Rep. *7*, 13888.

Uhlén, M., Fagerberg, L., Hallström, B.M., Lindskog, C., Oksvold, P., Mardinoglu, A., Sivertsson, Å., Kampf, C., Sjöstedt, E., Asplund, A., et al. (2015). Proteomics. Tissue-based map of the human proteome. Science *347*, 1260419.

Valenzuela, M.S., Green, N., and Liu, S. (2017). Identification of Berenil Target Sites in Plasmid pBR322. Int. J. Bioorganic Chem. Mol. Biol. *5*, 24–30.

Varghese, E., and Büsselberg, D. (2014). Auranofin, an anti-rheumatic gold compound, modulates apoptosis by elevating the intracellular calcium concentration ([ca2+]I) in mcf-7 breast cancer cells. Cancers (Basel). *6*, 2243–2258.

Verdin, E., Paras, P., and Van Lint, C. (1993). Chromatin disruption in the promoter of human immunodeficiency virus type 1 during transcriptional activation. EMBO J. *12*, 3249–3259.

Vogt, V. (1997). Retroviral Virions and Genomes.

Wandeler, G., Johnson, L.F., and Egger, M. (2016). Trends in life expectancy of HIV-positive adults on antiretroviral therapy across the globe. Curr. Opin. HIV AIDS *11*, 492–500.

Wang, D., Hicks, C.B., Goswami, N.D., Tafoya, E., Ribeiro, R.M., Cai, F., Perelson, A.S., and Gao, F. (2011). Evolution of Drug-Resistant Viral Populations during Interruption of Antiretroviral Therapy. J. Virol. *85*, 6403–6415.

Watson, J.A., Rumsby, M.G., and Wolowacz, R.G. (1999). Phage display identifies thioredoxin and superoxide dismutase as novel protein kinase C-interacting proteins: thioredoxin inhibits protein kinase C-mediated phosphorylation of histone. Biochem. J. *343 Pt 2*, 301–305.

Wei, X., Ghosh, S.K., Taylor, M.E., Johnson, V.A., Emini, E.A., Deutsch, P., Lifson, J.D., Bonhoeffer, S., Nowak, M.A., Hahn, B.H., et al. (1995). Viral dynamics in human immunodeficiency virus type 1 infection. Nature *373*, 117–122.

Weiss, R.A. (1993). How does HIV cause AIDS? Science *260*, 1273–1279.

Weiss, A., Wiskocil, R.L., and Stobo, J.D. (1984). The role of T3 surface molecules in the activation of human T cells: a two-stimulus requirement for IL 2 production reflects events occurring at a pre-translational level. J. Immunol. *133*, 123–128.

Wenzel, S., Schweimer, K., Rösch, P., and Wöhrl, B.M. (2008). The small hSpt4 subunit of the human transcription elongation factor DSIF is a Zn-finger protein with α/β type topology. Biochem. Biophys. Res. Commun. *370*, 414–418.

World Health Organization. (2018). Updated recommendations on first-line and second-line antiretroviral regimens and post-exposure prophylaxis and recommendations on early infant diagnosis of HIV: interim guidelines: supplement to the 2016 consolidated guidelines on the use of antiretroviral drugs for treating and preventing HIV infection. World Health Organization (access date: 23 April 2019)

Wilen, C.B., Tilton, J.C., and Doms, R.W. (2012). HIV: cell binding and entry. Cold Spring Harb. Perspect. Med. *2*, a006866–a006866.

Wong, J.K., Hezareh, M., Günthard, H.F., Havlir, D. V, Ignacio, C.C., Spina, C.A., and Richman, D.D. (1997). Recovery of replication-competent HIV despite prolonged suppression of plasma viremia. Science *278*, 1291–1295.

Wong, K., Parente, J., Prasad, K. V, and Ng, D. (1990). Auranofin modulated cytoplasmic free calcium in neutrophils by mobilizing intracellular calcium and inhibiting protein kinase. J. Biol. Chem. *265*, 21454–21461.

Wu, H., Liao, W., Li, Q., Long, H., Yin, H., Zhao, M., Chan, V., Lau, C.-S., and Lu, Q. (2018). Pathogenic role of tissue-resident memory T cells in autoimmune diseases. Autoimmun. Rev. *17*, 906–911.

Xu, W., Li, H., Wang, Q., Hua, C., Zhang, H., Li, W., Jiang, S., and Lu, L. (2017). Advancements in Developing Strategies for Sterilizing and Functional HIV Cures. Biomed Res. Int. *2017*, 1–12.

Xu, W.S., Parmigiani, R.B., and Marks, P.A. (2007). Histone deacetylase inhibitors: molecular mechanisms of action. Oncogene *26*, 5541–5552.

Yamamoto, D., Shima, K., Matsuo, K., Nishioka, T., Chen, C.Y., Hu, G.-F., Sasaki, A., and Tsuji, T. (2010). Ornithine decarboxylase antizyme induces hypomethylation of genome DNA and histone H3 lysine 9 dimethylation (H3K9me2) in human oral cancer cell line. PLoS One *5*, e12554.

Yang, X., Chen, Y., and Gabuzda, D. (1999). ERK MAP kinase links cytokine signals to activation of latent HIV-1 infection by stimulating a cooperative interaction of AP-1 and NF-kappaB. J. Biol. Chem. *274*, 27981–27988.

Yang, HC., Xing, S., Shan, L., K., Dinoso, J.,Shen, A., Zhou,Y., Shrum, C.K., Han,Y., Liu,J.O., Zhang,H., J.B., and Siliciano, R.F. (2009). Small-molecule screening using a human primary cell model of HIV latency identifies compounds that reverse latency without cellular activation. J. Clin. Invest. *119,* 3473–3486.

Yoo, M.-H., Xu, X.-M., Carlson, B.A., Patterson, A.D., Gladyshev, V.N., and Hatfield, D.L. (2007). Targeting thioredoxin reductase 1 reduction in cancer cells inhibits self-sufficient growth and DNA replication. PLoS One *2*, e1112.

Yoshida, M., Kudo, N., Kosono, S., and Ito, A. (2017). Chemical and structural biology of protein lysine deacetylases. Proc. Japan Acad. Ser. B *93*, 297–321.

Zayed, S., Hafez, A., Adolf, W., and Hecker, E. (1977). New tigliane and daphnane derivatives from Pimelea prostrata and Pimelea simplex. Experientia *33*, 1554–1555.

Zhang, H.-S., Liu, Y., Wu, T.-C., Du, G.-Y., and Zhang, F.-J. (2015). EZH2 phosphorylation regulates Tat-induced HIV-1 transactivation via ROS/Akt signaling pathway. FEBS Lett. *589*, 4106–4111.

Zhang, H., Du, Y., Zhang, X., Lu, J., and Holmgren, A. (2014). Glutaredoxin 2 Reduces Both Thioredoxin 2 and Thioredoxin 1 and Protects Cells from Apoptosis Induced by Auranofin and 4-Hydroxynonenal. Antioxid. Redox Signal. *21*, 669–681.

Zhou, H., Xu, M., Huang, Q., Gates, A.T., Zhang, X.D., Castle, J.C., Stec, E., Ferrer, M., Strulovici, B., Hazuda, D.J., and Espeseth, A.S. (2008). Genome-scale RNAi screen for host factors required for HIV replication. Cell Host Microbe. *4*, 495-504.

Zhou, Q., Li, T., and Price, D.H. (2012). RNA polymerase II elongation control. Annu. Rev. Biochem. *81*, 119–143.

Zhu, J., and Paul, W.E. (2008). CD4 T cells: fates, functions, and faults. Blood *112*, 1557–1569.

Zhu, J., Gaiha, G.D., John, S.P., Pertel, T., Chin, C.R., Gao, G., Qu, H., Walker, B.D., Elledge, S.J., and Brass, A.L. (2012). Reactivation of latent HIV-1 by inhibition of BRD4. Cell Rep. *2*, 807–816.

6 Abbreviations

abbreviation	full name
°C	Celisius degrees
AbeAdo	5'-(((Z)-4-amino-2-butenyl)methylamino)-5'-deoxyadenosine
ACE2	angiotensin converting enzyme 2
activ.	activation
AIDS	acquired immunodeficiency syndrome
AMD1	adenosylmethionine decarboxylase
AP-1	activator protein 1
APAO	acetylpolyamine oxidase
APC	antigen presenting cell
applic.	application
ASK-1	apoptosis signal-regulating kinase 1
ASXL3	additional sex combs like 3 (Drosophila)
AZT	3′-Azido-3′-deoxythymidine
b.d.	below detection
BRD4	bromodomain containing protein 4
bromo	bromodomain
BSA	bovine serum albumin
CAR	chimeric antigen receptor
CBX6	chromobox homolog 6
CCR5	C-C chemokine receptor type 5
CD	cluster of differentiation
CDK9	cyclin dependent kinase 9
chromo	chromodomain
conju.	conjugate
CpG	5'cytosine-phosphate-guanine3' (nucleotide sequence)
CTL	cytotoxic T lymphocytes
CXCR4	C-X-C chemokine receptor type 4
CXXC1	CXXC finger protein 1
CYLD	Cylindromatosis
DAO	diamine oxidase, a.k.a AOC1
dcSAM	decarboxylated S-adenosylmethioninamine
DFMO	difluoromethylornithine hydrochloride (ODC inhibitor)
DMEM	Dulbeccos modified eagle medium
DMSO	dimethyl sulfoxide
DNA	deoxyribonucleic acid
DNMT	DNA methyltransferases
DSIF	DRB sensitivity factor
e.g.	Latin: exempli gratia, English: for example
EDTA	ethylenediaminetetraacetic acid
eIF5A	eukaryotic translation initiation factor 5A
ELISA	enzyme-linked immuno assay
env	envelope gene (HIV)
FACS	fluorescence-activated cell sorting

abbreviation	full name
FC	flow cytometry
FCS	fetal calf serum
FITC	fluorescein isothiocyanate
FITC	fluorescein isothiocyanate
fw	forward (primer)
g	gram
Gag	group specific antigen (HIV)
GAPDH	glyceraldehyde 3-phosphate dehydrogenase
gDNA	genomic DNA
GFP	green fluorescent protein
GPX	glutathione peroxidase
GRX	glutaredoxin
h	hours
HAART	highly active antiretroviral therapy
HAT	histone acetyltransferase
HDAC	histone deacetylase
HEPES	4-(2-hydroxyethyl)-1-piperazineethanesulfonic acid
HIV	human immunodeficiency virus
HIV-1 M group	HIV-1 major group
HIVluc	HIV-1 derived reporter virus, expressing luciferase instead of *nef*, *env* deleted
HLA-DR	human leukocyte antigen – DR isotype
HMT	histone methyltransferase
HRP	horseradish peroxidase
HTS	high throughput screening
i.e.	Latin: id est, English: that is
IkB	inhibitor of κB
IKK complex	IκB kinase
iso.	isolation
IUPM	infectious units per million cells
IκB	inhibitor of kappa B
KAT6B	lysine acetyltransferase 6B
kb	kilobase
kDNA	kinetoplast DNA
LB	lysogeny broth
LPS	lipopolysaccharides
LRA	latency reversing agent
LTR	long terminal repeat (HIV)
MAPK	mitogen-activated protein kinases
mc	monoclonal
MGBG	methylglyoxal-bis-guanylhydrazone (inhibitor AMD1)
min	minutes
ml	mililiter
MOPS	3-(N-morpholino) propanesulfonic acid
mRNA	messenger RNA
MSH6	mutS homolog 6

abbreviation	full name
n.t.	not tested
$NADP^+$	nicotinamide adenine dinucleotide phosphate
NADPH	reduced form of nicotinamide adenine dinucleotide phosphate
nef	negative regulatory factor
NELF	negative elongation factors
NFAT	nuclear factor of activated T-cell
NFκB	nuclear factor kappa-light-chain-enhancer of activated B cells
NGS	normal goat serum
NHP	non-human primate
NLS	nuclear localization signal
NMS	normal mouse serum
ox	oxidized
p50/p65	NFκB heterodimer
PBMC	peripheral blood mononuclear cell
PBS	phosphate buffered saline
pc	polyclonal
PE	phycoerythrin
PEI	Paul-Ehrlich-Institut
PFA	paraformaldehyde
PHA	phytohaemagglutinin
PHD	plant homeodomain
PKC	protein kinase C
PRDX	peroxiredoxin
P-TEFb	postive transcriptional elongation factor b (complex)
PWWP	proline-tryptophan-tryptophan-proline containing domain
qPCR	quantitative PCR
qVOA	quantitative viral outgrowth assay
red	reduced
rev	reverse (primer)
RNA	ribonucleic acid
RNA Pol II	RNA polymerase II
RNAi	RNA interference
ROS	reactive oxygen species
RPL13A	60S ribosomal protein L13a
RPMI	Roswell Park Memorial Institute medium
RPS11	40S ribosomal protein S11
RPS27a	40S ribosomal protein S27a
RT-qPCR	reverse transcriptase qPCR
s	seconds
SAHA	Suberanilohydroxamic acid (a.k.a Vorinostat)
SAM	S-adenosylmethionine decarboxylase adenosyl methionine
SDS-PAGE	SDS polyacrylamide gel electrophoresis
seq	sequencing
SETD3	SET domain containing 3
shRNA	smal-hairpin RNA

abbreviation	full name
SIV	simian immunodeficiency virus
SIV cpz	SIV chimpanzee
SIV smm	SIV sooty mangabey
SMYD2	SET and MYND domain containing 2
SOC medium	super optimal broth with catabolite repression medium
sod.but.	sodium butyrate
SSAT	spermidine/spermine-N1-acetyltransferase
STAT	signal transducer and activator of transcription
TAE buffer	Tris-Acetate-EDTA buffer
TAR	trans-activating response element (HIV)
Tat	transactivator of transcription (HIV)
TBS-T	Tris-buffered saline with Tween 20
T_{CM}	central memory T cell
TCR	T-cell receptor
TE buffer	Tris-EDTA buffer
T_{EM}	effector memory T cell
TNFα	tumor necrosis factor alpha
TRRAP	transformation/transcription domain-associated protein
TRX	thioredoxin
T_{TM}	transitional memory T cell
TXNRD	thioredoxin reductase
USP22	ubiquitin specific peptidase 22
UV	ultraviolet
Vif	viral infectivity factor (HIV)
Vpr	viral protein r (HIV)
Vpu	viral protein u (HIV)
VSV-G	vesicular stomatitis Indiana virus glycoprotein
WB	Western blot
Δ	delta
µ	micro

7 List of figures and tables

7.1 List of figures

7.2 List of tables

8 Presentations

8.1 Oral presentations

2016: '*Identification of novel factors influencing HIV latency'*, follow-up EURECA meeting, Arbois (France)

2015: '*Identification of novel factors influencing HIV latency',* Paul-Ehrlich-Institut, Annual Research Retreat, Heidelberg (Germany)

8.2 Poster presentations

2017: '*Identification of novel factors influencing HIV latency',* Paul-Ehrlich-Institut, Annual Research Retreat, Ronneburg (Germany)

2016: '*Identification of novel factors influencing HIV latency',* Paul-Ehrlich-Institut, Annual Research Retreat, Ronneburg (Germany)

2015: '*Identification of novel factors influencing HIV latency',* 25th Annual Meeting of the Society for Virology, Bochum (Germany)

8.3 Publications

This thesis has not been published, also not in parts.

9 Curriculum Vitae

PERSONAL INFORMATION

Name: Alexandra Borch
Birth date: 09.01.1985
Birthplace: Neuhaus am Rennweg

PRACTICAL EXPERIENCE

01/2018—06/2019 CAR Engineer
TxCell SAS a Sangamo company, Valbonne (France)

11/2012—05/2014 Research Assistant
Evotec AG, Hamburg (Germany)
Department of Cellular Assays

EDUCATION

06/2014—12/2017 Paul-Ehrlich-Institut, Langen (Germany)
PhD thesis: “Identification of host factors influencing HIV latency”

10/2010—07/2012 International Master Program Molecular Medicine
Ulm University (Germany), Master of Science

09/2007—08/2010 International Bachelor Program Applied Biology
Bonn-Rhein-Sieg University of Applied Sciences (Germany), Bachelor of Science

PUBLICATIONS

Bonczkowski P, De Scheerder MA, Malatinkova E, **Borch A**, Melkova Z, Koenig R, De Spiegelaere W, Vandekerckhove L. (2016). Protein expression from unintegrated HIV-1 DNA introduces bias in primary in vitro latency models. *Sci. Rep.* 6:38329

Kumar A, Abbas W, Colin L, Khan KA, Bouchat S, Varin A, Larbi A, Gatot JS, Kabeya K, Vanhulle C, Delacourt N, Pasquereau S, Coquard L, **Borch A**, König R, Clumeck N, De Wit S, Rohr O, Rouzioux C, Fulop T, Van Lint C, Herbein G (2016). Tuning of AKT-pathway by Nef and its blockade by protease inhibitors results in limited recovery in latently HIV infected T-cell line. *Sci. Rep.* 6:24090.

Yu H, Usmani SM, **Borch A**, Krämer J, Stürzel CM, Khalid M, Li X, Krnavek D, van der Ende ME, Osterhaus AD, Gruters RA, Kirchhoff F. (2013). The efficiency of Vpx-mediated SAMHD1 antagonism does not correlate with the potency of viral control in HIV-2-infected individuals. *Retrovirology* 10:27.

Sterrenburg L, **Borch A**, Peeters BW, Pintér O, Zelena D, Roubos EW, Kozicz T. (2011). Acute ether stress differentially affects corticotropin-releasing factor and urocortin 1 in the Brattleboro rat. *Brain Res.* 1398:21-29.

10 Danksagung

Ich möchte mich herzlich bei Herrn Prof. Dr. Klaus Cichutek, der die Betreuung meiner Doktorarbeit übernommen hat, bedanken, sowie auch bei Frau Dr. Renate König, in deren Arbeitsgruppe ‘Host-Pathogen Interactions’ am Paul-Ehrlich-Institut ich meine Arbeit anfertigen konnte.

Frau Prof. Dr. Beatrix Süß danke ich für die unkomplizierte und nette Betreuung von Seiten der TU Darmstadt. Ich danke auch Herrn Prof. Dr. Alexander Löwer für seine Bereitschaft das Zweitgutachten für meine Arbeit zu übernehmen.

Darüber hinaus möchte ich mich bei allen Kooperationspartnern bedanken, vor allem bei Prof. Dr. Norbert Bannert für die Möglichkeit in seiner Arbeitsgruppe am Robert Koch-Institut zu forschen.

Danke auch an alle meine direkten Betreuer: Dr. Oliver Hohn, Dr. Nina Hein-Fuchs, Dr. Manja Burggraf, sowie Dr. Seifried und Dr. Melkova. Darüber hinaus auch ein dickes Dankeschön an meine inoffizielle Betreuerin Dr. Kerstin. Natürlich auch an die gesamte Forschergruppe: Lea, Max, Maïwenn, Esther, Heike, Christiane, Lise, Michaela und Pawel. Wir haben viel gelacht, hart gearbeitet und einiges erreicht. Ihr alle habt maßgeblich zum Gelingen und Durchhalten beigetragen. Ich danke euch dafür.

Ich möchte auch meiner Familie danken, daß sie immer hinter mir standen und nie müde wurden zu fragen, wie weit meine Doktorarbeit schon gediehen sei.

And a final thank you to my hon. I would have never gotten that far without you. Je bent mijn rots (en ik jouw branding).

11 Ehrenwörtliche Erklärung

Ich erkläre hiermit ehrenwörtlich, daß ich die vorliegende Arbeit entsprechend den Regeln guter wissenschaftlicher Praxis selbständig und ohne unzulässige Hilfe Dritter angefertigt habe.

Sämtliche aus fremden Quellen direkt oder indirekt übernommenen Gedanken sowie sämtliche von Anderen direkt oder indirekt übernommenen Daten, Techniken und Materialien sind als solche kenntlich gemacht. Die Arbeit wurde bisher bei keiner anderen Hochschule zu Prüfungszwecken eingereicht.

Darmstadt, den 02.10.2019

…….

Alexandra Borch

12 Appendix

Table S1: Primary screening hits derived from a genome-wide siRNA screen performed in HIVluc HEK293T cells, listed by their increasing Z-score.

OfficialSymbol	Z-Score	LocusLink	NCBI-Official Full Name
PRKCH	-3.2606	5583	protein kinase C, eta
PHYH	-3.2591	5264	phytanoyl-CoA 2-hydroxylase
RGS13	-3.1137	6003	regulator of G-protein signaling 13
STYX	-3.0499	6815	serine/threonine/tyrosine interacting protein
KRTCAP2	-3.0184	200185	keratinocyte associated protein 2
SLC22A18AS	-2.9664	5003	solute carrier family 22 (organic cation transporter), member 18 antisense
PGAM5	-2.933	192111	phosphoglycerate mutase family member 5
POLR2B	-2.9059	5431	polymerase (RNA) II (DNA directed) polypeptide B, 140kDa
MPV17L2	-2.8822	84769	MPV17 mitochondrial membrane protein-like 2
CNTRL	-2.8675	11064	centriolin
ACSM3	-2.7645	6296	acyl-CoA synthetase medium-chain family member 3
GREB1	-2.7446	9687	growth regulation by estrogen in breast cancer 1
POLR2E	-2.7021	5434	polymerase (RNA) II (DNA directed) polypeptide E, 25kDa
MED21	-2.6844	9412	mediator complex subunit 21
VGLL2	-2.6539	245806	vestigial like 2 (Drosophila)
LINC00652	-2.6432	29075	long intergenic non-protein coding RNA 652
SF3B1	-2.6389	23451	splicing factor 3b, subunit 1, 155kDa
SH3BP5L	-2.6267	80851	SH3-binding domain protein 5-like
SLC24A1	-2.6241	9187	solute carrier family 24 (sodium/potassium/calcium exchanger), member 1
SYNE4	-2.6114	163183	spectrin repeat containing, nuclear envelope family member 4
SF3B2	-2.5996	10992	splicing factor 3b, subunit 2, 145kDa
GGT7	-2.5881	2686	gamma-glutamyltransferase 7
ZNF157	-2.5813	7712	zinc finger protein 157
EEF1A2	-2.569	1917	eukaryotic translation elongation factor 1 alpha 2
RMND5B	-2.5303	64777	required for meiotic nuclear division 5 homolog B (S. cerevisiae)
RBM25	-2.5074	58517	RNA binding motif protein 25
SLC13A2	-2.5056	9058	solute carrier family 13 (sodium-dependent dicarboxylate transporter), member 2
NTN1	-2.496	9423	netrin 1
BUD31	-2.4837	8896	BUD31 homolog (S. cerevisiae)
ZNF205	-2.4826	7755	zinc finger protein 205
GTF3C4	-2.4821	9329	general transcription factor IIIC, polypeptide 4, 90kDa
KCTD18	-2.4668	130535	potassium channel tetramerization domain containing 18
HK2	-2.4252	3099	hexokinase 2
POLR2H	-2.4224	5437	polymerase (RNA) II (DNA directed) polypeptide H
ANXA13	-2.4188	312	annexin A13
POLR2I	-2.4173	5438	polymerase (RNA) II (DNA directed) polypeptide I, 14.5kDa

OfficialSymbol	Z-Score	LocusLink	NCBI-Official Full Name
SSPN	-2.4089	8082	sarcospan
ZNF599	-2.4022	148103	zinc finger protein 599
BCAS2	-2.385	10286	breast carcinoma amplified sequence 2
TMEM97	-2.385	27346	transmembrane protein 97
MED14	-2.3846	9282	mediator complex subunit 14
MZB1	-2.3711	51237	marginal zone B and B1 cell-specific protein
ST3GAL1	-2.3705	6482	ST3 beta-galactoside alpha-2,3-sialyltransferase 1
POLR2A	-2.3677	5430	polymerase (RNA) II (DNA directed) polypeptide A, 220kDa
IRF7	-2.3629	3665	interferon regulatory factor 7
SEC13	-2.3575	6396	SEC13 homolog (S. cerevisiae)
MYL3	-2.3574	4634	myosin, light chain 3, alkali; ventricular, skeletal, slow
SMAD4	-2.354	4089	SMAD family member 4
TMEM246	-2.3492	84302	transmembrane protein 246
PLEKHA5	-2.3482	54477	pleckstrin homology domain containing, family A member 5
KRT40	-2.348	125115	keratin 40
CAMKMT	-2.3474	79823	calmodulin-lysine N-methyltransferase
SERP1	-2.3398	27230	stress-associated endoplasmic reticulum protein 1
POMP	-2.3384	51371	proteasome maturation protein
POLR2K	-2.3372	5440	polymerase (RNA) II (DNA directed) polypeptide K, 7.0kDa
THOP1	-2.3269	7064	thimet oligopeptidase 1
PTMS	-2.3254	5763	parathymosin
SESN1	-2.3141	27244	sestrin 1
POLR2C	-2.3116	5432	polymerase (RNA) II (DNA directed) polypeptide C, 33kDa
KIAA2013	-2.3047	90231	KIAA2013
TPGS1	-2.3011	91978	tubulin polyglutamylase complex subunit 1
KIAA1109	-2.2765	84162	KIAA1109
PDZD4	-2.2734	57595	PDZ domain containing 4
SPRR2B	-2.2686	6701	small proline-rich protein 2B
PCNX	-2.2547	22990	pecanex homolog (Drosophila)
EFNB1	-2.2482	1947	ephrin-B1
PELI1	-2.245	57162	pellino E3 ubiquitin protein ligase 1
ADAM20	-2.2408	8748	ADAM metallopeptidase domain 20
LEPREL1	-2.2333	55214	leprecan-like 1
C16orf67	-2.2324	79014	chromosome 16 open reading frame 67
TMEM144	-2.2241	55314	transmembrane protein 144
WDR53	-2.2238	348793	WD repeat domain 53
C19orf48	-2.218	84798	chromosome 19 open reading frame 48
POLR2D	-2.2174	5433	polymerase (RNA) II (DNA directed) polypeptide D
CREBBP	-2.2101	1387	CREB binding protein
CCDC108	-2.209	255101	coiled-coil domain containing 108
LOC200213	-2.206	200213	hypothetical protein LOC200213
KIF19	-2.1759	124602	kinesin family member 19
PSME4	-2.1666	23198	proteasome (prosome, macropain) activator subunit 4

OfficialSymbol	Z-Score	LocusLink	NCBI-Official Full Name
KLRF1	-2.1604	51348	killer cell lectin-like receptor subfamily F, member 1
MGAT5B	-2.1569	146664	mannosyl (alpha-1,6-)-glycoprotein beta-1,6-N-acetyl-glucosaminyltransferase, isozyme B
ILF3	-2.1539	3609	interleukin enhancer binding factor 3, 90kDa
MAEL	-2.1528	84944	maelstrom spermatogenic transposon silencer
MYF6	-2.1511	4618	myogenic factor 6 (herculin)
CDH15	-2.1499	1013	cadherin 15, type 1, M-cadherin (myotubule)
C1orf51	-2.1411	148523	chromosome 1 open reading frame 51
RPL23	-2.1399	9349	ribosomal protein L23
SLC25A25	-2.1363	114789	solute carrier family 25 (mitochondrial carrier; phosphate carrier), member 25
C16orf71	-2.1279	146562	chromosome 16 open reading frame 71
NME7	-2.1256	29922	NME/NM23 family member 7
SLC39A14	-2.1249	23516	solute carrier family 39 (zinc transporter), member 14
PSMC4	-2.1211	5704	proteasome (prosome, macropain) 26S subunit, ATPase, 4
LOC257396	-2.1165	257396	uncharacterized LOC257396
FAM167B	-2.1159	84734	family with sequence similarity 167, member B
NUDT14	-2.113	256281	nudix (nucleoside diphosphate linked moiety X)-type motif 14
SEMA3A	-2.1126	10371	sema domain, immunoglobulin domain (Ig), short basic domain, secreted, (semaphorin) 3A
CD68	-2.1069	968	CD68 molecule
POLR2L	-2.1005	5441	polymerase (RNA) II (DNA directed) polypeptide L, 7.6kDa
XAGE2	-2.0994	9502	X antigen family, member 2
TMED1	-2.0991	11018	transmembrane emp24 protein transport domain containing 1
NFIX	-2.0985	4784	nuclear factor I/X (CCAAT-binding transcription factor)
NEK6	-2.0961	10783	NIMA-related kinase 6
POLB	-2.0955	5423	polymerase (DNA directed), beta
ICAM1	-2.0947	3383	intercellular adhesion molecule 1
PTRH2	-2.0895	51651	peptidyl-tRNA hydrolase 2
RRP15	-2.0862	51018	ribosomal RNA processing 15 homolog (S. cerevisiae)
SEMG1	-2.0832	6406	semenogelin I
C11orf40	-2.081	143501	chromosome 11 open reading frame 40
FKSG83	-2.0802	83954	FKSG83
OSBPL6	-2.0782	114880	oxysterol binding protein-like 6
IKBIP	-2.0757	121457	IKBKB interacting protein
RRAGB	-2.0743	10325	Ras-related GTP binding B
POLL	-2.0728	27343	polymerase (DNA directed), lambda
NCKAP1	-2.0723	10787	NCK-associated protein 1
RAN	-2.0703	5901	RAN, member RAS oncogene family
SCARB2	-2.0656	950	scavenger receptor class B, member 2
RIIAD1	-2.0597	284485	regulatory subunit of type II PKA R-subunit (RIIa) domain containing 1
GDPD2	-2.059	54857	glycerophosphodiester phosphodiesterase domain containing 2
DIRAS2	-2.0587	54769	DIRAS family, GTP-binding RAS-like 2

OfficialSymbol	Z-Score	LocusLink	NCBI-Official Full Name
RHOH	-2.0546	399	ras homolog family member H
TMEM256	-2.0533	254863	transmembrane protein 256
ZNF304	-2.048	57343	zinc finger protein 304
MS4A6E	-2.0464	245802	membrane-spanning 4-domains, subfamily A, member 6E
ELOVL3	-2.0415	83401	ELOVL fatty acid elongase 3
LOC129020	-2.0401	129020	hypothetical protein similar to topoisomerase (DNA) III beta (H. sapiens)
ZZEF1	-2.0386	23140	zinc finger, ZZ-type with EF-hand domain 1
RARRES1	-2.0363	5918	retinoic acid receptor responder (tazarotene induced) 1
XKR8	-2.0333	55113	XK, Kell blood group complex subunit-related family, member 8
ZNF2	-2.0315	7549	zinc finger protein 2
KPNB1	-2.027	3837	karyopherin (importin) beta 1
YWHAEP7	-2.0268	284100	tyrosine 3-monooxygenase/tryptophan 5-monooxygenase activation protein, epsilon pseudogene 7
PDAP1	-2.0237	11333	PDGFA associated protein 1
RRAS	-2.0165	6237	related RAS viral (r-ras) oncogene homolog
LRRC4B	-2.014	94030	leucine rich repeat containing 4B
ZNF700	-2.0137	90592	zinc finger protein 700
NPEPPS	-2.0122	9520	aminopeptidase puromycin sensitive
DDOST	-2.0117	1650	dolichyl-diphosphooligosaccharide--protein glycosyltransferase subunit (non-catalytic)
POF1B	-2.0086	79983	premature ovarian failure, 1B
MED31	-2.0078	51003	mediator complex subunit 31
CMC1	-2.0078	152100	C-x(9)-C motif containing 1
ACD	-2.0051	65057	adrenocortical dysplasia homolog (mouse)
DNAJB12	-2.0031	54788	DnaJ (Hsp40) homolog, subfamily B, member 12
ZSCAN10	-2.0029	84891	zinc finger and SCAN domain containing 10
NXF1	-2.0028	10482	nuclear RNA export factor 1
SLC12A1	-2	6557	solute carrier family 12 (sodium/potassium/chloride transporter), member 1
ENTPD8	2.0014	377841	ectonucleoside triphosphate diphosphohydrolase 8
TTC28	2.0027	23331	tetratricopeptide repeat domain 28
RUNX1T1	2.0046	862	runt-related transcription factor 1; translocated to, 1 (cyclin D-related)
NFKBIE	2.0086	4794	nuclear factor of kappa light polypeptide gene enhancer in B-cells inhibitor, epsilon
C10orf88	2.0118	80007	chromosome 10 open reading frame 88
TGOLN2	2.0121	10618	trans-golgi network protein 2
NXF5	2.0129	55998	nuclear RNA export factor 5
EML3	2.0144	256364	echinoderm microtubule associated protein like 3
ZNF557	2.0154	79230	zinc finger protein 557
SRF	2.0182	6722	serum response factor (c-fos serum response element-binding transcription factor)
CARF	2.0189	79800	calcium responsive transcription factor
C12orf10	2.0194	60314	chromosome 12 open reading frame 10
TLCD1	2.0195	116238	TLC domain containing 1
PLSCR4	2.0209	57088	phospholipid scramblase 4

OfficialSymbol	Z-Score	LocusLink	NCBI-Official Full Name
LAMB1	2.0226	3912	laminin, beta 1
GOLT1A	2.0227	127845	golgi transport 1A
PEX26	2.0241	55670	peroxisomal biogenesis factor 26
TMC6	2.0245	11322	transmembrane channel-like 6
CBLN1	2.0246	869	cerebellin 1 precursor
HOXC13	2.0257	3229	homeobox C13
C7orf62	2.0257	219557	chromosome 7 open reading frame 62
USP22	2.0267	23326	ubiquitin specific peptidase 22
SRRM2	2.0282	23524	serine/arginine repetitive matrix 2
C12orf5	2.0331	57103	chromosome 12 open reading frame 5
SLC25A29	2.0338	123096	solute carrier family 25 (mitochondrial carnitine/acylcarnitine carrier), member 29
FAM212B	2.035	55924	family with sequence similarity 212, member B
OMP	2.0415	4975	olfactory marker protein
ARMC12	2.0416	221481	armadillo repeat containing 12
ZCCHC13	2.0432	389874	zinc finger, CCHC domain containing 13
CRISPLD2	2.0465	83716	cysteine-rich secretory protein LCCL domain containing 2
SRD5A3	2.0482	79644	steroid 5 alpha-reductase 3
POU6F1	2.0545	5463	POU class 6 homeobox 1
ZYG11B	2.0549	79699	zyg-11 family member B, cell cycle regulator
ASXL3	2.058	80816	additional sex combs like 3 (Drosophila)
IL2RA	2.0608	3559	interleukin 2 receptor, alpha
KCNT1	2.0632	57582	potassium channel, subfamily T, member 1
FATE1	2.0634	89885	fetal and adult testis expressed 1
C6orf47	2.0688	57827	chromosome 6 open reading frame 47
LIN54	2.0704	132660	lin-54 homolog (C. elegans)
TNIP2	2.0712	79155	TNFAIP3 interacting protein 2
TM4SF18	2.0727	116441	transmembrane 4 L six family member 18
TSG101	2.0733	7251	tumor susceptibility 101
CDRT1	2.0761	374286	CMT1A duplicated region transcript 1
ZNF543	2.0768	125919	zinc finger protein 543
FAM129A	2.0777	116496	family with sequence similarity 129, member A
ZNF331	2.0786	55422	zinc finger protein 331
IFNA1	2.0815	3439	interferon, alpha 1
LNX1	2.0818	84708	ligand of numb-protein X 1, E3 ubiquitin protein ligase
DGCR2	2.0838	9993	DiGeorge syndrome critical region gene 2
CFHR3	2.0838	10878	complement factor H-related 3
INTS1	2.0838	26173	integrator complex subunit 1
RIMKLA	2.0847	284716	ribosomal modification protein rimK-like family member A
SDF4	2.088	51150	stromal cell derived factor 4
HYAL2	2.0949	8692	hyaluronoglucosaminidase 2
TAPBP	2.0952	6892	TAP binding protein (tapasin)
SCGB1A1	2.0968	7356	secretoglobin, family 1A, member 1 (uteroglobin)
C15orf41	2.0977	84529	chromosome 15 open reading frame 41

OfficialSymbol	Z-Score	LocusLink	NCBI-Official Full Name
SGCG	2.1035	6445	sarcoglycan, gamma (35kDa dystrophin-associated glycoprotein)
PPAPDC2	2.1054	403313	phosphatidic acid phosphatase type 2 domain containing 2
AK9	2.1055	221264	adenylate kinase 9
DLG1	2.1096	1739	discs, large homolog 1 (Drosophila)
GABRA4	2.1142	2557	gamma-aminobutyric acid (GABA) A receptor, alpha 4
DIS3L2	2.1142	129563	DIS3 mitotic control homolog (S. cerevisiae)-like 2
UBXN8	2.1154	7993	UBX domain protein 8
CHM	2.1158	1121	choroideremia (Rab escort protein 1)
LY6G5C	2.119	80741	lymphocyte antigen 6 complex, locus G5C
PCBD1	2.1206	5092	pterin-4 alpha-carbinolamine dehydratase/dimerization cofactor of hepatocyte nuclear factor 1 alpha
CATSPERB	2.1234	79820	catsper channel auxiliary subunit beta
ZFP36	2.1263	7538	ZFP36 ring finger protein
MBOAT2	2.1273	129642	membrane bound O-acyltransferase domain containing 2
HNRNPC	2.1285	3183	heterogeneous nuclear ribonucleoprotein C (C1/C2)
CBFA2T3	2.1292	863	core-binding factor, runt domain, alpha subunit 2; translocated to, 3
SNRPE	2.1333	6635	small nuclear ribonucleoprotein polypeptide E
BMPER	2.134	168667	BMP binding endothelial regulator
BRCTD1	2.1342	345499	BRCT domain containing 1
C9orf169	2.1372	375791	chromosome 9 open reading frame 169
TMEM184C	2.1432	55751	transmembrane protein 184C
YEATS4	2.1445	8089	YEATS domain containing 4
KAT6B	2.1472	23522	K(lysine) acetyltransferase 6B
ZNF415	2.148	55786	zinc finger protein 415
KIAA1715	2.1511	80856	KIAA1715
PAK1	2.1518	5058	p21 protein (Cdc42/Rac)-activated kinase 1
LOC257054	2.152	257054	similar to D-2-hydroxyglutarate dehydrogenase
REV1	2.1533	51455	REV1, polymerase (DNA directed)
ADAM32	2.1539	203102	ADAM metallopeptidase domain 32
MGC18216	2.1601	145815	hypothetical protein MGC18216
SNCA	2.1632	6622	synuclein, alpha (non A4 component of amyloid precursor)
NAP1L2	2.1649	4674	nucleosome assembly protein 1-like 2
ADAMTS5	2.1651	11096	ADAM metallopeptidase with thrombospondin type 1 motif, 5
SYT1	2.1659	6857	synaptotagmin I
APP	2.1673	351	amyloid beta (A4) precursor protein
SAFB	2.168	6294	scaffold attachment factor B
LMOD1	2.168	25802	leiomodin 1 (smooth muscle)
TNNT3	2.1699	7140	troponin T type 3 (skeletal, fast)
SLC25A15	2.1722	10166	solute carrier family 25 (mitochondrial carrier; ornithine transporter) member 15
MS4A2	2.1732	2206	membrane-spanning 4-domains, subfamily A, member 2
ADCK4	2.1775	79934	aarF domain containing kinase 4

OfficialSymbol	Z-Score	LocusLink	NCBI-Official Full Name
EXOSC3	2.1786	51010	exosome component 3
SMG6	2.1793	23293	SMG6 nonsense mediated mRNA decay factor
HSPC047	2.1794	29060	HSPC047 protein
OR2C1	2.1798	4993	olfactory receptor, family 2, subfamily C, member 1
LINC00323	2.1833	284835	long intergenic non-protein coding RNA 323
N4BP1	2.1834	9683	NEDD4 binding protein 1
SNUPN	2.1861	10073	snurportin 1
METTL21A	2.1884	151194	methyltransferase like 21A
TMEM9B	2.1887	56674	TMEM9 domain family, member B
HNRNPL	2.1888	3191	heterogeneous nuclear ribonucleoprotein L
USP45	2.1916	85015	ubiquitin specific peptidase 45
CIDEA	2.1949	1149	cell death-inducing DFFA-like effector a
ZC3H10	2.1962	84872	zinc finger CCCH-type containing 10
CCSER2	2.197	54462	coiled-coil serine-rich protein 2
ZNF830	2.2	91603	zinc finger protein 830
MILR1	2.2036	284021	mast cell immunoglobulin-like receptor 1
KCNE3	2.204	10008	potassium voltage-gated channel, Isk-related family, member 3
MAP2	2.2052	4133	microtubule-associated protein 2
SAGE1	2.2064	55511	sarcoma antigen 1
FLJ31821	2.2064	146268	hypothetical protein FLJ31821
APCS	2.2075	325	amyloid P component, serum
RABGAP1L	2.2081	9910	RAB GTPase activating protein 1-like
C1orf74	2.2095	148304	chromosome 1 open reading frame 74
DUSP15	2.2129	128853	dual specificity phosphatase 15
ARID5B	2.2132	84159	AT rich interactive domain 5B (MRF1-like)
F8A1	2.215	8263	coagulation factor VIII-associated 1
BEND5	2.2171	79656	BEN domain containing 5
CCNG2	2.2206	901	cyclin G2
PRPF38A	2.2208	84950	pre-mRNA processing factor 38A
BCO2	2.2225	83875	beta-carotene oxygenase 2
KIAA1456	2.2231	57604	KIAA1456
FLNB	2.2259	2317	filamin B, beta
PPRC1	2.2286	23082	peroxisome proliferator-activated receptor gamma, coactivator-related 1
MADCAM1	2.2327	8174	mucosal vascular addressin cell adhesion molecule 1
GDF9	2.2337	2661	growth differentiation factor 9
FAF1	2.2349	11124	Fas (TNFRSF6) associated factor 1
MRPS34	2.2351	65993	mitochondrial ribosomal protein S34
FBXO22	2.2365	26263	F-box protein 22
MMP10	2.2384	4319	matrix metallopeptidase 10 (stromelysin 2)
PCDH12	2.2407	51294	protocadherin 12
NDUFS4	2.2548	4724	NADH dehydrogenase (ubiquinone) Fe-S protein 4, 18kDa (NADH-coenzyme Q reductase)
PXK	2.2556	54899	PX domain containing serine/threonine kinase
DES	2.256	1674	desmin
C6orf57	2.2582	135154	chromosome 6 open reading frame 57

OfficialSymbol	Z-Score	LocusLink	NCBI-Official Full Name
PAF1	2.259	54623	Paf1, RNA polymerase II associated factor, homolog (S. cerevisiae)
TCP11	2.2619	6954	t-complex 11, testis-specific
NR6A1	2.2625	2649	nuclear receptor subfamily 6, group A, member 1
CBX6	2.2635	23466	chromobox homolog 6
SLC9A6	2.2662	10479	solute carrier family 9, subfamily A (NHE6, cation proton antiporter 6), member 6
RLTPR	2.2708	146206	RGD motif, leucine rich repeats, tropomodulin domain and proline-rich containing
USP5	2.2722	8078	ubiquitin specific peptidase 5 (isopeptidase T)
UGGT2	2.2751	55757	UDP-glucose glycoprotein glucosyltransferase 2
GAS2L1	2.2763	10634	growth arrest-specific 2 like 1
SLC25A23	2.2776	79085	solute carrier family 25 (mitochondrial carrier; phosphate carrier), member 23
KIAA1644	2.2776	85352	KIAA1644
CERS1	2.2832	10715	ceramide synthase 1
CCBL1	2.2865	883	cysteine conjugate-beta lyase, cytoplasmic
C4orf17	2.2928	84103	chromosome 4 open reading frame 17
FLJ32154	2.2947	149650	uncharacterized protein FLJ32154
SDE2	2.2952	163859	SDE2 telomere maintenance homolog (S. pombe)
KIAA0492	2.2998	57238	KIAA0492 protein
BEX1	2.3004	55859	brain expressed, X-linked 1
TGIF2LX	2.3004	90316	TGFB-induced factor homeobox 2-like, X-linked
ATP8A2	2.3025	51761	ATPase, aminophospholipid transporter, class I, type 8A, member 2
NUDT10	2.3025	170685	nudix (nucleoside diphosphate linked moiety X)-type motif 10
MACF1	2.3034	23499	microtubule-actin crosslinking factor 1
STXBP4	2.3045	252983	syntaxin binding protein 4
CXXC1	2.3053	30827	CXXC finger protein 1
KCNQ2	2.3054	3785	potassium voltage-gated channel, KQT-like subfamily, member 2
NAA38	2.3146	51691	N(alpha)-acetyltransferase 38, NatC auxiliary subunit
UTS2	2.3165	10911	urotensin 2
FOXP2	2.3174	93986	forkhead box P2
SHMT1	2.3182	6470	serine hydroxymethyltransferase 1 (soluble)
DANCR	2.3221	57291	differentiation antagonizing non-protein coding RNA
SLC25A22	2.3228	79751	solute carrier family 25 (mitochondrial carrier: glutamate), member 22
CALU	2.3231	813	calumenin
C3orf52	2.3248	79669	chromosome 3 open reading frame 52
CITED2	2.3255	10370	Cbp/p300-interacting transactivator, with Glu/Asp-rich carboxy-terminal domain, 2
LMCD1	2.3286	29995	LIM and cysteine-rich domains 1
TMEM120A	2.3307	83862	transmembrane protein 120A
TCF7	2.3338	6932	transcription factor 7 (T-cell specific, HMG-box)
GALNTL5	2.3381	168391	UDP-N-acetyl-alpha-D-galactosamine:polypeptide N-acetylgalactosaminyltransferase-like 5
PANX2	2.3384	56666	pannexin 2
PRDX4	2.3386	10549	peroxiredoxin 4

OfficialSymbol	Z-Score	LocusLink	NCBI-Official Full Name
RFESD	2.3403	317671	Rieske (Fe-S) domain containing
FAM65B	2.3427	9750	family with sequence similarity 65, member B
GCDH	2.3437	2639	glutaryl-CoA dehydrogenase
RNF41	2.3467	10193	ring finger protein 41
GCNT2	2.3492	2651	glucosaminyl (N-acetyl) transferase 2, I-branching enzyme (I blood group)
DENND5A	2.3547	23258	DENN/MADD domain containing 5A
ELMO3	2.3566	79767	engulfment and cell motility 3
EMC1	2.3595	23065	ER membrane protein complex subunit 1
PCID2	2.3637	55795	PCI domain containing 2
MEF2D	2.3742	4209	myocyte enhancer factor 2D
RHPN1-AS1	2.3762	78998	RHPN1 antisense RNA 1 (head to head)
SYCP3	2.3774	50511	synaptonemal complex protein 3
DZIP3	2.3778	9666	DAZ interacting zinc finger protein 3
BIRC5	2.3787	332	baculoviral IAP repeat containing 5
FAM73A	2.3794	374986	family with sequence similarity 73, member A
IL17A	2.383	3605	interleukin 17A
PCYT1A	2.3882	5130	phosphate cytidylyltransferase 1, choline, alpha
ARL6IP4	2.3968	51329	ADP-ribosylation-like factor 6 interacting protein 4
CSRP2	2.3992	1466	cysteine and glycine-rich protein 2
SCAND2P	2.4068	54581	SCAN domain containing 2 pseudogene
PFN4	2.4088	375189	profilin family, member 4
MTMR6	2.4129	9107	myotubularin related protein 6
NEDD4L	2.4129	23327	neural precursor cell expressed, developmentally down-regulated 4-like, E3 ubiquitin protein ligase
ANXA9	2.4149	8416	annexin A9
DHRS1	2.4151	115817	dehydrogenase/reductase (SDR family) member 1
CTTNBP2NL	2.4157	55917	CTTNBP2 N-terminal like
ZFP2	2.4157	80108	ZFP2 zinc finger protein
MCM2	2.4175	4171	minichromosome maintenance complex component 2
SMC5	2.4228	23137	structural maintenance of chromosomes 5
NDUFAF7	2.4231	55471	NADH dehydrogenase (ubiquinone) complex I, assembly factor 7
UPRT	2.4259	139596	uracil phosphoribosyltransferase (FUR1) homolog (S. cerevisiae)
ZNF593	2.427	51042	zinc finger protein 593
SENP3	2.4275	26168	SUMO1/sentrin/SMT3 specific peptidase 3
MAGEH1	2.4314	28986	melanoma antigen family H, 1
LOC113230	2.4322	113230	uncharacterized LOC113230
LNX2	2.4325	222484	ligand of numb-protein X 2
STARD3	2.4335	10948	StAR-related lipid transfer (START) domain containing 3
PRDX5	2.4355	25824	peroxiredoxin 5
LINC00342	2.4371	150759	long intergenic non-protein coding RNA 342
GP6	2.4386	51206	glycoprotein VI (platelet)
TRRAP	2.4388	8295	transformation/transcription domain-associated protein
LZTS1	2.4396	11178	leucine zipper, putative tumor suppressor 1

OfficialSymbol	Z-Score	LocusLink	NCBI-Official Full Name
SLC25A14	2.4484	9016	solute carrier family 25 (mitochondrial carrier, brain), member 14
DEPDC7	2.451	91614	DEP domain containing 7
REXO1	2.4529	57455	REX1, RNA exonuclease 1 homolog (S. cerevisiae)
SLC25A46	2.4611	91137	solute carrier family 25, member 46
GABPA	2.4668	2551	GA binding protein transcription factor, alpha subunit 60kDa
KY	2.4715	339855	kyphoscoliosis peptidase
AP2A2	2.4722	161	adaptor-related protein complex 2, alpha 2 subunit
ANXA5	2.4742	308	annexin A5
KIAA1731	2.4745	85459	KIAA1731
LINC00310	2.4773	114036	long intergenic non-protein coding RNA 310
ARHGEF39	2.4796	84904	Rho guanine nucleotide exchange factor (GEF) 39
CAMSAP2	2.483	23271	calmodulin regulated spectrin-associated protein family, member 2
A1BG	2.4844	1	alpha-1-B glycoprotein
ZNF321P	2.489	399669	zinc finger protein 321, pseudogene
PAQR8	2.4907	85315	progestin and adipoQ receptor family member VIII
TMEM121	2.4998	80757	transmembrane protein 121
NT5DC3	2.5001	51559	5'-nucleotidase domain containing 3
MGC45922	2.5008	284365	uncharacterized LOC284365
INCENP	2.5077	3619	inner centromere protein antigens 135/155kDa
SLC25A3	2.5095	5250	solute carrier family 25 (mitochondrial carrier; phosphate carrier), member 3
NFKBIA	2.5114	4792	nuclear factor of kappa light polypeptide gene enhancer in B-cells inhibitor, alpha
RNF183	2.512	138065	ring finger protein 183
FSCN3	2.5124	29999	fascin homolog 3, actin-bundling protein, testicular (Strongylocentrotus purpuratus)
TNFRSF10C	2.5136	8794	tumor necrosis factor receptor superfamily, member 10c, decoy without an intracellular domain
LARP4B	2.5172	23185	La ribonucleoprotein domain family, member 4B
NMI	2.5205	9111	N-myc (and STAT) interactor
CAPN2	2.5252	824	calpain 2, (m/II) large subunit
EXOSC8	2.5265	11340	exosome component 8
TRIM5	2.5268	85363	tripartite motif containing 5
USP39	2.5295	10713	ubiquitin specific peptidase 39
SAMD1	2.5317	90378	sterile alpha motif domain containing 1
LRRC9	2.5325	341883	leucine rich repeat containing 9
MGAT4B	2.5349	11282	mannosyl (alpha-1,3-)-glycoprotein beta-1,4-N-acetylglucosaminyltransferase, isozyme B
SLC19A2	2.5366	10560	solute carrier family 19 (thiamine transporter), member 2
BBOX1	2.5376	8424	butyrobetaine (gamma), 2-oxoglutarate dioxygenase (gamma-butyrobetaine hydroxylase) 1
SERINC2	2.5406	347735	serine incorporator 2
LPXN	2.5505	9404	leupaxin
FIGNL1	2.5519	63979	fidgetin-like 1
ZNF259	2.5524	8882	zinc finger protein 259
WDR5B	2.5526	54554	WD repeat domain 5B

OfficialSymbol	Z-Score	LocusLink	NCBI-Official Full Name
DNAH3	2.5529	55567	dynein, axonemal, heavy chain 3
LRP12	2.5568	29967	low density lipoprotein receptor-related protein 12
TMEM184A	2.5577	202915	transmembrane protein 184A
CLDN11	2.5617	5010	claudin 11
NUS1	2.566	116150	nuclear undecaprenyl pyrophosphate synthase 1 homolog (S. cerevisiae)
PHLDB3	2.5701	284345	pleckstrin homology-like domain, family B, member 3
CCNYL1	2.5722	151195	cyclin Y-like 1
EPS8L3	2.5798	79574	EPS8-like 3
DDX39A	2.58	10212	DEAD (Asp-Glu-Ala-Asp) box polypeptide 39A
USP29	2.5858	57663	ubiquitin specific peptidase 29
INHBE	2.5866	83729	inhibin, beta E
SEMA5B	2.5968	54437	sema domain, seven thrombospondin repeats (type 1 and type 1-like), transmembrane domain (TM) and short cytoplasmic domain, (semaphorin) 5B
TSPAN4	2.5979	7106	tetraspanin 4
SAMD3	2.5995	154075	sterile alpha motif domain containing 3
CTTN	2.6018	2017	cortactin
LSP1	2.6031	4046	lymphocyte-specific protein 1
ZNF383	2.6071	163087	zinc finger protein 383
RWDD4	2.6148	201965	RWD domain containing 4
GAL	2.6289	51083	galanin/GMAP prepropeptide
SAP18	2.6355	10284	Sin3A-associated protein, 18kDa
TFEB	2.6366	7942	transcription factor EB
GYPB	2.6404	2994	glycophorin B (MNS blood group)
ANO6	2.6448	196527	anoctamin 6
VCAM1	2.6462	7412	vascular cell adhesion molecule 1
SLC35A3	2.6462	23443	solute carrier family 35 (UDP-N-acetylglucosamine (UDP-GlcNAc) transporter), member A3
FAHD2B	2.6464	151313	fumarylacetoacetate hydrolase domain containing 2B
STX11	2.6491	8676	syntaxin 11
KIF20A	2.6537	10112	kinesin family member 20A
PPP6R2	2.6561	9701	protein phosphatase 6, regulatory subunit 2
SACS	2.6562	26278	spastic ataxia of Charlevoix-Saguenay (sacsin)
DICER1	2.6584	23405	dicer 1, ribonuclease type III
ANKRD31	2.6585	256006	ankyrin repeat domain 31
IKZF2	2.662	22807	IKAROS family zinc finger 2 (Helios)
TRAIP	2.6681	10293	TRAF interacting protein
HMGB2	2.67	3148	high mobility group box 2
STX12	2.6742	23673	syntaxin 12
TAMM41	2.6774	132001	TAM41, mitochondrial translocator assembly and maintenance protein, homolog (S. cerevisiae)
IRS1	2.6796	3667	insulin receptor substrate 1
ZSWIM1	2.6819	90204	zinc finger, SWIM-type containing 1
ATOX1	2.685	475	antioxidant 1 copper chaperone
MAMDC4	2.6883	158056	MAM domain containing 4
MTSS1	2.6958	9788	metastasis suppressor 1

OfficialSymbol	Z-Score	LocusLink	NCBI-Official Full Name
NCR3	2.7002	259197	natural cytotoxicity triggering receptor 3
E4F1	2.7053	1877	E4F transcription factor 1
NLE1	2.7073	54475	notchless homolog 1 (Drosophila)
KLF4	2.7084	9314	Kruppel-like factor 4 (gut)
UBE2E1	2.7088	7324	ubiquitin-conjugating enzyme E2E 1
UBL4A	2.7123	8266	ubiquitin-like 4A
PDGFA	2.7181	5154	platelet-derived growth factor alpha polypeptide
SEC31B	2.7198	25956	SEC31 homolog B (S. cerevisiae)
SLC47A2	2.7206	146802	solute carrier family 47 (multidrug and toxin extrusion), member 2
EIF1AX	2.7209	1964	eukaryotic translation initiation factor 1A, X-linked
CACNG2	2.7279	10369	calcium channel, voltage-dependent, gamma subunit 2
ZC3HAV1	2.7352	56829	zinc finger CCCH-type, antiviral 1
MRPL21	2.7403	219927	mitochondrial ribosomal protein L21
RAPGEFL1	2.7468	51195	Rap guanine nucleotide exchange factor (GEF)-like 1
TBRG1	2.7508	84897	transforming growth factor beta regulator 1
CNRIP1	2.7539	25927	cannabinoid receptor interacting protein 1
LMNA	2.7563	4000	lamin A/C
TIMP4	2.7571	7079	TIMP metallopeptidase inhibitor 4
DPCR1	2.7642	135656	diffuse panbronchiolitis critical region 1
DUS1L	2.7778	64118	dihydrouridine synthase 1-like (S. cerevisiae)
RARRES2	2.7791	5919	retinoic acid receptor responder (tazarotene induced) 2
FAM3D	2.7804	131177	family with sequence similarity 3, member D
C5orf17	2.7859	285685	chromosome 5 open reading frame 17
NCF2	2.7875	4688	neutrophil cytosolic factor 2
SIRPB1	2.7889	10326	signal-regulatory protein beta 1
MUC3B	2.7928	57876	mucin 3B, cell surface associated
FAM219B	2.7941	57184	family with sequence similarity 219, member B
PRG2	2.8016	5553	proteoglycan 2, bone marrow (natural killer cell activator, eosinophil granule major basic protein)
INADL	2.8032	10207	InaD-like (Drosophila)
KIAA1549L	2.8124	25758	KIAA1549-like
TTC3	2.8156	7267	tetratricopeptide repeat domain 3
DMRTC1	2.8175	63947	DMRT-like family C1
CEP55	2.8244	55165	centrosomal protein 55kDa
SETD3	2.8281	84193	SET domain containing 3
BCMO1	2.8322	53630	beta-carotene 15,15'-monooxygenase 1
CYLD	2.8376	1540	cylindromatosis (turban tumor syndrome)
RCVRN	2.8384	5957	recoverin
PEX12	2.8414	5193	peroxisomal biogenesis factor 12
KLK3	2.8482	354	kallikrein-related peptidase 3
C16orf54	2.8485	283897	chromosome 16 open reading frame 54
RASAL3	2.8519	64926	RAS protein activator like 3
TTC27	2.8735	55622	tetratricopeptide repeat domain 27
DMTF1	2.8782	9988	cyclin D binding myb-like transcription factor 1
ZNF526	2.8789	116115	zinc finger protein 526

OfficialSymbol	Z-Score	LocusLink	NCBI-Official Full Name
DCK	2.8848	1633	deoxycytidine kinase
RIC8A	2.887	60626	RIC8 guanine nucleotide exchange factor A
CIAO1	2.891	9391	cytosolic iron-sulfur protein assembly 1
LOC100499484-C9ORF174	2.8923	57653	LOC100499484-C9orf174 readthrough
PLIN1	2.8942	5346	perilipin 1
WDR4	2.8973	10785	WD repeat domain 4
ST8SIA5	2.9029	29906	ST8 alpha-N-acetyl-neuraminide alpha-2,8-sialyltransferase 5
TOR2A	2.908	27433	torsin family 2, member A
GLUD2	2.9103	2747	glutamate dehydrogenase 2
ACO2	2.9115	50	aconitase 2, mitochondrial
MYBL2	2.9225	4605	v-myb avian myeloblastosis viral oncogene homolog-like 2
FABP2	2.9235	2169	fatty acid binding protein 2, intestinal
APIP	2.9259	51074	APAF1 interacting protein
TMEM180	2.9331	79847	transmembrane protein 180
TAF7L	2.9355	54457	TAF7-like RNA polymerase II, TATA box binding protein (TBP)-associated factor, 50kDa
WDR89	2.9459	112840	WD repeat domain 89
C7orf71	2.9535	285941	chromosome 7 open reading frame 71
CABYR	2.9556	26256	calcium binding tyrosine-(Y)-phosphorylation regulated
FNDC4	2.9563	64838	fibronectin type III domain containing 4
KHDRBS3	2.9631	10656	KH domain containing, RNA binding, signal transduction associated 3
ARHGEF7	2.9673	8874	Rho guanine nucleotide exchange factor (GEF) 7
CREB3L3	2.9704	84699	cAMP responsive element binding protein 3-like 3
DACT3	2.982	147906	dishevelled-binding antagonist of beta-catenin 3
ACCS	2.9857	84680	1-aminocyclopropane-1-carboxylate synthase homolog (Arabidopsis)(non-functional)
QPRT	2.9871	23475	quinolinate phosphoribosyltransferase
SLITRK5	2.9917	26050	SLIT and NTRK-like family, member 5
KCNIP1	2.9971	30820	Kv channel interacting protein 1
FCGRT	3.0032	2217	Fc fragment of IgG, receptor, transporter, alpha
KIF3B	3.0058	9371	kinesin family member 3B
CCDC138	3.012	165055	coiled-coil domain containing 138
SLC25A1	3.0145	6576	solute carrier family 25 (mitochondrial carrier; citrate transporter), member 1
FAM216B	3.0248	144809	family with sequence similarity 216, member B
WDR75	3.0271	84128	WD repeat domain 75
EBLN2	3.0374	55096	endogenous Bornavirus-like nucleoprotein 2
TSGA10IP	3.041	254187	testis specific, 10 interacting protein
CLP1	3.0458	10978	cleavage and polyadenylation factor I subunit 1
BLVRA	3.049	644	biliverdin reductase A
CUL4A	3.0663	8451	cullin 4A
LRBA	3.0702	987	LPS-responsive vesicle trafficking, beach and anchor containing
KIAA0513	3.0757	9764	KIAA0513

OfficialSymbol	Z-Score	LocusLink	NCBI-Official Full Name
RALA	3.0797	5898	v-ral simian leukemia viral oncogene homolog A (ras related)
SLC25A45	3.0874	283130	solute carrier family 25, member 45
PRO0297	3.0901	29000	PRO0297 protein
ZNF578	3.0904	147660	zinc finger protein 578
PACSIN2	3.0942	11252	protein kinase C and casein kinase substrate in neurons 2
ABCC13	3.0987	150000	ATP-binding cassette, sub-family C (CFTR/MRP), member 13, pseudogene
SLC9B2	3.1094	133308	solute carrier family 9, subfamily B (NHA2, cation proton antiporter 2), member 2
NEDD9	3.1106	4739	neural precursor cell expressed, developmentally down-regulated 9
KIAA0226L	3.1123	80183	KIAA0226-like
DCN	3.121	1634	decorin
ATP6V1G2	3.1248	534	ATPase, H+ transporting, lysosomal 13kDa, V1 subunit G2
ARMC10	3.1394	83787	armadillo repeat containing 10
FGFBP3	3.1427	143282	fibroblast growth factor binding protein 3
ABO	3.1502	28	ABO blood group (transferase A, alpha 1-3-N-acetylgalactosaminyltransferase; transferase B, alpha 1-3-galactosyltransferase)
UBXN6	3.1506	80700	UBX domain protein 6
C20orf24	3.1578	55969	chromosome 20 open reading frame 24
LRRC34	3.1586	151827	leucine rich repeat containing 34
JSRP1	3.1591	126306	junctional sarcoplasmic reticulum protein 1
PDCD11	3.1741	22984	programmed cell death 11
RFTN2	3.1792	130132	raftlin family member 2
TCTN2	3.1897	79867	tectonic family member 2
DNASE1L3	3.1914	1776	deoxyribonuclease I-like 3
FAM192A	3.1924	80011	family with sequence similarity 192, member A
STAT4	3.202	6775	signal transducer and activator of transcription 4
MMP7	3.2094	4316	matrix metallopeptidase 7 (matrilysin, uterine)
DMKN	3.2165	93099	dermokine
C19orf54	3.2174	284325	chromosome 19 open reading frame 54
MBOAT7	3.2262	79143	membrane bound O-acyltransferase domain containing 7
WDR1	3.2412	9948	WD repeat domain 1
USH1G	3.2433	124590	Usher syndrome 1G (autosomal recessive)
TGIF2	3.2446	60436	TGFB-induced factor homeobox 2
SLC30A5	3.2459	64924	solute carrier family 30 (zinc transporter), member 5
SRL	3.2612	6345	sarcalumenin
MRPL32	3.2795	64983	mitochondrial ribosomal protein L32
PYCR1	3.289	5831	pyrroline-5-carboxylate reductase 1
PHLDB1	3.2914	23187	pleckstrin homology-like domain, family B, member 1
CFHR5	3.2959	81494	complement factor H-related 5
SLC8B1	3.3316	80024	solute carrier family 8 (sodium/lithium/calcium exchanger), member B1
OTUD7A	3.3601	161725	OTU domain containing 7A
ZNF418	3.3632	147686	zinc finger protein 418

OfficialSymbol	Z-Score	LocusLink	NCBI-Official Full Name
DAZL	3.366	1618	deleted in azoospermia-like
MMP12	3.3677	4321	matrix metallopeptidase 12 (macrophage elastase)
GTF3A	3.3899	2971	general transcription factor IIIA
TSNARE1	3.3917	203062	t-SNARE domain containing 1
PTBP2	3.4024	58155	polypyrimidine tract binding protein 2
ARFGAP3	3.4107	26286	ADP-ribosylation factor GTPase activating protein 3
HELB	3.4188	92797	helicase (DNA) B
C1orf173	3.4332	127254	chromosome 1 open reading frame 173
PEX3	3.4424	8504	peroxisomal biogenesis factor 3
TMEM261	3.451	90871	transmembrane protein 261
RGPD5	3.4586	84220	RANBP2-like and GRIP domain containing 5
CNOT11	3.4613	55571	CCR4-NOT transcription complex, subunit 11
GH2	3.4654	2689	growth hormone 2
GALNT14	3.4668	79623	UDP-N-acetyl-alpha-D-galactosamine:polypeptide N-acetylgalactosaminyltransferase 14 (GalNAc-T14)
CISD3	3.4681	284106	CDGSH iron sulfur domain 3
NDUFA5	3.4782	4698	NADH dehydrogenase (ubiquinone) 1 alpha subcomplex, 5
DSN1	3.489	79980	DSN1, MIS12 kinetochore complex component
PEX11B	3.4946	8799	peroxisomal biogenesis factor 11 beta
MUL1	3.5017	79594	mitochondrial E3 ubiquitin protein ligase 1
KRT24	3.5183	192666	keratin 24
CAMSAP1	3.5343	157922	calmodulin regulated spectrin-associated protein 1
INTU	3.5432	27152	inturned planar cell polarity protein
CENPO	3.5473	79172	centromere protein O
CSRNP3	3.5501	80034	cysteine-serine-rich nuclear protein 3
CSNK1E	3.5735	1454	casein kinase 1, epsilon
PUS7L	3.5768	83448	pseudouridylate synthase 7 homolog (S. cerevisiae)-like
PPP1R3B	3.5929	79660	protein phosphatase 1, regulatory subunit 3B
SLFN12	3.5983	55106	schlafen family member 12
MYEOV	3.5999	26579	myeloma overexpressed
KLRC4	3.6062	8302	killer cell lectin-like receptor subfamily C, member 4
ITGA2	3.6073	3673	integrin, alpha 2 (CD49B, alpha 2 subunit of VLA-2 receptor)
ZNF473	3.6115	25888	zinc finger protein 473
PRPF31	3.6131	26121	pre-mRNA processing factor 31
NRIP3	3.6247	56675	nuclear receptor interacting protein 3
COMMD5	3.6276	28991	COMM domain containing 5
KIAA1239	3.6362	57495	KIAA1239
GALM	3.6366	130589	galactose mutarotase (aldose 1-epimerase)
KRI1	3.6472	65095	KRI1 homolog (S. cerevisiae)
S100A7A	3.6549	338324	S100 calcium binding protein A7A
KRT86	3.6612	3892	keratin 86
HEATR4	3.6952	399671	HEAT repeat containing 4
HSPA2	3.6964	3306	heat shock 70kDa protein 2
ZNF11B	3.6964	7558	zinc finger protein 11B

OfficialSymbol	Z-Score	LocusLink	NCBI-Official Full Name
FAM178B	3.7261	51252	family with sequence similarity 178, member B
YIPF1	3.7402	54432	Yip1 domain family, member 1
ASPRV1	3.7537	151516	aspartic peptidase, retroviral-like 1
C14orf178	3.7782	283579	chromosome 14 open reading frame 178
MMP23B	3.8209	8510	matrix metallopeptidase 23B
NANS	3.8261	54187	N-acetylneuraminic acid synthase
TOB1	3.85	10140	transducer of ERBB2, 1
FIBIN	3.8696	387758	fin bud initiation factor homolog (zebrafish)
TMEM86A	3.9272	144110	transmembrane protein 86A
GAS2L2	3.9373	246176	growth arrest-specific 2 like 2
RLBP1	3.9969	6017	retinaldehyde binding protein 1
CYP2C9	4.034	1559	cytochrome P450, family 2, subfamily C, polypeptide 9
FAM200B	4.0377	285550	family with sequence similarity 200, member B
SYNE1	4.0379	23345	spectrin repeat containing, nuclear envelope 1
CORO1B	4.039	57175	coronin, actin binding protein, 1B
WDR47	4.0722	22911	WD repeat domain 47
C2orf48	4.077	348738	chromosome 2 open reading frame 48
ETV7	4.0865	51513	ets variant 7
KIF3C	4.0909	3797	kinesin family member 3C
PLOD1	4.0922	5351	procollagen-lysine, 2-oxoglutarate 5-dioxygenase 1
ATP2A1	4.1042	487	ATPase, Ca++ transporting, cardiac muscle, fast twitch 1
ZNF253	4.1083	56242	zinc finger protein 253
PEX19	4.1134	5824	peroxisomal biogenesis factor 19
SCN11A	4.1307	11280	sodium channel, voltage-gated, type XI, alpha subunit
KLHDC10	4.1618	23008	kelch domain containing 10
PGAP3	4.1642	93210	post-GPI attachment to proteins 3
RUVBL2	4.1801	10856	RuvB-like AAA ATPase 2
C14orf119	4.1862	55017	chromosome 14 open reading frame 119
SH2B3	4.2096	10019	SH2B adaptor protein 3
SMYD2	4.2379	56950	SET and MYND domain containing 2
EDDM3A	4.2572	10876	epididymal protein 3A
ST3GAL4	4.2852	6484	ST3 beta-galactoside alpha-2,3-sialyltransferase 4
HSPB2	4.2885	3316	heat shock 27kDa protein 2
WNK2	4.3026	65268	WNK lysine deficient protein kinase 2
KCNJ8	4.3405	3764	potassium inwardly-rectifying channel, subfamily J, member 8
MEG3	4.3407	55384	maternally expressed 3 (non-protein coding)
ST6GAL2	4.3672	84620	ST6 beta-galactosamide alpha-2,6-sialyltranferase 2
PREB	4.3798	10113	prolactin regulatory element binding
C1orf131	4.3955	128061	chromosome 1 open reading frame 131
COMMD3	4.4093	23412	COMM domain containing 3
MSH6	4.4118	2956	mutS homolog 6
KCNK13	4.4143	56659	potassium channel, subfamily K, member 13
NELFCD	4.4289	51497	negative elongation factor complex member C/D
WDR17	4.4423	116966	WD repeat domain 17

OfficialSymbol	Z-Score	LocusLink	NCBI-Official Full Name
GKN2	4.5036	200504	gastrokine 2
PYCARD	4.5416	29108	PYD and CARD domain containing
PPP1R21	4.5452	129285	protein phosphatase 1, regulatory subunit 21
DCTN2	4.5876	10540	dynactin 2 (p50)
BRD4	4.588	23476	bromodomain containing 4
KCNQ1DN	4.6621	55539	KCNQ1 downstream neighbor (non-protein coding)
RRN3	4.6878	54700	RRN3 RNA polymerase I transcription factor homolog (S. cerevisiae)
FAM120B	4.7001	84498	family with sequence similarity 120B
ZC3H13	4.708	23091	zinc finger CCCH-type containing 13
ZDHHC2	4.7192	51201	zinc finger, DHHC-type containing 2
DMRTB1	4.7524	63948	DMRT-like family B with proline-rich C-terminal, 1
NAA15	4.7604	80155	N(alpha)-acetyltransferase 15, NatA auxiliary subunit
MMP26	4.7838	56547	matrix metallopeptidase 26
UTP6	4.8308	55813	UTP6, small subunit (SSU) processome component, homolog (yeast)
LOC285733	4.8759	285733	hypothetical LOC285733
CRYBB2	4.8773	1415	crystallin, beta B2
ANPEP	4.943	290	alanyl (membrane) aminopeptidase
SLC22A18	4.951	5002	solute carrier family 22, member 18
NCSTN	4.9557	23385	nicastrin
TMEM125	5.025	128218	transmembrane protein 125
SNTA1	5.0916	6640	syntrophin, alpha 1
TNP1	5.1668	7141	transition protein 1 (during histone to protamine replacement)
RBM6	5.2019	10180	RNA binding motif protein 6
ITPKB	5.3147	3707	inositol-trisphosphate 3-kinase B
MDH2	5.3526	4191	malate dehydrogenase 2, NAD (mitochondrial)
PRKRIR	5.3715	5612	protein-kinase, interferon-inducible double stranded RNA dependent inhibitor, repressor of (P58 repressor)
TOX3	5.5324	27324	TOX high mobility group box family member 3
ZNF256	5.5416	10172	zinc finger protein 256
COL6A5	5.6382	256076	collagen, type VI, alpha 5
OVOL2	5.6559	58495	ovo-like zinc finger 2
VWC2	5.6948	375567	von Willebrand factor C domain containing 2
CMTM4	5.8988	146223	CKLF-like MARVEL transmembrane domain containing 4
WWC1	5.9123	23286	WW and C2 domain containing 1
MESP1	6.1065	55897	mesoderm posterior 1 homolog (mouse)
ATF7IP2	6.1733	80063	activating transcription factor 7 interacting protein 2
EFCAB5	6.3777	374786	EF-hand calcium binding domain 5
THSD7B	6.4392	80731	thrombospondin, type I, domain containing 7B
ANTXR2	6.4397	118429	anthrax toxin receptor 2
MDGA1	6.4535	266727	MAM domain containing glycosylphosphatidylinositol anchor 1
TUG1	6.8214	55000	taurine up-regulated 1 (non-protein coding)
ND3	6.906	4537	NADH dehydrogenase, subunit 3 (complex I)
GOLGA2P5	7.837	55592	golgin A2 pseudogene 5

OfficialSymbol	Z-Score	LocusLink	NCBI-Official Full Name
DNAJC12	8.2913	56521	DnaJ (Hsp40) homolog, subfamily C, member 12
SUSD1	9.5587	64420	sushi domain containing 1
HYOU1	14.1959	10525	hypoxia up-regulated 1